UNIVERSITÉ DU QUÉBEC

THÈSE
PRÉSENTÉE À
L'UNIVERSITÉ DU QUÉBEC À CHICOUTIMI
ET
L'INSTITUT DE GÉOCHIMIE
L'ACADÉMIE CHINOISE DES SCIENCES
POUR L'OBTENTION
DU DOCTORAT EN RESSOURCES MINÉRALES

PAR

GUAN-QING LU

LE LIEN GÉNÉTIQUE ENTRE LA MINÉRALISATION EN OR ET EN MERCURE ET L'ÉVOLUTION PÉTROLIFÈRE - LE CAS DE DÉPÔT D'OR ET MERCURE DE DANZHAI

MAI 1994

Bibliothèque
Paul-Émile-Boulet

UQAC
Université du Québec
à Chicoutimi

Mise en garde/Advice

Afin de rendre accessible au plus grand nombre le résultat des travaux de recherche menés par ses étudiants gradués et dans l'esprit des règles qui régissent le dépôt et la diffusion des mémoires et thèses produits dans cette Institution, **l'Université du Québec à Chicoutimi (UQAC)** est fière de rendre accessible une version complète et gratuite de cette œuvre.

Motivated by a desire to make the results of its graduate students' research accessible to all, and in accordance with the rules governing the acceptation and diffusion of dissertations and theses in this Institution, the **Université du Québec à Chicoutimi (UQAC)** is proud to make a complete version of this work available at no cost to the reader.

L'auteur conserve néanmoins la propriété du droit d'auteur qui protège ce mémoire ou cette thèse. Ni le mémoire ou la thèse ni des extraits substantiels de ceux-ci ne peuvent être imprimés ou autrement reproduits sans son autorisation.

The author retains ownership of the copyright of this dissertation or thesis. Neither the dissertation or thesis, nor substantial extracts from it, may be printed or otherwise reproduced without the author's permission.

A Genetic Link

Between the Gold-Mercury Mineralization and Petroleum Evolution

-A case of the Danzhai Gold-Mercury Deposit

By

Guan-Qing LU

A thesis in partial fulfillment of the requirements for the degree of Doctor of Philosophy at l'Université du Québec à Chicoutimi, Chicoutimi, Québec, Canada, and the Institute of Geochemistry, the Chinese Academy of Sciences, Guiyang, Guizhou Province, P. R. China.

May 1994

Abstract

The Danzhai gold-mercury deposit is situated in the eastern region of Guizhou province, southwest of P. R. China.

The Danzhai deposit is one of the gold-mercury-antimony-barite deposits in the Sandou-Danzhai ore belt, which is controlled by regional fault system F_1. The host rocks are Upper Cambrian and Lower Ordovician carbonates. Wall rock alteration is dominated by silicification and carbonatization. The major mineral assemblages consist of cinnabar, arsenopyrite, stibnite, pyrite and realgar, orpiment as well as barite. Chemical analyses show that gold is positively correlated with arsenic so that the gold may be mainly associated with arsenic minerals. The Au/Ag ratio is always greater than 1 in the gold ore. Hydrocarbons, particularly bitumen, are abundant in both the host rocks and the ore. The geological characteristics of the Danzhai gold-mercury deposit is quite similar to that of Carlin gold deposit in the western U.S.A except the Danzhai deposit is rich in organic matter and not associated with igneous rocks.

A number of gold-mercury-antimony-barite deposits are distributed in or around the Majiang-Danzhai oil trap, and all of these deposits are present under the ancient interface between petroleum and oilfield brine (-500 m). Field observation shows that a variety of forms of hydrocarbon occur not only in the host carbonates but in the ore deposit as well. Patch-like bitumen, veinlet bitumen as well as stylolite-like bitumen host sulfide minerals such as arsenopyrite and cinnabar while metal sulfides such as cinnabar and gangue minerals also host bitumen. Besides bitumen, paraffin wax is also found in the deposit. An organic petrography study demonstrates that the bitumen in the minerals from the deposit is identical to the bitumen in the former Majiang-Danzhai oil trap. The bitumen is actually pyrobitumen, with a high reflectance, a mosaic texture, and an anisotropic nature but without fluorescence. The reflectance of bitumen from the deposit is high, varying from 2 to 3.8%, and the temperature calculated from this reflectance ranges from 150 to 210°C, indicating that the petroleum in the Majiang-Danzhai oil trap reached the thermal natural gas stage.

Fluid inclusion examination reveals important information about the ore-forming fluids. A variety of hydrocarbon inclusions are identified, including: (1) liquid methane inclusions; (2) bitumen inclusions; (3) paraffin wax inclusions; (4) heavy oil inclusions, and various combinations. Liquid methane inclusions are found in both metallic minerals such as cinnabar and realgar and gangue minerals such as quartz, calcite, dolomite and barite. The heavy oil inclusions are more abundant in carbonate minerals such as calcite and dolomite than in other minerals such as quartz and cinnabar. The spatial relationship between the liquid methane inclusions and cinnabar and realgar demonstrates that the hydrocarbon inclusions are a significant part of ore-forming fluid. The homogenization temperatures of aqueous inclusions range from 130-210 °C and the salinities detected from 5.2 - 19.3 wt. %NaCl equivalent. Solid probe mass spectrometry confirms that hydrocarbons, particularly methane, are the most important constituent of the fluid inclusions. The methane in some inclusions is as high as 69.8 mole percent. Some heavy hydrocarbon molecules are also detected by the mass spectra. The spectra of a sample from the second stage of mineralization displays a complete separation indicating a dominant unmixing of the CH_4 and H_2O phases. Another spectra of a sample from the third stage of mineralization displays an complete separation indicating a marked unmixing of H_2O and CO_2 phases.

Argon isotope data of three quartz samples from the Danzhai gold-mercury deposit show that the initial $(^{40}Ar/^{36}Ar)_0$ value is much higher than 295.5, the $(^{40}Ar/^{36}Ar)_0$ value of modern atmosphere, which is common in most formation waters or oilfield brines. The isochron ages for the three quartz samples are 2783 Ma, 3047 Ma and 2250 Ma respectively, which are obviously much older than reasonable mineralization age, even much older than that of Cambrian and Ordovician host sedimentary rocks. This high excess argon is interpreted to be the result of the formation water or oilfield brine leaching radiogenic ^{40}Ar from the Lower Cambrian black shale, subsequently precipitated in the Danzhai gold-mercury deposit.

Lead isotope data exhibit characteristics of common, rather than radiogenic lead. They are homogeneous, and belong to highly evolved μ value lead, which are widely distributed over South China. These characteristics are different from the lead isotope data of Mississippi Valley-type lead zinc deposits, but similar to that of most stratiform deposits

hosted in sedimentary rocks. Lead isotope data in the deposit plots on the evolution curve of the Upper Crust in the plumbotectonic model. The model age of ore lead is in the neighborhood 400 Ma, equivalent to the end of Silurian period. Therefore, lead isotopes in the deposit indicate derivation from the host sedimentary rocks.

Evidence described above suggests that gold and mercury mineralization in the deposit was related to the petroleum evolution in the Majiang-Danzhai oil reservoir. The oil and associated brine leached the metals and sulfur from the Lower Cambrian black shale and other host rocks and subsequently precipitated them to form the Danzhai deposit.

Résumé Prolongé

Le dépôt d'or et de mercure de Danzhai, qui fait l'objet de cette étude, est situé dans le district oriental de Guizhou (Chine du sud-ouest), province célèbre pour sa production de mercure. Quelques cent dépôts de mercure, antimoine, arsenic, or et barytine sont présents dans ce district et dans la région voisine, la province de Hunan. Danzhai était très connu comme un des plus grands dépôts de mercure en Chine. Il était exploré et exploité comme dépôt de mercure pendant plus d'une trentaine d'années.

Dès le début des années 1980, en comparant les caractères géologiques du dépôt d'or et de mercure de Danzhai avec ceux du dépôt d'or de type-Carlin dans l'ouest des États-Unis, une réévaluation de la mine de mercure a été effectuée pour trouver de l'or. Les travaux géologiques détaillée ont démontré que la minéralisation d'or est actuellement associée à la minéralisation de mercure, il est aussi d'une importance industrielle indépendante.

1. L'environnement tectonique

La colonne stratigraphique de la région orientale de la province de Guizhou est presque complète à partir du Protérozoïque jusqu'au Trias Inférieur-Moyen, et comprend les carbonates et les flyschs du Paléozoïque Supérieur, les carbonates du Paléozoïque Inférieur intercalés occasionnellement par des shales et des roches clastiques protérozoïques légèrement métamorphisées.

L'environnement tectonique de la région orientale de Guizhou est encore problématique. Le concept bien accepté est que la Chine méridionale, particulièrement la région d'étude, est située dans le bouclier de Yangtze. Mais cette interprétation est remise en question par Hsü et al. (1988, 1989) qui proposent un modèle de chevauchement. Les

différentes interprétations de l'environnement tectonique du sud de la Chine résultent des diverses interprétations du Groupe de Banxi. Hsü et al. (1988, 1989) assument que le Groupe de Banxi est segmenté par un océan (océan de Banxi), limité par deux continents séparés Yangtze et Huanan (sud de la Chine) pendant la période pré-Mésozoïque. L'océan fut fermé au Trias Supérieur et le Huanan chevaucha le continent de Yangtze. Mais dans la région d'étude, le Groupe de Banxi est clairement sous-jacent aux roches sédimentaires cambriennes et siniennes. Par conséquent, il appartient au Protérozoïque comme il est traditionnellement accepté. Donc, du moins dans la région orientale de Guizhou, l'interprétation orthodoxe est plus raisonnable que le modèle de chevauchement.

Le district étudié est situé dans la partie moyenne du synclinorium Kaili-Fanchen , qui comprend plusieurs plis successifs de direction N-NE et des failles de direction N-NO et NO. L'importante faille régionale F1 coupe le synclinorium dans la région de Sandou-Danzhai. Les failles subsidiaires reliées à F1 sont très nombreuses et la plupart sont orientées N-S ou NNE. Beaucoup de dépôts de mercure, or, arsenic, antimoine sont associés avec ces failles qui constituent la ceinture minéralisée de Sandou-Danzhai.

2. Les caractères géologiques du dépôt d'or et de mercure de Danzhai

Les roches hôtes du dépôt d'or et de mercure de Danzhai sont les carbonates de l'Ordovicien Inférieur et Cambrien Supérieur, ayant des structures bréchifiées, litées et laminées. Les corps minéralisés en or et mercure se présentent principalement dans les failles, quelquefois dans les lits. Les altérations périphériques présentent des assemblages de basse température tels que la silicification et la carbonatisation. Les assemblages de minéraux sont principalement: les sulfures d'arsenic, de mercure, d'antimoine comme le cinabre, l'arsénopyrite, la stibine, la pyrite, le réalgar, l'orpiment et la barytine. Les minéraux d'or ou l'or finement greinu n'ont pas été observés aux microscopes optique et à balayage électronique, mais les analyses chimiques et les analyses par activation neutronique ont montré qu'il existe une corrélation positive entre l'or et l'arsenic. Ainsi, l'or peut être est associé à des minéraux d'arsénic comme l'arsénopyrite, le réalgar, l'orpiment ou la pyrite arsénifère. Le rapport Au/Ag est toujours supérieur à 1 dans les corps aurifères, mais inférieur à 1 dans les roches hôtes et les dépôts de mercure. Les métaux de base ne sont pas concentrés dans les corps minéralisés ou dans les roches hôtes. Les hydrocarbures,

particulièrement les bitumes sont abondants dans les roches hôtes, et aussi dans les corps minéralisés. Évidement, les caractéristiques géologiques du dépôt d'or et de mercure de Danzhai sont presque identiques à celles du dépôt d'or de type-Carlin dans l'ouest États-Unis par autre le dépôt de Danzhai n'est pas associé à des roches ignées.

3. La concentration des hydrocarbures et la minéralisation d'or et de mercure

Les bitumes sont largement distribués dans les roches sédimentaires paléozoïques dans la région orientale de Guizhou. Les grès bitumineux sont surtout présents dans la seconde unité de la Formation de Wengxiang, Silurien ($S_{1\text{-}2}w^2$) et dans la Formation de Honghuaran, Ordovicien Inférieur (O_{1h}) de la région de Majiang, Duyun, Danzhai et Kaili. L'investigation sur le terrain montre que la concentration de bitume fut contrôlée définitivement par le plis de Majiang et les strates sus-mentionnées . Même dans la seconde unité de Wengxiang, les bitumes sont seulement concentrés dans le niveau plus bas que le coutour -500 m du plis de Majiang. Au-dessus de ce niveau, aucun grès bitumineux n'a pu être observé même dans le même lit de grès. Ainsi, le niveau -500 m est probablement la limite entre le pétrole et les saumures de champs pétrolifères. Cet ancien réservoir est appelé le réservoir pétrolier de Majiang-Danzhai.

Plusieurs dépôts de mercure, d'antimoine, d'or et de barytine sont distribués dans ou autour de cet ancien réservoir pétrolier. La ceinture minéralisée de Sandou-Danzhai est aussi située dans l'extension de ce réservoir pétrolier. Les minéralisations tendent à être enrichies là où la concentration en hydrocarbures est modérée, mais ne le sont pas là où les bitumes sont extrêmement enrichis , pauvres ou absents. Il est remarquable que tous les dépôts de mercure, antimoine, arsenic, or et barytine se trouvent en-bas de -500 mètres, interface possible entre le pétrole et la saumure du champ pétrolifère.

Beaucoup de formes d'hydrocarbures se présentent aussi dans les roches hôtes carbonatées cambriennes et ordoviciennes de ce dépôt. Les bitumes sont présents dans les pores des carbonates laminées et/ou des carbonates litées. Ils remplissent aussi les stylolites et les géodes dans les carbonates. En plus, les bitumes mesurant quelques centimètres, se présentent sous forme de veines dans les roches carbonatées. Les hydrocarbures sont présents également dans le dépôt, dans les veines et dans les corps minéralisés. Les

hydrocarbures souvent observés sont des bitumes dispersés dans le quartz, les carbonates et la barytine et ils peuvent être facilement distingués par leur couleur. Par exemple, les calcites et les veines de quartz de couleur noire, les calcites tâchetées en noir sont souvent observées dans le dépôt. Les bitumes "en plaque", en veinules et stylolite renferment souvent des sulfures tels que l'arsénopyrite, la pyrite, et le cinabre. Le cinabre et la gangue de minéraux englobent les bitumes. Une autre forme d'hydrocarbure solide, la cire minérale aussi identifiée dans le dépôt, est caractéristisée par une couleur brune et brun-foncée et se présente en filonnets parfois associée au bitume ou isolée. Comme le bitume, la cire minérale est souvent associée aux sulfures tels que l'arsénopyrite, la pyrite, le cinabre. L'examen attentif au microscope montre l'absence des zones réactionnelles dans ces hydrocarbures solides, ce qui exclut probablement une formation des hydrocarbures avant la venue du fluide minéralisateur. Par conséquent, il est conclu que ces hydrocarbures coprécipitaient avec les minéraux hôtes et les minéraux sulfurés. Ceci suggère que ces hydrocarbures étaient une partie significative du fluide minéralisateur, c'est-à-dire que les minéralisations d'or et de mercure dérivaient probablement du pétrole et/ou des saumures des champs pétrolifères associées à l'ancien réservoir pétrolifère de Majiang-Danzhai.

La pétrographie organique a démontré que les bitumes dans les roches hôtes, les veines et les minéraux du dépôt sont identiques aux bitumes du réservoir pétrolier de Majiang-Danzhai. La réflectance des bitumes à partir des différents stades de minéralisation du dépôt est élevée et varie entre 2 et 3.8%. Les températures calculées à partir de cette réflectance est de l'ordre de 150-210°C. Les bitumes sont actuellement les pyrobitumes à réflectance élevée, à texture en mosaïque et de nature anisotropique. L'investigation de la fluorescence souligne que les bitumes ont perdu leur fluorescence. Donc, le pétrole présent dans le réservoir de Majiang-Danzhai a atteint le stade de gaz naturel thermogénique, qui est le dernier stade de l'évolution du pétrole pendant la formation du dépôt d'or et de mercure de Danzhai.

4. L'étude des inclusions fluides

L'examen des inclusions fluides de minéraux hôtes des différents stades de minéralisations de ce dépôt révèle quelques informations importantes au sujet du fluide minéralisateur. Plusieurs inclusions d'hydrocarbures sont identifiées dont: (1) à méthane

liquide; (2) à bitume; (3) à cire minérale; (4) à huile lourde et bien sur des combinaisons de ces inclusions. Les inclusions d'huiles lourdes sont présentes seulement dans le second stade de minéralisation et quelques inclusions contenant des huiles lourdes sont rencontrées dans le troisième stade de minéralisation. D'autres types d'inclusions hydrocarbures sont observées à des stades variées de minéralisation.

Les inclusions fluides d'hydrocarbures sont les plus abondantes dans plusieurs minéraux de différents stades de minéralisation. Les inclusions de méthane liquide sont ubiquistes dans les minéraux métallifères tels que le cinabre, le réalgar et les minéraux de la gangue tels que le quartz, la calcite, la dolomite et la barytine. Les inclusions d'huiles lourdes ont tendance à se concentrer dans les carbonates tel la calcite et la dolomite. La relation spatiale entre les inclusions de méthane liquide, le cinabre et le réalgar démontre que les inclusions d'hydrocarbures sont la fraction la plus important du fluide minéralisateur. Il est exceptionnel que plusieurs types d'inclusions hydrocarbures en quantité importante sont uniques dans un dépôt. Évidemment, l'étude des inclusions fluide confirme que ces hydrocarbures constituaient une partie importante de fluide minéralisateur et avaient probablement joué un rôle important dans la transport et la dépôt des éléments minéralisateurs.

Les salinités enregistrées par les inclusions aqueuses varient entre 5.2 et 19.3 .% en pois eq. NaCl. avec une moyenne de 7.3 % en pois eq. NaCl.. La plupart d'entre elles ont une à deux fois la salinité de l'eau de l'océan (3.2 % en pois NaCl.), seulement quelques échantillons exposent des salinités élevées. Les températures d'homogénéisation des inclusions aqueuses sont comprises entre 130 et 210 °C, la plupart d'entre elles sont concentrées dans l'intervalle de 140 à 180 °C. Ces températures sont considérablement plus élevées que celles de la plupart des environnements de la diagenèse sédimentaire et que celles des dépôts de plomb et zinc de MVT, mais elles sont équivalentes à celles des saumures de gaz naturel.

L'immiscibilité des fluides est observé dans le stade de minéralisation. Différentes conditions de démixion sont trouvées dans beaucoup d'occasions. L'immiscibilité enregistrée par les inclusions de fluides dans le dépôt est celle entre les phases aqueuse et des hydrocarbures, particulièrement le méthane liquide. Les investigations exposent deux

principaux types d'inclusions fluides intimement associées dans le même étalage planaire indiquant qu'elles sont captées dans les mêmes conditions en présence d'un fluide miscible des hydrocarbures et de saumure, mais leurs températures d'homogénéisation et leur salinités sont différentes.

L'étude par spectrométrie de masse à sonde solide confirme que les composants des hydrocarbures, particulièrement le méthane, sont d'importants constituants des inclusions fluides. L'abondance du méthane dans quelques inclusions est aussi élevée que 69.8 moles pour-cent. Des molécules d'hydrocarbures lourds sont aussi détectées par spectromètre de masse. Par comparaison de spectre de spectromètre de masse des phases de gaz distinctes au dessus bursts totale, un spectre démontre une séparation complète indiquant une immiscibilité dominante des phases CH_4 et H_2O dans le second stade de minéralisation. Un autre spectre cependant expose une immiscibilitie dominante des phases de H_2O et CO_2 dans le troisième stade de minéralisation. Une quantité élevée en hydrocarbures dans les inclusions fluides corrobore que les hydrocarbures constituaient une partie importante du fluide minéralisateur et que les minéralisations d'or et de mercure dans le dépôt étaient reliées à l'évolution pétrolière régionale du réservoir de Majiang-Danzhai.

5. Étude isotopique

De nombreuses investigations démontrent que, la valeur initiale de $(^{40}Ar/^{36}Ar)_0$ dans l'eau de formation ou des saumures des champs pétrolifères est souvent autour de 295.5, (valeur de $^{40}Ar/^{36}Ar$ de l'atmosphère moderne). Les donnés isotopiques sur l'argon de trois échantillons du dépôt, montrent un excès de ^{40}Ar. Le rapport initial de $(^{40}Ar/^{36}Ar)_0$ pour chacun des échantillons ou chacune des étapes d'écrasement est plus élevé que la valeur de l'atmosphère moderne. Les âges pour trois échantillons de quartz sont respectivement 2783 Ma, 3047 Ma et 2250 Ma. Évidemment, ils sont plus anciens que l'âge raisonnable de minéralisation, et même plus ancien que celle de roches sédimentaires hôtes cambriennes et ordoviciennes. Il y a deux façons d'interpréter l'excès d'argon anormal. D'une part, l'intervalle d'âge de ces échantillons est similaire à celui des roches ignées (e.g.: basaltes coussinés). Leurs valeurs initiales de $(^{40}Ar/^{36}Ar)_0$ sont très élevées et leur spectre est caractérisé aussi par une forme en selle. L'excès ^{40}Ar peut dériver du manteau et traverser la croûte supérieure par dégazage. D'autre part, les strates hôtes du dépôt appartiennent au

Cambrien et à l'Ordovicien, mais les dépôts similaires sont aussi présents dans les anciennes strates tels que le Cambrien Inférieure, le Sinien et même le Groupe Protérozoïque de Banxi. Les minéraux argileux sont enrichis dans ces strates, particulièrement dans les shales noirs du Cambrien Inférieur, qui sont largement distribués au dessus du craton de Yangtze, et considéré comme le principal niveau source de l'huile et des minerais de la région. Par conséquent, l'eau de formation ou saumure du champ pétrolifère peut lessiver le ^{40}Ar radiogénique à partir de ces strates riches en K, et le précipiter postérieurement dans le dépôt d'or et de mercure de Danzhai. La dernière interprétation semble plus raisonnable que la première. La miscibilité de deux fluides distincts n'est pas identifiée ici, puisque de la seconde à la dernière minéralisation, l'isotope d'argon n'a aucun changement significatif.

Le plomb en trace dans la stibine est isolé avec succès à partir des composants majeurs tels que Sb et S pour l'étude d'isotope de plomb parce qu'il n'y a pas de galène disponible dans le dépôt. Les données sur les isotopes du plomb indiquent du plomb commun, plutôt que du plomb radiogénique. Les isotopes de plomb de tous les échantillons des différents corps minéralisés sont homogènes et ont une valeur μ plomb évolué élevée, lesquelles sont largement distribués au sud de la Chine. Ces caractéristiques de l'isotope du plomb dans le dépôt sont totalement différentes de celles de dépôts de Pb-Zn de MVT, mais sont similaires à celles des dépôts stratifiés des roches sédimentaires. En accord avec le modèle "plombotectonique" de Doe et Zartman (1979), les données sur les isotopes du plomb se situent dans le coube d'évolution de la croûte supérieure. Donc, l'origine de l'isotope du plomb dans les dépôts est dérivée des roches sédimentaires cambro-ordoviciennes. L'âge modèle du plomb des minerais est autour de 400 Ma, équivalent à la fin du Silurien.

6. L'évolution du pétrole et des minéralisations d'or et de mercure

En accord avec les travaux de Han et al.(1982) sur le pétrole, les strates qui sont des sources possibles d'huile dans la région sont: le cambrien inférieur, la formation ordovicienne de Honghuaran et la formation silurienne de Wengxiang. Mais seuls les shales noirs du cambrien inférieur sont importants comme source d'huile parce que 97.96% de l'huile brute du réservoir pétrolier de Majiang-Danzhai peut venir de ces shales noirs. Cette hypothèse est aussi supportée par les études isotopiques, par exemple, les isotopes du soufre

du cinabre et de la stibine indiquent que le soufre est venu des roches sédimentaires; l'isotope d'argon anormalement riche en excès d'argon, qui peut s'interpréter raisonnablement par l'huile et les saumures associées qui lessivent l'argon radiogénique des shales noirs; l'étude des isotopes du plomb montre aussi que le plomb en trace dans la stibine est d'origine sédimentaire. Donc, les sources de minerai de ce dépôt et la source de pétrole du réservoir sont venues des mêmes strates, soit les shales noirs du cambrien inférieur.

L'association intime entre la minéralisation de mercure et l'évolution du pétrole est bien documentée, la discussion suivante est donc concentrée sur la relation entre l'or et le pétrole. L'huile brute peut extraire l'or et d'autres métaux des roches sédimentaires, comme le démontrent les expériences effectuées par Ling (1989). La capacité d'extraction de l'or dépend de la nature de l'huile. L'huile brute riche en composants hétéroatomiques a une grande capacité d'extraction parce que le composantes hétéroatomiques peuvent piéger l'or et les autres métaux. Il est à noter que l'huile brute moderne dans quelques champs pétrolifères est minéralisée en or, jusqu'à quelques ppm.

La réflectance des bitumes est plus élevée que 2% dans le dépôt et aussi dans l'ancien réservoir de pétrole. L'étude des inclusions fluides montre que le fluide minéralisateur est surtout composé de méthane et des autres hydrocarbures fortement évolués. Ces évidences suggèrent que l'évolution du pétrole dans le réservoir pétrolier s'approche du stade de gaz naturel thermogénique, l'huile brute pendant ce stade est séparée thermiquement du méthane et des pyrobitumes solides. L'or, les autres métaux et le soufre sont libérés par la séparation des molécules hétéroatomiques. La combinaison des métaux et du soufre a produit les minéralisations.

Les saumures associées peuvent aussi lessiver l'or et les autres métaux à partir des roches sédimentaires. Mais sa capacité d'extraction est souvent inférieure à celle de l'huile brute correspondante. Les saumures ont eu aussi la capacité de lessiver la silice des roches sédimentaires à une température plus élevée. Lors de la réduction de la température, la silice remplacera le calcaire pour produire la silicification ou encore pour précipiter sous forme de veines de quartz. Le dépôt des métaux à partir des saumures peut être causé par une

diminution de la température, une baisse de pression ou une augmentation de la fugacité d'oxygène.

ACKNOWLEDGEMENTS

This thesis is part of the joint program of Université du Québec à Chicoutimi (UQAC) and the Institute of Geochemistry, Chinese Academy of Sciences (IGCAS). I would like to thank the following individuals and organizations for their contributions and help in the preparation of this thesis.

The graduate studies and the preparation of the thesis were supervised by Prof. Jayanta Guha and Prof. Huanzhang Lu and Prof. Edward Chown at UQAC, for their constant guidance and motivation. This thesis was prepared under their careful supervision.

Equal thanks are proferred to the supervisor on the side of IGCAS, Prof. Guangzhi Tu, and co-supervisor Xianpei Chen. Their confidence in this project and frequent direction was critical for the smooth completion of this thesis.

The author has also greatly benefited from the suggestions and discussions of many individuals both in UQAC and IGCAS. They include: Prof. Woussen, Prof. Pierre Cousineau, Prof. Alain Rouleau, Mr. Denis Coté, Dr. Guoxiang Chi, Ms. Michèle Mainville, Ms. Jeannette See, Dr Junsou, Liu, Mr. Bernard Lapointe, Mr. Daniel Bandy-Ayera, Mr. Amar Dahmani at UQAC; Prof. Weihua Yang, Prof. Keyou Yang, Prof. Ouyang Ziyan, Prof. Jiamo Fu, Prof. Yuzhuo Qiu, Prof. Xiuzhang Wang, Prof. Jingping Cheng, Prof. Zhonggang Wang, Prof. Jixi Shi, Prof. Nansheng Chen; Dr. Tianbao Bai, Dr. Yongzhang Zhou, Mr. Qiu Huaning, Dr. Wenjin Yang, Ms Sunrong Li, Mr. Zhifeng Xiao(IGCAS). Their suggestions and assistance have been greatly appreciated.

Access to the studied mines and the general geological information was provided by the geologists working in the Danzhai Gold-Mercury Mine, Yata Mine, Getang Mine, Zhimotang Mine, and the Bureau of Geology and Mineral Resources of Guizhou Province, P. R. China.

This study was partly funded by AUCC-ACDI (project #912-282/14218). necessary accessory support was also provided by IGCAS scholarship, the Open Laboratory of Ore Geochemistry affiliated to the Chinese Academy of Sciences, and the Etudes Avancées et Recherche of UQAC.

Specially thank is to Prof. Gérard Woussen, director of the Ph.D program of the Sciences de la Terre at UQAC; Ms. Ruming Peng, head of the Education Office of IGCAS; and Mr. Michael Trembaly, administrative assistant of the AUCC project, Ms Louise Varagnolo, director of CAMEC.

Finally, thanks are given to Prof. Reinhard Hesse in the Geological Department, McGill Universtiy for accessing the equipment of bitumen reflectance measurement, and Prof. Robert Lamarche, Department of Biology, who provided facilities for fluorescence microscopy.

TABLE OF CONTENTS

LIST OF TABLES

LIST OF FIGURES

LIST OF PLATES

CHAPTER I:
INTRODUCTION

§ 1.1. Gold History

Of all natural elements, gold has been called the first folly of man, the whore of civilization for more than 5,000 years (Boyle, 1984). In different cultures of human history, gold has been firstly used as decoration and and monetary unit for its great natural beauty and universal durability. Gold exploration and mining have a long history, and the most noble of metals is many things to different persons. To the economic geologists and geochemists it is a rare and noble metal, the geochemistry of which is intricate and complex. So, gold presents a challenge to mineralization theory, prospecting strategy, and to the study of its geochemical behavior (Boyle, 1979, 1984).

The recent wave of gold exploration commenced in the early 1970's (Craigie, 1986). The wave was further motivated by the rise of the price of gold from about $200 in 1979 to nearly $700 (U.S.) an ounce by the end of the same year, and finally led to the gold rush of the 1980s (Keays and Skinner, 1988). With this gold rush, new concepts of geological and geochemical environments favorable for gold, improved exploration methodology were put forward and new or improved gold mineralization theories were presented, which were summarized in a series of volumes, including Gold'82, The Geology, Geochemistry and Genesis of Gold Deposits (Foster, 1984), Proceedings of Gold '86, (Macdonald, 1986), Gold History and Genesis of Deposits (Boyle, 1984), Archean Lode Gold Deposits in Ontario (Colvine et al., 1984, 1988), The Geology of Gold Deposits: The Perspective in 1988 (Keays and Skinner, 1988), and Gold Metallogeny and Exploration (Foster, 1991), and numerous papers in scientific journals.

§ 1.2. Sedimentary Rock-Hosted Disseminated Gold Deposits

Sedimentary rock-hosted disseminated gold deposits are classified as Carlin-type gold deposits or invisible gold deposits. As a type of gold deposit, it is the latest to be discovered and mined. It was first described in the west of the United States in 1962 (Radtke et al., 1980; Berger and Bagby, 1991; Bonham, 1988). However, during the past two decades, sedimentary rock-hosted, disseminated precious metal deposits have become an important source of gold because of their tremendous reserves and huge production (Berger and Bagby, 1991; Alvarez and Noble, 1988).

Recently, Berger and Bagby (1991) defined Carlin-type gold deposits and Carlin-like gold deposit. They classified carbonate-replacement gold deposits associated with alkaline igneous intrusions similar in many, but not all, respects to the Carlin-type, as "Carlin-like gold deposits". Although a consensus has not been reached as to what is a Carlin-type gold deposit, it can be characterized by the following criteria: (1) sedimentary host rocks, mostly carbonates; (2) the gold is invisible even under the microscope or common electron microscope; (3) the hydrothermal alteration is simple, principally consisting of silicification, carbonatization and pyritization, with low temperature assemblages; (4) the mineral assemblage is dominated by sulfide minerals such as pyrite, arsenopyrite, cinnabar, realgar, orpiment, stibnite, and barite is frequently observed; (5) ore-forming elements are chalcophile elements Au, Ag, Hg, Sb, As, but the deposits have low base metal contents such as Cu, Pb, Zn, and the ratio of Au/Ag is commonly greater than 1 in the ore; (6) ore-bodies are usually controlled by faults, sometimes by the stratification; (7) most of these deposits are not associated with magmatic rocks while some of them are (e.g. in western U.S.A.); (8) most of these deposits are rich in carbonaceous materials. If a gold deposit shows the characteristics mentioned above, it can be classified as a sedimentary rock-hosted disseminated gold deposit, a Carlin-type gold deposit, or a invisible gold deposit.

A number of sedimentary rock-hosted disseminated gold deposits have been recognized in 1980 in the southwest and northwest provinces in the People's Republic of

China (Fig. 1.1). They are principally located in southwestern Guizhou, northwestern Guangxi and eastern Yunnan. These adjoining locations form a triangle which is known as the "gold triangle" area by geologists. The similar deposits are also reported in other localities, such as the eastern region of Guizhou province, north of Sichuan province, Hunan province, Henan province and (Fig. 1.1). A great number of sedimentary rock-hosted deposits or prospects are being explored in this area of P. R. China. Five of this kind of gold deposits from the southwest of Guizhou province were described in the Western literature by Cunningham, et al. (1988), showing that the geological characteristics of these sedimentary rock-hosted disseminated gold deposits, or prospects, bear remarkable resemblance to that of Carlin gold deposit of the western of United States. They are hosted in Permian to Triassic limestone and dolomite, and are not associated with magmatism or metamorphism; the gold is invisible and occurs in sulfides such as pyrite and arsenopyrite, realgar, orpiment; the alteration pattern is simple, dominated by silicification, carbonatization; the mineral assemblage is arsenopyrite, pyrite, cinnabar, realgar, orpiment, stibnite, barite. The size of these deposits is not yet established, but most of them contain gold with economic significance at an average grade of 3 to 7 grams per metric ton.

§ 1.3. Previous Geological Investigations and the Scope of Problems in the Danzhai Gold-mercury Deposit

The Danzhai gold-mercury deposit, the focus of this study is situated in the eastern region of Guizhou province, which is a province famous for its mercury production (Fig. 1.1). Several tens of different sized mercury, antimony, arsenic and barite deposits are present in this region and adjoining area of Hunan province. Danzhai was known previously as one of the biggest mercury deposits in P. R. China, and has been explored and mined as a mercury deposit for more than thirty years. Systematic regional geological investigation and mapping of the Danzhai mercury mine area began in the early 1950's, and a geological report and a series of geological maps were presented by the No.4 Geological Team of Guizhou (1964). The Danzhai mercury deposit as well as other mercury, antimony, arsenic and barite deposits in the area were then considered as typical telethermal deposits. Recently, they have been classified as typical stratiform and stratabound deposits (Zhang, 1983).

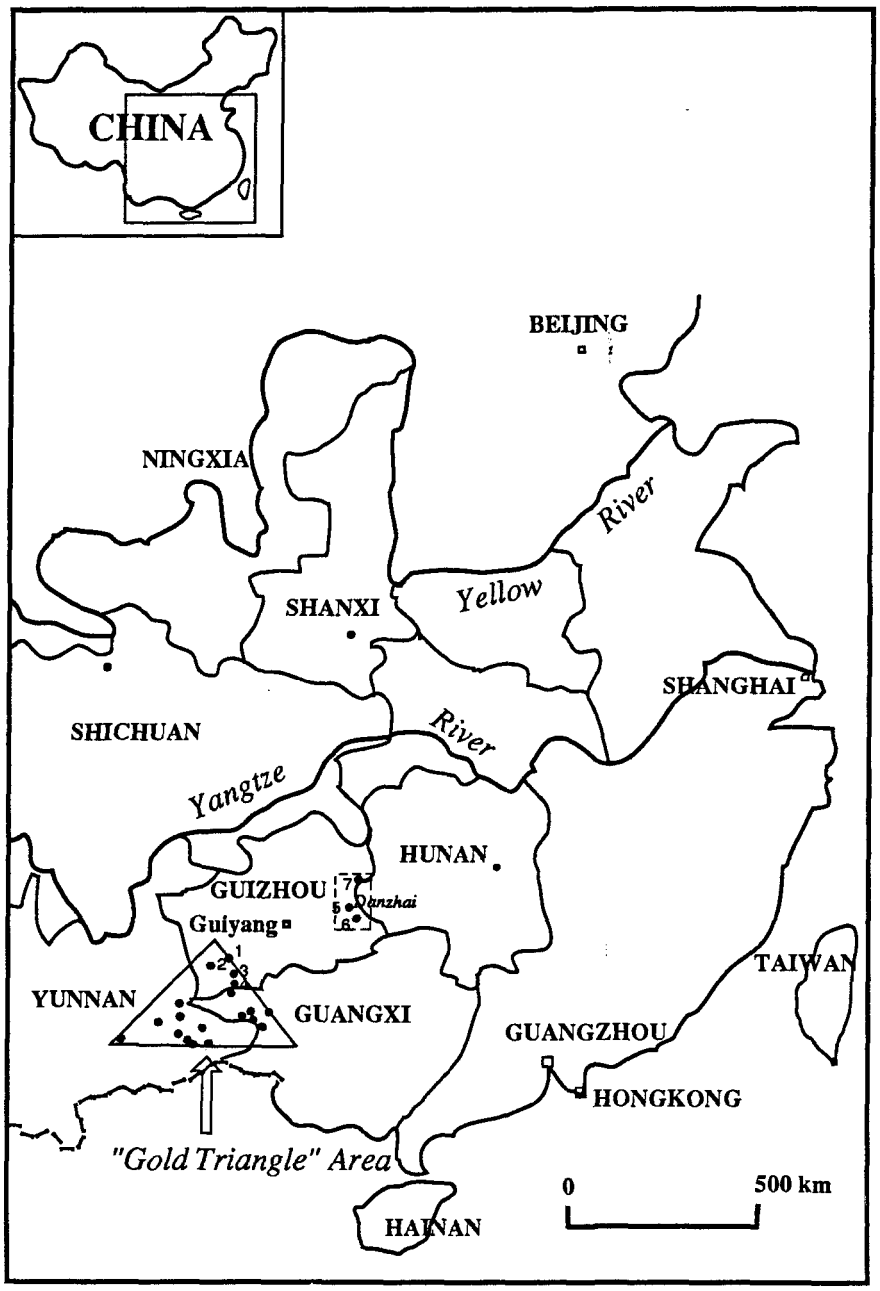

Fig. 1.1 Triangle showing the distribution of Carlin-type gold deposits (solid circle) in Southwest Guizhou, Northwest Guangxi and East Yunnan province and other reported locations in the People's Republic of China. The dotted line rectangle showing the Guizhou-Hunan mercury ore field. Some important deposits mentioned in this study are as follows: 1. Gotang deposit; 2. Zhimotang deposit; 3. Yata deposit; 4. Banqi deposit; 5. Danzhai deposit; 6. Miaolong deposit; 7. Wanshan deposit.

Since early 1983, after comparison of the geological characteristics of the Danzhai mercury deposit with those of the Carlin-type gold deposits in the western U.S.A, re-evaluation and re-prospecting of this mercury mine as a gold mine was undertaken and a detailed geological survey and exploration showed that gold mineralization is also of economic importance in Danzhai.

The genesis of the Danzhai gold-mercury deposit and many other similar deposits in the area by a process similar to or related to petroleum evolution was proposed by Tu (1983, 1984, 1987, 1988). The similarities between petroleum evolution and the formation of these "active ore-forming elements" (e.g. Hg, As, Sb) deposits were noted. Chen et al (1986) and Fu (1988, 1990) also considered that these mercury, antimony, arsenic, gold and barite deposits in the Sandou—Danzhai ore belt, are related to the hydrocarbon evolution of an ancient oil field. Hydrocarbon investigation aimed at prospecting for petroleum carried out by Han et al.(1982) found several tens of meters of bituminous sandstone in the second member of Wengxiang formation, Silurian ($S_{1\text{-}2}w^2$) in the eastern region of Guizhou. Detailed field surveys and laboratory tests revealed the existence of the Majiang-Danzhai petroleum reservoir in the area. Based on the spatial association of regional mercury, antimony, arsenic, gold and barite deposits with the Majiang-Danzhai oil trap, Chen et al.(1986) believed that the these deposits were derived from the regional hydrocarbon evolution. Evidence offered by Chen et al.(1986), depends on two coincidences between regional mineralization and petroleum evolution: (1) the spatial distribution of Sb, Hg, As, Au and barite mineralizations coincident with the distribution of the ancient oil field in the region; and (2) the temperature obtained from the measurement of reflectance of bitumen from the host rocks of the deposits in this area which is in good agreement with the ore-forming temperature. No further evidence was offered to establish a genetic connection between the regional mineralization and hydrocarbon evaluation.

A schematic comparison was recently made by Tu (1990) among the three biggest Carlin-type gold deposits in the world: The gold deposits of western U. S. A., southwestern Guizhou, in southwest China, southwest Qinling, in northwest China. He divided the mineralization of the gold deposits in southwestern Guizhou into two principal periods. A synsedimentary period, during which ore-forming elements such as Au, Hg, Sb, As, Tl, U were concentrated in fine-grained pyrite and carboniferous materials hosted in Phanerozoic

ore-source strata, followed by a remobilization period, during which gold and associated ore-forming elements were remobilized and transported to favorable structures, where gold and other ore-forming elements were precipitated. The remobilization period occurred during the Yanshanian Orogeny. The energy or potential heat sources to remobilize and transport the gold and associated elements were associated with the tectonic movements.

Even though the fundamental geological setting for the Danzhai gold-mercury deposit is clear, a number of problems remain to be solved. For example, the recognition of the gold deposit of the region as a Carlin-type is still subject to controversy, and the origin of the gold mineralization is contentious. The principal problems concerning the Danzhai gold-mercury deposit are discussed in the following:

Organic material such as bitumen is abundant in the Danzhai gold-mercury deposit as well as in other deposits in this area. A similar situation also exists in the Carlin-type gold deposits elsewhere in the world, such as the Carlin gold deposit of western U.S.A. Radtke and Scheiner (1970) indicate that carbonaceous materials are enriched in the deposit, and played an important role in the gold mineralization, but the field surveys and laboratory tests revealed that the gold mineralization appears to be no more controlled by arsenopyrite or other sulfide minerals than by these organic materials. The genetic relationship between gold mineralization and carbonaceous materials is still unclear.

The Danzhai gold-mercury deposit and other deposits are spatially distributed in or around the Majiang-Danzhai petroleum reservoir, but the spatial association between them does not necessarily mean that they are genetically connected. Obviously, detailed investigation of spatial and temporal relationship between them should be undertaken. This investigation, together with other geological and geochemical studies, may confirm or deny possible genetic links.

The nature of the ore-forming fluid, its composition and physico–chemical characteristics such as temperature, pressure as well as density are important aspects, which may be used to discriminate between petroleum and/or associated oilfield brines or other kinds of ore-forming fluid. Fluid inclusions derived from petroleum evolution should be rich in oil, bitumen, or other forms of hydrocarbons whereas fluid inclusions from a fluid of epithermal origin will be

dominated by aqueous and carbon dioxide inclusions, and will probably show boiling features (Romberger, 1985). Fluid inclusion investigations, therefore, should give an important insight to the identification of the ore-forming fluid of the Danzhai gold-mercury deposit.

Only a few inorganic geochemical studies have been done on the Danzhai gold-mercury deposit, and few stable isotopic analyses have been done. Zhang (1983) and Chen et al. (1986) analyzed the sulfur isotopes of sulfide minerals as well as $\delta^{13}C$-$\delta^{18}O$ of calcite and dolomite from the veins of the deposit. Their data are insufficient to distinguish whether the mineralization is related to petroleum evolution or not, even though these isotope investigations proved that the sulfur, carbon as well oxygen originated from sedimentary rocks, it certainly does not mean that the metals are of the same origin. Argon and lead isotope investigation, however, may serve the purpose, to discriminate the provenance of the gold and mercury mineralization, because these two isotopes can indicate the original sources of the mineralization, the mantle, the lower or upper crust or a combination. Therefore, an argon and lead isotopic survey may be critical to determine the origin of the mineralizing elements such as gold and mercury.

§ 1.4. Objectives of This Study

This study was designed to:

(1) investigate the spatial and temporal relationship of the host rocks, alterations and gold-mercury mineralizations in the Danzhai gold-mercury deposit;

(2) survey the spatial and temporal connection between the ancient Majiang Danzhai petroleum reservoir and the regional mercury, antimony, arsenic, gold and barite mineralization in the eastern region of Guizhou;

(3) characterize the composition and behavior of the ore-forming fluids in the ore minerals (cinnabar, realgar) and associated gangue minerals (quartz, calcite, dolomite) by fluid inclusion studies in order to establish a link between them. Particular attention is paid

on the ubiquitous hydrocarbon fluid inclusions as well as their connection with regional hydrocarbon evolution.

(4) elucidate the role of fluid evolution in gold and mercury deposition, with respect to the temperature, pressure, and composition of the ore-forming fluid.

(5) scrutinize the possible origin of the ore-forming elements and fluids and its importance elucidating the history of the Danzhai gold-mercury deposit.

The principal objective is to construct the relationship between the host rocks, alteration and gold-mercury mineralization, to establish a correlation between the hydrocarbon evolution and gold-mercury mineralization, and to examine the evolution of ore-forming fluid with the progress of alteration and mineralization.

§ 1.5 Methodology

In order to attain the objectives, the following methods will be applied:

(1) compilation of the regional tectonic setting, the regional stratigraphy, the regional magmatism and metamorphism as well as the regional association of the ore deposits.

(2) detailed field geological investigation, and setting of the deposit, the mineral assemblages, the alteration patterns, the crosscutting veins of both mineralizations and alterations.

(3) Petrograhic studies of the different gold orebodies have been carried out to verify the different mineralization and alteration patterns. Sixty sample from different orebodies with different type of mineral association, the host rocks, altered host rocks with different stage of alteration were collected.

(4) The spatial relationship between different types and/or stages of alteration and mineralization, in order to establish a temporal sequence between them.

(5). Solid hydrocarbons such as bitumen and paraffin wax are commonly observed, and associated with the gold-mercury mineralization in the Danzhai gold-mercury deposit. Distinct solid hydrocarbons will be identified and their maturity will be measured. Attention will be paid to the spatial and temporal relationships between the solid hydrocarbons and gold-mercury mineralization. Their possible genetic links are to be examined in detail.

(6) Bitumen reflectance in the Danzhai gold-mercury deposit is measured to compare with bitumen in the host rock of the deposit as well as bitumen in the Majiang-Danzhai oil trap for recognizing the maturity of all the bitumen and the connection between these different occurrences of bitumen. Hydrocarbons are usually characterized by fluorescence, and hydrocarbons with different maturity show distinct fluorescence. Therefore, the fluorescence of different forms of hydrocarbons will also be examined to categorize their maturity.

(7) Fluid inclusion studies: Two group of fluid inclusions are found of different compositions, hydrocarbon and aqueous fluid inclusions. The hydrocarbon fluid inclusions are dominant in most stage of mineralization. Other significant information with regard to the characteristics of ore–forming fluid, may be measured or calculated such as the temperature, the pressure and the salinity of the ore-forming fluid. The fluid inclusion study has been performed at the University of Quebec, Chicoutimi, using microthermometry methods by heating and freezing stages: Chaixmeca heating and freezing stage (Nancy, France), and U.S.G.S. Gas-flow heating and freezing system. The volatile composition of fluids hosted in quartz and calcite were analyzed by solid probe mass spectrometry (Guha et al. 1990, 1991) to determine the composition of fluid inclusions, to distinguish the unmixing of fluid and to measure the decrepitation temperature of the fluid inclusions.

(8) Argon isotopes were examined as an indicator of the origin of mineralization. Unlike many other elements, argon is a noble gas and non-reactive with other elements, it is therefore a good indicator of its primary provenance. Isotope investigation will examine if the argon came from the mantle, atmosphere or another source. Argon has also the potential to determine the age of mineralization by ^{39}Ar-^{40}Ar plateau age. This study expects to show if a deep-seated magmatic fluid, an oil-field brine, or underground water took part in the gold and mercury mineralization, or if it is a combination of these fluids.

(9) Lead isotopic study was also applied as a tracer of gold-mercury mineralization. Since base metal minerals are rare in the Danzhai gold-mercury deposit, trace lead isolated from stibnite was applied to lead isotopic study, which proved successful in distinguishing the geological provenance of the gold and mercury mineralization. This can corroborate or deny the results from the argon isotope study.

CHAPTER II:

REGIONAL GEOLOGICAL SETTING

§ 2.1. Introduction

The Danzhai gold-mercury deposit is located in the eastern region of Guizhou province, southwest China. It is an important deposit of the Sandou-Danzhai ore belt consisting of several tens of known deposits of mercury, antimony, arsenic, gold and barite.

Sedimentary rocks are the host to a great number of different sized mercury, antimony, arsenic, gold and barite deposits in the Guizhou-Hunan mercury ore field. The mercury deposits in other countries are usually related to volcanic rocks, although occasionally occurring in sedimentary rocks, these tend to be clastic rocks such as sandstone or siltstone. In China, however, more than 90% of mercury mineralization is hosted in carbonate rocks.

From a stratigraphic view, even though mercury mineralization in China is present in strata of many periods, 80% of the mercury reserves are concentrated in Cambrian and Lower Ordovician strata, and about 15% of mercury reserves are present in Permian and Lower Triassic strata. The mercury mineralization in the sedimentary rocks of other periods is insignificant (Hua, 1982).

§ 2.2. Regional Stratigraphy

The major strata that crop out in the eastern region of Guizhou Province consists of Lower Paleozoic argillaceous carbonates, shale as well as Upper Paleozoic carbonate and

flysch. Proterozoic clastic rocks of the Banxi Group outcrop in the east. This assemblage in south China is called the Yangtze craton.

§ 2.2.1. Proterozoic Erathem

Banxi Group, Proterozoic: The Banxi Group occurs throughout the study area, particularly in the east part of Fig. 2.1, and is composed of low grade metamorphosed littoral clastic rocks, up to 20 km in total thickness. It is divided into two subgroups by an unconformity.

Lower Subgroup of Banxi Group: The Lower Subgroup is constituted of marine eruptive rocks (ophiolite suite), arenaceous argillaceous flysch and carbonates, more than 8.3 km in thickness.

Upper Subgroup of Banxi Group: The Upper Subgroup overlies the Lower Subgroup unconformably with a conglomerate at base and is 12 km thick in its area of maximum development. It consists of marble, tuffaceous rocks and black slate. Black flysch is prevalent and cross bedding, ripples on sole marks are usually observed in flysch. A recurring cyclothem is composed of conglomeratic arenite-arkose, quartz arenite and slate.

Sinian System, Proterozoic: the period from 800 to 570 Ma is called Sinian System in China with a map symbol Z (c.f.: Guizhou Geological Bureau, 1973)(Fig. 2.1). It is extensively developed in the Yangtze craton and overlies the Upper Subgroup of Banxi Group. It is principally composed of glacial sediments and is divided into the Upper Subsystem and the Lower Subsystem.

The Lower Subsystem of the Sinian is defined as three groups of glacial sedimentary rocks: The first Group (or Wuyi Group) consists of morainal arenaceous conglomerate, arkose and sericite slate, with dolomite breccia or dolomite and occurs at the base occasionally containing lenticular hematite ore. The second Group (Baidu Group): The lower member of this group is composed of siltstone and silty slate containing dolomite and conglomerate, the upper member is composed of black carbonaceous shale, bearing plant fragments of "*Laminarites*" with intercalated sedimentary rhodochrosite and hematite ore.

The third Group (or Lijiapo Group): Grey green colored with purple colored massive glacial drift deposit, containing tillite bearing argillaceous sandstone intercalated with laminated mudstone and/or slate. The component of tillite is so complicated that it includes a variety of rocks such as magmatic rocks, quartzite, arenite, tuff, phyllite, and slate. The grain size of the breccia is highly variable, ranging from 1 meter in diameter to several centimeters in diameter. Striae are observed on the surface of blocks in the tillite.

Upper Subsystem of Sinian is developed in Zhunyi, Kaiyang region and classified into two groups. The Dushantou Group is composed of sandstone, multicolored shale and black carbonaceous shale. It is an important phosphorous producing sequence (called basal phosphate ore beds). The Denying Group is composed by dolomite, chert as well as phosphate ore (called Middle phosphate ore beds)..

§ 2.2.2. Paleozoic Erathem

Cambrian System: The rocks of the Cambrian system are widely distributed in the study area, consisting of littoral arenaceous shale and silty carbonates. The Middle to Upper Cambrian is dominated by limestone and dolomite, particularly banded and brecciated carbonate rocks. The Lower Cambrian system is constituted of black shale intercalated with some carbonates, the bottom of which is composed of massive phosphatic sediment and phosphate concretions, 1 m thick (called upper phosphate ore beds).

Ordovician System: The rocks of the Ordovician system occur in association with the Cambrian System, constituted principally of littoral carbonates and clastic rocks. The Upper Ordovician is generally absent in the study area. The Middle Ordovician consists of shale, the bottom of which is dominated by lenticular conglomerate. The Lower Ordovician is composed of limestone, dolomite and shale.

Silurian System: The Upper Silurian System is absent in the study area, only the Wengxiang formation of Lower to Middle Silurian systems occurs, consisting of littoral shale intercalated with sandstone as well as limestone. Some fossils such as *Stomatograptus sinensis, Monoclimacis cf. adunca, M. cf. vomerinus etc.* Purple colored sandstone is

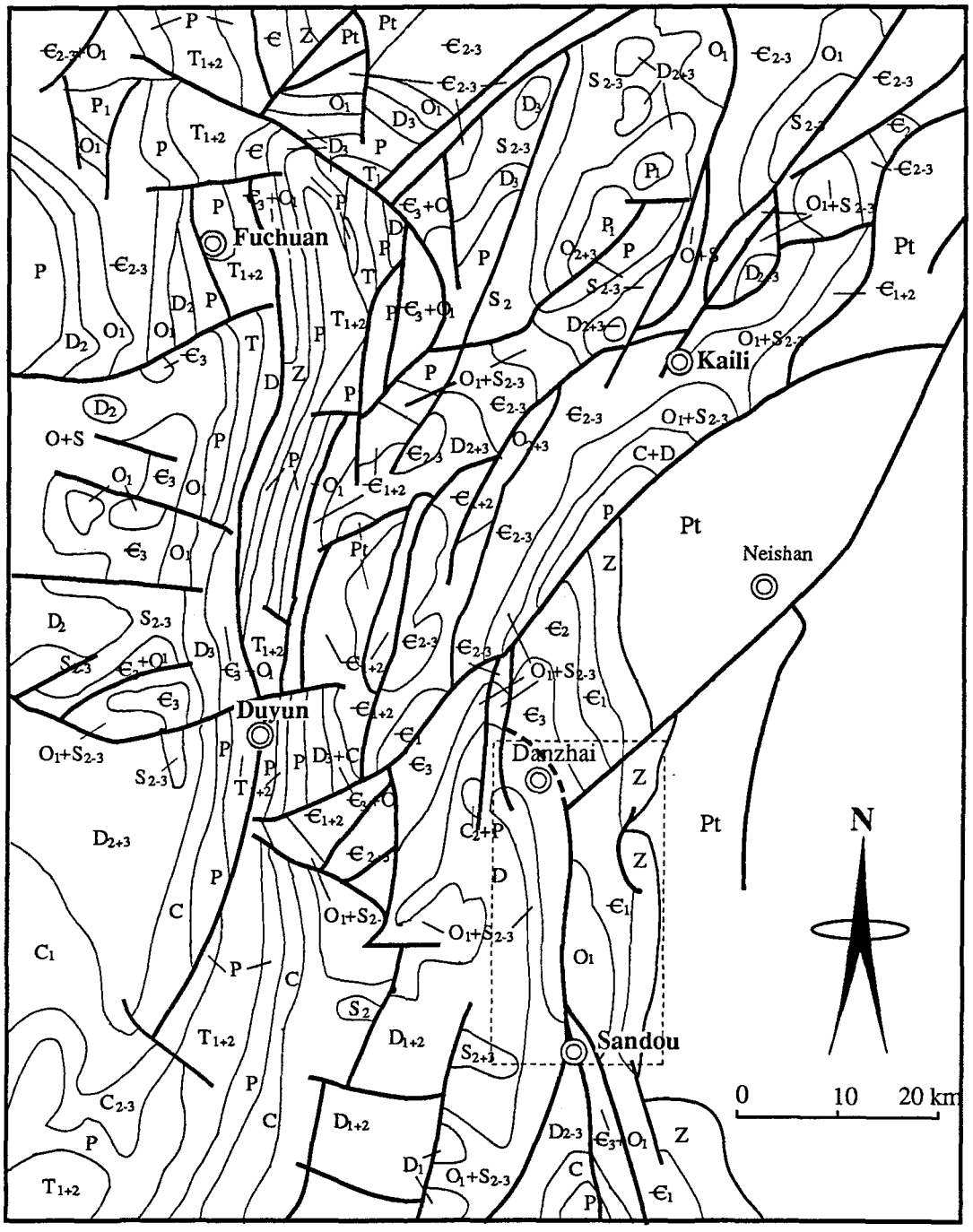

Fig. 2.1 Geological map in the eastern region of Guizhou province. The rectangle represents the Sandou-Danzhai ore belt shown in Fig. 3.2 (Modified after Guizhou Geological Bureau, 1973).

present on the top. In the Majiang, Kaili, Duyun, Danzhai and Sandou area, the second member of the Wengxiang formation is composed of black colored bituminous sandstone.

Devonian System: The Lower Devonian system is constituted of quartz arenite, intercalated with shale, locally hematite bedding is present. The Middle Devonian is dominated by dolomite, limestone, and marl intercalated with arenaceous shale. In Duyun, it contains ferruginous sandstone, ooïd hematite (called "Duyun-type iron ore"), with widely varying thickness. The Upper Devonian System, is composed of dolomite and limestone.

Carboniferous System: The Carboniferous system principally crops out in the southeast corner of Fig. 2.1. The Lower Carboniferous consists of carbonates, locally intercalated with arenaceous shale. The Middle and Upper Carboniferous are made up of limestone and dolomite in the study area and change to shales and bearing bauxite, hematite, and coal seams in the north of Guizhou Province.

Permian System: The Permian system is distributed in the core of synclines and overlaps on older strata in the study area. The Lower Permian is dominated by limestone, but at its base, the Liangshan group contains 0 to 50 meters of sandstone intercalated with arenaceous shale, locally bearing lenticular coal beds. The Upper Permian is constituted of limestone, chert and shale, locally bears beds of siderite ore. Most of the Carlin-type gold deposits and antimony, arsenic deposits in southwest of Guizhou are hosted by the Permian system.

§ 2.2.3. Mesozoic Erathem

Triassic System: This system is present in the northeast and southwest parts of Fig. 2.1, Lower and Middle Triassic usually occurs with the Permian system in the core of the synclines. The Middle Triassic consists of four sedimentary assemblages: clastic rocks, clastic rocks intercalated with carbonates, carbonates intercalated with clastic rocks and carbonates. Locally, it contains anhydrite and halite deposits. The Lower Triassic comprises limestone and dolomite. Some gold, antimony, arsenic deposits hosted in the rocks of this System in the southwest region of Guizhou province.

Other strata younger than Triassic are terrigenous sediments which are occasionally present in the core of synclines in northeast Guizhou but are rarely seen in the study area.

Note that, at least in the study area, the Banxi Group clearly underlies the Lower Paleozoic argillaceous carbonates, and the Sinian System commonly overlaps unconformably on the Banxi Group.

Recently this well accepted model has been questioned by Hsü et al.(1987, 1988, 1989, 1990). The different recognition of tectonic setting in south China results from a different interpretation of the Banxi Group, Proterozoic, therefore the regional stratigraphy is described here. Hsü et al. (1988) invoked a thrust model and interpreted that the southern China area was an ocean (called the Banxi Ocean) bounded by two separate continents, called Yangtze and Huanan (South China) respectively during pre-Mesozoic time (Fig. 2.2 and Fig. 2.3). A pre-Devonian accretionary prism was formed at the northwestern active margin of the Huanan continent (the Proterozoic clastics and lower Paleozoic flysch). During the early Devonian, the margin became passive and carbonate rocks were deposited unconformably on top of the accretionary prism (the Lower Paleozoic carbonate rocks). The ocean was closed in the late Triassic and the Huanan terrane was overthrust onto the Yangtze continent. As a result of this collision, S-type granite was formed in Huanan during the Mesozoic. Then in late Mesozoic time the Huanan terrane which is attached to the Yangtze terrane was overthrust in turn by another microcontinent further to the southeast, the Donnanya (southeastern Asia) continent.

This debate is still open and no consensus has been reached yet. The key issue is the recognition of the Banxi Group, consisting of slightly metamorphosed unfossiliferous clastic rocks, locally containing ophiolite blocks. The orthodox interpretation considered the Banxi Group as a Precambrian basement, the core of Yangtze craton, but Hsü et al (1988, 1989) interpret it to be an ophiolitic melange in the suture zone between two colliding microcontinents, and call it the Banxi ophiolite melange. The collision took place in Mesozoic time (Hsü et al. 1988).

§ 2.3. Regional Tectonic Setting

Two contradictory explanations were proposed for the tectonic setting in the region. One is the well-accepted theory that considered South China as a craton (e.g. Zhang et al., 1984, Xiong and Coney, 1985), the Yangtze craton, another is a recently proposed hypothesis that suggests that South China was formed as a consequence of the collision of two separate continents (Hsü et al. 1987, 1988, 1989).

The well-accepted interpretation for the tectonic setting in China indicated that most of south China, including the eastern part of Yunnan Province, Guizhou Province Hunan province, Jiangxi Province, Anhui Province, Jiangshu Province and Zhejiang provinces, are underlain by the Yangtze craton, which is composed of Proterozoic crystalline rocks overlain by Paleozoic and Lower to Middle Triassic marine sedimentary rocks and Upper Triassic continental sedimentary rocks (Xiong and Coney, 1985).

In the eastern region of Guizhou province (Fig. 2.1), low grade metamorphic littoral clastic rocks, marble, tuffaceous rocks, well developed black flysh as well as an ophiolite suite (for example, in Fanjinshan area) of Banxi Group crops out extensively, the total thickness of this assemblage is as much as 20 km. As described before, the Banxi Group is a complicated unfossilliferous group consisting of Lower and Upper subgroups. It is overlain by the Sinian system, and then from Cambrian to Middle Triassic Systems. The widely occurring Proterozoic Banxi Group is believed to constitute the core of Yangtze craton.

The stratigraphy in the study area (Fig. 2.1) shows a jump from east to west. The Cambrian to Lower Ordovician strata occurring in the eastern region of Guizhou are the host rocks of hundreds of mercury, antimony, arsenic, gold and barite deposits. Triassic and Permian rocks generally crop out in the cores of synclines and in partly exposed reefs that were topographic highs during the Triassic. In southwest Guizhou Province, however, Permian to Lower Triassic rocks crop out extensively, and are the host strata of the Carlin-type gold and other mercury, antimony, arsenic deposits of different sizes (Guizhou Geological Bureau, 1973).

Devonian to Triassic littoral carbonate rocks were deposited on a broad cratonic platform in Guizhou Province, near the west edge of the Yangtze craton. Reef facies mark the edge of the craton, and turbidites intercalated with argillaceous rocks were deposited on the continental slope. The area was uplifted during Late Triassic time and was covered by widespread terrestrial deposits, including coal beds. The rocks were folded and faulted during the Yanshanian orogeny, 190 to 65 Ma. Gentle to moderately tight folds, sometimes associated with high-angle faults, trend generally eastward.

In summary, it is generally considered that the Proterozoic Banxi Group, composes the core of the Yangtze Craton, and the Sinian, the Lower to Upper Paleozoic and Mesozoic rocks formed the folded belt, which is principally composed by platform carbonate deposited on the craton. All the different rocks in the study area were folded and faulted in the Yanshanian Orogeny (Zhang et al., 1984, Xiong and Coney, 1985).

The eastern region of Guizhou Province is situated in the transitional zone from the core of the Yangtze craton, the Banxi Group, to the accretionary belt, strata aged from Cambrian to Triassic (Fig.2.1). The different interpretations of the tectonic setting of this area will certainly influence thinking about the formation of regionally distributed mercury, antimony, arsenic, gold and barite mineralizations. As shown earlier, the stratigraphy consists of an almost continuous sequence from Banxi Group, overlain in turn by Sinian, Cambrian, Ordovician, Silurian, Devonian, Carboniferous, Permian, to Lower Triassic rocks. No metamorphism is observed in the Cambrian to Triassic sedimentary rocks, and no magmatic activity (except in the Banxi Group) either. The collision belt and overthrust suggested by Hsü (1988) has not been observed in the eastern region of Guizhou Province (Fig.2.2 and Fig. 2.3). The evidence offered by Hsü et al. (1988, 1989) to support the overthrust model, for example, the Lantien, Loping and Xishan window, may exist locally in the eastern provinces of China such as Anhui, Zhejiang Province (Fig. 2.4), but certainly, not all the Banxi Group overlaps on the Lower Paleozoic. In the study area, for example, the Cambrian and Sinian sedimentary rocks overlie the little metamorphosed clastic rocks of the Banxi Group unconformably in the whole eastern region of Guizhou and adjoining areas of Hunan province. Obviously, from the field investigation of study area,

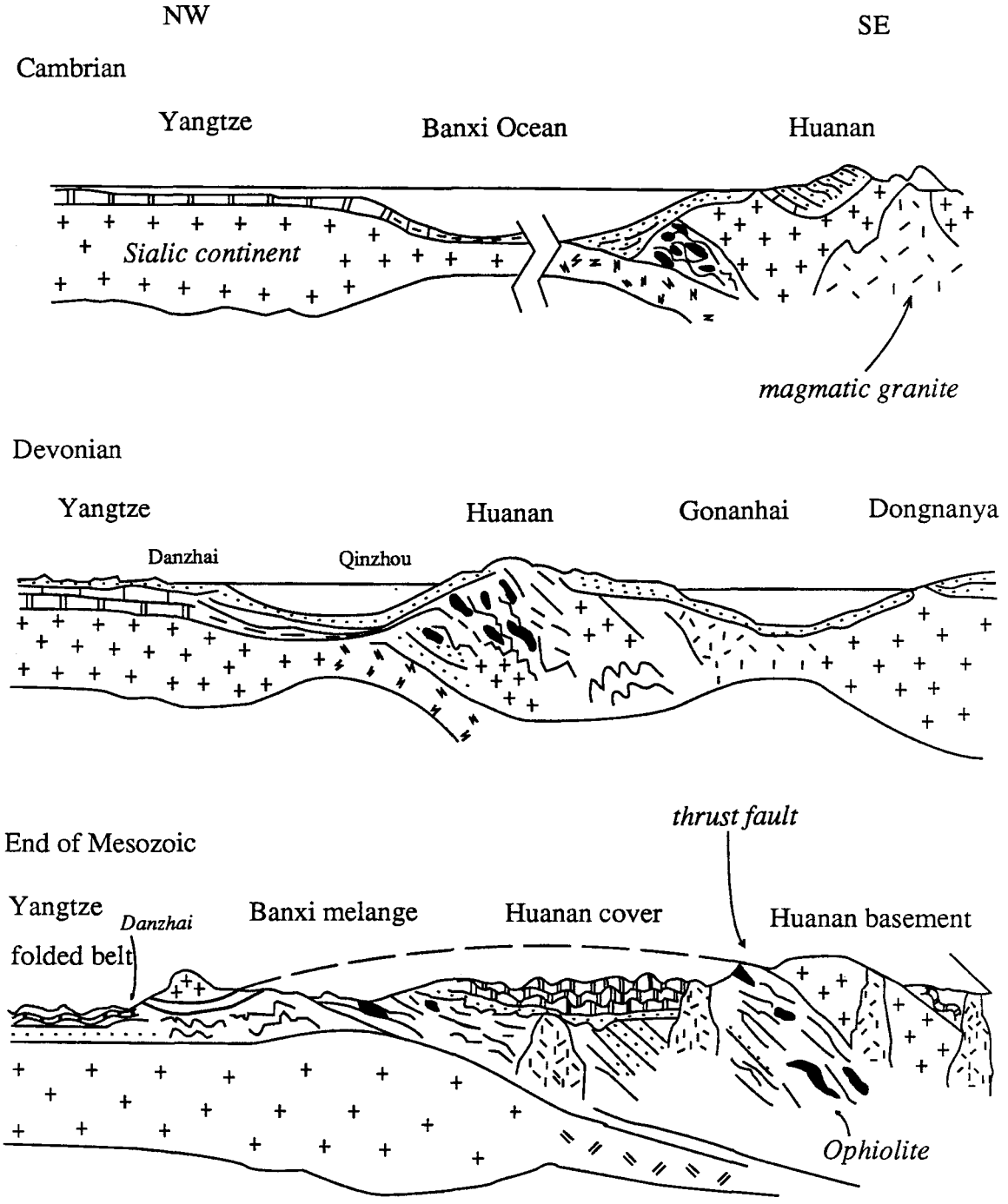

Fig. 2.2 Synthesized sections across the Fig. 2.3 from the NW to SE showing schematic tectonic evolution of South China (After Hsü et al., 1990).

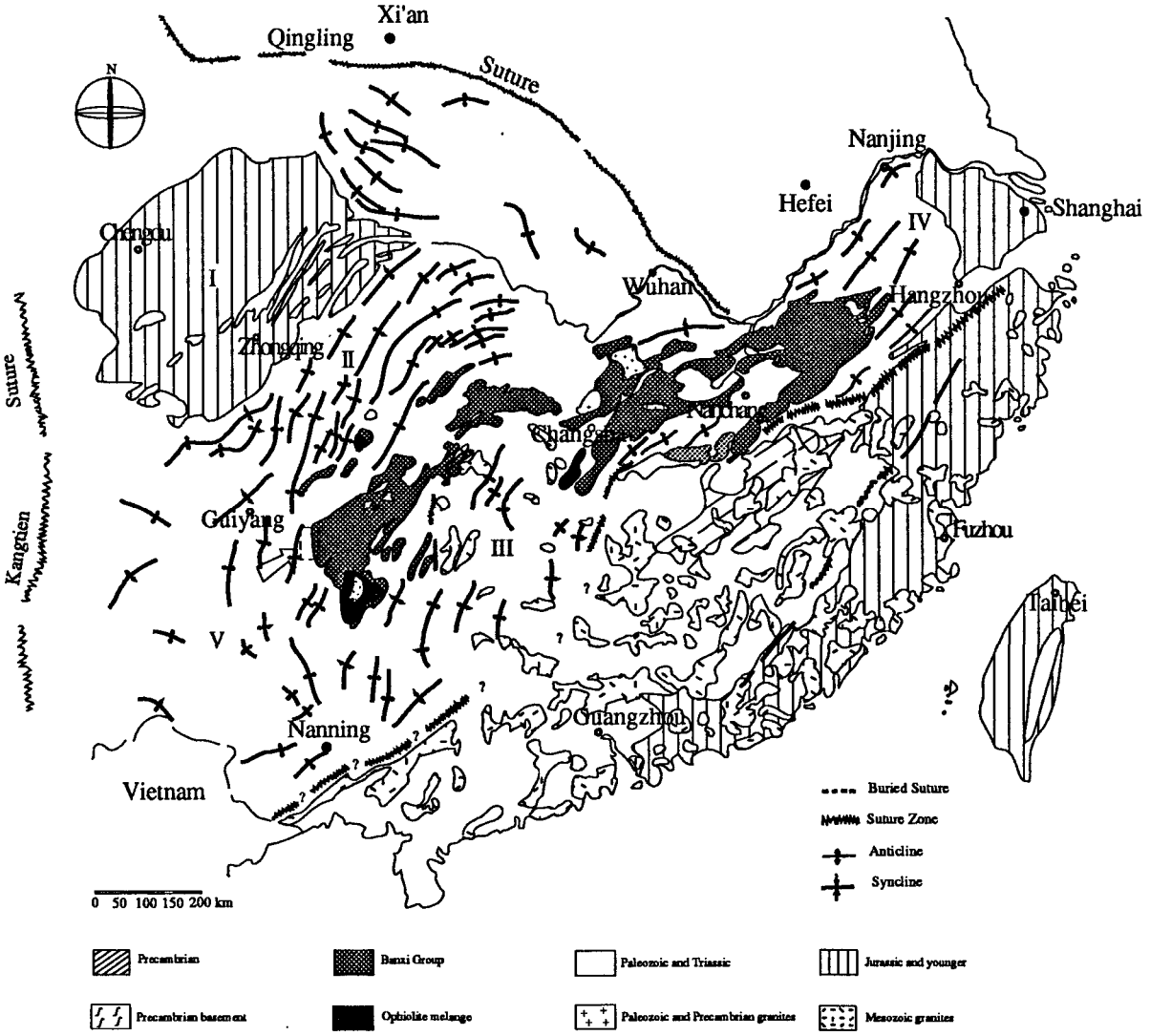

Fig. 2. 3 Tectonic setting in South China, an overthrust model proposed by Hsü et al.(1990). Tectonic units: Sichuan Basin; II and IV, Yangtze fold belt; III Hunan fold belt; V, western Guangxi deformed belt. The small rectangle near Guiyang represents the study area (After Hsü et al., 1990).

the first interpretation appears more acceptable, that is, the study area is located on a craton, not in a thrust belt.

§ 2.4. Regional Geological Structures

Several orogenies influenced the geological structures in the eastern region of Guizhou from the Proterozoic to the Triassic. The first important orogeny is the Wulin Orogeny, which divided the Upper and Lower Proterozoic. The Lower Proterozoic strata, tightly folded and metamorphosed, form the basement of the Yangtze craton. The Upper Proterozoic strata overlies the Lower Proterozoic unconformably. The Caledonian orogeny also influenced the strata before the Devonian, but the most important orogeny which determined the regional geological structures is the Yanshanian orogeny, from 190 to 65 Ma. Rocks older than Late Triassic were pervasively folded and faulted during the Yanshanian orogeny (Fig.2.4). The basement structures formed during the Wulin orogeny and Caledonian orogenies were reactivated and penetrated the cover strata during the late Yanshanian orogeny.

Three structure systems are developed in the study area, the longitudinal structure system, the latitudinal structure system and the New Huaxia structure system (Guizhou geological Bureau, 1973). These structures, formed or reactivated in the Yanshanian orogeny (190 to 65 Ma), are the most important structures controlling mineralizations in the region.

1. Longitudinal structure system: The Longitudinal structure system is dominant in the whole study area, many N-S striking anticlines and synclines are displayed, associated N-S striking faults. These structures are cut by the latitudinal structure system at both the north and the south end of Fig. 2.4. Some antimony, mercury and arsenic mineralization occur in the Longitudinal structure system.

2. Latitudinal structure system: The latitudinal structure system occurs in the southwest corner of Fig. 2.4, and is the eastern part of an E-W structure system in South Guizhou, consisting of an E-W striking anticline and a group of E-W striking faults.

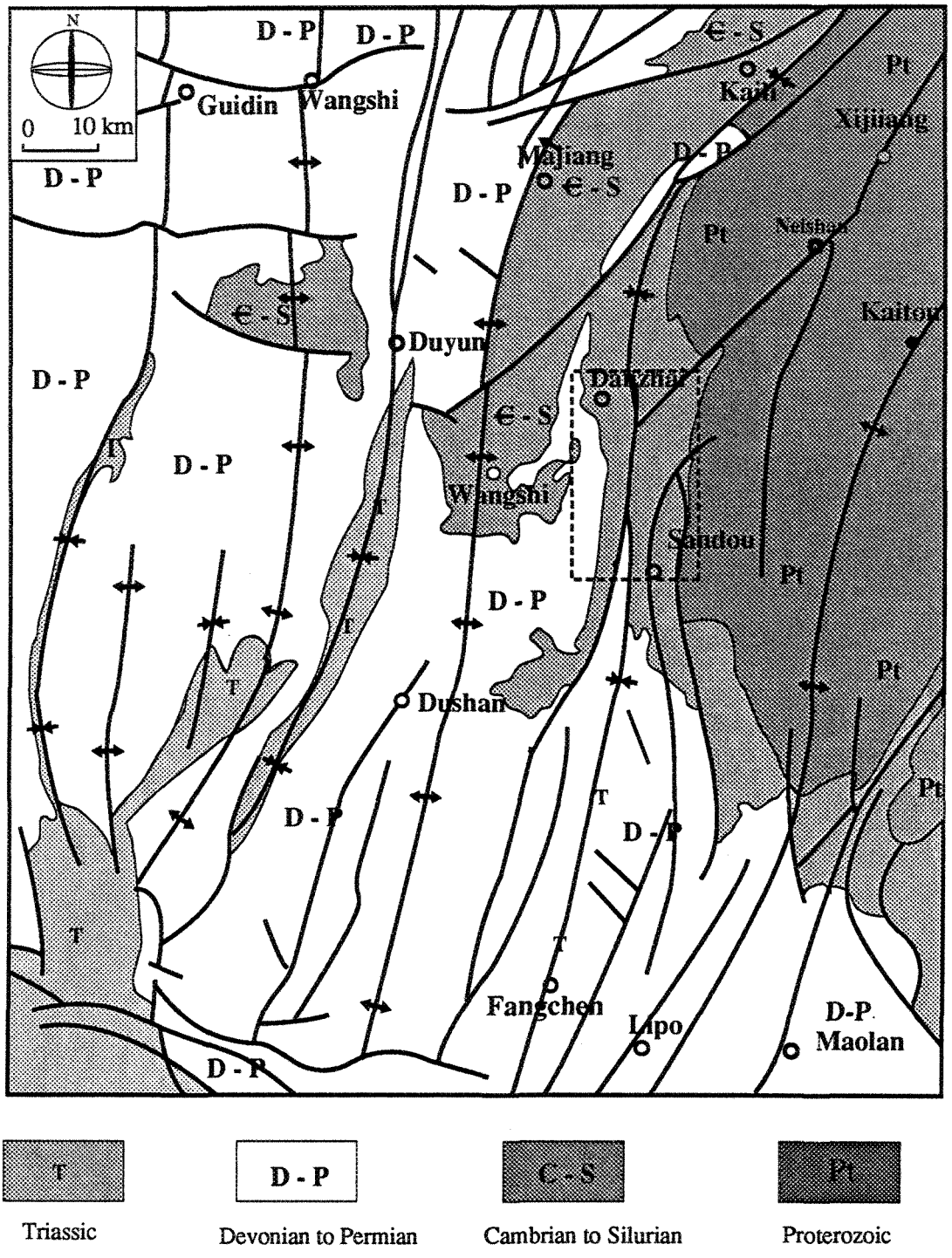

Fig. 2. 4 Geological structures in the eastern region of Guizhou Province. The rectangle represents the Sandou-Danzhai ore belt shown in Fig. 3.2.

3. New Huaxia structures system: Structures of this system are the most important structures related to mineralization in the region, and they are present in the eastern part of the area (Fig. 2.4). The New Huaxia structure system constitutes a series of folds and faults striking NNE and some shear zones with a NNW direction. In the study area, two regional first-order structures are preserved. The Neishan anticlinorium is present in the east, and Kaili-Fangchen synclinorium occurs in the west. The Neishan anticlinorium is covered by low grade metamorphic rocks of the Proterozoic Banxi Group. Some antimony, mercury, and gold mineralization is distributed in faults in the Neishan anticlinorium. The Kaili-Fangchen synclinorium is composed of different orders of NNE-striking folds, NNW-striking as well as NW-striking faults. It has an "S" form and is divided into three parts, called the north, middle and south part.

The north part of the area, from Kaili to Danzhai, at the head of the "S" is an arc 44 km in length, and 8 to 12 km in width. The axis of the synclinorium changes from NE to NNE from Kaili to Danzhai. The north part of the synclinorium is cut by a NE striking fault in Nangao. Some large barite deposits and some medium and small sized antimony and mercury deposits are hosted by the faults and second order folds in the Kaili to Danzhai part of the Kaili-Fangchen synclinorium.

The middle part is situated in the waist of the "S" from Danzhai to Sandou region. It has a length of 35 km, and width of 5-8 km. It is covered by the Cambrian and Ordovician strata, and some Sinian and Proterozoic Banxi Group rocks in the west as well. An important fault (F_1) cuts the synclinorium in the Sandou-Danzhai area. Second order faults are well developed, and most of them strike N-S or NNE in the area. Many different sized mercury, gold, arsenic, antimony deposits are associated with these faults, which comprise the so-called Sandou-Danzhai ore belt.

The south part is the tail of the "S", which extends from Sandou to Fangchen. It is about 100 km long and about 30 km wide. The Kaili-Fangchen synclinorium is divided into several second order folds, and some of these second order folds are cut by the Sandou-Lipo

fault. In contrast to the north and middle parts, the rocks in the south part are much younger, composed of Upper Paleozoic and even Mesozoic strata.

§ 2.5. Summary

The stratigraphy in the eastern region of Guizhou Province is almost continuous from Proterozoic to Middle-Lower Triassic, and is primarily composed of low grade metamorphosed Proterozoic clastic rocks mainly outcrop in the east.part; Upper Paleozoic carbonate and flysch; Lower Paleozoic carbonates, occasionally intercalated by shale.

The recognition of the tectonic setting in the region are still contentious. The well accepted concept is that south China, particularly the area studied is situated on the Yangtze Craton, but this interpretation is recently questioned by Hsü et al.(1987,1988, 1989, 1990), and a thrust model is proposed instead. The different recognitions of tectonic setting in south China results from the different interpretation of the Banxi Group. Hsü et al.(1988,1989) assumed that the Banxi Group accumulated in an ocean (called the Banxi Ocean) bounded by two separate continents, called the Yangtze and the Huanan (South China) during pre-Mesozoic time. The ocean was closed in the late Triassic and the Huanan terrane was overthrust onto the Yangtze continent. But in the region studied, the Banxi Group clearly underlies the Cambrian and Sinian sedimentary rocks, so it belongs to Proterozoic as traditionally believed. Therefore, at least in the eastern region of Guizhou, the orthodox interpretation is more reasonable than the overthrust model.

The area studied is located in the middle part of the Kaili-Fanchen synclinorium, which is composed of different order NNE-striking folds, NNW and NW-striking faults. The regionally important fault F_1 cuts the synclinorium in the Sandou-Danzhai area. Second order faults related to F_1 are well developed, and most of them strike to N-S or NNE. A variety of different sized mercury, gold, arsenic, antimony deposits are associated with these faults, which comprises the so-called Sandou-Danzhai ore belt.

CHAPTER III:

GEOLOGICAL CHARACTERISTICS OF THE DANZHAI GOLD-MERCURY DEPOSIT

§ 3.1. Introduction

The Danzhai gold-mercury deposit, the focus of this study, is situated in the mountainous eastern region of Guizhou province, a well known area for mercury production. Hundreds of different sized mercury, antimony, arsenic and barite deposits are present in this region and the adjoining area of Hunan province. In the Sandou-Danzhai ore belt, for example, several tens of mercury, antimony, arsenic and barite deposits are associated. The Danzhai mercury deposit is the biggest one among them. The gold, mercury, antimony, arsenic, and barite mineralizations are spatially associated not only in the same ore field or ore belt, but within the same deposit as well. It is noteworthy that almost all of the newly-found sedimentary rock-hosted, disseminated gold deposit are associated with mercury, antimony or arsenic mineralization in P. R. China. Previously, they were identified as different sized mercury, antimony or arsenic deposits. For example, the Yata gold deposit, reported by Cunningham et al.(1988) in western literature, was mined orginally as a small antimony deposit.

Danzhai was known to be of the biggest mercury deposits in P. R. China, and has been explored and mined as a mercury deposit for more than thirty years. Systematic regional geological investigation and mapping of the Danzhai mercury mine area commenced in the early 1950's, and a geological report and a series of geological maps were presented by the No.4 Geological Team of Guizhou (1964).

Comparison of the geological characteristics of the Danzhai mercury deposit with those of the Carlin-type gold deposits in the west U.S.A, demonstrates a strong resemblance between them. Re-evaluation and re-prospecting of the mercury mine as a gold prospect was undertaken and proved this assumption to be true, the Danzhai mercury deposit was actually associated with gold mineralization. Detailed geological surveys and exploration reveal that the gold mineralization is also of independent economic importance. Several exploitable gold orebodies and a large volume of wall rocks, untouched during the mercury production, have been proven to contain extensive gold mineralization grading from 3 to 9 ppm. Exploration for gold is still going on, the gold reserves are not yet established.

§ 3.2. Host Sedimentary Rocks In The Sandou-Danzhai Ore Belt

The host rocks for the Danzhai gold-mercury deposit as well as many other mercury, antimony, arsenic and gold deposits in the Sandou-Danzhai ore belt belong to the Early Ordovician and Late Cambrian (Fig. 3.1). They are dominated by carbonates, occasionally intercalated with shales. The stratigraphic column shown in Fig. 3.1 indicates the specific host strata of different mercury, antimony and gold deposits in the Sandou-Danzhai ore belt.

The formations hosting the mineralization in the Sandou-Danzhai ore belt include the Guotang Formation, Lower Ordovician (O_{1g}); Sandou Formation, Upper Cambrian(C3s), the Yangjiawan Formation, Upper Cambrian(C3y) and the Dafadong Formation, Middle Cambrian (C2df), which are characterized by carbonates with a variety of structures such as massive carbonate, laminated carbonate, banded carbonate, lenticular carbonate, as well as brecciated carbonate. The following is a brief description of these four Formations:

§ 3.2.1. Dafatong Formation (C_2df), Middle Cambrian

This formation, mainly distributed in the north part of the Sandou-Danzhai ore belt (Fig.3.2), is dominated by gray colored laminated and banded limestone, occasionally intercalated with massive brecciated dolomite. It is the host strata of the Xiawuni mercury deposit. Thin section examination shows that these carbonates consists principally of fine to medium grained calcite and dolomite, with a high percentage of clay minerals in this

Fig. 3.1 Composite Stratigraphic column of the Sandou-Danzhai ore belt

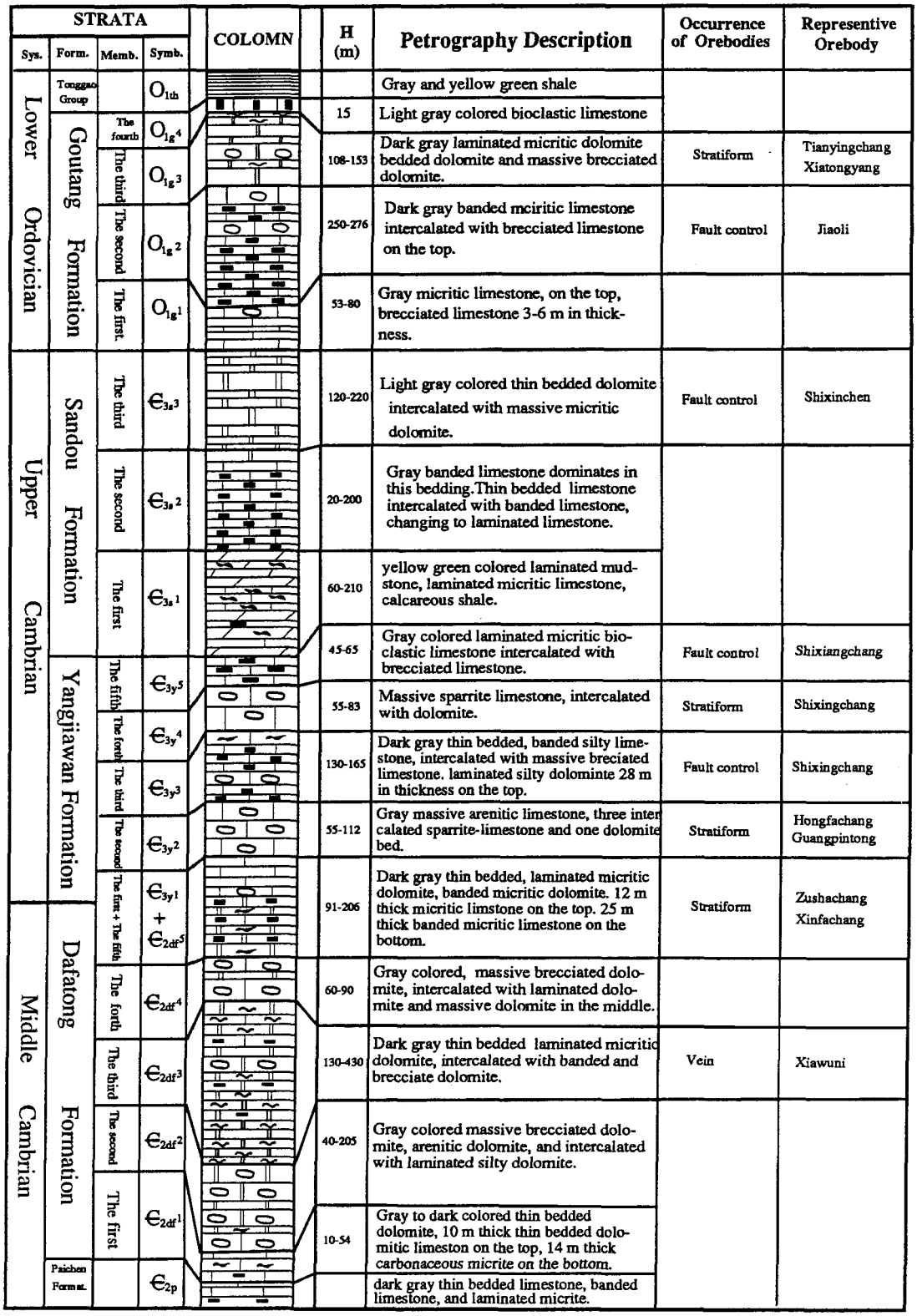

laminated and banded limestone. Organic matter is also ubiquitous, and bitumen, in particular, is present. Organic carbon in this formation is as high as 0.39% (Chen et al., 1986).

§ 3.2.2. Yangjiawan Formation (C_3y), Upper Cambrian

The orebodies of the Danzhai gold-mercury deposit occur in the Upper Cambrian Yangjiawan Formation(C3y), as are many other deposits such as Shixiangchang, Hongfachang as well as Guangpintong gold-mercury deposits in the ore belt. This Formation is distinguished by dark gray banded and laminated micrite intercalated with several layers of massive brecciated limestone. The thickness of the massive brecciated limestone varies widely and ranges from less than one meter to more than thirty meters locally. Some of this massive brecciated limestone occurs in lenses whose thickness changes sharply with localities. Big blocks of limestone twenty to fifty centimeters in diameter are occasionally observed within the banded and/or laminated limestone. Petrographic observation of these rocks indicates that the unaltered host rocks consist of 55-85 percent micritic calcite and clay, 15 – 40 percent dolomite spar and microspar as well as 1–3 percent medium-grained pyrite. The pyrite occurs as euhedral crystals ranging from 30-150 μm in size, and is commonly aligned in fine layers parallel to the bedding. Fresh rock quite often contains specks, films, and coatings of carbonaceous materials. Bitumen commonly fills the pores of calcite or dolomite, or concentrated in veinlets and stylolites in the carbonate rocks. Chemical analysis reveals that most samples of fresh unaltered rock from numerous localities contained abundant organic carbon, ranging from 0.48 to 0.87 % by weight in the third member of this formation (C_3y^3) (Chen et al., 1986), much higher than the average organic carbon content of carbonates.

§ 3.2.3. Sandou Formation (C_3s), Upper Cambrian

The Sandou Formation is distributed over all the Sandou-Danzhai ore belt and hosts the Shixinchin mercury deposit. The rocks in this formation are characterized by dark gray colored thin bedded to banded limestone, intercalated with several layers of shale. Microscope examination indicates that these rocks consist of 50 to 60 percent medium-grained calcite, 20 to 25 percent dolomite, 10 to 15 percent clay minerals (probably illite). In

many localities, these limestones have a shaly character and show a distinct light-gray to tan color on fracture surfaces and bedding planes. This weathered appearance is due to oxidation of pyrite and carbonaceous materials, the removal of carbonates and local formation of iron oxides.

§ 3.2.4. Guotang Formation (O_{1g}), Lower Ordovician

The Lower Ordovician Guotang Formation (O_{1g}), is mainly present in the southern part of the Sandou-Danzhai ore belt(Fig. 3.2), several mercury and gold deposits such as Tianyinchang gold-mercury deposit and Xiatongyang gold-mercury deposit are located in this formation. The fresh unaltered rocks of this formation are mainly composed of dark gray, laminated micritic dolomite, massive dolomite as well as massive brecciated dolomite. Mineralogically these rocks contain 60 to 75 percent dolomite, 10 to 20 percent calcite. Other constituents are fine-grained quartz and clay minerals. Carbonaceous materials are seen in thin sections, particularly dispersed bitumen is a significant minor component of the host rocks.

Sedimentary petrofacies analysis show that the sedimentary depositional environment of these carbonates was the margin of a sedimentary basin, which is evidenced by the carbonate debris flows, grain flows as well as huge fallen carbonate blocks from the adjoining carbonate platform. It is also confirmed by the curly bedding and slumping bedding in banded and laminated limestone as well as carbonate breccia. The fossils found in these rocks are trilobite, graptolite, and crinoidea. It is accordingly believed that distribution of Sandou-Danzhai ore belt was spatially coincident with a sedimentary basin margin near a platform slope.

Even though there are some distinctions between different formations of the host strata in the Sandou-Danzhai ore belt, the lithology is always dominated by limestone and dolomite with different structures. It is quite similar to the host rocks of the Carlin gold deposit in the west of U.S.A.(Radtke and Scheiner, 1970; Radtke et al., 1980). Similarly, the four formations of the host strata are also rich in carbonaceous material and diagenetic pyrite. Cinnabar is observed in the fresh unaltered carbonates as a minor constituent as well,

Fig. 3.2 Geological Map of the Sandou-Danzhai ore belt (After No. 4 Geological team, 1964).

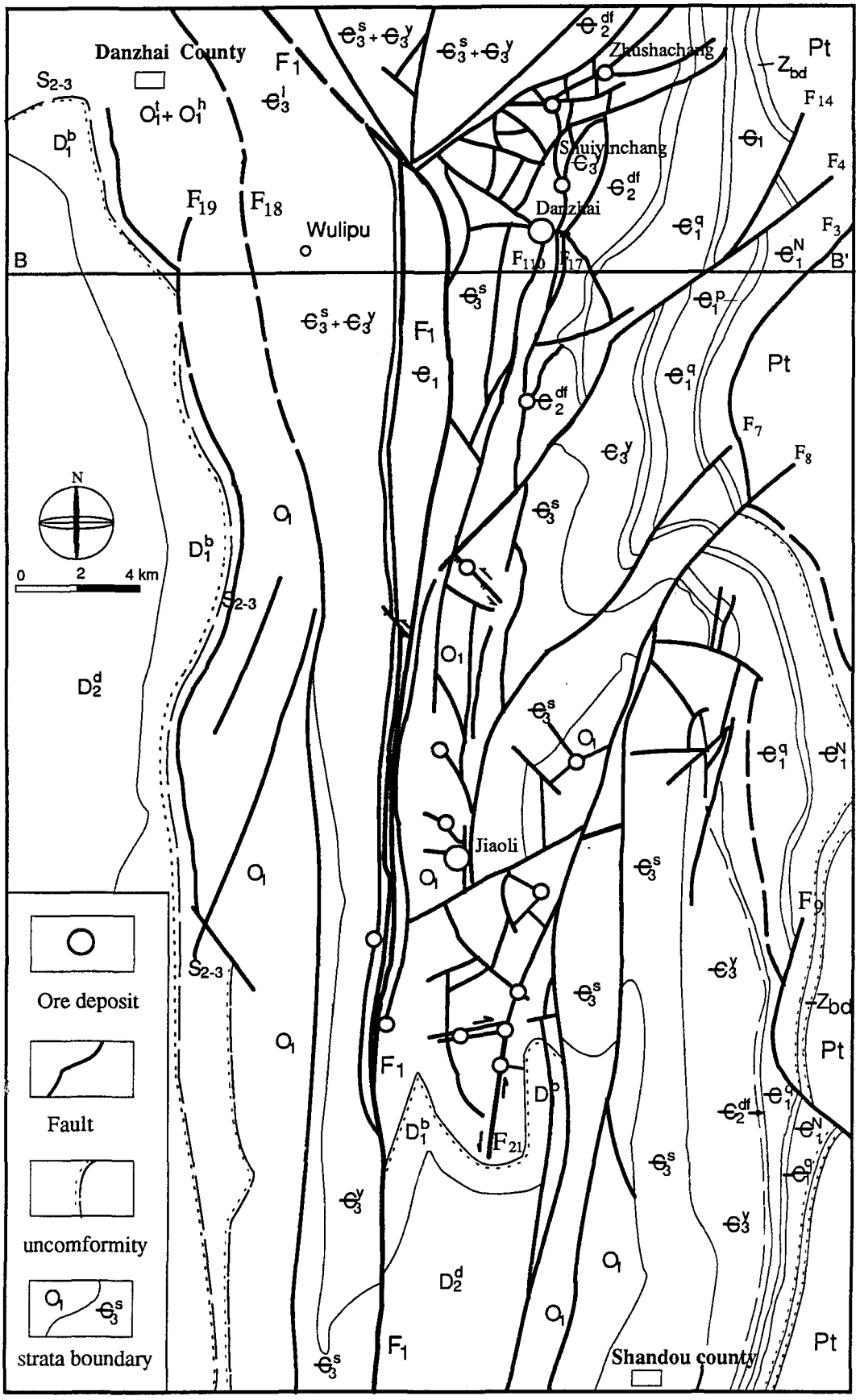

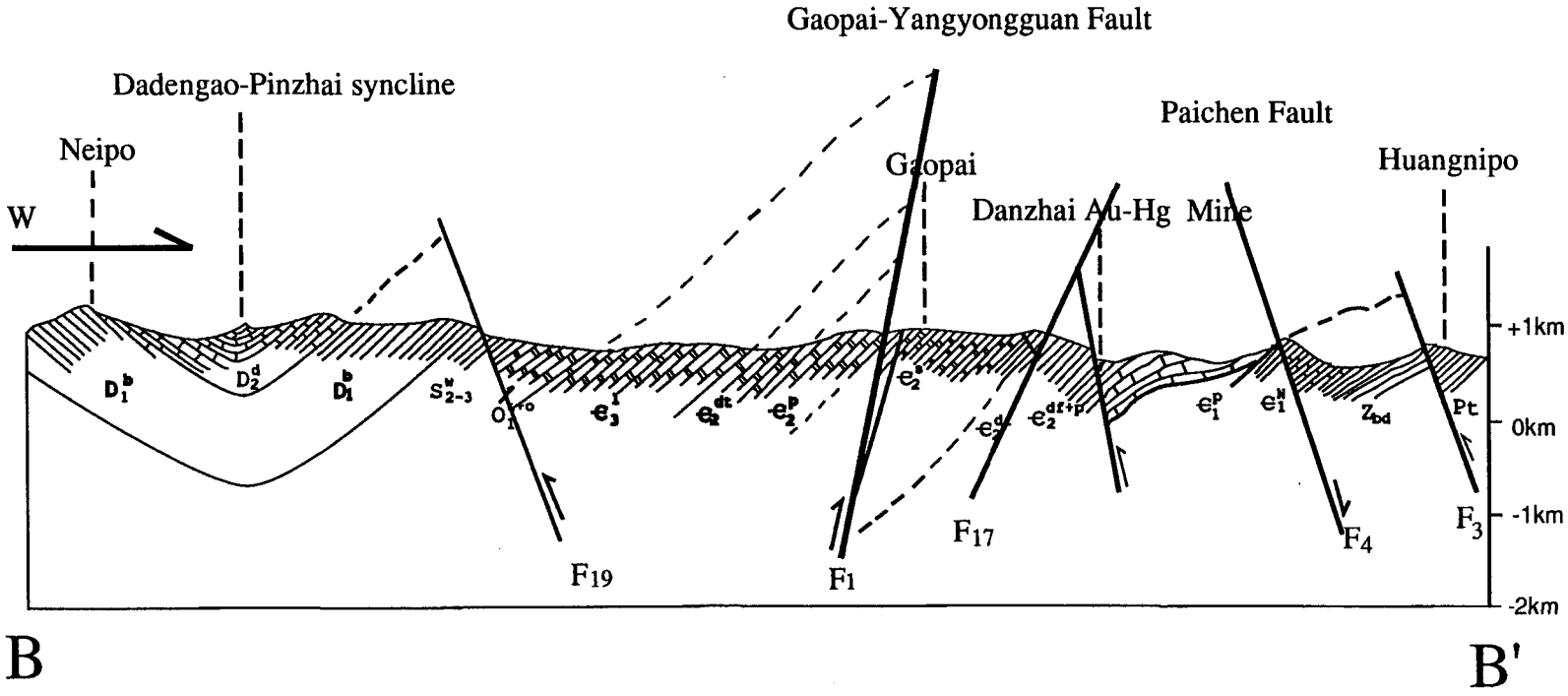

Fig. 3.3 Regional Cross Section in the Danzhai Gold Mercury Deposit (Location and legend are indicated in Fig. 3.2) (modified after No. 4 geological team, Guizhou Bureau of Geology).

which is considered evidence that these Cambrian or Ordovician strata were the source strata of regional mercury mineralization (Hua, 1982).

§ 3.3. Structural Controls of Gold And Mercury Mineralization

Many different sized mercury, antimony, arsenic, gold as well as barite deposits or prospects occur in faults. The relationship between these deposits and the different size structures is discussed by their order of size.

§ 3.3.1. Regional Structures

As described in an earlier chapter, the study area is situated in Kaili-Fangchen synclinorium which has a length of 145 km, and a width of 5-12 km. The Sandou-Danzhai ore belt is located in the middle part of Kaili-Fangchen synclinorium. This part is 35 km long and 5-12 km wide as shown in Fig. 3.2.

§ 3.3.2. Structural controle of the Sandou-Danzhai Ore Belt

The Sandou-Danzhai ore belt occurs on the east flank of the Zhushachang-Deimenzhai syncline (Fig. 3.2, Fig. 3.3), a second order fold in the regional Kaili-Fangchen synclinorium. The Zhushachang-Deimenzhai syncline is an open fold, with low dip angle. It is composed of Devonian and Silurian strata in the core and Ordovician and Cambrian strata on its east flank. It curves and changes direction from NE to NNE in Gaopai, and its axis plunges to the SSW.

The southeast limb of the Zhushanchang-Deimenzhai syncline is cut off by fault F_1 as well as by many other second order faults near F_1. F_1 is a fault of regional importance and can be seen in Fig. 2.1 and Fig.2.4. It is a N-S-oriented, west dipping reverse fault, and the most extensive fault in Sandou-Danzhai ore belt. It is only about 30 km long in the Sandou-Danzhai ore belt and cuts the Cambrian and Ordovician strata at surface, but in total, it is 80 km long and cuts through all the strata from the Devonian, through the Carboniferous, the Permian as well as the Lower Triassic to the south of the Sandou-

Danzhai ore belt (Fig. 2.1 and Fig. 2.4). Obviously, F_1 is a fault either formed, or at least reactivated in the Yanshanian Orogeny.

Second order faults are well developed on the east flank of the Zhushachang-Deimenzhai anticline. These lower order faults are divided into two blocks by the regional fault F_1 : the west upper block of F_1 only few N-S oriented second order faults occur, such as F_{18}, F_{19} are paralell to F_1 but their dip direction contrary to F_1 (Fig. 3.2; Fig.3.3). In the east block (lower block), however, several groups of faults are present. As shown in Fig. 3.2, the second order faults in the east blocks are densely concentrated near F_1, but none of them cut through F_1. Only a few NE-oriented faults such as F_4, F_3, F_7 and F_8 extend to the eastern margin of the area (Fig. 3.2), far from F_1. These spatial relationships suggest that the second order faults are related to the regional fault F_1.

Second order faults in the east block of F_1 can be classified into three groups by their orientation, a NNE, a NE and a NW group. The first two groups of faults are relatively big faults at the local scale, and are several kilometers in length. The NNE-oriented faults are commonly cut off by NNE-oriented faults, for example, F_4 a NE-oriented fault is cut off by F_{17} and F_{110}, which are NNE-oriented faults. The NW-oriented faults, however, are usually of small scale, several hundreds meters or one kilometer in length, and are generally limited or terminated by the other two fault groups.

At the south end of the Sandou-Danzhai ore belt, Lower Devonian strata overlie the Lower Ordovician strata unconformably, which provides an opportunity to observe the temporal sequences between the second order faults, regional fault F_1 as well as the strata. Fig. 3.2 illustrates that all of the three groups of second order faults are not present in the Devonian rocks even though F_1 is. This spatial relationship suggests that these second order faults were formed before the Devonian, as was the regional fault F_1 since these second order faults were evidently related to it. Accordingly, it is concluded that F_1 was produced in the Caledonian Orogeny but reactivated in theYanshanian Orogeny since it cuts the strata from Devonian, Carboniferous, Permian to Lower Triassic as indicated earlier, but the second order faults do not cut strata later than Devonian.

The gold and mercury mineralization are controlled by the regional fault F_1 and related to second order faults. Their relationship is discussed as follows: Firstly, all the deposits in the ore belt are located east of the regional fault F_1, and no mercury, gold or any other mineralization has been documented to the west of F_1. Secondly, mercury and gold mineralization is observed in brecciated fragments within this fault, implying that F_1 was also mineralized. Thirdly, the ore deposits tend to be present in the second order faults near F_1 rather than far from F_1, for instance, in a given fault, the portion near F_1 is usually highly altered and mineralized whereas the portion far from F_1 is less altered or unaltered and not mineralized. Fourthly, the deposits are usually present at the intersection between the NNE-oriented group and the NE-oriented group of second order faults near F_1. Lastly, no mineralization has been reported in the Devonian strata to the south end of the Sandou Danzhai ore belt because no second order faults associated with F_1 occur there. Therefore, the mercury and gold mineralization in the Sandou-Danzhai ore belt tends to be concentrated in the second order faults near the regional fault F_1. This evidence suggests that regional fault F_1 probably served as conduit for the ore-forming fluid, and the second order faults provided the locations for the deposition of ore-forming elements. The mineralization probably took place before the Devonian.

§3.3.3. Structural Control of The Danzhai Gold-Mercury Orebodies

In the Danzhai Gold-Mercury deposit, there are two major groups of faults with the same direction but with different characteristics, one of which consists of reverse faults, and the other of normal faults. In addition, bedding plane faults are usually present in the mine area. These three groups of faults are usually several hundreds of meters or 1 to 3 kilometers long. With the exception of fault F_{110}, they are not shown on Fig. 3.2 since they are too small. The relationship between these faults and the distribution of orebodies is described as follows:

1. The NNE reverse faults, including F_{110}, F_{246}, F_{240}, F_{241}, are characterized by breccia, schistose structural lenses and mylonitized rocks, all of which are silicified, carbonatized as well as mineralized. For example, the main mercury orebody in Danzhai occurs in F_{110}.

1) F_{110}: it comprises several second order faults, ranging from the Shuiyinchang-Yangwuhe by the Danzhai Gold-Mercury mine, to meet with F4, which is seen in Fig. 3.2. It is 5 km long, 2-4 meters wide, striking NE, dipping to the SE, with a vertical throw of 25 to 50 meters. Several subzones are recognized: the schistose subzone, the schistose and brecciated subzone, and the mylonite subzone, The reverse fault was extensively carbonatized, locally silicified as well as mineralized with mercury. It is the most important mineralization-controlling reverse fault for mercury mineralization.

2). F_{246}: it is located in the western lower block of F110, and meets F_{110} in the north. It is about 1 km long, striking 20-50°, dipping to the SE, with a dip angle of 45-75°. The reverse fault is 1 to 2 m wide and consists of several subzones similar to that of F_{110}. Silicification and carbonatization are present in the subzones, and both gold and mercury mineralization are important.

3) F_{240}: it is situated in the western end of the deposit, dips to the east, at an angle of 70°. It is about 400 m long, and local mineralization occurs in this small reverse fault.

4) F_{241}: it is located in the western end of the deposit, curves in an arc, strikes to the NNE and dips 68° to the SEE. and is 3 meters wide. The limestone and mudstone in the reverse fault are brecciated, silicified, carbonatized, and contain gold and mercury mineralization represented by cinnabar, arsenopyrite and pyrite.

2. Normal faults with a NNE direction: These comprise mainly F_{243}, F_{244}, F_{245}, F_{247}, which are distributed in the middle part of the deposit, as shown in Fig. 3.4 .

1) F_{243}: it dips 45-66° to SE, shows a wavelike variation along its strike. Its vertical shift ranges from 1 to 2 meters, its width ranges from 1 to 3 meters. The brecciated rocks are silicified, pyritized, and contain Au, Hg mineralization as well. The No.2 gold orebody is hosted by this fault .

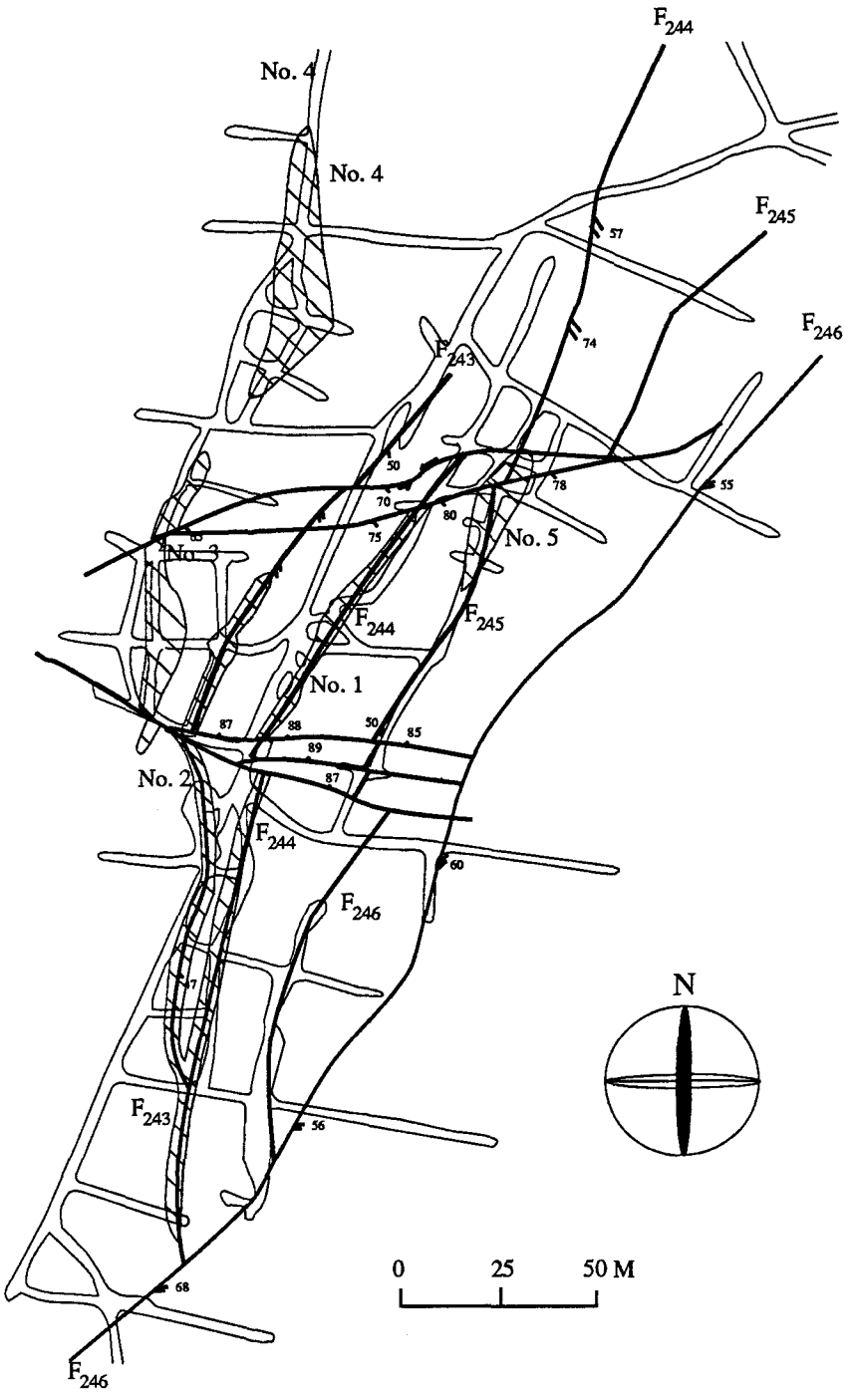

Fig. 3.4 Geological map of 405 Level, Danzhai mine showing faults and ore zones (the host rocks in this Level belong to the Upper Cambrian Yangjiawan Formation).

2) F_{244}: it dips 35-60° to SEE, and is 400 meters long. Its vertical shift ranges from 1 to 3 meters. The brecciated rocks in the fault were silicified, pyritized, and also contain Au, Hg mineralization. This fault is the host fault to the No.1 gold orebody (Fig. 3.4).

3) F_{245}: it is parallel to F_{244} and similar to F_{244} in many ways. It strikes 020°-030°, and dips 35-55° to the SE. It is 400 meters long, and its vertical shift ranges from 1 to 3 meters. The brecciated rocks in the fault were silicified, pyritized, and also contain Au, Hg mineralization. It is the ore controlling fault of the No.5 orebody .

4) F_{247}: it is located on the east upper block of F_{246}, dips 65° to SE. it ranges from 1 to 2 meters in width, and up to 1 km in length. Its vertical shift is about 3-7 meters.

3. Bedding-plane faults: These are commonly observed in the brecciated limestone and thin bedded laminated and/or banded limestone, particularly in the fourth member of the Yangjiawan Group. The bedding planes are usually concentrated with carbonaceous materials with bright color, locally filled with stibnite and cinnabar. The intense reverse fault movement on the bedding-plane fault is a favorable structure for gold and mercury mineralization. For instance, both the No.3 and No. 4 gold orebodies are present in a bedding-plane fault.

In summary, gold and mercury mineralization of the Danzhai Gold-Mercury orebodies are controlled by faults of different orders.

§ 3.4. Mineralizations and Alterations

The major alterations associated with the gold and mercury orebodies are silicification and carbonatization. Both the alteration and mineralization are distributed principally along reverse faults, normal faults as well as bedding plane faults. They become generally more intense within fault breccias, gradually dying out in the undeformed country rocks. The alterations are accompanied by corresponding veins and/or veinlets and associated with distinct extensive gold or mercury mineralization. For example, even in the last stage of quartz and calcite veining, usually considered devoid of mineralization, when examined

under the microscope contains disseminated gold-bearing arsenopyrite and pyrite although it is not an important gold mineralization.

The fractures, such as reverse or normal faults, influence the pattern of mineralization and alteration. In the normal faults, huge calcite veins which range from 1 to 4 meters are developed, and mercury and antimony as well as gold mineralization are concentrated in the veins and silicified breccias. In the reverse faults, however, the silicification and gold-mercury mineralization is also highly developed, and the quartz and carbonate veins system is replaced by veinlets of quartz, calcite and dolomite. Several stages of mineralization have been established from their crosscuting relationships and mineral assemblage and are described in the following section.

§ 3.4.1. The First Mineralization Stage

The first stage of mineralization is characterized by gold mineralization with no mercury mineralization. Two distinct type of gold mineralization are classified in the first mineralization stage:

The first type of gold mineralization is composed of banded ore, which has no obvious differences in appearance from the banded carbonate (Plate 1A). The banded carbonates consist of alternating bands, one composed of micritic carbonate and some clay minerals, appears black in color, and the other composed of fine-grained calcite or dolomite spar, appears clear and light grey in color. The gold-bearing arsenopyrite and pyrite are highly concentrated in the light grey colored, fine-grained carbonate band, particularly at the base of the white band. In the black carbonate band, however, arsenopyrite or pyrite is rarely observed (Plate 1B and Plate 1C). As a rule, the rectangle-shaped (along c axis) or rhombic shaped (across the c axis) grains of arsenopyrite, 0.1 to 0.5 mm in length, are disseminated in the fine-grained calcite. No crosscutting relationship has been observed between the the arsenopyrite, pyrite and calcite under the microscope. This banded ore has been cut by subsequent carbonate vein systems. Several important characteristics are noteworthy: (1) some of its is associated with silicification which produced calcedony while other is not associated with any alteration. (2). carbonaceous material is not rich in the

banded ore, which is distinct from other types or stages of mineralization; (3) No mercury minerals such as cinnabar are observed; (4) chemical analysis indicates the gold abundance is high, ranging from 30 to 150 g/t in the banded ore.

The second type of gold mineralization is characterized by silicified host rocks, especially silicified carbonate rocks. As in the first type of gold mineralization, arsenopyrite and pyrite occur as rectangle-shaped (along c axis) or rhombic shaped (across the c axis) crystals, about 0.1 to 0.5 mm in length, and are disseminated in fine-grained quartz or chalcedony. Cinnabar is not associated with the ore similar to the first type. Two important features distinguish it from the first type, one is the association of carbonaceous materials (Plate 1D), and the other is the association with silicification. The first stage of silicification is composed of fine-grained quartz or chalcedony. Chalcedony is microcrystalline and/or cryptocrystalline, the grain size is generally between 0.005 – 0.01 mm. Generally speaking, the first stage silicification is pervasively distributed along faults, with no evident associated quartz veins.

The common characteristics of first and second type of gold mineralization are the similar size and shape of arsenopyrite and pyrite, and the absence of mercury mineralization. The temporal relationship between the first and the second type of gold ore in the first mineralization stage is not clear, but it is certain that both of them were cut by the subsequent calcite and quartz veins.

§ 3.4.2. The Second Mineralization Stage

The second stage of mineralization is important for both mercury and gold mineralization. It formed the principal carbonate vein systems and was mined for mercury production. It is also characterized by two types of ore which are as follows:

The first type of ore is the carbonate veins, with associated cinnabar, stibnite, pyrite and arsenopyrite. The carbonate veins are as wide as 1 to 4 meters, generally filling the normal faults, but not present in the reverse faults. For example, big coarse-grained carbonate veins are present with mercury and gold mineralization in the No. 5, No. 3 and No.4 orebodies. Silicified breccia sof various sizes are commonly observed in or near the

carbonate veins which are intensely mineralized with gold and considered to belong to the first mineralization stage (Plate 2A). Under the microscope, the carbonate veins consist of both calcite and dolomite, and are usually 10 to 50 mm in size. Cinnabar occurs as subhedral crystals which range from 0.1 to 30 mm in size, disseminated in the veins. Stibnite is characterized by its acicular or columnar shape, and also occurs as big crystals. Arsenopyrite and pyrite are present as fine grains and are disseminated in the borders of the crystals of calcite or dolomite or in fissures in the carbonate veins. Quartz is occasionally seen as a minor component occurring with anhedral and /or hypidiomorphic texture, with a grain size between 0.05 – 0.1 mm. It is interesting to note that the white colored calcite veins are spotted by black sparkles. The second type of ore is formed of the carbonate veins associated with cinnabar, realgar, orpiment, stibnite and carbonaceous materials (Plate 2B). These carbonate veins are small and tens of centimeters wide. Cinnabar is similar to the first type, but the arsenopyrite and pyrite are not seen in this assemblage. Instead of arsenopyrite, other arsenic-bearing minerals such as realgar and orpiment are present. Realgar and orpiment always occur together as coarse crystals.

These two types of ore are distributed in different levels of the mine. The the first type of mercury gold mineralization is usually present in the deep levels in the deposit such as the 405 level, and the 280 level whereas the second type of mercury gold mineralization occurs near the surface, for example, the 690 level.

§ 3.4.3. Third Mineralization Stage

The third mineralization stage is composed of barite veinlet systems as well as associated host carbonate rocks with different intensity of silicification (Plate 2C).

The barite veinlets are well developed in these carbonate host rocks. Besides the barite, cinnabar and quartz are also present in the veinlets, and arsenopyrite and pyrite are sparsely disseminated in the barite. These veinlets are several centimeters wide and develop in several groups with different orientations. These veinlets are highly developed in reverse faults, and appears to have cemented the brecciated host rocks. The host rocks are usually less intensely silicified or even unsilicified carbonates in which arsenopyrite and pyrite are disseminated, occasionally stibnite is seen in unaltered carbonates. Carbonaceous materials

are usually concentrated in the host rocks as well as in the veinlets. In a word, the third mineralization stage is characterized by mercury mineralization in barite veinlets and gold mineralization in the host carbonate rocks.

§ 3.4.4. Last Stage of Quartz and Carbonate Veins

Last stage quartz and carbonate veins also have associated arsenopyrite and pyrite, but not associated with cinnabar and stibnite. Arsenopyrite and pyrite are so sparsely disseminated in the veins that they are of no importance for gold mineralization.

The quartz veins range from 10 to 100 centimeters thick, and consists of euhedral coarse quartz, sometimes containing quartz vugs. The wall rocks of the last stage of quartz vein are generally less silicified or unsilicified. The carbonate veins are as wide as 50 to 120 centimeters, composed of euhedral coarse calcite or dolomite. The carbonate veins are also spotted with black sparkles and occasionally contain visible bitumen (Plate 2D).

The major minerals occurring in the Danzhai gold-mercury deposit are listed in Table 3.1 and Table 3.2 according to their temporal sequence.

§ 3. 5. Occurrence of Gold

The occurrence of gold is critical to define a Carlin-type gold deposit. It is mysterious since native gold or gold minerals are not commonly observed under different microscopic magnification or even under the scanning electron microscope. That is why the Carlin-type gold deposit is called an invisible gold deposit. Considerable investigation has been undertaken in order to find the exact occurrence of gold in the Carlin-type gold deposits in the U.S.A.

As early as 1951, Joralemon (1951) observed gold at Getchell, Nevada associated with pyrite, marcasite, quartz, and realgar. He recognized both native gold and electrum, and reported laboratory tests that indicate that most of the gold occurs as inclusions in pyrite. The more porous grains are the best hosts, with the gold occurring near grain margins and

Table 3.1 Relative abundance of minerals in the different stages of the Danzhai gold-mercury deposit

	Mineralization Stages			
Mineral	**I**	**II**	**III**	**IV**
chalcedony	+++	++		
quartz	++	+	++	+++
calcite		+++	+	+++
dolomite		+++	+	++
arsenopyrite	+++	++	+	+
cinnabar		+++	++	
realgar		+++		
orpiment		+++		
stibnite		+++	++	
barite			+++	
pyrite	+	++	++	+

Table 3.2 Mineral Assemblage Related to Gold and Mercury Mineralization

1. Mineral assemblage related to gold mineralization (GMA)			
GMA1	calcite	arsenopyrite	pyrite
GMA2	chalcedony, quartz	arsenopyrite	pyrite
GMA3	quartz	realgar, orpiment	cinnabar
GMA4	calcite	cinnabar, stibnite	arsenopyrite, pyrite
2. Mineral assemblages related to mercury mineralization (MMA)			
MMA1	quartz	calcite	cinnabar, stibnite
MMA2	barite	cinnabar	quartz
MMA3	calcite	stibnite	native mercury

rarely in the cores. Joralemon (1951) observed gold rimming quartz grains, both as individual, large grains and as clusters of very tiny grains. The clusters are elongate parallel to the bedding. The gold with the quartz-realgar veins is paragenetically late and follows the main period of gold deposition.

Radtke and Scheiner (1970) determined empirically that, when the organic content of the ore exceeded 0.3 wt. %, there was a significant percentage of gold with organic material, and concluded that organic carbon played an important role in the deposition of gold at Carlin. Wells and Mullens (1973) studied the distribution of gold in the Carlin and the Cortez mines and found that most of the gold was within or on pyrite, and little, if any, gold was contained in carbonaceous material. Hausen and Park (1986) also examined the carbonaceous ore at Carlin and found that most of the gold was on and within pyrite and to a much lesser degree in the carbonaceous matter.

Using a high-resolution synchrontron X-ray fluorescence technique, Chao et al. (1986) also failed to discover any gold in areas of carbonaceous material within a gold-rich sample from the Horse Canyon deposit, and stated that "We believe that the carbonaceous material in Carlin-type deposits may have been important in the chemistry of the ore-carrying solutions, but played no significant role in metal transport."

Geologists consider that most of the gold in Carlin-type gold deposits is very irregularly distributed. At Carlin, Radtke (1985) found the gold to occur as a thin coating or film on pyrite, locally on the surfaces of amorphous carbon, encapsulated in silica, and dispersed in auriferous pyrite within grains of realgar. The majority of the gold at Carlin is within or on pyrite. Wells and Mullens (1973) examined the occurrence of gold at the Carlin and Cortez Mines and found it mainly within arsenian pyrite and in arsenian rims around pyrite grains. Tafuri (1987) observed gold in the Mercur deposit in two forms, as free gold surrounded by quartz and calcite in disseminated ores, and as inclusions in marcasite. Tafuri (1987) also speculated that arsenian pyrite contains gold, because separates of this pyrite always contain assayable amount of gold.

High-resolution transmission and Auger electron microscopy examination determined that gold is present in two habits (Hochella et al., 1986; Bakken et al. 1989): (1)

as discrete particles that vary from 50 to 200 Å in diameter that are encapsulated primarily in pyrite, but also in cinnabar and quartz, and (2) as free gold particles up to 100 Å in diameter that are associated with illite.

Attempts to find fine-grained gold or gold minerals such as electrum in ore of the Danzhai deposit by microscope and scanning electronic microscope examination have not been successful. Even in the realgar orpiment sample containing 328.57 g/t of gold determined by chemical analysis, no fine-grained gold grains or gold minerals were observed.

Table 3.3 and Table 3.4 list the data from chemical and Neutron Activation Analysis respectively. Gold shows a strong positive correlation with arsenic in both analyses,. For example, S_1-03 and S_1-22 are, two samples from the first stage of mineralization, the banded ore in the carbonate band in which arsenopyrite is highly concentrated. Arsenic is high, 5.15% and 25.01% respectively, gold is accordingly rich in both of them, 50 g/t and 150 g/t . The highest gold content is found in a realgar and orpiment sample, 328.57 g/t, but this positive correlation is not shown in the wall rocks or in the mercury ore (Fig. 3.5). Obviously, gold is closely associated with arsenic-rich minerals such as arsenopyrite, realgar, orpiment as well as arsenian pyrite, so all the arsenic minerals are gold-bearing minerals in the Danzhai gold-mercury deposit. Cathelineau et al.(1988) indicated the gold tends to concentrate in arsenopyrite from most physical and chemical conditions of depostion in hydrothermal deposits. Evidently, further work should be done to determine the exact occurrence of gold in this arsenic minerals.

As in the Carlin deposit, Au/Ag ratios of the Danzhai deposit are always higher than 1, and a positive correlation is shown between Au and Au/Ag ratios in the gold ore (Au > 1 ppm). In the wall rocks or in the mercury ore, however, Au/Ag ratios are usually less than 1 (Fig. 3.6).This is a common characteristic in a Carlin-type gold deposit, as distinguished from other types of gold deposit (Radtke and Scheiner, 1970; Radtke, 1985; Bagby and Berger, 1991). Base metals are not concentrated in the ores or wall rocks, and usually in the neighborhood of their Clarke values. Thallium is a metal enriched in the Carlin gold deposit, but remains at its Clarke value level (0.45 ppm) in the Danzhai deposit.

Table 3.3 Ore metals in the Danzhai gold mercury deposit by chemical analysis

Sample	Au (ppm)	As (ppm)	Ag (ppm)	Hg (ppm)	Sb (ppm)	Au/Ag
S1-03	50.00	51500.00	0.58	51.60	13.00	86.66
S1-06	0.54	750.00	1.46	18.90	5.00	0.37
S1-12	0.33	150.00	0.03	7.45	4.00	9.94
S1-15	0.25	1400.00	0.88	44.70	28.00	0.29
S1-22'	1.00	1500.00	0.13	21.30	52.00	7.87
S1-22	150.00	250100.00	2.05	147.90	380.00	73.28
S1-23	2.50	700.00	0.10	23.30	5.00	25.77
S1-26	1.79	3000.00	1.75	22.80	15.00	1.02
S1-28	7.50	3800.00	1.46	11.40	3.00	5.13
Sx-01	328.57	531900.00	4.68	438.00	420.00	70.21
Sx-02	33.93	40100.00	0.39	474.60	10.00	88.13
S2-01	0.08	3800.00	0.19	11.10	3.00	0.45
S2-02	0.25	700.00	1.46	32.10	2.00	0.17
S2-06	0.05	1900.00	1.46	30.40	5.00	0.03
S2-11	15.89	2200.00	1.46	152.70	2.00	10.86
S2-13	25.00	3700.00	0.61	412.20	380.00	40.98
S3-03	0.04	220.00	1.75	8.50	1.00	0.02
S3-06	11.43	2400.00	0.88	20.40	1.00	13.03
S3-07	0.26	1200.00	0.26	19.80	2.00	1.01
S4-01	0.15	1100.00	2.92	19.14	8.00	0.05
S4-01'	1.07	1200.00	1.17	47.40	5.00	0.92
S4-02	0.19	720.00	0.88	118.50	440.00	0.22
S4-03	1.07	450.00	0.26	27.50	18.00	4.17
S4-05	1.43	650.00	0.10	72.60	68.00	14.64
S4-07	5.89	4000.00	0.38	27.50	3.00	15.39
S4-13	13.93	4300.00	0.38	27.90	65.00	36.37
S5-01	0.07	30.00	4.09	84.80	1.20	0.02
S5-02	0.23	420.00	0.51	60900.00	620100.00	0.45
S5-03	0.90	500.00	0.08	494.40	2.00	11.65
S5-04	0.48	3600.00	0.77	3100.00	173600.00	0.63
S5-04'	0.10	110.00	3.95	160.50	4.00	0.02
S5-06	1.79	720.00	3.80	25.50	13.00	0.47
S14-01	2.62	4500.00	2.05	91.50	80.00	1.28
S14-12	3.22	2100.00	0.88	105.30	250.00	3.67
W-01	0.22	50.00	2.92	20.60	1.00	0.08
W-02	0.36	230.00	2.05	12.37	5.00	0.17
W-03	0.11	25.00	4.39	9.90	1.20	0.03

Table 3.4 Metals analyzed by Neutron Activation in the Danzhai gold mercury deposit

Sample	Au (ppm)	As (ppm)	Ba (ppm)	Sb (ppm)	Cu (ppm)	Pb (ppm)	Tl (ppm)	Ge (ppm)	V (ppm)
Clark	0.004	1.80	425.00	0.20	55.00	12.50	0.45	1.50	135.00
S4-01(1)	0.03	43.56	182711.10	14.86	11.00	60.00	0.60	1.80	2.70
S1-22	100.67	52888.41	n.d.	564.62	151.00	80.00	5.00	2.20	5.40
S1-18(2)	n.a.	n.a.	n.a.	n.a.	19.00	60.00	0.80	2.40	20.00
S14-12	1.40	515.43	n.d.	197.82	19.00	110.00	0.90	1.10	30.00
Sx-01	8.35	7518.76	n.d.	1409.94	68.00	100.00	0.60	2.50	13.80
Sx-02	62.00	73073.33	n.d.	2296.70	41.00	90.00	0.70	6.30	17.50
Dz-02	n.a.	n.a.	n.a.	n.a.	19.00	50.00	0.80	4.50	75.50
Dz-06	0.04	33.27	4916.88	7.07	53.00	60.00	0.60	20.20	33.80
Dz-3(1)	7.68	2430.68	371.70	116.59	64.00	90.00	0.40	3.70	27.50
Dz-16(2)	42.45	13133.66	156.21	114.72	53.00	20.00	0.60	2.80	10.00
Dz-19(2)	n.a.	n.a.	n.a.	n.a.	19.00	190.00	0.60	3.20	22.50
Dz-21(1)	0.23	233.73	220.64	53.17	38.00	80.00	0.40	5.20	17.50
Dz-21(2)	0.50	286.99	117.96	81.91	23.00	30.00	1.00	4.50	10.00
S5-04	n.a.	n.a.	n.a.	n.a.	49.00	210.00	0.20	3.70	6.50
Dz-3(2)	18.04	5383.66	217.32	149.11	45.00	70.00	0.30	4.20	9.50
S4-01	n.a.	n.a.	n.a.	n.a.	30.00	20.00	0.20	2.70	11.20
S1-18(1)	95.28	75770.00	n.d.	1095.32	79.00	70.00	0.50	5.50	6.80
Dz-01	9.09	3670.99	181.99	810.93	37.00	110.00	0.40	4.70	6.30
S5-07	5.54	181.05	n.d.	6880.68	26.00	460.00	0.50	5.60	8.10
W-01	0.11	71.71	194.88	34.16	19.00	80.00	0.30	4.50	1.90
S5-10	6.38	1567.88	n.d.	2627.52	23.00	170.00	0.60	2.20	6.00
Dz-23(2)	n.a.	n.a.	n.a.	n.a.	19.00	60.00	0.70	3.30	5.00
W-03	n.a.	n.a.	n.a.	n.a.	23.00	50.00	0.80	2.50	7.00

n.a. = not analyzed; n. d. = not detected.

Samples are analyzed in the Universite of Quebec at Chicoutimi.

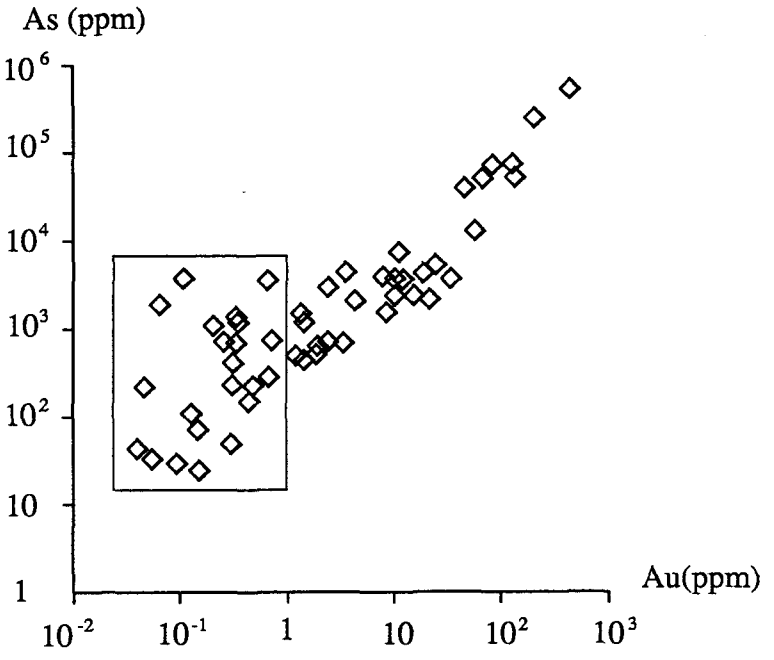

Fig. 3.5 Correlation between gold and arsenic shows a positive correlation in the gold ore (Au > 1 ppm), but this correlation is not shown in the wall rock or mercury ore (Au < 1ppm, within the rectangle).

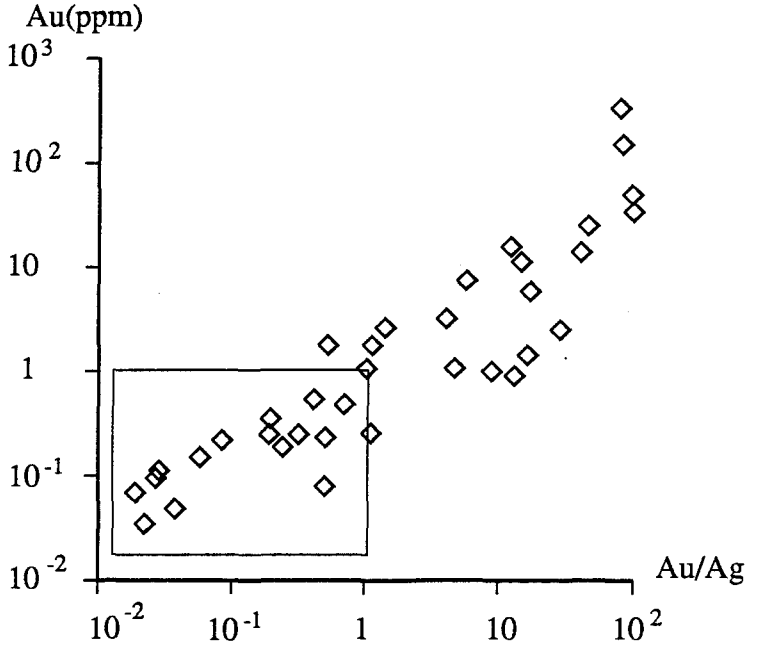

Fig. 3.6 The Au/Ag ratio is always higher than 1 in the gold ore (Au > 1 ppm), but less than 1 in the wall rocks or mercury ore (Au < 1ppm). This is a common characteristic of Carlin-type gold deposits.

§ 3.6. Mineral Assemblage

Knowing that the gold is principally associated with arsenic minerals, the gold ore mineral assemblage and the mercury ore mineral assemblage can be clearly distinguished. The principal metallic minerals in the deposit are cinnabar, stibnite, arsenopyrite, pyrite, realgar, orpiment as well as barite. Different mineral assemblages occur in the different stage of mineralization and different orebodies.

The mineral assemblages related to gold mineralization consist of four groups: (1) calcite - arsenopyrite- pyrite; (2) chalcedony-quartz - arsenopyrite-pyrite; (3) quartz-realgar-orpiment-quartz-calcite; (4) calcite–stibnite-cinnabar- arsenpyrite, pyrite. The first type is dominant in the banded ore which is believed to belong to the first mineralization stage. The second type is also attributed to the first stage of mineralization accompanied by silicification. These types of mineral assemblage are mainly found in the No.1, No.3 and parts of the No.4 orebodies, the third type is important in the second mineralization stage, but is only observed near the surface. The last type occurs in calcite veins, associated with extensive mercury mineralization.

The mineral association related to mercury mineralization includes: (1) quartz–calcite, dolomite–cinnabar–stibnite; (2) barite-cinnabar-quartz; (3) calcite–stibnite–native mercury. The first type of assemblage dominates the second mineralization stage. It is present as large veins and is very important for mercury mineralization. For example in the No.5 orebody, several meter-wide calcite veins contain cinnabar and stibnite crystals. The second type is seen in the third mineralization stage occurring in the No.4 orebody. The last assemblage may be related to secondary processes.

Even though the gold and mercury mineralization is associated in the Danzhai gold-mercury deposit, it is noteworthy that they are not always associated in all stages of mineralization. The first stage of mineralization is dominated by gold mineralization, and is not associated with mercury mineralization at all. The gold mineralization tends to be concentrated in the altered host rocks, particularly silicified, carbonaceous carbonates.

Mercury mineralization tends to accumulate in veins and veinlets, associated with gold mineralization .

§ 3.7. Schematic Comparison Of Geological Characteristics Between The Danzhai Gold-mercury Deposit and the Carlin Gold Deposit

The Carlin gold deposits in Nevada, U.S.A. have been studied in detail (Joralemon, 1951; Hausen and Kerr, 1968; Radtke and colleagues, 1970, 1980, 1985; Bagby and Berger, 1991). The fundamental geological characteristics of the deposit have been documented in detail even though the genesis of Carlin gold deposit is still contentious. It is therefore possible to compare the geological characteristics between the Danzhai gold-mercury deposit and the Carlin gold deposit.

§ 3.7.1. Nature of the host rocks

The host rocks of the Danzhai gold-mercury deposit and of Carlin gold deposit are almost the same, both of them are dominated by carbonates. In the case of the Danzhai gold-mercury deposit, the host rocks are dark-grey colored carbonates with different structures such as brecciated carbonate, banded limestone, laminated carbonate and thin bedded carbonates, sometimes intercalated with shale. The carbonates belong to the Lower Ordovician to Upper Cambrian strata. In the Carlin deposit, the Lower Silurian to Lower Devonian Roberts Mountains Formation is the host rock of the deposit, which is also dominated by dark-gray, fine-grained, laminated dolomitic limestone containing some silt (Evans, 1980).

§ 3.7.2. Structural Control of the Deposits

The Roberts Mountains thrust is a prominent structure of regional importance for the gold mineralization in the Carlin area, and the Carlin gold deposit is located near the crest of the Tuscarora anticline within an area where high-angle normal faults have broken the range into numerous blocks and produced intense shattering of the lower plate carbonate rocks near the trace of the Roberts Mountains thrust. Radtke et al.(1980) believe that these high-

angle normal faults in and near the deposit served as channels for the hydrothermal solutions.

In Danzhai, the situation is quite similar. F_1 is an important regional fault, and is mineralized itself in the Danzhai area. Three groups of second order faults related to F_1 have also broken the area into numerous blocks. The gold and mercury mineralizations usually are located in the intersection of the NNE-oriented and NE-oriented second order faults in localities near F_1. Obviously, F_1 served as the channel for ore-forming fluid, and the associated second order faults provided the sites for gold and mercury deposition.

§ 3.7.3. Occurrence of Gold

No detailed investigation on the occurrence of gold has been done so far in Danzhai, but it is certain that gold is invisible under the microscope or even under the scanning electronic microscope. Based on chemical analysis as well as Neutron Activation Analysis, gold shows positive correlation with arsenic, which may suggest that gold occurs in one or more of arsenopyrite, realgar, orpiment as well as arsenian pyrite. Wells and Mullens (1973) examined the occurrence of gold at the Carlin and Cortez Mines and found it mainly within arsenian pyrite and in arsenian rims around pyrite grains.

§ 3.7.4. Association of Alterations

The alterations in the Danzhai gold-mercury deposit are simple and clear, that is, several stages of silicification and carbonatization and associated different stage of quartz, carbonate and barite veins or veinlets. No pre-ore stage veins have been observed, neither did an oxidized acid leaching occur. The alterations in the Carlin gold deposit seem quite complicated. For example, Bakken and Einaudi (1986) carefully describe the alterations in the Carlin gold mine, and divide the alteration zones into 'recrystallized calcite', 'incipient silicification', 'moderate silicification', 'intense silicification', and 'complete silicification'. The vein or veinlet systems are also quite complex, and different in the hanging wall and footwall of the main orebodies. Based on observed cross-cutting relations, the veinlets observed in the Roberts Mountains Formation overlying the main orebody in order of

decreasing age were divided into nine types (type A to I). Although not all the veinlets were associated with gold mineralization, they can be classified into several stages related to different geological activities: (1). The calcite (type A), calcite ± quartz ± hydrocarbon (type B) in the hanging wall as well as the quartz veinlets (type F) in the footwall of the orebody are considered to have formed prior to the hydrothermal activity. They belong to veinlets that predate hydrothermal activity and are not related to gold mineralization. (2) The veinlets that are associated with hydrothermal alteration are calcite ± dolomite veinlets (type C) in the hanging wall and carbonate ± barite ± quartz veinlets (type E) in and periphery of the orebody. They are considered to be related to gold mineralization. (3) Barite ± sphalerite ± galena veins (type I) consist of white, euhedral quartz and barite fills vugs in bedded jasperoid and jasperoid veins that developed after the rocks were altered. They belong to veinlets that postdate hydrothermal activity. The calcite veinlets (type D) cut all features in the deposit and are probably related to weathering.

Evidence presented suggest that most of the acid-leaching and oxidation in the orebodies and surrounding rocks occurred during boiling in the late-stage hydrothermal fluids (Radtke et al., 1980). This acid leaching process complicated the primary geological characteristics of the Carlin gold deposit. Similar processes did not exist in the Danzhai gold-mercury deposit, so the primary geological characteristics in the Danzhai gold-mercury deposit are well preserved.

§ 3.7.5. Mineralization Association

The mineralization is regionally associated with other similar deposits both in Carlin and in Danzhai. For instance, a number of gold deposits occur together in the Carlin region while a great deal of gold, mercury, antimony and barite deposits are associated in the Sandou-Danzhai ore belt. In the southwest of Guizhou, the situation is the same. Many gold deposits are present in the same area, and their geological characteristics are quite similar. There are some differences though, in Carlin only gold is of economic importance, but in Danzhai, both gold and mercury are of independent economic importance. Base metal minerals are present in Carlin, for example, in barite ± sphalerite ± galena veins, but in Danzhai, these base metal minerals are nearly absent. Chemical analyses show that the base metals both in the host rocks and in the ore are in the level of their Clarke values.

§ 3.7.6. Associated Igneous Rocks

A great contrast exists between the Carlin gold deposit and the Danzhai gold-mercury deposit regarding to this aspect. In the eastern region of Guizhou and in "Gold Triangle Area" of southwest Guizhou, north Guangxi and east Yunan, neither magmatism nor metamorphism is associated with the gold mineralization. In the Carlin area, Nevada, U.S.A., however, igneous rocks occur within, or in the vicinity of, nearly all of the Carlin-type gold deposits. Granodioritic stocks as well as granodiorite to granite dykes are found in the Getchell, Gold Acres, Goldstrike, Northumberland, and White Caps deposits, and magnetic anomalies suggest the presence of large granitic bodies beneath other deposits such as Carlin. The Carlin-like deposits in central Montana and the South Dakota are closely associated with alkaline igneous rocks including syenite and alkaline granite. In most districts, the igneous rocks are intensely altered by hydrothermal fluids, and ore commonly occurs in fractures parallel to the intrusions (Radtke et al. 1980; Berger and Bagby, 1991).

§ 3.7.7. Associated Carbonaceous Materials

The carbonaceous materials in the Carlin gold deposit and other similar gold deposits in the area are pervasive. For instance, Kuehn and Bodnar (1984) found pyrobituminous material within fluid inclusions in calcite ± quartz ± hydrocarbon veins at Carlin; Radtke (1985) found that mineralized rocks contain significantly more organic carbon (0.5-0.6 wt. %) than unmineralized rocks (0.2-0.4 wt.%); Hausen and Park (1986) found that the ores at Carlin, Getchell, and Alligator Ridge contain bituminous matter that is mostly petroleum residues emplaced in the host rocks prior to gold mineralization. Furthermore, Hausen and Park (1986) concluded from a study of the Carlin deposit and from comparisons with other deposits that the domed and faulted structures associated with some Carlin-type gold deposits had been petroleum reservoirs. In the Danzhai gold-mercury deposit as well as other deposits in the east region of Guizhou province, bitumen veins, or hydrocarbon bearing veins and veinlets are ubiquitous, and bitumen is particularly

extensive, carbonaceous materials are rich both in the host rocks and in the veins. This subject will be discussed in detail in the next chapter.

§ 3.8. Summary

Danzhai was well known as one of the biggest mercury deposits in P. R. China, but recent investigations show it is actually associated with gold mineralization as well. The host rocks of the deposit are Lower Ordovician and Upper Cambrian carbonates with different structures such as brecciated carbonate, banded carbonate, laminated carbonate. The gold and mercury orebodies are mostly located in faults, some are also present along bedding plane faults. No igneous rocks are observed regionally, so a heat source for mineralization may not be derived from magmatic activity. The peripheral alterations are low temperature associations such as silicification, carbonatization. The principal mineral assemblage is sulfides of arsenic, mercury and antimony such as cinnabar, arsenopyrite, stibnite, pyrite and realgar, orpiment as well as barite. No fine-grained gold or gold minerals have been observed under the optical or the scanning electron microscope, but whole rock chemical analysis shows that the gold has a strong positive correlation with arsenic so that the gold may be mainly associated with arsenic minerals such as arsenopyrite, realgar, orpiment, or arsenian pyrite. The Au/Ag ratio is always greater than 1 in the gold ore but less than 1 in the wall rocks and the mercury ore. Base metals are not concentrated in the ore or wall rocks. Hydrocarbon veins, particularly bitumen are extensive, organic matter is concentrated both in the host rocks and in the veins; Evidently, the geological nature of the Danzhai gold-mercury deposit is quite similar to that of Carlin-type gold deposits in the western U.S.A except for the associated igneous rocks.

CHAPTER IV:

SOLID HYDROCARBON CONCENTRATIONS AND THEIR RELATIONSHIP WITH GOLD-MERCURY MINERALIZATION

§ 4.1. Introduction

Many metallic ore deposits hosted by sedimentary rocks are associated with hydrocarbons such as bitumen and/or oil (Bohdan, 1990; Barton, 1982; Parnell, 1988; Raymond et al, 1987; Saxby, 1976). For example, the association of bitumen and oil with Mississippi Valley-type lead-zinc deposits was described by Anderson (1991), Anderson and Macqueen (1982), Giordano(1985), Gize and Barnes, 1987, Henry et al. (1992), Leventhal (1990), Macqueen and Powell (1983), Marikos et al. (1986), Pering (1973), Powell and Macqueen(1984), and the relationship between uranium mineralization and associated organic matter has been elucidated by Curiale et al. (1983), Leventhal et al.(1986, 1987a), Meunier et al., (1990, 1991), Parnell and Eakin (1987), Parnell (1988), Hansley and Spirakis (1992). Other deposits such as copper mineralization hosted in sandstone and/or limestone are also considered to be somewhat related to hydrocarbons or associated brines (Kelly and Nishioka 1985, Sverjensky, 1987); The association of hydrocarbons and sedimentary rock-hosted mercury deposits in Austria, California, Germany, Italy, Peru, Spain, Texas and China are documented by many geologists (Parnell, 1988; Shi, 1991; Peabody and Einaudi 1992). This association between hydrocarbon and metallic ore deposits suggests that the oil and/or associated oilfield brines may play a significant role in the formation of the corresponding deposits. For example, Sverjensky(1984, 1987) considered that oil field brines could be the ore-forming solution for Mississippi valley-type lead-zinc-fluorite-barite deposits as well as for sediment-hosted Cu-rich deposits.

Bitumen and/or other forms of organic matter are also concentrated in Carlin-type gold deposits. For example, in the Carlin gold deposit, Western U.S.A., Radtke and Scheiner (1970) reported that three forms of organic matter are associated with gold: (1) an activated carbon component; (2) a mixture of high-molecular-weight hydrocarbons usually associated with the activated carbon components; and (3) an organic acid, similar to "humic acid", containing functional groups capable of interacting with gold organic compounds. Another Carlin-type gold deposit reported in Peru is also rich in organic matters (Noble and Vidal, 1990). The situation is the same in the Carlin-type gold deposits in the P.R. China (e.g.: Cunningham et al, 1988).

The nature and role of organic matter in the mineralizing processes responsible for the genesis of Carlin-type deposits has been studied by a number of workers. At Carlin, Radtke (1985) found that mineralized rocks contain significantly more organic carbon (0.5-0.6 wt. %) than unmineralized rocks (0.2-0.4 wt.%). A similar study at Jerritt Canyon found < 0.1 wt.% organic carbon in unmineralized rocks and 0.3-0.5 wt.% in mineralized rocks (Leventhal et al., 1987b). Hausen and Park (1986) concluded from a study of the Carlin deposit and from comparisons with other deposits that doming and faulting associated with some Carlin-type gold deposits had been petroleum reservoirs. A number of studies have been conducted to characterize the nature of the carbonaceous material. Hausen and Park (1986) concluded that the ores at Carlin, Getchell, and Alligator Ridge contain bituminous matter that is mostly petroleum residues emplaced in the host rocks prior to gold mineralization. Kuehn and Bodnar (1984) found pyrobituminous material within fluid inclusions in calcite ± quartz ± hydrocarbon veins at Carlin. Gize and Barnes (1987) studied the thermal history, oxidation, and re-working of organic matter at Carlin, and concluded that there was evidence for multiple generations of bitumen, indicative of a pulsing of the incoming brines during the original migration of the organic matter. During hydrothermal activity, the carbonaceous material was heated, partly volatilized, and mobilized locally by the hydrothermal solutions (Hausen and Park, 1986).

The role of carbonaceous material in the transport and precipitation of gold has been somewhat controversial. Radtke and Scheiner (1970) determined empirically that, when the organic content of the ore exceeded 0.3 wt. %, there was a significant percentage of the gold with the organic material, and concluded that organic carbon played an important role in the

deposition of gold at Carlin. Wells and Mullens (1973) studied the distribution of gold in the Carlin and Cortez mines and found that most of the gold was within or on pyrite, and little, if any, gold was contained in carbonaceous material. Hausen and Park (1986) also examined the carbonaceous ore at Carlin and found that most of the gold was on and within pyrite and to a much lesser degree in the carbonaceous matter.

Thus, previous investigations show that although carbonaceous materials are enriched in Carlin-type gold deposits everywhere, the genetic relationship between these carbonaceous materials and gold mineralization is still unclear.

§ 4.2. Former Majiang-Danzhai Petroleum Reservoir

The second member of The Wengxiang Formation ($S_{1\text{-}2}w^2$) consists of silty or fine-grained quartz sandstone intercalated with silty shale. The thickness of this member varies from 20-38 meters in the area, but it can be as thick as 100 meters locally. Field surveys show that black colored sandstone in this member of the Silurian Wengxiang Formation in the Majiang, Duyun, Danzhai and Kaili area of eastern Guizhou proved to be bituminous sandstone (Han et al., 1982). Even though this second member can be 100 meters thick, the greatest thickness of bituminous sandstone in this member is only 27.8 meters (Fig. 4.1). Detailed laboratory tests demonstrate that the bitumen principally fills pore spaces between sand grains in the sandstone.

Regional investigation demonstrates that the carbonates in the Lower Ordovician Honghuaran Formation(O_{1h}), underlying the Wengxiang Formation, are also rich in bitumen. In comparison with the second member of the Wengxiang Formation, the abundance of bitumen in the Honghuaran Formation is considerably lower. The carbonate of the Honghuaran Formation is composed of packstone and grainstone, in which primary pores, diagenetic vugs and fissures are extensively developed. The bitumen fills these primary and secondary pores and fissures.

Although the sandstone in the second member of the Wengxiang formation ($S_{1\text{-}2}w^2$) and the carbonate in the Honghuaran Formation (O_{1h}) is widely distributed in the

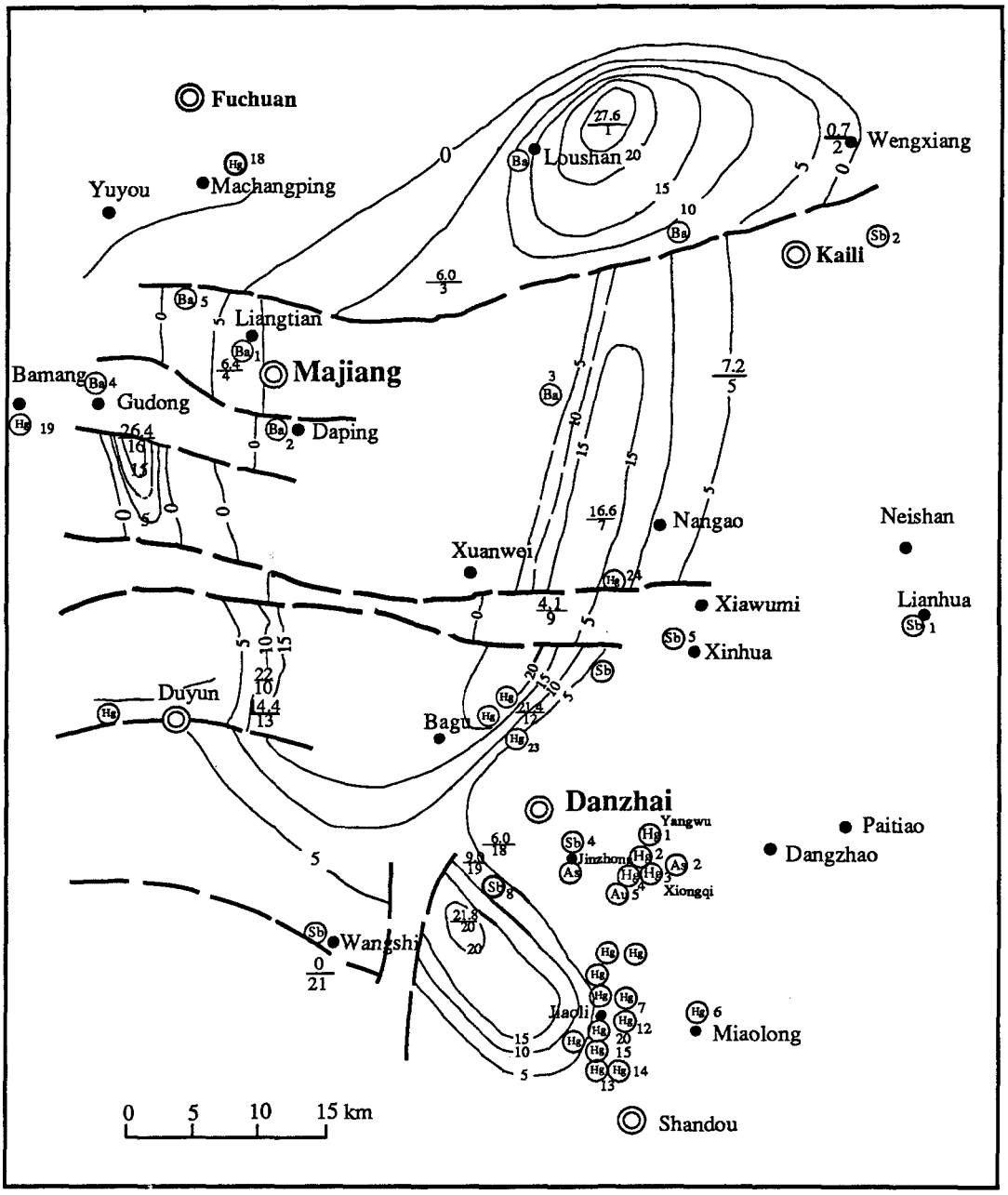

Fig. 4. 1 The isopach of Silurian bituminous sandstone and the distribution of mercury, antimony, gold and barite deposits and prospects in the eastern region of Guizhou province (Modified after Han et al., 1982, and Chen et al., 1986). $\frac{4.2}{17}$: The numerator indicates the thickness of biutminous sandstone while the denomerator shows the total thickness of the second member of the Silurian Wengxiang Formation.

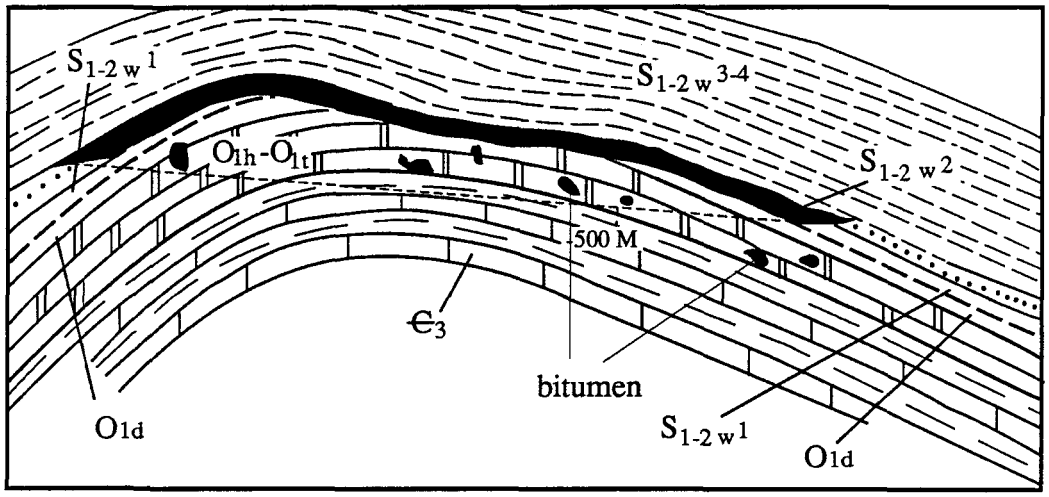

Fig. 4.2 The Majiang anticline and the second member of the Silurian Wengxiang Formation, and the Lower Ordovician Honghuaran Formation controlling the distribution of bitumen. All the bituminous sandstone is present in the -500 meters contour in the region (modified after Han et al., 1982).

eastern region of Guizhou, the bitumen distribution in them is not uniform over the area. The distribution of bitumen is controlled significantly by the Majiang anticline (Fig. 4.2), which formed in Late Caledonian orogeny, was a north-south striking, gently dipping (the dip angle of west flank is 3 - 4 ° and that of east flank is only 1 - 3°) anticline. The core of this anticline is composed of the carbonate of the Honghuaran formation (O_{1h}) while the two flanks are comprised of the sandstone of the second member of the Wengxiang Formation ($S_{1-2}w^2$) (Fig. 4.2).

The distribution of Silurian bituminous sandstone was controlled by both the Majiang anticline and the sedimentary rocks in its core and flanks. Even in the Majiang anticline and in the second member of The Wengxiang Formation, the bitumen is not pervasively distributed in different levels. In the sandstone of the second member of the Wengxiang Formation, for example, bitumen is extremely concentrated in the level above the -500 m contour of the Majiang anticline. Below this level, however, no bituminous sandstone can be found even in the same member. These sandstones gradually turn into silty limestone along the western flank of the anticline, and no bituminous sandstone is observed even though they are located above the -500 m contour. For example, in Kaili, the sandstone in the second member of the Wengxiang Formation ($S_{1-2}w^2$) is as thick as 65 meters, but only 0.7 meter at the top is rich in bitumen. In Sandou, the thickness of the same sandstone bed is 35 meters, but the bituminous sandstone is concentrated in the top 17 meters, so upper black colored sandstone contrasts with the lower white colored sandstone. In Duyun, to the south of the Wangshi fault, the thickness of the same sandstone is as great as 160 meters, but bituminous sandstone is not present. Therefore, Han et al. (1982) concluded that the Silurian bituminous sandstone represented a petroleum trap in the Silurian period, and the boundary of the bituminous sandstone, is at the -500 meter elevation in the structure.

The primary oil reserves of this destroyed oil trap is estimated at 1.6 billion tonnes (Han et al., 1982). Three possible oil source strata are recognized and examined in the region are: the Lower Cambrian (C_1), the Lower Ordovician Honghuaran Formation (O_{1h}) as well as the Silurian Wengxiang Formation ($S_{1-2}w^2$), but the thickness of the Lower Ordovician Honghuaran Formation(O_{1h}) and the Silurian Wengxiang Formation($S_{1-2}w^2$) is

too small to have produced such a tremendous petroleum reserve. The Lower Cambrian is composed of black shale with a thickness extending from 109 to 1032 meters, and its average organic carbon abundance is as high as 0.70%. It is therefore considered that the Lower Cambrian black shale is the principal oil-forming strata of the Majiang-Danzhai petroleum reservoir (Han et al., 1982). In addition, trace element investigation of the possible oil source strata indicated that, the Lower Cambrian black shale is enriched not only in organic matter, but also in ore-forming elements such as mercury, gold, arsenic and phosphorus. Therefore, the Lower Cambrian black shale is a possible provenance of the mercury and gold in the region as well (Chen et al., 1986).

§ 4.3. Regional Hydrocarbon Concentration and Mineralizations

The isopach of Silurian bituminous sandstone in the second member of the Wengxiang Formation($S_{1\text{-}2}w^2$) represents the former petroleum reservoir (Fig. 4.1). It is impressive that in or around this former oil trap, a great number of mercury, antimony, arsenic, gold and barite deposits or showings are present (Chen et al., 1986). A similar situation is also reported elswhere, mercury mineralization where is hosted in sedimentary rocks is usually associated with an oil reservoir (Rudakhov, 1973; Peabody and Einaudi, 1992). Rudakhov (1973) points out that mercury is so abundant in some oil and gas fields that mercury anomalies are used in prospecting for hydrocarbons.

Further geological investigation shows that different types of ore deposit are distributed in distinct localities of the former oil trap (Fig. 4.1). For example, the barite deposits or showings are definitely distributed in the center of the former oil trap in the Cambrian-Ordovician strata, but in the same locality, other ore deposits such as mercury, antimony and gold deposits are scarce. Only a few mercury and antimony showings have been found within the Silurian bituminous sandstone, and most of them are not of economic importance. The mercury, antimony and gold deposits with significant economic importance, however, tend to be present in localities where the Silurian bituminous sandstone wedges out, or outside but adjoining the bituminous sandstone. These deposits are present in the Cambrian-Ordovician carbonates rather than the Silurian bituminous sandstone.

The oil trap was controlled by the Majiang anticline as well as the strata of the second member of the Wengxiang Formation ($S_{1-2}w$) and the Lower Ordovician Honghuaran Formation, but the mercury deposits as well as other associated deposits tend to concentrate where the hydrocarbon is moderately concentrated, they do not occur where the hydrocarbons are extremely enriched (e.g.: Silurian bituminous sandstone or the pure bitumen veins in Cam-Ordovician carbonates,), nor where the hydrocarbons are scarce or absent. The mercury, antimony, arsenic, gold and barite deposits are principally concentrated in the organic-matter-enriched Cambrian and Ordovician carbonates, other than the Silurian bituminous sandstone itself. The situation is similar for barite deposits in the same area. This distribution of the metallic ore deposits is probably controlled by the former petroleum and oilfield brine interface, because these deposits or prospects are commonly present under or near the -500 meter contour (Han et al., 1982; Chen et al., 1986).

The bitumen concentration in the Majiang-Danzhai oil trap is not distributed equally on the east and west flanks of the Majiang anticline. The isopach of the Silurian bituminous sandstone demonstrates that the hydrocarbons are more concentrated in the east flank than in the west. This is interpreted to be the result of the sedimentary facies controlling the hydrocarbon enrichment. It is remarkable that the occurrence of metallic ore deposits coincides significantly with the hydrocarbon concentration, and the mercury, antimony, gold mineralization is more common on the east flank than the west flank. For example, the Sandou - Danzhai ore belt is situated on east flank of the former oil trap.

This regional spatial association between these metallic ore deposits and the former Majiang-Danzhai petroleum reservoir implies that the regional mineralizations are related to the petroleum evolution.

§ 4.4. Hydrocarbon Concentration in the Danzhai Gold-mercury Deposit

Field surveys show that various forms of organic matter occur in the host carbonate rocks of the Danzhai gold-mercury deposit. For example, laminated bitumen is present in the laminated and/or banded carbonate; the stylolites and vugs formed by the diagenesis of carbonates are also usually filled with bitumen. Bright-colored shiny bitumen is commonly

seen in fissures, fractures, faults and along stratification planes. The bitumen veins range up to several centimeters in thickness, are intercalated in the Upper Cambrian carbonates (Plate 3A). This bitumen is usually black, shiny and with a brittle and conchoidal fracture. Some metal sulfides such as pyrite and cinnabar can be seen within them.

Bitumen is also present in both veins and ores of the deposit, for instance, dispersed bitumen is commonly observed in quartz, carbonate and barite veins, and can easily be distinguished by its color. Black colored calcite, quartz as well as black-spotted calcite are commonly seen in the Danzhai gold-mercury deposit. The scattered bitumen is so abundant in some quartz veins that they show an unusual black color instead of the common white color (Plate 3B).

Further microscopic investigation demonstrates that various forms of dispersed bitumen, such as patch-like bitumen, veinlet bitumen as well as stylolite-like bitumen, are closely associated with gold and mercury mineralization. In addition, the scattered bitumen occurs not merely in gangue minerals such as calcite, quartz, dolomite and barite, but also in ore minerals such as cinnabar.

Patch-like bitumen is hosted by quartz crystals of the second mineralization stage(Plate 3C). Bitumen, in turn, hosts arsenopyrite, a principal gold-bearing mineral. This occurrence is quite common in the second mineralization stage. Note that the so-called patch-like bitumen is actually big solid bitumen inclusions enclosed in quartz, calcite or cinnabar, which will be discussed in detail in a later chapter.

Bitumen veinlets are associated with arsenopyrite, pyrite and cinnabar (Plate 3D), and several tiny quartz crystals are precipitated from the hydrocarbon veinlet as well. The host mineral of the hydrocarbon veinlet is calcite. Arsenopyrite, pyrite and cinnabar are concentrated only in the hydrocarbon veinlet and no such ore minerals are seen in the calcite which hosted the bitumen veinlet.

Apart from the commonly observed bitumen, another kind of solid hydrocarbon, natural paraffin wax, is also found in the Danzhai gold-mercury deposit. This light colored, transparent solid hydrocarbon is also called ozokerite. It is characterized by a brown to dark

brown color, and occurs as thin stringers sometimes together with bitumen sometimes apart. Similar to bitumen, paraffin wax is also usually associate with metal sulfides. Paraffin wax is seen to associated with arsenopyrite, pyrite, cinnabar as well as the veinlet bitumen(Plate 3E and Plate 3F).

Stylolite-like and patch-like hydrocarbons host metallic minerals. These metallic minerals tend to be richer in bitumen than in paraffin wax (Plate 4A and 4B). Paraffin wax is usually associated with bitumen, but occasionally, paraffin wax is independently associated with metallic minerals.

Stage by stage investigation shows that hydrocarbons, particularly bitumen, are associated with different stage of mineralization. As mentioned above, the first mineralization stage consists of arsenopyrite and/or pyrite, and dominated by gold mineralization. As shown in Plate 1D, scattered bitumen is concentrated in the fine-grained quartz and chalcedony and arsenopyrite. The second mineralization stage is characterized with cinnabar, realgar, orpiment, stibnite, arsenian pyrite and/or pyrite, and accompanied by the gangue minerals such as calcite, dolomite and quartz. Both mercury and gold mineralization are important, the solid bitumen and paraffin wax, particularly the patch-like, veinlet hydrocarbons are mostly concentrated in calcite and quartz veins of the second stage of mineralization. The third mineralization stage is composed of barite, cinnabar, quartz, calcite and pyrite, in which hydrocarbons are also present in scattered forms. The last mineralization stage consists of euhedral quartz crystals, and calcite; solid bitumen and paraffin wax are also commonly present as patch-like, veinlet and stylolite-like forms.

Evidence described above clearly shows that the gold and mercury mineralization is associated with a variety of forms of hydrocarbons, such as patch-like bitumen, veinlet bitumen, as well as stylolite-like bitumen and paraffin wax in the different stages of mineralization. Two important questions about their temporal connection arise. First, what is the temporal relationship between the hydrocarbons and their host minerals? More precisely, if a quartz crystal hosts some bitumen, does it necessarily mean that the quartz and bitumen co-precipitated from the same fluid, or did the hydrocarbons just fill cavities or fissures in the earlier formed quartz, as various forms of hydrocarbons fill pores in the carbonate rocks? Second, are these ore minerals such as arsenopyrite and cinnabar co-

precipitated with the bitumen or captured by the bitumen? Two possibilities should be considered here, one that the bitumen and ore minerals deposited from the same ore-forming fluid at the same time, and a second possibility that, the bitumen deposited in advance, but it reacted with later ore-forming fluids and resulted in the precipitation of cinnabar and arsenopyrite.

The temporal relationship between bitumen and its host mineral may be partly resolved by petrographic evidence. As shown in Plate 4C, three triangular bitumen inclusion *a, b, c,* are enclosed in two quartz crystals. Bitumen A is actually a solid inclusion, obviously trapped in the process of quartz crystallization, while the other two bitumen inclusions *b* and *c* are filled in the borders of quartz crystals. These are interpreted to be later infillings, but their shape, color and reflectance are the same as bitumen *a*.. It is reasonable to suppose that bitumen *a* precipitated in the process of crystallization of its host mineral, quartz, the bitumen *b* and *c* precipitated subsequently from the same fluid as bitumen *a*, and did deposit from another fluid later on. This problem will be further discussed in the chapter on hydrocarbon fluid inclusions.

The second question is quite difficult to answer, but one way to solve the puzzle was proposed by Kelly and Nishioka (1985). If a hydrothermal fluid interacted with hydrocarbons, bitumen or oil, for example, hydrocarbons will capture some metallic minerals but a reaction zone will also be produced around the bitumen. Attempts to find a reaction zone were made in the examination of the hydrocarbon-bearing samples from the different mineralization stages, but no such a reaction zone was found around bitumen or paraffin wax. It is therefore considered that the metallic minerals such as arsenopyrite and cinnabar are co-precipitated with hydrocarbons. Furthermore, the hydrocarbons are assumed to play a significant part in the ore-forming fluid.

Many documented cases of sedimentary rock-hosted mercury and antimony deposits are associated with bitumen. In the Plamennoye mercury-antimony deposit, for instance, Vershkovshaya et al (1972) indicate that, the highest mercury content occurs with the maximum bitumen enrichment. A similar case is present in the Danzhai gold-mercury deposit, where mercury and gold mineralization is commonly associated with hydrocarbons in different occurrences. A variety forms of hydrocarbon are abundant not only in the

Danzhai gold-mercury deposit, but also in many other sedimentary rock-hosted mercury, antimony, arsenic and barite deposits or prospects in the eastern region of Guizhou (Han et al., 1982; Chen et al., 1986, Fu, 1988). This suggests that the Danzhai gold-mercury mineralization is probably related to petroleum evolution and/or the associated oilfield brine of the former Majiang-Danzhai petroleum reservoir.

§ 4.5. Reflectance of Bitumen

Bitumen occurs in distinct groups, which are classified as prediagenetic, syngenetic and postdiagenetic. The last group of bitumen is important for the petroleum evolution in a petroleum reservoir, and its reflectance is generally lower than that of the other two groups of bitumen (Robert, 1988). Bitumen reflectance is measured in order to to investigate whether the bitumen in the minerals of the Danzhai gold-mercury deposit is comparable to that of the Majiang-Danzhai oil trap or not, and to what stage of petroleum evolution it belongs.

The measurement of bitumen reflectance on polished thin sections were carried out at the Geological Department, McGill University on a Zeiss Universal microscope (oil immersion objective EPI 40/0.85 Pol) equipped with a RACIP28 photomultiplier tube and digital recording unit, using monochromatic green light (546nm). Polished glass standards with %R. values of 1 and 1.67 served to calibrate the photometer readings, the maximum and minimum reflectance (Rmax' and Rmin'), respectively. Bireflectance (BI) is the arithmetic difference between the measured maximum and minimum reflectance values: BI=Rmax'- Rmin'. Random reflectance (Rm) was also measured. One or more reflectance measurements were made on each organic fragment, depending on fragment size.

The bitumen reflectance in the Majiang-Danzhai petroleum reservoir was first studied by Han et al.(1982). Samples from different localities in the oil trap gave an average reflectance high (R_{mean} (%)), ranging from 2.0 to 5.9, but most fell in the range from 2.0 to 3.5. The reflectance of bitumen from the Cambrian host rocks of the Danzhai gold-mercury deposit (Chen et al., 1986), gave the same result as that of Han et al.(1982). The present study finds bitumen reflectance in the minerals from the different mineralization stages in the

deposit to have a high reflectance in the range from 2.5 to 3.8 % (Table 4.1). There is no significant variation of bitumen reflectance from stage to stage of the mineralization except that bitumen in the last stage of quartz and calcite veining is considerably lower reflectance than that of the other stages (Fig. 4.3). Therefore, from the bitumen reflectance standpoint, there is no distinction between bitumen in the Danzhai gold-mercury deposit and the bitumen from the host rocks or the bitumen from the Majiang-Danzhai petroleum reservoir.

It is noteworthy that the temperatures, calculated from the reflectance of bitumen from each distinct stage of mineralization in the Danzhai gold-mercury deposit, vary from 150 to 210 °C.

Low-rank dispersed bitumen is generally isotropic. As the grade of thermal maturation increases, bitumen develops optical anisotropy. In polished thin sections, this material exhibits a fine-grained mosaic texture composed of randomly oriented anisotropic domains. Even micro-areas that appear isotropic at 400X magnification are shown at higher magnification to be composed of submicron-size anisotropic particles (King, 1963). Similar mosaic textures are observed in most high-rank carbonaceous materials, whether naturally formed (Gize and Barnes, 1987) or experimentally pyrolyzed, and are interpreted to be the result of thermal changes in the physical structure of the organic matter. Mosaic elements are interpreted to represent domains of quasigraphitic crystallities, composed of sheets or stacks of alky-substituted polynuclear aromatic structures (Sanada et al., 1973; Yen, 1975). When formed in an anisotropic stress field, these quasigraphitic domains tend to adopt a preferred orientation perpendicular to maximum compressive stress (Levine and Davis, 1989). Therefore, The bitumen in the Danzhai gold-mercury deposit is actually pyrobitumen, which is insoluble in carbon disulfide (CS_2), has high reflectance values, with a high level of surface anisotropic reflectance under oil immersion objective lens. Some of the pyrobitumen exhibits various forms of mosaic texture, shrinkage cracks and degassing pores caused by thermal maturation.

Table 4.1 Bitumen reflectance in the Majiang-Danzhai oil trap and the Danzhai depsoit

Sample	Location	Age	Petrography	$\bar{R}$max(%)	Reference
1. Bitumen reflectance in the former Majiang-Danzhai petroleum reservoir					
803-504	Yanzhai, Danzhai	$S_{1-2}w^{2}$	sandstone	2.00	1
803-43	Loubang, Duyun	$S_{1-2}w^{2}$	sandstone	2.5	1
803-212	Modaoshi, Majiang	O_{1h}	carbonate	2.74	1
L6-114	Xinren, Danzhai	O_{1h}	carbonate	2.78	1
L6-117	Banzhuang, Duyun	O_{1h}	carbonate	2.85	1
803-516	Hobazhai, Duyun	O_{1h}	carbonate	2.80-3.91	1
803-124	Jiazhao, Sandou	O_{1h}	carbonate	3.31	1
803-136	Pojiao, Duyun	O_{1h}	carbonate	3.52	1
803-133	Gaogentian, Duyun	O_{1h}	carbonate	3.68	1
803-62	Dawan, Duyun	O_{1h}	carbonate	3.24-5.90	1
2. Bitumen reflectance in the host rocks of the Danzhai gold mercury deposit					
Z07	Danzhai mine	$\in_{2}$ df	dolomite	1.48-1.51	2
Z06	Danzhai mine	$\in_{2}$ df	dolomite	2.34-2.37	2
Z05	Danzhai mine	$\in_{2}$ q	limestone	1.54-1.58	2
not named	Danzhai mine	$\in_{1}$ zn	concrete	3.47-3.55	2
not named	Danzhai mine	$\in_{1}$ zn	limestone	1.45-1.49	2
not named	Danzhai mine	$\in_{1}$ zn	limestone	2.32-2.35	2
not named	Danzhai mine	$\in_{1}$ zn	diagenetic vein	3.02-3.09	2
W-02	Danzhai mine	$\in_{1}$ zn	limestone	2.52	3
W-03	Danzhai mine	$\in_{1}$ zn	limestone	2.43	3
3. Bitumen reflectance in the vein and the ores in the Danzhai gold mercury deposit					
S1-03	Danzhai mine	I*	gold ore	2.55	3
S1-23	Danzhai mine	I	gold ore	2.2	3
S4-02	Danzhai mine	II	quartz vein	2.43	3
S1-12	Danzhai mine	II	quartz vein	2.75	3
S5-01	Danzhai mine	II	calcite vein	2.91	3
S2-02	Danzhai mine	II	carbonate vein	2.48	3
S5-06	Danzhai mine	II	mercury ore	2.9	3
S5-01	Danzhai mine	II	mercury ore	3.12	3
S5-10	Danzhai mine	II	gold ore	2.67	3
S2-13	Danzhai mine	II	gold ore	2.75	3
Sx-01	Danzhai mine	II	realgar	2.56	3
S4-02	Danzhai mine	III	barite veinlet	2.83	3
S4-01	Danzhai mine	III	barite veinlet	2.65	3
S5-04	Danzhai mine	IV	quartz vein	2.42	3
S5-03	Danzhai mine	IV	quartz vein	2.78	3
S3-07	Danzhai mine	IV	quartz vein	2.58	3
S5-01	Danzhai mine	IV	calcite vein	2.69	3
S4-12	Danzhai mine	IV	calcite vein	2.19	3

1 = Han et al. (1982); 2 = Chen et al. (1986); 3 = this study.

* I, II, III, IV indicate the mineralizaiton stage.

A

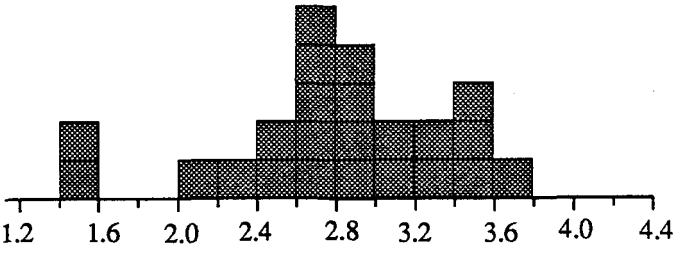

Fig. 4.3 A Histograms of bitumen reflectance in the Majiang-Danzhai petroleum reservoir and in the host rocks in the Danzhai deposit (Data from Table 4.1).

B

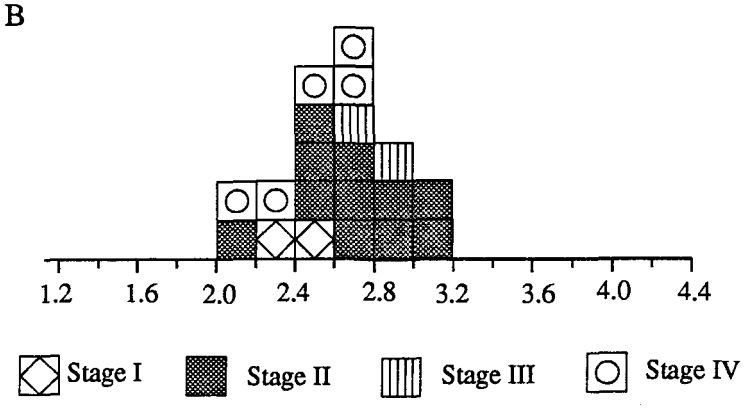

Fig. 4.3 B Histograms of bitumen reflectance in the different stages of veins and ores of the Danzhai gold mercury deposit (Data from Table 4.1).

§ 4.6. The Fluorescence of Solid Hydrocarbons

Fluorescence is another important property used to discriminate petroleum and to determine the evolutionary degree of the hydrocarbon. The fluorescence of bitumen and paraffin wax were measured under a variety of conditions. Four different excitation bands were used: 365, 390, 445, and 510 nm. Emission spectra were scanned manually using a quartz wedge monochromator/ photometer. This experiment was carried out in the Biology Department, McGill University.

Experimental results show that not all of the examined bitumen are fluorescent, nor is paraffin wax under excitation bands of 365, 390, 445 nm. Under the 510 nm excitation band, however, some paraffin wax has a strong red fluorescence (Plate 4D), but many others are not fluorescent at all.

That fact the solid hydrocarbons in the Danzhai gold-mercury deposit lost their fluorescence confirms that these hydrocarbons are overmature (Jacob, 1983, 1985; Bertrand et al., 1986). The fluorescent property of hydrocarbons will decrease, and will finally be lost with increase of petroleum maturity. From the study of the reflectance and anisotropy of bitumen, it is concluded that hydrocarbons in both the Danzhai gold-mercury deposit and the Majiang-Danzhai petroleum reservoir are highly evolved, overmature petroleum, which are classified in the thermal gas stage in petroleum evolution (Tissot and Welte, 1984).

§ 4.7. Conclusion

Bitumen is widely distributed in the Palaeozoic sedimentary rocks in the study area. In particular, bituminous sandstone occurs in the second member of the Silurian Wengxiang Formation ($S_{1\text{-}2}w^2$) as well as the Ordovician Honghuaran Formation(O_{1h}) in the Majiang, Duyun, Danzhai and Kaili areas. Detailed field investigation and laboratory tests show that bitumen concentration is significantly controlled by both the Majiang anticline and the strata mentioned above. Even in the second member of the Wengxiang Formation, bitumen are only located above -500 m contour of the Majiang anticline, below this level, no bituminous

sandstone could be found even in the same sandstone unit. The -500 meter contour is probably the former boundary between petroleum and oilfield brine. This hydrocarbon trap is called the Majiang-Danzhai petroleum reservoir.

Numerous mercury, antimony, arsenic, gold and barite deposits or showings are distributed in or around this former oil reservoir. The so-called Sandou - Danzhai ore belt is situated at the limit of petroleum evolution of the former oil trap. Different types of ore deposit are distributed in particular localities around the former oil trap. The mineralization is more abundant where hydrocarbon is moderately concentrated, rather than where the hydrocarbon is extremely enriched (e.g.: pure bitumen veins, or bituminous sandstone), or where the hydrocarbon is scarce or absent. Surprisingly, all the mercury, antimony, arsenic, gold and barite deposits in the area are located under the -500 meters contour, believed to be the ancient interface between petroleum and oilfield brine.

Field observations show that a variety forms of hydrocarbons occur in the host carbonate rocks and in the ore of the Danzhai gold-mercury deposit. Bitumen is present in the laminated and/or banded carbonate, and fill stylolites and vugs in the carbonates. Bitumen veins range up to several centimeters in thickness, and are intercalated in the host carbonate rocks of the Danzhai gold-mercury deposit.

Beside occurring in the wall rocks, dispersed bitumen is also present in the quartz, carbonate and barite veins and can easily be distinguished by its color. Black colored calcite, quartz veins as well as black-spotted calcite are frequently found in the Danzhai gold-mercury deposit.

Patch-like bitumen, veinlet bitumen, as well as stylolite-like bitumen commonly host sulfide minerals such as arsenopyrite, pyrite and cinnabar, and cinnabar can also host bitumen. Patch-like bitumen is actually a big solid inclusion hosted in quartz, calcite or barite. It is concluded that bitumen co-precipitated with the host and the sulfide minerals. Careful examination shows no reaction zone around in the bitumen grains, which excludes the possibility that the early formed bitumen reacted with a later ore-forming fluid.

Another solid hydrocarbon, natural paraffin wax, is also found in the Danzhai gold-mercury deposit. It has a characteristic brown to dark brown color, occurs as thin stringers, sometimes with bitumen and sometimes independently. Paraffin wax is usually associated with metal sulfides such as arsenopyrite, pyrite and cinnabar.

This evidence suggests that hydrocarbons are a significant part of the ore-forming fluid, and the Danzhai gold-mercury mineralization as well as the regional mercury, antimony, arsenic, gold and barite mineralizations are probably derived from the evolution of petroleum and/or the associated oilfield brine of the former Majiang-Danzhai petroleum reservoir.

The organic petrography study demonstrates that the bitumen in the minerals from the studied deposit corresponds to the bitumen in the former Majiang-Danzhai oil trap as well as the bitumen in the host rocks. The reflectances of bitumen from different stages of mineralization of the Danzhai gold-mercury deposit is high, varying from 2 to 3.8%. The temperature calculated from this reflectance ranges from 150 to 210 °C. The bitumen is actually pyrobitumen, with a mosaic texture as well as an anisotropic nature.

Fluorescence investigation of the bitumen confirms the result of the organic petrography study. The bitumen lost its fluorescence, because it is overmature. It is therefore concluded that the hydrocarbons in the Majiang-Danzhai petroleum reservoir reached the thermal natural gas stage when the Danzhai gold-mercury deposit was formed.

CHAPTER V:

FLUID INCLUSIONS

§ 5.1. Introduction

The association of solid hydrocarbons such as bitumen and paraffin wax with gold and mercury mineralization suggest that oil and/or oilfield brine probably played an important role in the mineralization of the Danzhai gold-mercury deposit. An investigation of ore-forming fluid is necessary to confirm or deny this assumption. Fluid inclusion study has proved to be the most useful tool in unveiling the characteristics of the ore-forming fluid (e.g.: Roedder, 1979, 1984). Generally speaking, fluid inclusion examination can offer the following important information about the ore-forming fluid: (1) temperature; (2) pressure; (3) density; (4) composition and many other characteristics such as the pH and Eh. Obviously, this information is critical in the recognition of the ore-forming fluid of the Danzhai gold-mercury deposit.

A number of fluid inclusion studies have been undertaken on Carlin-type gold deposits in the west of United States by Nash (1972), Radtke et al.(1980), Kuehn and Rose (1986) and Rose and Kuehn (1987). Nash (1972) obtained a homogenization temperature of 175±25 °C, yielding an ore-forming temperature of 200 °C with pressure correction. Slack (Radtke et al. 1980) considered that the consistent presence of both liquid-rich and vapor-rich inclusions in the same mineral plate represented the boiling process and classified three types of inclusions: type I: fluid inclusions contain a liquid and a vapor phase, the bubble usually makes up 5 to 30 percent of the total volume of the inclusion, which are liquid fluid inclusions; Type II: inclusions composed of a liquid and a vapor phase, in which the volume of vapor equals or exceeds that of the liquid phase, which are gaseous fluid inclusions; Type III: inclusions composed of three phases-liquid water, liquid CO_2 and

vapor ($H_2O + CO_2$) phase, which are carbon dioxide inclusions. Radtke et al. (1980) pointed out that no daughter minerals or other phases such as hydrocarbons or iron oxides have been found in any inclusions of any type in Carlin samples. Recently, Kuehn and Rose (1986) and Rose and Kuehn (1987) found pre-ore veins containing both methane-bearing and high-CO_2 inclusions indicative of pressures of formation on the order of $7.5x10^7$-$16x10^7$ pascals. In the ore-forming paragenesis, they found two broad generations of fluids, one a low-salinity, high-CO_2, high-H_2S fluid associated with the gold deposition stage and another low-salinity, low-CO_2 fluid found in late-stage and peripheral minerals. Beside Radtke et al.(1980) no other authors found evidence for widespread boiling of either the ore-depositing fluids or the late-stage fluids and concluded that the ore was deposited through cooling, most likely during the mixing of two distinct fluids.

Hydrocarbon fluid inclusions are found in many sedimentary rock-hosted metal deposits, particularly Mississippi Valley-type (simplified as MVT) lead-zinc-barite-fluorite deposits (Burruss, 1981; Roedder, 1984). Many cases of yellow to brown colored oil-bearing fluid inclusions hosted in fluorite and/or in sphalerite in MVT lead zinc or fluorite deposits are documented (e.g.: Etminan and Hoffman, 1989; Moser et al., 1992; Rankin, 1990; Roedder, 1962, 1984). The oil inclusions in MVT lead-zinc-barite-fluorite deposits are of low maturity, as defined by color and fluorescence.

Some investigations regarding to the Carlin-type gold deposit in the U.S.A. indicated that hydrocarbon fluid inclusions are also present in pre-ore veins. For example, Kuehn and Bodnar (1984) found pyrobituminous material within fluid inclusions in calcite ± quartz ± hydrocarbon veins at Carlin, some methane-bearing fluid inclusions in pre-ore veins described by Kuehn and Rose (1986). These authors considered the hydrocarbon fluid inclusions related to petroleum evolution. None of them considered that gold mineralization in western U.S.A could be related to the petroleum evolution, but rather that the petroleum evolution was prior to gold mineralization.

The relationship between organic inclusions and mercury mineralization in several mercury deposits in the eastern region of Guizhou, including the Wanshan mercury deposit, the Danzhai gold-mercury deposit, the Datongla mercury deposit and the Lula mercury deposit is outlined by Shi (1991). He considered that organic matter plays an important role in the transport and deposition of mercury.

deposit is outlined by Shi (1991). He considered that organic matter plays an important role in the transport and deposition of mercury.

§ 5.2. Hydrocarbon Fluid Inclusions

Hydrocarbon fluid inclusions are the dominant inclusions found in the Danzhai gold-mercury deposit, so they are discussed first.

§ 5.2.1. Classification of Hydrocarbon Fluid Inclusions

All the transparent minerals occurring in the deposit such as quartz, calcite, dolomite, and barite were examined for fluid inclusions as well as two translucent ore minerals, cinnabar and realgar. A variety of hydrocarbon fluid inclusions are ubiquitous, and even dominate in some stages of mineralization. Uncommon high rank hydrocarbon fluid inclusions, such as bitumen inclusions, heavy oil inclusions and paraffin wax inclusions may also be identified.

The classification of hydrocarbon fluid inclusions is based on their optical characteristics. Four types of hydrocarbon inclusions are recognized: (1) Light hydrocarbon inclusions are dominated by methane, which is present as a transparent supercritical fluid instead of a common gas phase. Liquid methane inclusions are ubiquitous, and can be seen in every host mineral of the different mineralization stages. It occurs as different generations, both primary and secondary inclusions; (2) Bitumen inclusions are black to dark brown colored, solid inclusions, also distributed in every mineralization stage. (3) Paraffin wax inclusions, are translucent, colorless or brown-colored solid inclusions at room temperature, usually associated with bitumen inclusions. (4) Heavy oil inclusions are present as oil droplets in aqueous inclusions or in liquid methane inclusions. They are usually black or dark brown in color, either viscous liquid or solid. The last type, heavy oil inclusions are observed only in the second and third mineralization stage, while others are found in every mineralization stage (except the first stage, because the chalcedony and fine-grained quartz is too tiny to host visible fluid inclusions). In addition, there are many fluid inclusions which are a combination of the four components.

Note that the bitumen and paraffin wax inclusions occur as solid phases at room temperature, but they were liquids when they were captured, so these inclusions are considered to be fluid inclusions.

§ 5.2.2. Identification of Hydrocarbon Fluid Inclusions

The hydrocarbon fluid inclusions described above are not commonly observed in metallic ore deposits, so the identification and the generation of these hydrocarbon inclusions as well as their relationship to mineralization and these hydrocarbon inclusions is discussed in detail here.

A. Liquid Methane Inclusions

Light hydrocarbon inclusions are ubiquitous in both metallic and gangue minerals in the Danzhai gold-mercury deposit. Contrary to the general rule, the light hydrocarbon inclusions in these minerals are liquid rather than gaseous phases. They are actually a supercritical methane fluid. These supercritical methane fluid inclusions generally occur as just one phase, except where mixed with solid hydrocarbons such as bitumen or paraffin wax. The light hydrocarbon inclusions appear to be liquid, transparent and colorless, and may easily be mistaken for pure aqueous inclusions. When the inclusions are frozen at -81 - -87 °C, a bubble appears and moves, and the bubble grows as freezing proceeds. In some cases, one or two white, translucent solid phases appear in the process of freezing, which are considered to be paraffin wax dissolved in the liquid methane inclusions (Kvenvolden and Roedder, 1971).

Liquid methane inclusions are an important consituent of the fluid inclusions in ore minerals. For example, irregular-shaped colorless large liquid methane inclusions are present in cinnabar, the most important mercury mineral in the deposit (Plate 5A). Some black inclusions may be dominated by bitumen (Plate 5B). Similarly, liquid methane inclusions are also observed in realgar, although they are quite small and vary from 2 to 6 μm in size. Liquid methane inclusions are enclosed in quartz (Plate 5C), but note that one of them is attached to a cinnabar crystal captured by the quartz. Although most of the wall of

occurrence shows that the inclusions are of primary origin and related to mercury mineralization.

Primary, pseudosecondary or secondary liquid methane inclusions predominate in many gangue minerals as well. Plate 5D shows a well-developed growth zone in a quartz crystal. At high amplification, these growth zones are composed of hydrocarbon inclusions, most of them liquid methane, some are composed of bitumen or paraffin wax, still others are aqueous (Plate 6A). Pseudosecondary liquid methane inclusions in quartz crystals (Plate 6B), and the fluid inclusions in the interior zone are obviously connected to the exterior dark zone, which is dominated by densely-populated tiny liquid methane and bitumen inclusions. Evidently, the interior liquid methane inclusion zone was formed when the exterior zone crystallized. Therefore, the interior liquid methane inclusions are pseudosecondary. There are many liquid methane and some aqueous inclusions hosted in the interior zone (Plate 6C). Secondary fluid inclusions are also commonly observed along healed microcracks, the composition of these secondary fluid inclusions is usually dominated by liquid methane and associated with tiny crystals of cinnabar. Both liquid methane and small cinnabar crystals are hosted in calcite as secondary inclusions, which implies that mercury can be dissolved in the liquid methane. In one instance, a liquid methane inclusion was observed to contain a small cinnabar crystal as well, but it is not clear whether this is a daughter mineral or captured mineral.

B. Bitumen Inclusions

Bitumen inclusions are generally large, their diameter is in the range of 10 to 50 μm. The so-called patch-like pyrobitumen within the crystals of calcite or quartz mentioned in the previous chapter could also be considered as huge solid bitumen inclusions. They are probably the biggest bitumen inclusions in the deposit, commonly several mm in size, and some of them contain pyrite, arsenopyrite or cinnabar.

Bitumen inclusions hosted in quartz, calcite and barite are black and solid phase in room temperature (Plate 6D). A group of single solid phase bitumen inclusions in quartz is shown in Plate 7A, but one of the biggest inclusions which was partly cut in sample preparation can be seen under reflected light. The contrast between the same bitumen inclusion under transmitted and under reflected light is exhibited in Plate 7A and Plate 7B.

Observation under reflected light(Plate 7B) shows that the black colored fluid inclusions in Plate 7A are solid bitumen, and the reflectance of this bitumen inclusions is 2.8% on average.

No color variation of patch-like, stylolite-like, and veinlet bitumen has been seen under transmitted light through the different stages of mineralization. However, the color of bitumen in these inclusions changes with the different mineralization stage. For instance, in the second and third stage, the bitumen inclusions are black (e.g.: Plate 6D, 7A) whereas the bitumen inclusion in the last stage is a brown color. Several bitumen inclusions in the last stage of quartz vein are brown (Plate 7C), some of them occur with liquid methane. The brown bitumen and colorless methane are present in the same inclusion, but their phases are clearly separate, bitumen is solid whereas methane is liquid.

Although some bitumen inclusions are present as a single solid phase, that is, pure solid bitumen inclusions, some of them are composed of two or three phases with mixtures of liquid methane and/or paraffin wax. Plate 7D illustrates a bitumen inclusion with three spheres. The spheres are white compared to liquid methane which is colorless. No change in the physical state was observed during freezing to -180 °C, but they melt when heated to 50 °C. The spheres are not fluorescent, therefore, the three white solid spheres are assumed to be paraffin wax within the black solid bitumen inclusion. Another three component bitumen inclusion is shown in Plate 8A. The three components are bitumen (black), paraffin wax (white, in the upper-right border of the bitumen inclusion) and liquid methane (colorless, separating from bitumen). These two inclusions are actually connected, not separate, but nearly necked down. Plate 8B shows the same situation, where a small bitumen inclusion and a bitumen-bearing liquid methane inclusion are almost necked down

C. Paraffin Wax Inclusions

Paraffin wax is a colorless or white, somewhat translucent, hard wax consisting of a mixture of solid straight-chain hydrocarbons ranging in melting point from 48° to 66 °C. Natural occurring paraffin wax is also called ozokerite or mineral wax, and its color may vary from colorless, light-yellow to dark-brown, depending on admixtures of bitumen.

As with liquid methane inclusions and bitumen inclusions, paraffin wax inclusions are observed in several stages of mineralization. Actually, most occurrences of paraffin wax inclusions are associated either with bitumen, or liquid methane inclusions. Paraffin wax inclusions are as abundant as bitumen inclusions but less common than liquid methane inclusions.

As a rule, if paraffin wax is associated with bitumen, it is usually present as a solid phase (Plate 8C), but if paraffin wax is associated with liquid methane, it can be present as either a solid phase or dissolved in the liquid methane. The solid phase can be observed under the microscope at room temperature while the dissolved phases are seen in the process of freezing.

Paraffin wax inclusions in the Danzhai gold-mercury deposit vary in color from colorless to brown, depending on whether it is mixed with bitumen or not, and the amount of bitumen. The colorless paraffin wax inclusions are generally associated with liquid methane inclusions while the brown ones are associated with bitumen inclusions.

Only a few documented cases are reported about paraffin wax inclusions. They were described as a colorless, birefringent solid phase. In a case reported by Levine et al.(1991), for example, several varieties of organic inclusions are present in the euhedral quartz crystals hosted in fractures in Cambrian-Ordovician carbonate rocks near Quebec city area. The paraffin wax in this example is a white, translucent, fibrous, commonly birefringent solid phase. In the case of the Danzhai gold-mercury deposit, however, the paraffin wax is not birefringent, even though it has the other characteristics described above. On heating, the solid paraffin wax inclusions melt between 60 to 90 °C, which corresponds to the characteristics of paraffin wax.

Unlike bitumen inclusions, paraffin wax inclusions are not commonly documented in ore deposits. Only two references are known in the hydrocarbon inclusion literature, the paraffin wax inclusions in both of these example come from quartz veins in sedimentary rocks, rather than ore deposits. They are actually paraffin wax-bearing fluid inclusions, the paraffin wax is dissolved in or associated with other hydrocarbon constituents or an aqueous phase (Kvenvolden and Roedder, 1971; Levine et al., 1991). These fluid inclusions are

related to petroleum evolution, for example, the organic fluid inclusions hosted in quartz which occurs as fracture fillings in sedimentary rocks of Taconian Allochthon near Québec City are derived from Middle Ordovician carbonaceous shales, and are still within the petroleum window (Levine et al. 1991).

D. Heavy Oil Inclusions

Oil inclusions have been reported in many MVT lead zinc deposits. They are as yellow to brown in color, fluorescent under short-wave ultraviolet light and immiscible with aqueous fluids so that they are quite easily recognized (Kvenvolden and Roedder, 1971, Blasch and Coveney, 1988; Roedder, 1984).

Oil inclusions in the Danzhai gold-mercury deposits seem to be of high maturity, and occur as densely concentrated droplets of dark brown color. The heavy oil droplet inclusions occur in the calcite of the major stage of gold and mercury mineralization (Plate 8D). In one inclusion, several viscous, densely concentrated oil droplets occur together. The adjoining inclusions are probably pure heavy oil inclusions. But none of them are fluorescent. Cinnabar and other metal sulfide are also present in the same calcite crystal which hosts these heavy oil fluid inclusions.

Oil droplet-bearing fluid inclusions are also found in barite in the third mineralization stage. Four dark brown droplets are seen in an aqueous fluid inclusion (Plate 9A), these droplets are probably heavy oil.

Heavy oil inclusions are seen in the second mineralization stage, some oil droplet-bearing inclusions are also observed in barite from the third mineralization stage, but this kind of inclusion is not found in the last stage of quartz veining. The frequency of occurrence of heavy oil inclusions is low, mainly concentrated in calcite, dolomite and barite, no heavy oil inclusions are observed in quartz, whether from the second, third or the last mineralization stage.

§ 5.2.3. Fluorescence of Hydrocarbon Fluid Inclusions

Numerous investigations (Kvenvolden and Roedder, 1971; Burruss, 1981; Levine et al., 1991; McLimans, 1987) demonstrate that hydrocarbon fluid inclusions are strongly fluorescent, so fluorescent microscope examination is a practical way to discriminate between hydrocarbon fluid inclusions. As early as 1898, Reese utilized fluorescence to identify petroleum inclusions in quartz (Roedder, 1984). Kvenvolden and Roedder(1971) and Roedder (1984) considered fluorescence investigation to be a simple and effective way to identify organic inclusions. Recently, Burruss et al.(1980) and Burruss (1981) have demonstrated that the distinctive fluorescence color of various hydrocarbon phases can offer valuable information on the timing of hydrocarbon migration.

Samples from the Danzhai gold-mercury deposit were examined under a variety of conditions. Four different excitation bands 365, 190, 445, and 510 nm were applied. Emission spectra were scanned manually using a quartz wedge monochromator photometer.

Unfortunately, none of the hydrocarbon fluid inclusions, either liquid methane inclusion, heavy oil droplets in the inclusions, bitumen inclusion, or paraffin wax inclusion are fluorescent. One heavy oil inclusion may be an exception, under 365, 190, 445 nm band, it does not fluorescent, but under the 510 nm excitation band, the heavy oil droplet in one inclusion shows a strong red color effect. It is not clear whether it represents fluorescence or not. Evidently, the fluorescent effect of the hydrocarbon inclusions is consistent with that of solid hydrocarbons described in the previous chapter.

The reason why some hydrocarbon inclusions do not fluoresce has been interpreted by Jacob (1983). Organic matter is commonly fluorescent at low grade, but this property is lost with increasing rank. This suggests a fairly high grade of maturity for the hydrocarbon fluid inclusions, which is in good agreement with the results of solid hydrocarbon reflectance. The same argument may explain why the paraffin wax is not birefringent.

§ 5.3. Other Fluid Inclusions

Although hydrocarbon fluid inclusions dominate in every mineralization stage, some aqueous inclusions are also observed in most host minerals. Based on their phases at room temperature, the aqueous inclusions can be classified as follows:

§ 5.3.1 Aqueous inclusions

Liquid inclusion, two phase, liquid and vapor, the volume of the liquid in the inclusion is greater than 50% while the volume of the bubble is less than or equal to 50%. In the deposit, the bubble in this kind of fluid inclusions is usually between 1-15%, especially if the host mineral is calcite or cinnabar.

§ 5.3.2. Gas rich inclusions

Type I: gas inclusions, two phases, vapor and liquid, with the volume of gas in the inclusion being greater than or equal to 50%. The gas in the inclusion can be vapor or water, CO_2, CH_4. Strictly speaking, only the the fluid inclusion with the condition mentioned above and homogenized to pure gas phase may be called a gas inclusion. Gas inclusion usually occur with a group of aqueous fluid inclusions and is believed to represent unmixing.

Type II: Pure gas inclusions, one phase, without liquid, occur in many host minerals, for example, in quartz, cinnabar, calcite and barite as secondary inclusions.

§ 5.3.3. Daughter mineral bearing inclusions

These inclusions can be divided into two types: Liquid + daughter mineral, without vapor phase, is a two phase fluid inclusion. This kind of fluid inclusion occurs occasionally in quartz and also in barite, but is not observed in realgar or cinnabar.

Liquid + vapor + daughter mineral, three phases fluid inclusion, like the type V inclusion, is principally present in quartz and barite.

According to Radtke (1984), daughter minerals are not present in the fluid inclusions of the Carlin gold deposit in western U.S.A. This kind of inclusion with one or even two daughter minerals are observed in the Danzhai mine. For example, two daughter minerals are present in one fluid inclusion of the second mineralization stage (Plate 9B). Both of these daughter minerals are columnar, one with high birefringence and high extinction angle, the other non-birefringent but with parallel extinction.

Carbon dioxide and carbon dioxide-bearing inclusions occur in significant amounts in the Carlin gold deposit, western U.S.A.(Radtke, 1984, Kuehn and Rose, 1986, Rose and Kuehn, 1987), but in the Danzhai gold-mercury deposit, the carbon dioxide inclusions are not observed. Only a few carbon dioxide-bearing fluid inclusions are seen occasionally in the Danzhai deposit, which is also detected by microthermometry study.

§ 5. 4. Distribution of Fluid Inclusions in Relation to Mineralization

A great number of hydrocarbon inclusions such as liquid methane, bitumen, paraffin wax and heavy oil inclusions, together with aqueous inclusions, are hosted in both metallic minerals such as cinnabar and gangue minerals such quartz, calcite, dolomite, barite and in the different mineralization stages of the Danzhai gold-mercury deposit. It is noteworthy that the different types of fluid inclusion are not homogeneously distributed in the different mineralization stages in the deposit.

The first mineralization stage is dominated by gold mineralization, gold-bearing minerals such as arsenopyrite and pyrite are associated with chalcedony and fine-grained quartz. The quartz crystals are so tiny that no fluid inclusions are visible, but pyrobitumen fills fissures and occurs on the border of quartz crystals.

The second mineralization stage is characterized by cinnabar, realgar, orpiment, stibnite, arsenian pyrite and/or pyrite, and accompanied by calcite, dolomite and quartz. Various types of fluid inclusions are present in this stage. Liquid methane and aqueous

inclusions are seen in all the minerals mentioned above. Bitumen inclusions are observed in quartz, calcite and cinnabar, and paraffin wax inclusions are usually associated with bitumen inclusions. Heavy oil inclusions are present in calcite. The liquid methane inclusions demonstrate a close relationship with this stage of mineralization.

The third mineralization stage is constituted of cinnabar, barite, quartz, calcite and pyrite. The fluid inclusions of this stage are also characterized by liquid methane inclusions, bitumen and paraffin wax inclusions are also observed in both barite and quartz. One inclusion containing oil spheres occurs in barite. Aqueous inclusions are not commonly observed.

The last stage of mineralization consists of euhedral quartz crystals, calcite, and some sparsely disseminated arsenopyrite and pyrite. The euhedral quartz is rich in tiny hydrocarbon inclusions. The hydrocarbon inclusions are so densely distributed that the quartz is dark in color under the microscope. Other hydrocarbon inclusions such as bitumen and paraffin wax inclusions are also observed but neither heavy oil inclusions or oil-bearing inclusions are seen in the minerals of this stage. The bitumen inclusions of this stage are brown, differing from the black inclusions of other stages.

The quantity of different fluid inclusions changes from stage to stage, and it is very difficult to quantify the different stages. The proportion of the different types of fluid inclusions in different mineralization stages is quantified in Fig. 5.2.

§ 5.5. Salinities and Homogenization Temperatures of Aqueous Inclusions

The microthermometric studies were carried out on doubly polished thick sections using a Chaixmeca and a USGS heating and freezing stage (Roedder, 1984). Microthermometric results are summarized in Fig. 5.1, which shows the salinity variations between different stage of mineralizations. The recorded salinities vary between 5.2 and 19.3 wt.% NaCl eq. with a mean salinity of 7.3 wt% NaCl eq. Most salinities of aqueous inclusions are in the range of one to two times the salinity of seawater (3.2 wt% NaCl), only

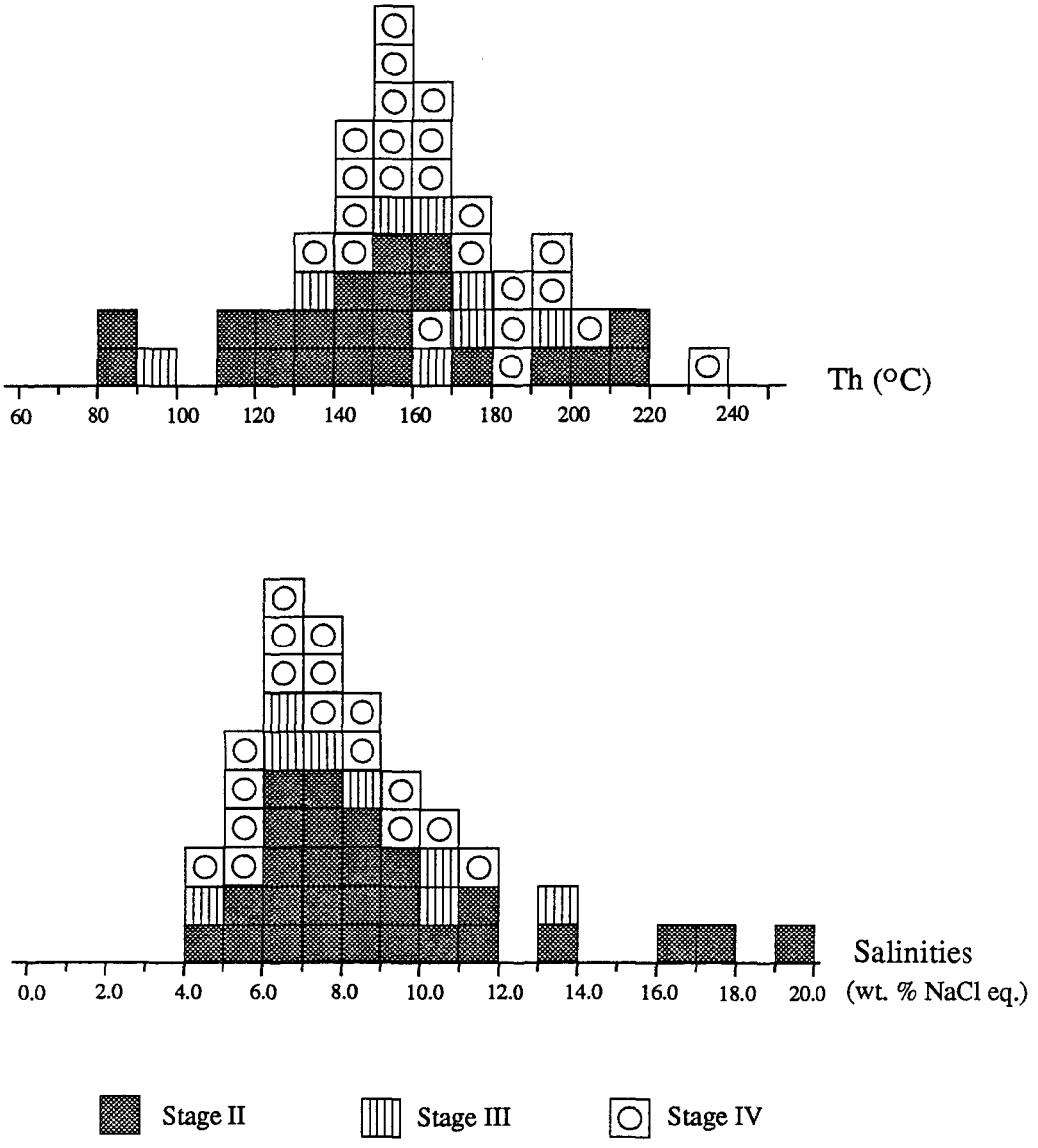

Fig. 5.1 Hostograms of homogenization temperatures and salinities of aqueous inclsuions from different mineralization stages in the Danzhai gold- mercury deposit.

a few samples exhibit higher salinities. No significant variation of the salinities of aqueous inclusions are displayed from stage to stage of mineralization.

Obviously, the salinities of aqueous inclusions in Danzhai are higher than that of the Carlin-type gold deposit, western U.S.A. For example, a fluid inclusion study from the Meikle Mine, Carlin Trend, Northern Nevada indicates a salinity range of 1.7 to 2.5 wt % NaCl equivalent (Lamb et al., 1992). Note that this is even considerably lower than seawater salinity (3.2%). Even though they are considerably higher than that of the Carlin-type gold deposits in western U.S.A., the salinities of fluid inclusions in Danzhai are significantly lower than Mississippi Valley-type lead zinc deposits. Many investigations show that the salinity of MVT lead zinc deposits generally exceeds 15 wt.% NaCl equivalent, and frequently exceed 20 %, yet NaCl daughter minerals are almost never found. All examples of salinities under 10 % are from secondary inclusions or very late-stage minerals (Roedder, 1967).

The fluid inclusion survey of sedimentary diagenetic environments by Roedder (1979) gave a general impression that the fluid inclusion salinity in these environments is high. For example, the fluid inclusion salinities from crystal-line geodes, vugs and veins in sediments are moderately to strongly saline (16 - 25 % NaCl eq.). The freezing temperatures of fluid inclusions in diagenetic sphalerite hosted in bituminous coals from coal mines in central Missouri corresponds to a strongly saline brine (>22 % Na eq.) (Roedder, 1984). Therefore, as summarized by Roedder (1979), most environments of sedimentary diagenesis, at least those recorded by fluid inclusion, involved the presence of a saline brine. However, this general conclusion is challenged by some recent fluid inclusion investigations in natural gas fields. As an example, Wang et al.(1991) reported that the gas field brine in the Weiyuan gas field, Sichuan Province, China has a salinity ranging from 4.3 - 17.0 wt.% NaCl equivalent, and the salinities in Chuanzhong oil field, Sichuan Province, China are between 7.1 - 11.6 wt. % NaCl equivalent. So, not all oil field brines are highly saline, but are certainly more saline than seawater. The salinities of fluid inclusions in Danzhai are equivalent to the Weiyuan gas field and the Chuanzhong oil field in Sichuan Province, Southwest China.

The homogenization temperatures of fluid inclusions vary from 130 to 210 °C, most of them concentrate in the range of 140-180 °C. No significant variations of homogenization temperature are observed from stage to stage of the mineralization. Fluid inclusion investigations of sedimentary diagenetic environments show that the temperatures are low, in the range of 45 to 150 °C (e.g. Roedder, 1979). MVT lead zinc deposits, particularly deposits in the United States, show that during the ore-forming stage, temperatures were generally between 100° and 150°C, and rarely as high as 200 °C. Oilfield brines are considered to be the analogue of the MVT deposits ore-forming fluid(Sverjensky, 1984, 1987). The temperature range of these deposits corresponds to the temperatures of present-day oilfield brines. The temperatures of the brines in natural gas fields are significantly higher those of the oilfield brines. For instance, fluid inclusions in overgrowth calcite and in calcite and quartz filling in geodes, vugs and cracks of the dolomite reservoir in the Weiyuan gas field show that the temperatures range from 80-160 °C to 200-240 °C. The usual temperature range of oilfield brine is 80-160 °C, and the temperature range of the gas field brine is 200-240 °C. Hydrocarbons will thermally crack into methane at higher temperature, so the hydrocarbons had evolved to the overmature stage. Investigations described earlier indicate that the hydrocarbons in the study area are in the overmature stage.

§ 5.6. Microscopic Evidence for Unmixing

Fluid unmixing is observed in all stage of mineralization. Unlike the boiling condition found in many ore deposits, the unmixing recorded by fluid inclusions in Danzhai is the result of immiscibility between aqueous and hydrocarbon phase, particularly liquid methane.

Two major fluid inclusion types occur intimately associated in the same planar arrays indicating that they were trapped under the same conditions in the presence of a mixed fluid of coexisting hydrocarbon and brine, although their homogenization temperature and salinities are quite different.

A subhedral quartz crystal occuring in a bitumen veinlet, in which metal sulfides such as cinnabar, arsenopyrite, pyrite are present, is assumed to have being co-precipitated with the hydrocarbon veinlet and the metal sulfides. The host mineral of the hydrocarbon veinlet

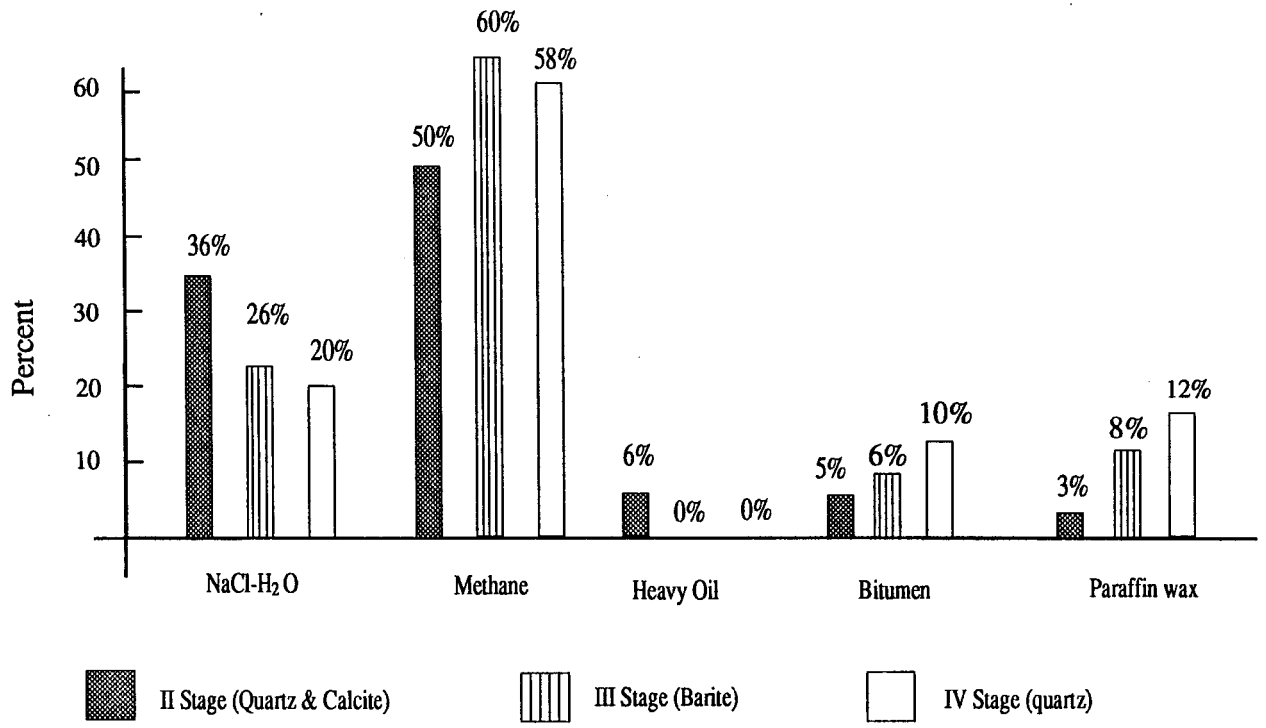

Fig. 5.2 The relative abundance of different type fluid inclusions in the different mineralization stages.

is calcite. A group of fluid inclusions in this quartz crystal (Plate 9C), probably represents the unmixing assemblage of an aqueous and a hydrocarbon fluid. Bitumen-bearing liquid methane inclusions, aqueous liquid inclusions, and gas inclusions are present in this unmixing assemblage. These inclusions have a similar size and are not aligned, no microcrack was observed in this tiny subhedral quartz crystal. The isolated, randomly distributed occurrence of these fluid inclusions suggest that they are primary inclusions. It is therefore considered that they represent an unmixing assemblage.

Fluid inclusions in the growth zones of quartz shown earlier (Plate 5D, 6A), are dominated by hydrocarbon inclusions, particularly liquid methane inclusions, but some aqueous inclusions are rarely seen in the growth zones. All of these fluid inclusions contained within growth zones are considered to be primary in origin. The closely spatial association between aqueous and hydrocarbon inclusions may imply that these primary inclusions were trapped under the same conditions from a mixed fluid of coexisting hydrocarbon and brine. and are the result of unmxing of liquid methane and brine.

Liquid methane inclusion and aqueous inclusion are commonly observed coexisting in the same crystal (Plate 9D). They are probably primary inclusions since they are randomly distributed do not occur along a healed crack.

Hydrocarbons can dissolve in water, and water can be dissolved in liquid hydrocarbons (Price,1978 a,b; 1979; Price et al., 1983). The solubility of hydrocarbons in water depends on temperature and pressure. For example, methane solubility greatly increases with increasing pressure in the high temperature range (T> 300 °C) whereas it is almost stable with increasing pressure at lower temperatures (70 - 250 °C). Methane solubility is sensitive to temperature variation in a wide pressure range, and increases quickly with increasing temperature.

The appropriate temperature for the Danzhai gold-mercury deposit lies in the lower temperature range (70 - 250 °C), so pressure deviation is unlikely play an important role in the unmixing of hydrocarbon and brine, but the temperature decrease is probably a significant factor leading to the unmixing.

§ 5. 7. Study of Fluid Inclusions by Solid Probe Mass Spectrometry

The microscopic fluid inclusion investigation demonstrates that the fluid composition in the Danzhai gold-mercury deposit is different from that of the Carlin-type gold deposits in the western U.S.A. It is obviously necessary to test the result of this observation by analyzing the composition of these fluid inclusion.

Recently, Guha et al.(1990, 1991) developed a method to determine the volatile composition of fluid inclusions using solid probe mass spectrometry. Compared to commonly used mass spectrometric and gas chromatographic methods (e.g.: Baker and Smith, 1986), the most important advantages of this technique are as follows (1) Some error sources in mass spectrometric techniques are reduced, for example, gases dissipated during grinding or by catalytic reactions, gases released from the walls of the chamber and the pump, and problems linked to the introduction of gases in the source or ionization chamber are avoided. (2) A small amount of sample material is needed so that the experimental results can be correlated with specific inclusion types. (3)The fluids unmixing can be recognized by comparing the decrepitation temperature with the spectra of specific inclusion types. (4) Its capability to match the presence of gases in inclusions in quartz with those in associated sulfides, accordingly confirming or denying the presence of similar fluids which were trapped by both gangue and ore minerals.

§ 5. 7. 1. Experimental Procedure

The the critical steps of the experimental procedure are outlined here as described in detail by Guha et al.(1990). The most important part of the analytical system, is a temperature programmable solid probe insert, fitting directly onto the ion source of a VG-12-1250 mass spectrometer. The sample tube is held tightly at the level of tube holder and therefore permits adequate contact with the heater. The heating rate of the probe can change from 0 to 750 °C per minute in steps of 0.1 °C and can be programmed to run between ranges of temperature.

Before analysis, the samples are examined under the microscope in order to characterize the types and generations of fluid inclusions as well as their decrepitation temperatures. The part to be analyzed is then cut from the sample for specific analysis. The fragments are first heated for 12 hours at 100 °C to eliminate adsorbed water. The probe tip and the sample tube are heated in the mass spectrometer under vacuum at 650 °C for 10 min. If no gases are detected after this procedure, the sample is then put in the sample tube and the probe is again heated to 100 °C for a few minutes before analysis. The probe with the sample is then inserted into the mass spectrometer and heated under high vacuum. The heating ranges for this study are from 100 to 500 °C, at 20 °C a step, and are programmed separately for each analysis.

The emissions from bursts of fluid inclusions have been analyzed by the Single Ion Monitoring (SIM) program, which examines an assigned m/e value for each desired channel. The channels are chosen by relative abundance of components from scanning all possible volatile components. The selected channels for this study are CH_4, H_2O, H_2S, CO_2, N_2 and some heavy hydrocarbons (the maximum capability of the machine is to monitor 26 channels at the same time). The detection limit of this experiment can be as low as sub-picogram.

A computer program (VG Software) integrates surface areas of peaks produced by the decrepitations and automatically traces the baseline above background. The background is therefore completely eliminated from the entire spectrum. The program creates a data base of relative abundances of gases from which any desired ratio can be calculated.

§ 5. 7. 2. Sample Preparation

All samples examined were quartz, which contain fluid inclusions of several types and origins. Consideration was taken to select representative samples for every mineralization stage, that is, the second, third and last stage of mineralization. Unfortunately, the crystals of chalcedony are too small to find visible fluid inclusions under an ordinary optical microscopes, so no sample of the first mineralization mineralization was tested. Care was also paid to different type of fluid inclusion too, particularly the hydrocarbon and the aqueous group, which were preselected under the microscope.

Secondary fluid inclusions were avoided in the preselection of samples, even though some secondary fluid inclusions occur along microcracks, most of them are filled with liquid methane and tiny cinnabar crystals.

Eight quartz sample were tested for light gases which dominate the fluid inclusions and proved the high accuracy for the solid mass probe spectrometry analysis (Guha et al., 1990; 1991). Three quartz samples H5D, H5E, H5Eb from two different parts of the same thin section S_4-01, associated with cinnabar, arsenopyrite and pyrite from the second mineralization stage. H5D was selected from the part dominated by aqueous inclusions while both H5E and H5Eb were taken from the part dominated by liquid methane inclusions. The parts are divided into two sample for analysis to compare results and to calculate the accuracy of analysis. H5F was chosen from sample Sx-01, which is associated with cinnabar, realgar, orpiment and calcite, in which both silicification and carbonatization are present. Unlike other samples selected, this sample was taken by chance, not preselected. H5H was also taken randomly from sample S5-03, which is associated with barite, quartz and cinnabar from the third mineralization stage. Both H5B and H5C were preselected from different parts of the sample S4-02, H5B represents the aqueous inclusions whereas the H5C contains liquid methane inclusions.

Three other quartz sample were tested for heavy hydrocarbons by Solid Mass Probe Spectrometry analysis. H5I(S_4-04), H5J (S_5-07) and H5K (S_4-18) were examined for heavy hydrocarbon from the second, third and last stage of mineralization respectively. Some heavy oil inclusions are observed under the microscope in H5I (S_4-04).

§ 5. 7. 3. Experimental Results

The analytical results are consistent with the microscopic observations (Table 5.1). Hydrocarbons, particularly liquid methane are dominant in these fluid inclusions. In the group of liquid methane inclusions, analysis indicates that methane abundance ranges from 51.48 to 68.15 mole percent. An unexpected result was the high methane abundance in the aqueous group, usually in the range of several percent, the highest being 44.91 mole percent. The content of N_2 in the samples is consistently low, in the neighborhood of 1 mole percent, but with one exception, N_2 is as high as 13.88 mole percent in sample H5H.

Table 5.1 Volatile composition in the fluid inclusions analyzed by Solid Mass Probe Spectrometry (Mole percent)

No.	Sample	CH_4(16)	H_2O(18)	N_2(28)	H_2S(34)	CO_2(44)
H5B	S_4-20	15.89	80.87	1.17	0.98	1.89
H5C	S_4-20	68.15	27.41	1.89	0.00	2.55
H5D	S_4-01	4.30	79.40	1.43	0.02	15.02
H5E	S_4-01	67.41	28.37	1.47	0.00	2.75
H5Eb	S_4-01	59.13	37.50	1.11	0.01	2.27
H5F	S_x-01	63.76	31.69	1.72	0.00	2.83
H5G	S_2-10	44.91	51.48	1.85	0.00	1.76
H5H	S_5-16	5.50	58.33	13.88	0.31	21.97
H5I	S_4-04	38.56	56.82	1.20	0.10	1.67
H5J	S_5-07	67.91	29.23	0.86	0.00	1.98
H5K	S_4-18	61.47	34.89	1.12	0.01	2.47

The H_2S in all these samples is always low, consistently less than 1 mole percent, usually 0.01 mole percent. The CO_2 content of in these samples is low as well, commonly 2 mole percent. Two exceptions should be noted, one in sample H5H, of 21.97 mole content of CO_2, another is from sample H5D, 15.62% CO_2. Both of these are aqueous inclusions.

Heavy hydrocarbons are also detected, the masses of significant quantity are 76, 104, 148, 193, 200, 204 (Fig. 5.3). It is not known what kinds of hydrocarbon molecules these masses represent, these are of low abundance compared to the common components such as CH_4 and H_2O, the highest content among them with a mass 200, constituted 0.57 mole percent of sample of H5I.

§ 5. 7. 4. Discussion

The remarkably high CH_4 content of the fluid inclusions in the samples from the Danzhai gold-mercury deposit has been confirmed as a dominant and/or common component, consistent with microscopic observations. The analyzed data corroborate that the composition of the fluid inclusions from the Danzhai gold-mercury deposit is not completely comparable to that of the Carlin-type gold deposits in the western U.S.A. (Kuehn and Rose, 1986; Rose and Kuehn, 1987), but is in good agreement with that of the other mercury deposits in the same area documented by Shi (1991).

The decrepitation temperature of methane tends to be lower than that of other gases such as H_2O, CO_2 and H_2S. The most important peaks of CH_4 usually vary from 150° to 400 °C. This trend, however is not seen in other components. For example, the decrepitation temperature for the important peaks of H_2O, CO_2 and H_2S depend on the sample. No significant peaks of any components are present at temperatures higher than 500 °C. Microscope examination of the analyzed quartz chips confirm that all visible fluid inclusions decrepitated in the experiment.

The spectra of samples from the second mineralization stage demonstrate that although inclusions may have a high CH_4 or H_2O content, all the inclusions show a mixture of both. For example, in sample H5B (from sample S_4-02), methane spectra extend over a wide range from 150 to 500 °C, while that of other gases such as H_2O, CO_2, N_2, H_2S also

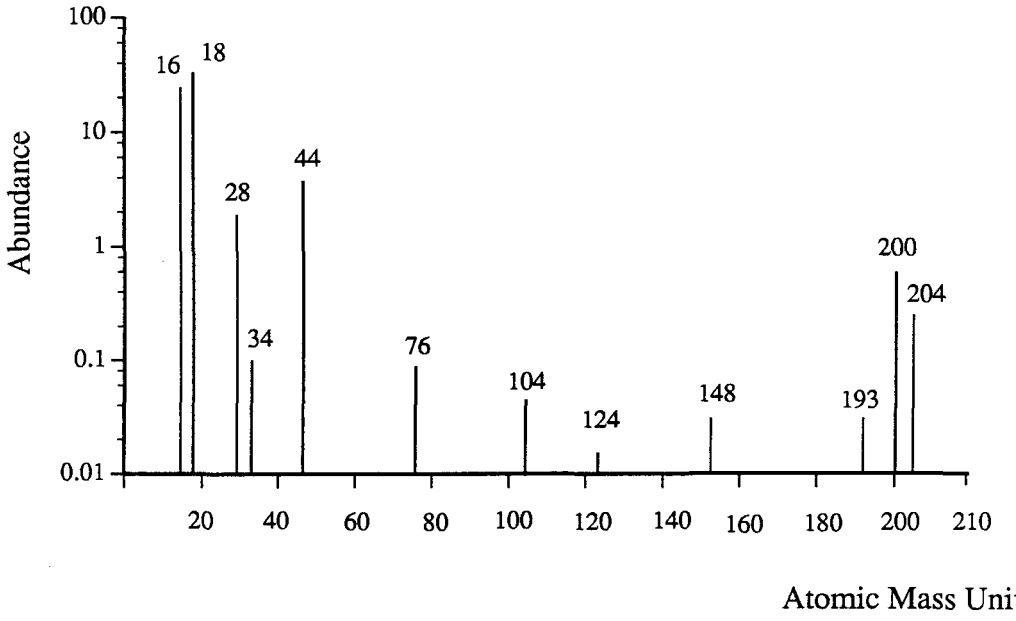

Fig. 5.3 The relative abundance versus mass showing the presence of CH_4(16), H_2O(18), N_2(28), H_2S (34), CO_2(44) and other masses such as 76, 104, 124, 148, 193, 200, 204. The exact hydrocarbon molecules of the these masses is unknown.

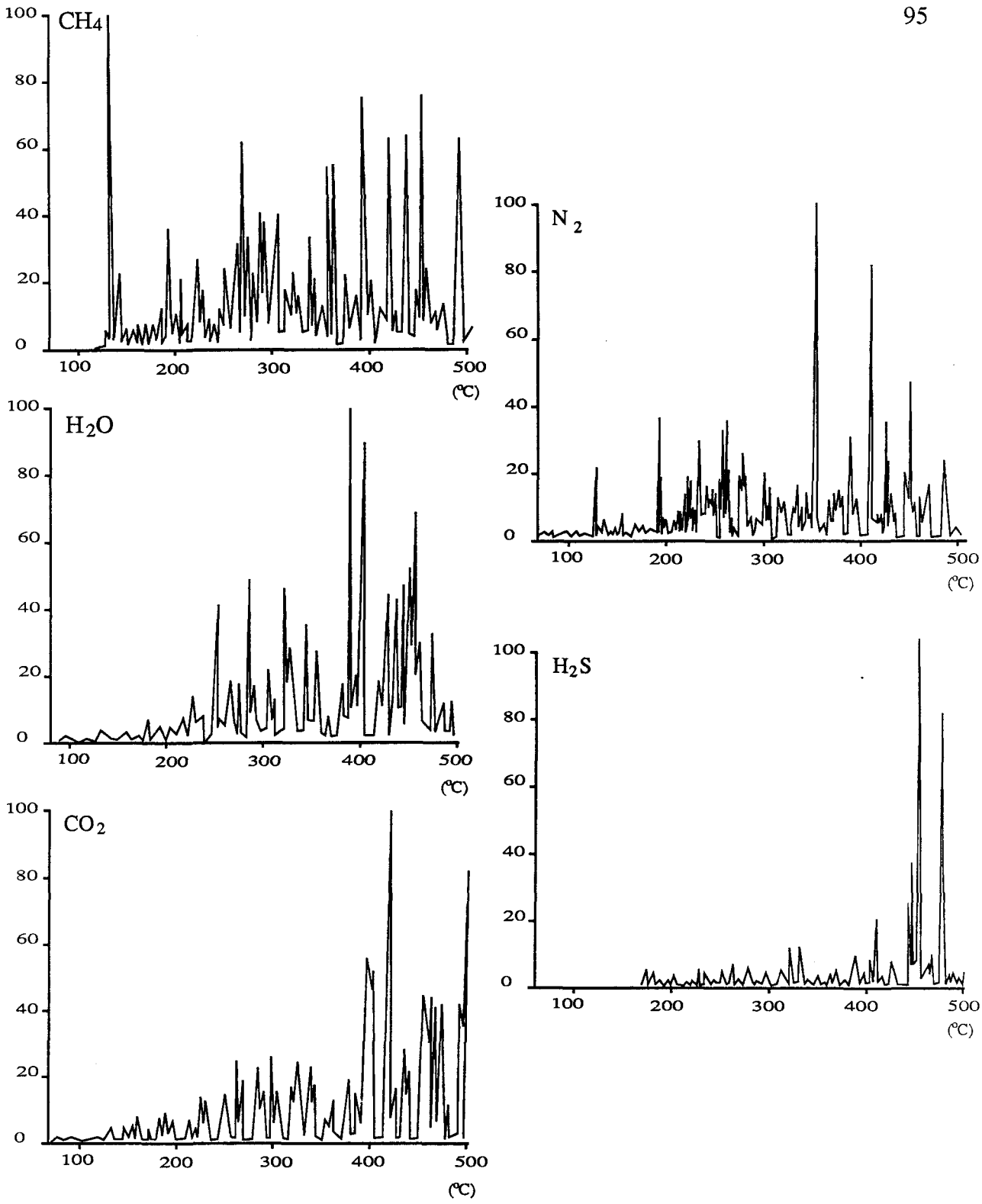

Fig. 5.4 Mass spectra of fluid inclsuions of sample H5B, showing the spectra of CH_4being widely distributed while the spectra of other gases such as H_2O, CO_2, N_2, and H_2S tend to concentrate in the high temperature range (350 -500° C).

exhibit a wide range, from 350 to 500 °C (Fig. 5.4). It is therefore considered that these gases are hosted in the same types of fluid inclusions at least in the higher temperature range. This tendency is also seen in the inclusions from the third and the last mineralization stage.

One of the major concerns in the analysis of the composition of fluid inclusions in the Danzhai gold-mercury deposit is the mechanism of the deposition of gold and mercury. Microscope investigation of the fluid inclusions described earlier shows that unmixing is possible in this deposit. One advantage of solid probe mass spectrometry study is the ability to analyze the mass spectra of the gas at various temperatures of decrepitation. Unmixing between methane and oilfield brine may be the cause of deposition of ore-forming elements. For instance, a rapid drop in pressure would probably purge the CH_4 and CO_2 from the aqueous phase, or inversely, purge the H_2O from liquid methane (in this case, methane is the dominant phase and in the other case, water is the dominant phase). Peaks resulting from the release of the gases occur at distinct temperatures may reflect decrepitation of inclusions of different composition (Guha et al., 1991). Fluids that have experienced extreme CH_4-H_2O unmixing will form inclusions with CH_4- and H_2O-rich end members decrepitating at distinct temperatures. Even though the decrepitation of fluid inclusions is determined by various factors, these populations of distinct fluid inclusion types will be automatically discriminated by comparison of mass spectrometer spectra of distinct gas phases over total bursts. A spectra (H5E) from sample S4-01, the second stage of mineralization, displays a complete separation indicating complete unmixing of the CH_4 and H_2O phases. The most important methane peaks are in 180 to 250 °C range whereas those of H_2O extend from 380 to 460 °C (Fig. 5.5). H5E is a methane dominated sample, in which the CH_4 content is 59.13 mole percent and that of H_2O is 37.50 mole percent. The CO_2 content of this sample is low, only 2.27 mole percent, it shows no peak separation in the spectra. This does not mean no phase separation occurs since the separated phase may have the same decrepitation temperature. Another spectrum (H5H) from the sample S5-03, the third mineralization stage, however, displays a complete separation indicating a marked unmixing of H_2O and CO_2 phases (Fig.5.6). The most significant spectra of H_2O are concentrated between 350 and 450 °C while those of CO_2 are focused in a narrow range from 450 to 500 °C. H5H is a H_2O dominated sample, in which the H_2O content is 58.33 mole percent, and CO_2 is 21.97 mole percent. The CH_4 content is low, only 5.50 mole

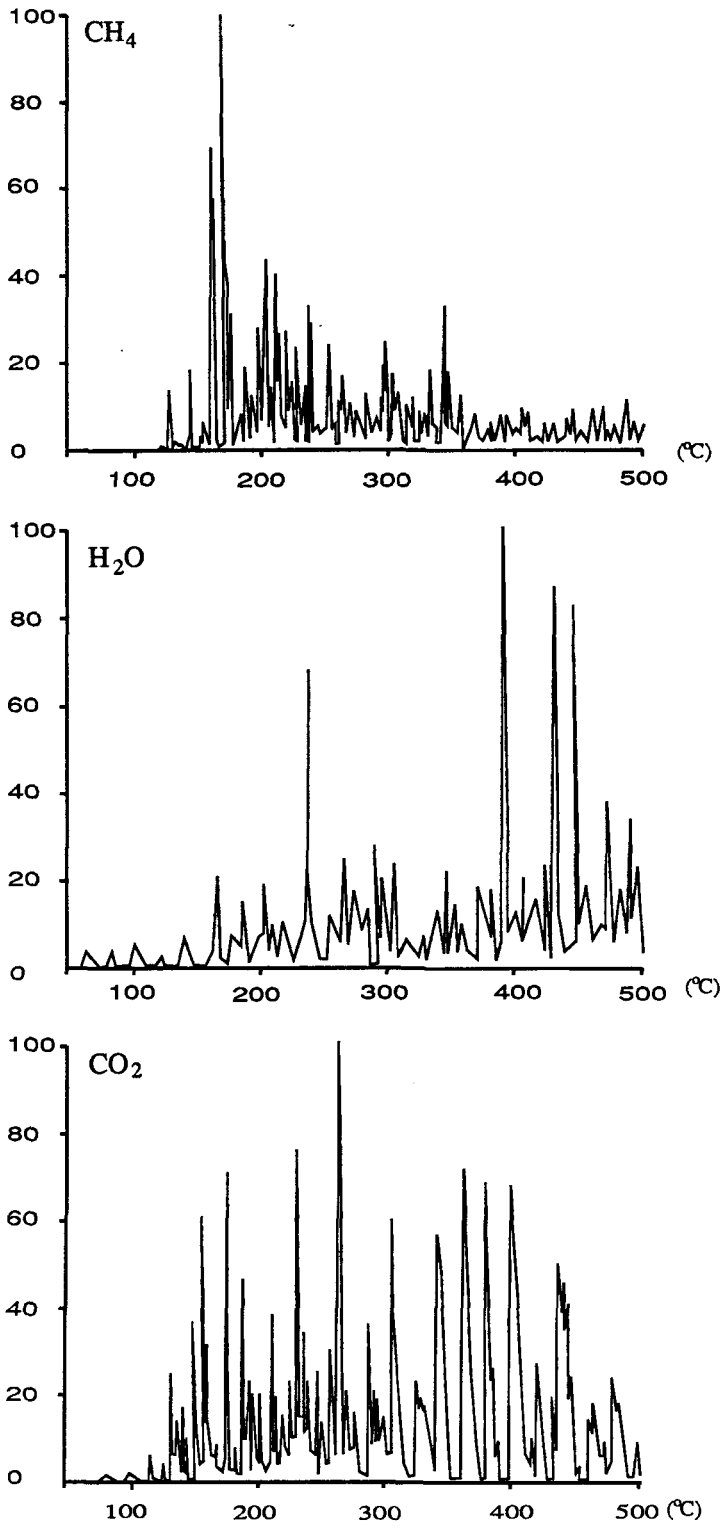

Fig. 5.5 Mass spectra of fluid inclusions of sample H5E showing the unmixing of CH_4 and H_2O that the peaks of CH_4 extend from 180 to 250 °C while the peaks of the H_2O spectra are concentrated in the temperature ranges from 390 -500° C. CO_2 shows no phase separation.

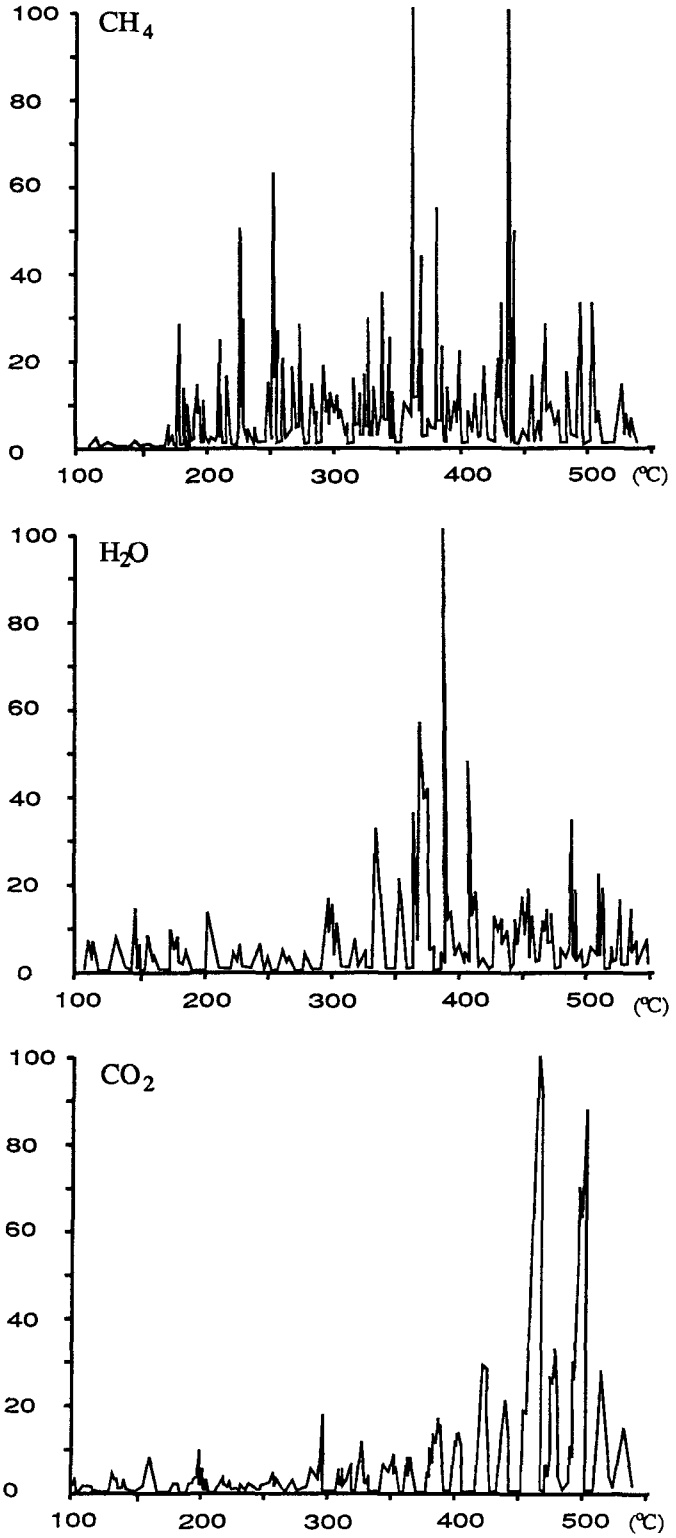

Fig. 5.6 Mass spectra of fluid inclusions of sample H5H indicating unmixing of H_2O and CO_2. the spectra of H_2O extend from 350 to 450°C while two important peaks are present in the temperature from range 450 to 500°C. The CO_2 content in this sample is 21. 97 mole percent.

percent, it displays no peak separation spectra . For the last mineralization stage, neither CH_4 - H_2O peak separation spectra nor CH_4 and CO_2 peak separation spectra is shown by the mass spectra comparison, but this does not mean that phase separation did not occur since some evidence of unmixing is observed under the microscope. It is reasonable to presume that unmixing of CH_4-H_2O, or H_2O-CO_2 is the mechanism of the deposition of gold and mercury in second and third mineralization stages.

The H_2S content of fluid inclusions is consistently lower than other common components. In two of the analyzed quartz samples, H5B(S4-02) and H5H (S5-03), the H_2S content is as high as 0.98 mole percent and 0.31 mole percent respectively. The spectra of H_2S of H5B, shown in Fig. 5.4, seem to correspond to the high temperature spectra range of methane, which probably suggests that H_2S is dissolved in the liquid methane.

§ 5.8. Summary

The investigation of fluid inclusion in different host minerals and different mineralization stages in the Danzhai gold-mercury deposit reveal some surprising information about the ore-forming fluids.

A variety of hydrocarbon inclusions are found in the deposit studied, which include (1) liquid methane inclusions; (2) bitumen inclusions; (3) paraffin wax inclusions; (4) heavy oil inclusions, and various combinations of all above. Heavy oil inclusions are only present in the second mineralization stage and some heavy oil-bearing inclusions are seen in the third mineralization stage. Other hydrocarbon inclusions are observed in various mineralization stages. Some solid hydrocarbon inclusions, paraffin inclusions, for example, are not a commonly observed component in the ore deposit.

Hydrocarbon inclusions predominate in a variety of minerals in different mineralization stages. Liquid methane inclusions are found in both metal minerals such as cinnabar and realgar as well as gangue mineral such as quartz, calcite, dolomite and barite. The heavy oil inclusions tend to concentrate in carbonate minerals such as calcite and

dolomite. The spatial relationship between the liquid methane inclusions and cinnabar and realgar demonstrates that the hydrocarbon inclusions are a significant part of ore-forming fluid. Fluid inclusion observation suggests that the liquid methane or supercritical methane fluid probably has the capability of dissolving mercury and other ore-forming elements .

The fluorescence of hydrocarbon is commonly used as a critical feature to discriminate among the hydrocarbon inclusions. All types of hydrocarbon inclusions in the Danzhai gold-mercury deposit, however, have lost their fluorescent property. This suggests that the hydrocarbons in the deposit studied are overmature.and corresponds to the results obtained by bitumen reflectance previously described,

A variety of aqueous inclusions are also observed in the host minerals, but no carbon dioxide-rich inclusions were noted. The salinities of these aqueous inclusions are in the range 5.2 to 19.3 wt. % NaCl equivalent, which are considerably higher than the salinities of fluid inclusions in Carlin-type gold deposits in western U.S.A., but lower than the fluid inclusion salinities of MVT lead zinc deposits. Homogenization temperatures of the fluid inclusions are from 130 - 210 °C, considerably higher than an oilfield brine, but equivalent to a gas field brine.

The tremendous quantity of hydrocarbon components in the fluid composition of the studied deposit demonstrated that the ore-forming fluid in the Danzhai gold-mercury deposit is different from that of Carlin gold deposit in the western U.S.A, even though other geological characteristics are quite similar.

The types of hydrocarbon inclusions and the ratio of hydrocarbon inclusions over all fluid inclusions are unique in an individual ore deposit. Even though some oil inclusions are present in the MVT lead-zinc-barite-fluorite deposits, generally, these hydrocarbon inclusions do not dominate in the deposits, but are just a minor constituent of the ore-forming fluid. The hydrocarbons are usually of low or middle maturity so they are usually fluorescent. The hydrocarbon inclusions in the Danzhai gold-mercury deposit, however, are the dominant inclusion type in the ore-forming fluid for various mineralization stages. Obviously, the hydrocarbon component in the deposit may have played an important role in the migration and deposition of ore-forming elements.

It is certain that the types and characteristics of hydrocarbon components are distinct from the hydrocarbons reported from a variety of ore deposits. They are quite similar to that of thermogenic natural gas fields. Many cases show that thermogenic natural gas is dominated by methane inclusions and associated with other hydrocarbon inclusions such as bitumen and heavy oil inclusions. The hydrocarbons in a thermogenic gas field lose their fluorescence since they are usually subjected to a higher temperature than that of common oilfields.

The solid probe mass spectrometry study confirms that the hydrocarbon components, particularly methane, are the most important constituent of the fluid inclusions. The methane content of some inclusions is as high as 69.8 mole percent. Some heavy hydrocarbon molecules are also seen in the mass spectra.

Comparison of mass spectrometer spectra of distinct gas phases over total bursts show the spectra displaying a complete separation indicating unmixing of CH_4 and H_2O phases in the second mineralization stage. Another spectrum, however, displays a complete separation indicating unmixing of H_2O and CO_2 phases in the third mineralization stage. It is thus reasonable to presume that unmixing of CH_4-H_2O, or H_2O-CO_2 is the deposition mechanism for gold and mercury in the second or third mineralization stages.

CHAPTER VI:

ARGON ISOTOPE INVESTIGATION OF QUARTZ ASSOCIATED WITH MINERALIZATION

§ 6.1. Introduction

The field geological investigation, petrographic observation and fluid inclusion examination in the Danzhai gold-mercury deposit reveal that the gold and mercury mineralization is likely related to regional petroleum evolution. This relationship has been examined by isotopic studies which offer additional information regarding the origin of ore-forming fluids.

Isotope studies were undertaken to complement previous efforts to trace the origin of the deposit (Zhang, 1983; Chen et al., 1986). Both these studies reported that the sulfur isotopic composition of the Danzhai gold-mercury deposit is of sedimentary origin. Zhang (1983) reported $\delta^{34}S$ values of 20 cinnabar samples, ranging from +11.5 to 22.5 ‰, with an average of 17.2 ‰, Chen et al.(1986) examined 15 samples of cinnabar, with an average value of + 17.05 ‰. These results are identical with those determined for sedimentary rocks of the region (Hua, 1982)(Fig. 6.1). Various investigations indicated that the sulfur isotopic composition of cinnabar or stibnite in all of the mercury, antimony and gold deposits in the East Guizhou region, is homogeneous and rich in the heavy sulfur isotope ^{34}S, that is to say, the $\delta^{34}S$ value in these deposits is always positive, ranging from 10 to 20 ‰ $\delta^{34}S$. These sulfur isotope values indicate that the sulfur has been derived from sedimentary rocks (e.g.: Brown, 1967, Field, 1966).

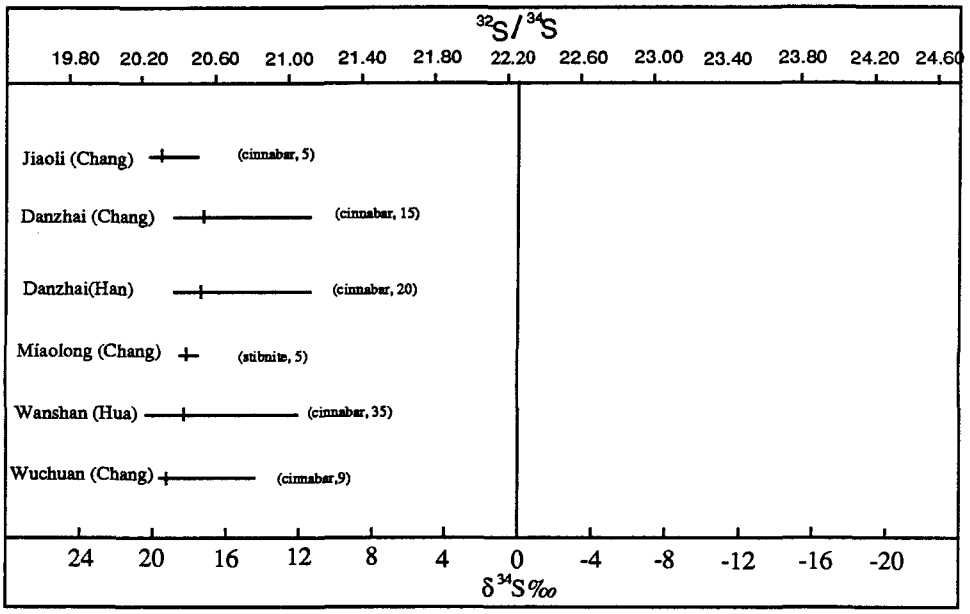

Fig. 6.1 Sulfur isotopic composition of mercury, gold and antimony deposits in the eastern Guizhou region(compiled after Chen et al. (1986), Hua (1982) and Zhang(1983)). The Jiaoli gold-mercury deposit, Danzhai gold-mercury deposit, Miaolong gold-antimony deposit, Wanshan mercury deposit and Wuchuan mercury deposit are all hosted by Cambrian or lower Ordovician carbonates (Number of samples analyzed is within brackets).

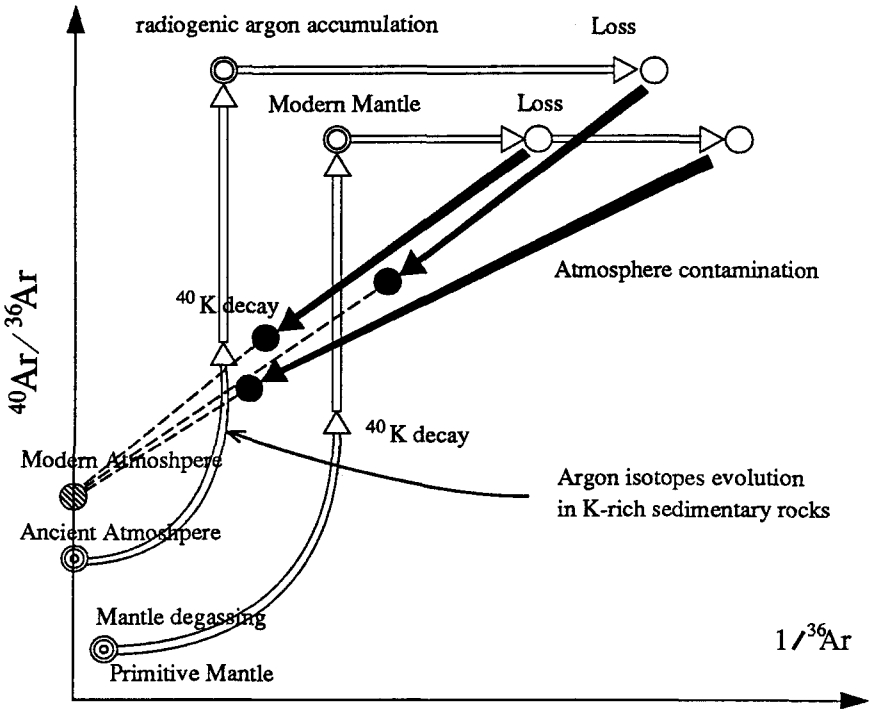

Fig. 6.2 Two different evolution paths for Argon isotopes: 1. Mantle degassing, evolution and contamination with atmosphere; 2. K-rich sedimentary rocks *in-situ* K-decay and radiogenic argon accumulation and mixing with atmosphere.

These studies point out that the source of sulfur in the sulfide minerals in the Danzhai gold-mercury deposit is the host sedimentary rocks. However, sulfur of sedimentary origin in a deposit does not mean that all of the ore-forming materials such as gold and mercury are also of the same origin. For example, an ore-forming fluid of deep derivation may mix with sulfur-rich formation water in the sedimentary rocks and result in the metal sulfide deposition. Therefore, other isotopic studies are necessary to investigate the source of the other ore-forming elements.

Argon isotopes may be applied to trace the origin of mineralization. The first important feature is that the principal ore-forming elements are Hg, Sb, As and Au. Apart from gold, Hg, Sb and As are the most prominent ore-forming elements or so-called "active" ore-forming elements (Tu, 1983). In the family of the ore-forming metals, Hg is a metal that is the easiest to transport as a volatile phase at low temperature in the process of mineralization (White et al., 1974, Varekamp and Busack, 1981). Another important feature is that methane, an evident volatile component, was concentrated in the ore-forming fluid. In this situation, noble gas isotopes such as argon may provide a useful tool to reveal the origin and history of the ore-forming fluid. Unlike other active elements which are continually transferred between solid and fluid phases to a degree that often masks their original sources, argon is a noble gas, unreactive with other components and without a phase transformation, so argon is always a gaseous phase under crustal and mantle conditions. Argon isotope investigations show that, even in a deep sedimentary basin, the atmospheric isotopic composition of argon is preserved in materials and their abundance pattern is recognizable (Cadogan, 1977, Mazor and Bosch, 1987). The associated water and oil of some natural gas fields are reported dominated by atmospheric argon (Podosek and Honda, 1980; Bosch and Mazor, 1988; Nagao et al., 1981). The application of the ^{40}Ar-^{39}Ar dating technique to minerals containing fluid inclusions may open a new way of studying the sources and interactions of fluids in the crust as well as dating the minerals hosting these fluids (Kelley et al., 1986; Turner, 1988; Turner et al., 1990; Turner and Wang, 1992).

As with other isotopes, the composition of argon isotopes principally depends on its source. Generally speaking argon isotopes may have three distinct provenances which are distinguishable: 1. the mantle or lower crust (primary or initial argon); 2. the atmosphere;

and 3. the ^{40}K decay. The relationship of argon between these sources is outlined in Fig. 6.2.

In the first case, the K-Ar method may be used to date potassium rich minerals such as K-feldspar or mica. In the Danzhai gold-mercury deposit, however, the host rocks are carbonates, and no potassium rich minerals occur in the vein, ore or alteration. Accordingly, it is not feasible to date the age of mineralization in the Danzhai gold-mercury deposit by the K-Ar technique.

Argon isotopes have proven to be a useful tool to distinguish the origin of the ore-forming elements (Kelley et al. 1986; Turner 1988). Pioneer noble gas investigation of formation waters from deep sedimentary basins revealed that noble gas may be derived from above (atmosphere, hydrosphere and uppermost crust) or from below (lower crust and upper mantle)(Mazor and Bosch, 1987). For instance, if the argon isotope which was captured by a mineral in Danzhai gold-mercury deposit originated from the mantle or lower crust, the ore-forming fluid may be postulated to be of the same origin. For the same reason, if the excess argon captured by a mineral in the deposit originated from the atmosphere, the ore-forming fluid are supposedly derived from a surface source such as underground water or an oil-field brine. Another possibility to be considered is a combination of these two sources. For example, the ore-forming elements such as Hg, As, Au were derived from the upper mantle or lower crust, transported to upper crust, where they mixed and reacted with underground water or other upper crust derived fluid and resulted in the mineralization. In this case, argon from a deep source could be contaminated or modified by atmoshperic argon.

Previous studies (e.g. Mazor and Bosch, 1986; Bosch and Mazor, 1988) indicate that the argon isotopes in most formation waters or oil brines are of atmospheric origin, and may be modified in some degree. Argon isotopes can be used to date the age of the formation water, oil brine and natural gas. Apparently, the argon isotopes may help to establish to the age of the gold-mercury mineralization and demonstrate the origin of the ore-forming elements in the Danzhai gold-mercury deposit.

§ 6.2. Sample Description

Quartz was chosen for argon isotope analysis to trace the origin of mineralization, firstly because it is a mineral of low-potassium content, and the ^{40}K decay may be neglected, and all argon in the mineral is excess argon, which may provide original information about the ore-forming fluid. Secondly, its texture has the great advantage of capturing argon and protecting it from dissipation. Thirdly, silicification is the most important alteration related to both gold and mercury mineralization in the deposit studied.

Three quartz samples were collected from the three different stages of quartz veins, which include: (1) sample Dz-01, a quartz vein from the second stage of silicification consisting of pure quartz and some cinnabar, arsenopyrite and stibnite, is an important stage for both gold and mercury mineralization; (2) sample Dz-02, a barite, quartz and cinnabar vein with pyrite from the third mineralization stage, which consists mainly of barite, quartz and some calcite crystals; and (3) sample Dz-03, coarsely euhedral quartz vugs connected to quartz veins which represent the last stage of silicification. If the argon isotopic composition was diluted by the atmosphere, the discrepancy should appear from the second stage to the last stage of alteration, and it will constrain the original sources of argon isotopes.

The three quartz samples were carefully examined under the microscope for fluid inclusions. In sample Dz-01, primary fluid inclusions (5-50 μm) are the dominant population. And some secondary inclusions are also situated along microcracks. Both primary and secondary fluid inclusions are rich in liquid methane, and some tiny cinnabar crystals are present with secondary fluid inclusions along microcracks. The population and the size of the secondary fluid inclusions is much lower than the primary ones, therefore, the contribution of secondary fluid inclusions to the argon isotope composition of the whole sample is negligible. In sample Dz-02, fluid inclusions are sparsely distributed and range from 3 to 10 μm in size. All of them are considered to be primary fluid inclusions, and can be classified into two groups; aqueous inclusions and liquid methane inclusions. The aqueous inclusions are less abundant but larger in size while the liquid methane inclusions are more abundant but smaller in size in comparison to the aqueous ones. Sample Dz-03 contains few fluid inclusions commonly less than 5 mm in diameter, chiefly aqueous and liquid methane inclusions.

§ 6.3. Experimental Method

The *In-vacuo* crushing technique, proposed by Kelley et al.(1986), is a useful way to detect argon isotopes. This technique was firstly applied in China by Qiu and Dai (1989). They proved that, the *In-vacuo* crushing technique is superior to the stepped heating technique in some ways, particularly for analyzing argon isotopes in fluid inclusions.

Prior to irradiation, samples were cleaned ultrasonically in Analar-grade methanol and deionized water and then encapsulated in evacuated quartz vials. They were irradiated with a suite of cherts at the Herald reactor in Chendu, in 1990. Analysis was carried out within a few months of irradiation and Ca analyses were also possible, an important aspect in view of the presence of dolomite. The irradiation was monitored using Hb3gr. The following irradiation parameters were determined: J=0.0135±0.00015, a=(K/Ca)/(^{37}Ar/^{39}Ar)=0.448 (conversion factor for K/Ca weight ratio), and b=(K/Cl)/(^{38}Ar/^{39}Ar)=3.64 (conversion factor for K/Cl wight ratio), for all samples (Berger and York, 1970; 1981).

The three quartz samples were crushed to a grain size of 0.4 to 0.6 mm. They were separated by electromagnet and purified by hand picking under a binocular microscope, then cleaned in an ultrasonic bath. the samples received a neutron fluency of around 4.05 x10^{18} n.cm^{-2}.

The samples were crushed to a size less than 0.5 μm, assuming that most of the fluid inclusions were broken open.

Prior to analysis the blanks were reduced by heating the crusher to 120 °C overnight, using heating tape. The samples were crushed repeatedly *in vacuo* using a magnetically operated pestle (Kelley et al. 1986; Qiu and Dai, 1989). Gases released by crushing were gathered and analyzed in a 15 cm radius high-sensitivity chamber. The various argon isotopes were determined by analyzing aliquots of atmospheric argon at regular intervals. Blanks were measured before and during each series of measurements.

The level of the ^{40}Ar system blank was $3x10^{-10}$ cm^3 STP, with the $^{40}Ar/^{36}Ar$ ratio close to that of air. Blanks for the other isotopes were negligible in relation to the neutron induced argon. The number of crushings per extraction (see table 6.1 to 6.2) was increased throughout the experiment in an attempt to maintain the levels of argon available for analysis. Crushing was continued until the gas release diminished significantly. The final powder of crushed quartz is dark in color and smaller than 0.5 μm in diameter.

§ 6.4. Results

The results are summarized in Table 6-1 to 6-3. The only argon isotope data listed specifically are those for ^{40}Ar and ^{36}Ar . The measurements of ^{39}Ar , ^{38}Ar and ^{37}Ar have been subjected to the usual corrections. Any attempt to understand the significance of the data and to make comparisons between samples irradiated with different fluencies demands that this conversion be made, now that the ^{40}Ar-^{39}Ar methodology is extended beyond the simple task of measuring radiometric ages. A second feature of the data is that abundances are expressed throughout in percent. There are at least four sources of the Ar isotopes released in these experiments:

(1) The characteristic isotope diagnostic of the presence of atmospheric argon is ^{36}Ar. Atmospheric ^{40}Ar (denoted as $^{40}Ar_A$) also accompanies the ^{36}Ar. Where it has been necessary to estimate the amount of atmospheric ^{40}Ar, the modern $^{40}Ar/^{36}Ar$ ratio of 295.5 has been assumed. The Cambrian and/or Ordovician atmospheric ratio was lower than the modern value, by an unknown amount. However, in all the samples analyzed atmospheric ^{40}Ar is minor in comparison to other sources and the assumption introduces no significant error. ^{40}Ar, to which this atmospheric correction has been applied, is denoted as $^{40}Ar^*$. $^{40}Ar^*$ is itself a mixture of two components, (radiogenic) $^{40}Ar_K$ and (excess) $^{40}Ar_E$; these are described below.

Table 6.1 $^{40}Ar/^{39}Ar$ data of sample Dz-01

Step	Drops	$^{40}Ar/^{36}Ar$	$^{39}Ar/^{36}Ar$	$^{40}Ar^{*}\%$	$^{40}Ar/^{39}Ar$	$^{39}Ar\%$	Age (Ma, 1SD)
J = 0.0480868							
1	6	615.12	0.33	51.96	978.62	3.76	6986.1±117.0
2	6	744.55	0.30	60.31	1494.08	1.29	7736.4±397.4
3	8	754.54	1.98	60.84	231.44	8.43	4502.3±51.9
4	12	1023.19	3.45	71.12	211.15	8.83	4351.0±39.5
5	20	921.54	1.90	67.93	328.69	7.76	5090.6±45.6
6	25	849.74	1.14	65.22	486.92	4.28	5764.4±105.7
7	35	885.85	2.98	66.64	198.37	11.42	4248.8±31.6
8	45	902.11	1.06	67.24	570.11	5.00	6038.1±83.1
9	60	937.00	0.83	68.46	773.67	3.55	6572.1±99.4
10	70	933.30	0.91	68.34	700.83	6.51	6398.6±52.7
11	80	999.37	0.30	70.43	2314.22	1.90	8517.1±242.4
12	90	892.08	2.47	66.87	241.56	15.06	4573.2±39.8
13	100	1169.90	1.20	74.74	727.78	4.28	6464.8±86.9
14	130	1273.99	0.91	76.80	1076.39	2.84	7154.5±118.4
15	150	1308.68	1.70	77.42	597.03	5.11	6118.5±62.8
16	180	1342.20	0.85	77.98	1226.92	2.52	7386.5±169.9
17	250	1314.70	1.94	77.52	525.33	6.46	5895.9±45.7

Table 6.2 $^{40}Ar/^{39}Ar$ data of sample Dz-02

Step	Drops	$^{40}Ar/^{36}Ar$	$^{39}Ar/^{36}Ar$	$^{40}Ar^{*}\%$	$^{40}Ar/^{39}Ar$	$^{39}Ar\%$	Age (Ma, 1SD)
J = 0.0439360							
1	7	858.82	24.47	65.58	23.02	26.41	1260.9±9.4
2	8	1200.62	42.59	75.36	21.25	22.04	1189.7±7.2
3	16	688.26	22.72	57.05	17.29	40.47	1019.5±3.0
4	20	1054.96	1.17	71.99	649.94	0.60	6109.1±11.4
5	40	918,26	3.33	67.82	186.99	6.11	4004.6±13.3
6	60	1077.26	1.06	72.57	734.20	0.78	6322.0±77.9
7	80	772.37	1.29	61.74	369.68	1.52	5136.9±41.7
8	90	1309.20	0.70	77.43	1451.60	0.24	7524.7±347.4
9	100	1347.38	0.67	78.07	1559.71	0.24	7652.4±434.7
10	130	1400.52	1.57	78.90	704.43	0.41	6249.6±177.4
11	150	1403.79	1.67	78.95	664.39	0.43	6147.5±189.4
12	220	1678.27	3.06	82.39	452.36	0.75	5481.8±96.5

Table 6.3 $^{40}Ar/^{39}Ar$ data of sample Dz-03

Step	T(°C)	$^{40}Ar/^{36}Ar$	$^{39}Ar/^{36}Ar$	$^{40}Ar^{*}\%$	$^{40}Ar/^{39}Ar$	$^{39}Ar\%$	Age (Ma, 1SD)
J = 0.0435209							
1	50	715.18	1.80	58.68	233.17	9.48	4350.1±234.45
2	50	791.53	1.77	62.67	279.49	4.42	4649.9±569.4
3	60	709.63	1.85	58.36	223.94	5.20	4283.9±553.8
4	100	876.36	2.34	66.28	248.33	6.65	4453.78±443.3
5	160	503.58	2.36	41.32	88.19	8.39	2844.2±766.9
6	250	360.15	2.65	17.95	24.38	11.07	1304.9± -781.8
7	400	1769.01	16.60	83.29	88.75	13.60	2853.2±385.0
8	1000	28513.37	479.05	98.94	58.90	17.75	2292.5±1650.8
9	1400	581.31	13.24	49.15	21.59	23.45	1195.0± -275.2

(2) Radiogenic ^{40}Ar (denoted as $^{40}Ar_K$) together with its parent K (determined by way of ^{39}Ar) is present in the three samples, but with very low abundance.

(3) Excess (Parentless) ^{40}Ar (denoted as $^{40}Ar_E$) is present in all the samples analyzed and is presumed to reside in liquid methane fluid inclusions and/or aqueous fluid inclusions and to represent ^{40}Ar degassed or leached from the crust. Aqueous fluids trapped in fluid inclusions are, except in the case of trapped surface water, saline and contain appreciable amounts of Cl, which in these experiments is measured by way of neutron induced ^{38}Ar. For this reason the presence of an excess component is sought through correlation between ^{40}Ar and ^{38}Ar (expressed as Cl equivalent). A component of ancient atmospheric ^{36}Ar and ^{40}Ar dissolved in these brines is also present and shows a correlation with Cl.

(4) Three samples analyzed contain a very small proportion of calcite and dolomite, identified in the Ar analyzed by way of ^{37}Ar and indicated in the tabulated data as Ca equivalent.

There is a definite variation among the three samples. Their significant features shown in tables 6.1 to 6.3 are discussed in the following. Since sample Dz-01 contains, in a most extreme form, all the features that are considered important, this will be discussed first.

§ 6.4.1. Sample Dz-01

This sample is a representative of the second stage of mineralization, an important stage for both gold and mercury mineralizations.

The most surprising feature on crushing Dz-01 was the very large quantity of $^{40}Ar^*$ released. Examination of Table 6.1 shows that in all 17 steps of crushing, the $^{40}Ar^*$ is always greater than 51.96%, the highest being 77.98%. The sample showed a tendency from the beginning to the end of crushing, of high $^{40}Ar^*$ abundance. As a consequence, the $^{40}Ar/^{36}Ar$ also shows the same tendency, and the $^{40}Ar/^{36}Ar$ is always a high ratio, from 615.12 at the beginning of crushing, to 1314.70 at the end. Apparently, the $^{40}Ar/^{36}Ar$ values for all steps of crushing of this sample are much higher than the modern atmospheric

ratio, 295.5. This indicates that tremendous excess argon was released by the crushing process of quartz.

In contrast to $^{40}Ar^*$, the quantity of ^{39}Ar released from this quartz sample is definitely low. Its abundance is generally less than ten percent, with only two exceptions, one is in the seventh step of crushing, where 11.42% ^{39}Ar is released; the other is in the twelfth step of crushing, where 16.06% ^{39}Ar is released. This characteristic low content of ^{39}Ar demonstrates that radiogenic argon is of little importance in the quartz sample.

The apparent age of the sample is higher than the acceptable age of either mineralization or host sedimentary rocks. Fig. 6.3 shows that the multistage age spectrum of the quartz sample is very complicated. The lowest apparent age is 4351.01±39.52 Ma while the highest apparent age is 7386.48±169.90 Ma. It is noteworthy, the so-called "saddle shaped" age spectra are usually interpreted as an indication of excess ^{40}Ar in the sample (Lanphere and Dalrymple, 1976; Turner et al. 1990, Qiu and Dai, 1989; Turner and Wang, 1992). In the diagram (Fig. 6.3), several "saddle shaped" variations are present.

The $^{40}Ar/^{36}Ar$-$^{39}Ar/^{36}Ar$ isochron diagram (Fig. 6.4) indicates that, in the Dz-01 quartz sample, the correlation coefficient of the data from each step of crushing is 0.5625. The initial $(^{40}Ar/^{36}Ar)_0$ for the mineralization is 708.51±64.12, double that of the modern atmosphere. The isochron age for the mineralization is 2817.79 Ma, which is not acceptable for the real age of mineralization.

§ 6.4.2. Sample Dz-02

Sample Dz-02 is a quartz sample from the third stage of mineralization, which is of importance for mercury mineralization, the minerals associated with this sample are barite and cinnabar.

This quartz sample also has a large quantity of $^{40}Ar^*$ similar to sample Dz-01 (Table 6.2), and extends, from the beginning to the end of crushing, the $^{40}Ar^*$ increased gradually, from the first step of crushing with 65.58% to the last crushing step with 82.39%.

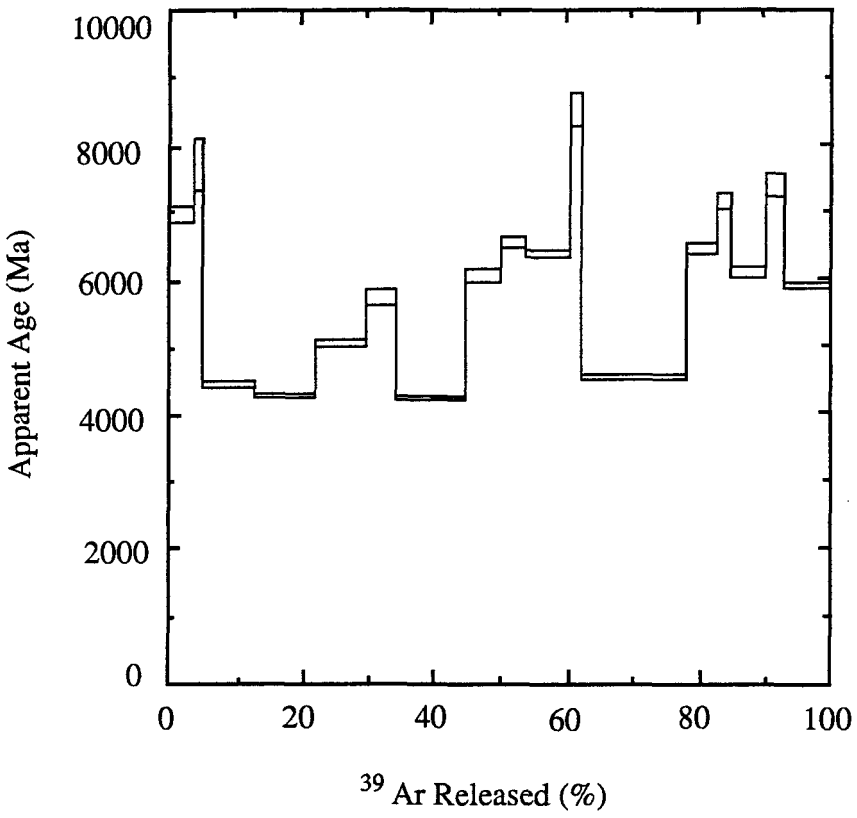

Fig.6.3 Multistage age spectra of argon isotopes of sample Dz-01 showing several so-called "saddle shaped" spectra, and both the highest apparent and lowest apparent age are much higher than the acceptable age of mineralization.

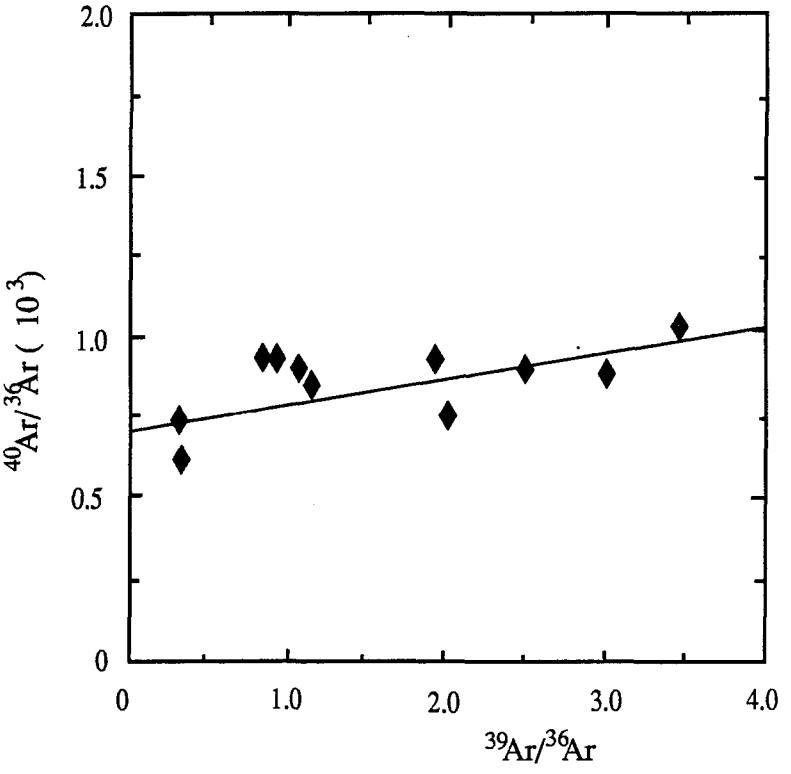

Fig. 6.4 $^{40}Ar/^{36}Ar$--$^{39}Ar/^{36}Ar$ isochron diagram of sample Dz-01
R=0.5624781; S=78.35 36.20; Io=708.51 64.12; T=2817.79 Ma.

The $^{40}Ar/^{36}Ar$ values from different steps of crushing are also high, ranging from 688.26 to 1678.27. The highest $^{40}Ar/^{36}Ar$ value is more than 5 times that of the modern atmosphere.

As shown in table 6.2 and Fig. 6.5, an increase of ^{39}Ar is noticeable. In the first three stages of crushing, the ^{39}Ar abundance is high, and varies from 26.41%, 22.04% to 40.47%. The apparent age for these three steps is 1133 Ma on average, but for the remaining nine crushing steps, the ^{39}Ar abundance decreases abruptly, and is generally less than 1%. The apparent ages for these nine steps range from 4006.63 Ma to 7652.73 Ma, and 6070.07 Ma on average. Moreover, the $^{40}Ar/^{36}Ar$-$^{39}Ar/^{36}Ar$ isochron diagram displays unexpected results. The correlation coefficient and the slope of the isochron are negative (Fig. 6.6). These abnormal characteristics are contradictory to to all known argon isotope data. A possible explanation for it is that these data come from two different groups of fluid inclusions, which had two distinct initial $(^{40}Ar/^{36}Ar)_0$ values.

§ 6.4.3. Sample Dz-03

Sample Dz-03 is from several euhedral quartz crystals connected to the last stage of quartz veining, and of no importance to either gold or mercury mineralizations.

The euhedral quartz crystals host only a few fluid inclusions, so it is very difficult to detect the argon by the *in-vacuo* crushing technique. Therefore, the step heating technique was applied for this sample. Even so, the available noble gas for isotopic measurement is scarce, which influences the accuracy of the data and the quality of the analysis, therefore the isotopic data for this sample are presented here only for reference.

The isotopic data for Dz-03 are tabulated in table 6.3. In total, nine heating steps were undertaken from 50 to 1400 °C. The $^{40}Ar^*$ abundances for different heating steps are also high, 59.62% on average, but show no tendency to increase from the first to last heating step. The $^{40}Ar/^{36}Ar$ ratios are high for each heating step, generally in the neighborhood of 750, but when the temperature reached 1000 °C, the $^{40}Ar/^{36}$ ratio become tremendously high, 28513.37.

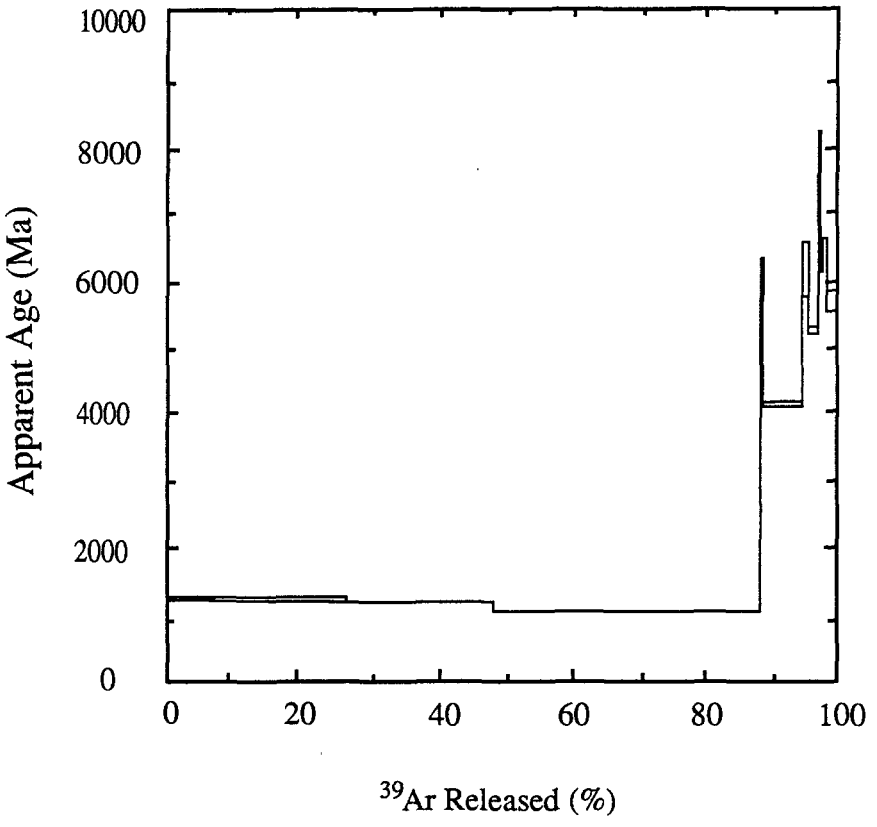

Fig. 6.5 Age spectra of sample Dz-02. The first three steps released a relative large quantity of ^{39}Ar, the remaining nine steps released only a small quantity.

The apparent age for this sample is also high, ranging from 1195.02 to 4649.94 Ma (Fig. 6.7). The isochron age of this sample is 2250 Ma which is not acceptable for the age of the mineralization, either. The initial ($^{40}Ar/^{36}Ar)_0$ is 576.2, which is higher than that of modern atmosphere, but a little lower that of the second mineralization stage.

§ 6.5. Discussion and Element Correlations

There are a number of key observations that should be summarized in order to interpret the geological significance of the Ar isotope data.

1. Excess ^{40}Ar dominated in all three samples. The initial $(^{40}Ar/^{36}Ar)_0$ ratio for each of the samples is much higher than that of the modern atmosphere. The $^{40}Ar/^{36}Ar$ ratio is always high in each step of crushing or heating.

2. The isochron ages for the three quartz samples are 2783, 3047 and 2250 Ma respectively. Evidently, they are much older than the Cambrian and Ordovician host carbonate rocks, and thus much older than a possible mineralization age.

3. ^{39}Ar is of low abundance in all three quartz samples. ^{39}Ar is also of low abundance in each step of crushing or heating, generally, in the range of several percent. Sample Dz-02, the first three steps of crushing released a large quantity of ^{39}Ar relative to the others, ranging from 20% to 40%. For the remaining nine steps of crushing, however, the ^{39}Ar abundance is usually less than 1%.

4. Table 6.4 and 6.5 show the correlation coefficients between different argon isotopes, such as ^{40}Ar, $^{39}Ar(K)$, $^{38}Ar(Cl)$, $^{37}Ar(Ca)$ and ^{36}Ar. The data in the two tables demonstrate that $^{39}Ar(K)$, $^{38}Ar(Cl)$, $^{37}Ar(Ca)$ show positive correlation. For example, in sample Dz-01, their correlation coefficients are: $^{37}Ar(Ca)$ to $^{38}Ar(Cl)$ is 0.5849; $^{37}Ar(Ca)$ to $^{39}Ar(K)$ is 0.7425; $^{38}Ar(Cl)$ to $^{39}Ar(K)$ is 0.7418. The correlation coefficients with regard to the sample Dz-02, are even higher, close to 1: $^{37}Ar(Ca)$ to $^{38}Ar(Cl)$ is 0.9719; $^{37}Ar(Ca)$ to $^{39}Ar(K)$ is 0.9814; $^{38}Ar(Cl)$ to $^{39}Ar(K)$ is 0.9617.

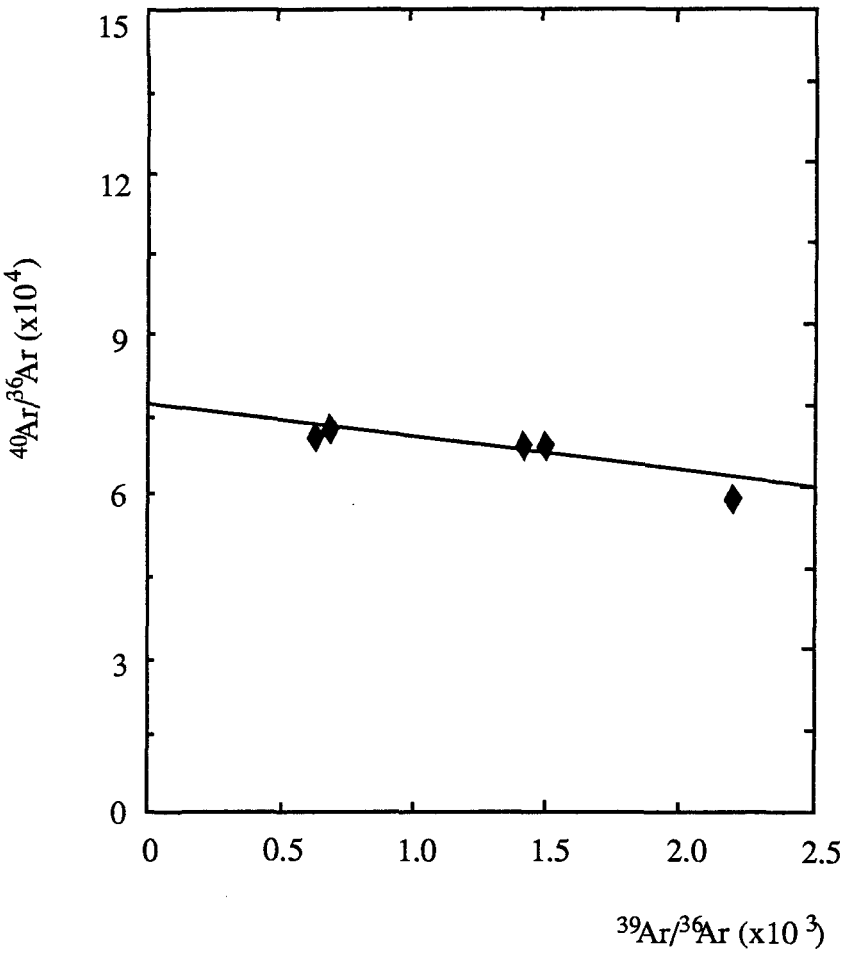

Fig. 6.6 $^{40}Ar/^{36}Ar$-$^{39}Ar/^{36}Ar$ isochron diagram of sample Dz-02.
R = -0.9298; $(^{40}Ar/^{36}Ar)_0$ = 1205.3; S = -0.0834; I = 0.0008;
T = 3047.7035.

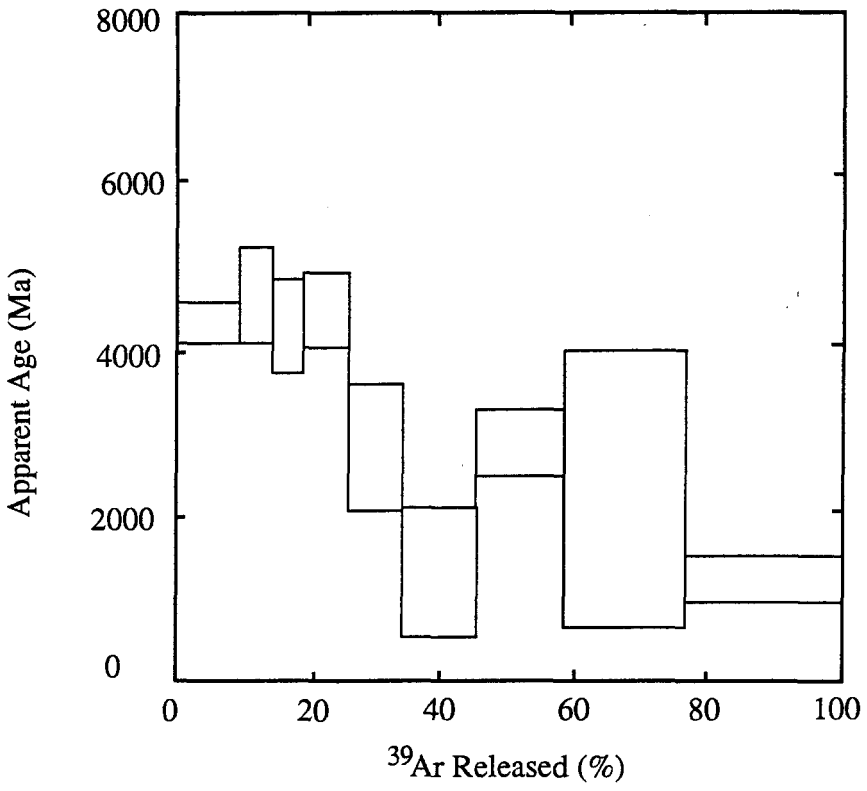

Fig. 6.7 Mutistage age spectra of argon of sample Dz-03 from quartz vugs.

5. The correlation between ^{40}Ar and $^{39}Ar(K)$ is extremely low, -0.0406 for sample Dz-01, and 0.3441 for sample Dz-02. The correlation between ^{40}Ar and ^{36}Ar, however, is definitely positive, the correlation coefficient being 0.5579 for the sample Dz-01 and 0.8754 for the sample Dz-02.

The principal characteristics of the argon are to be considered first, and the problem of excess ^{40}Ar will be discussed separately. Low abundance of $^{39}Ar(K)$ in the three samples is to be expected, since the host mineral is pure quartz, and potassium impurity in quartz is negligible, but the first three steps of crushing of sample Dz-02 released a relatively high quantity of ^{39}Ar which was not anticipated. To interpret this anomaly, it is important to consider the occurrences of the gas in quartz. Generally, the noble gas occupies imperfections in the mineral, such as, fluid inclusions, and sites in the crystal lattices. The lattice occupied argon is normally released in the high temperature range of step heating, but as the argon in the sample Dz-02 is released by crushing, the contribution of lattice argon is negligible, therefore it is concluded that all the argon of this sample is derived from fluid inclusions. As mentioned before, fluid inclusions in this sample are classified into two groups, one is the group of large aqueous fluid inclusions, and the other is the group of liquid methane inclusions, which are of relatively small size. It is assumed that in the process of crushing, the large fluid inclusions are broken first and the smaller ones are crushed subsequently. Accordingly, the first three steps of crushing released a large quantity of $^{39}Ar(K)$ principally from the aqueous fluid inclusions, the remaining nine steps of crushing released little $^{39}Ar(K)$ mostly coming from the liquid methane fluid inclusions. The low abundance of $^{39}Ar(K)$ in the sample Dz-01 and Dz-03 is explained in the same way. In these samples, liquid methane inclusions dominate, and the aqueous fluid inclusions are of relatively small importance. This also helps to understand the negative correlation coefficient from different steps of crushing in sample Dz-02, and a negative slope of the isochron as well. But why is the abundance of $^{39}Ar(K)$ in liquid methane and in aqueous inclusions so different? One possibility is the solubility of $^{39}Ar(K)$ in aqueous solution is different from that in liquid methane (Mazor and Bosch, 1987), and another possibility is that the K abundance in the aqueous fluid inclusions is higher than in liquid methane.

The $^{39}Ar(K)$, $^{38}Ar(Cl)$, $^{37}Ar(Ca)$ are positive correlated in the two samples analyzed by step crushing. Investigation by Turner et al, (1990), Turner and Wang (1992), Qiu and Dai, (1989) shows that the relationship between $^{39}Ar(K)$, $^{38}Ar(Cl)$, $^{37}Ar(Ca)$ revealed that they came from fluid inclusions hosted by quartz. It is anticipated that the correlation between ^{40}Ar and $^{39}Ar(K)$ which is extremely low, shows that the ^{40}Ar is not *in-situ* radiogenic ^{40}Ar decayed from potassium. The high positive correlation between ^{40}Ar and ^{36}Ar suggests that they have the same provenance, and originated from the decay of potassium in clay minerals or other K-rich minerals.

§ 6.6. Origin of Excess Argon

Rama et al.(1965) provide a good summary of excess argon investigations between 1956 and 1965. At that time, however, excess argon was considered an impurity and an obstacle to K-Ar dating. Its interference with the radiogenic argon formed by *in situ* potassium decay needed to be considered, otherwise, excess argon influenced the results of K-Ar dating. At this time, Rama et al.(1965) pointed out that the excess argon is hosted by fluid inclusions in minerals such as quartz, feldspar, fluorite.

The identification of excess ^{40}Ar in rocks and minerals by analyzing the $^{40}Ar/^{36}Ar$-$^{39}Ar/^{36}Ar$ age spectrum was first introduced by Lanphere and Dalrymple (1971). After many similar examinations (e.g. Lanphere and Dalrymple 1971; 1976), scientists reached a consensus, that the "saddle-shaped" age spectra is diagnostic of excess ^{40}Ar. Generally, "saddle-shaped" age spectra, typical of excess ^{40}Ar-bearing igneous intrusives, are those in which the apparent ages of successive increments decrease systematically to a minimum value at intermediate values of ^{39}Ar release and then increase. The minima approaches but does not reach as low as the true age of the rocks(Harrison and McDougall, 1988; Herzler and Harrison, 1988). Detailed study showed that the "saddle-shaped" age spectra, however, are not always indicative of the presence of excess ^{40}Ar, since the same pattern is also found for rocks that have experienced partial loss of ^{40}Ar through thermal metamorphism. With regards to the Danzhai gold-mercury deposit, multistage "saddle shaped" age spectra are present in all three samples, particularly in sample Dz-01. Regional

Table 6.4 Correlations between ^{36}Ar, $^{37}Ar(Ca)$, $^{38}Ar(Cl)$, $^{39}Ar(K)$, and ^{40}Ar of the quartz sample (Dz-01) from second mineralization stage.

	^{36}Ar	$^{37}Ar(Ca)$	$^{38}Ar(Cl)$	$^{39}Ar(K)$	^{40}Ar
^{36}Ar	1.0000				
$^{37}Ar(Ca)$	0.2919	1.0000			
$^{38}Ar(Cl)$	0.0851	0.5848	1.0000		
$^{39}Ar(K)$	0.0404	0.7424	0.7418	1.0000	
^{40}Ar	0.5579	0.2549	0.4475	-0.0407	1.0000

Table 6.5 The correlation between ^{36}Ar, $^{37}Ar(Ca)$, $^{38}Ar(Cl)$, $^{39}Ar(K)$, and ^{40}Ar of the quartz sample (Dz-02) from third mineralization stage.

	^{36}Ar	$^{37}Ar(Ca)$	$^{38}Ar(Cl)$	$^{39}Ar(K)$	^{40}Ar
^{36}Ar	1.0000				
$^{37}Ar(Ca)$	0.6906	1.0000			
$^{38}Ar(Cl)$	0.7528	0.9719	1.0000		
$^{39}Ar(K)$	0.6526	0.9814	0.9637	1.0000	
^{40}Ar	0.8754	0.3630	0.4369	0.3441	1.0000

geological investigation indicates that, thermal metamorphism was not a major factor in the study area.

The $^{40}Ar/^{36}Ar$-$^{39}Ar/^{36}Ar$ isochron diagrams (Fig. 6.4, Fig. 6.6) show apparent isochron ages which are much higher than the postulated mineralization age (Caledonian Orogeny or Yanshanian Orogeny), and even older than the age of its host rocks (Late Cambrian and Early Ordovician). Evidently, the apparent age is not an acceptable mineralization age. In an $^{40}Ar/^{36}Ar$-$^{39}Ar/^{36}Ar$ isochron diagram, when the abscissa ^{39}Ar tends to zero, the ordinate tends to the initial $(^{40}Ar/^{36}Ar)_0$ intercept. For modern atmosphere, the value is 295.5, but in different geological times, the initial $^{40}Ar/^{36}Ar$ ratio of the atmosphere is different, the older periods having a lower ratio. However, in Fig.6-3, the initial $^{40}Ar/^{36}Ar$ ratio as high as 708.51, twice that of the modern atmosphere, and of course much higher than that of a coeval atmospheric $^{40}Ar/^{36}Ar$ value. This indicates that the quartz captured gas of a high initial $^{40}Ar/^{36}Ar$ value, that is, excess or parentless argon was trapped.

Huge quantities of excess argon definitely influence the isochron age. For the samples studied, the abundance of excess argon is so high that the isochron cannot give the correct age of quartz crystallization. That is why, all of the isochron ages, and age spectra cannot be considered as the age of mineralization.

Where did the excess argon come from and what is its geological significance? Generally, there are four different types of excess ^{40}Ar-bearing materials which have been recognized (Seidemenn, 1976): (1) rocks containing a clathrate-like argon trap phase, such as cordierite, beryl; (2) intrusive igneous rocks with the common rock-forming minerals occluding ambient argon during growth; (3) extrusive igneous rocks which trapped ambient argon by rapid cooling of a melt; (4) metamorphic minerals that presumably crystallized under high argon partial pressures. Apparently, these excess ^{40}Ar-bearing materials exist in the igneous and metamorphic environment. Neither magmatic nor metamorphic activities were observed in the study area. Geological investigations clearly defined that the Danzhai gold-mercury deposit is a low-temperature hydrothermal deposits. Apparently, the model proposed by Seidemenn (1976) is not applicable to the deposit under study.

The age spectra of sample Dz-01(Fig. 6.3) are indeed similar to those of intrusive igneous and eruptive igneous rocks. Initial $(^{40}Ar/^{36}Ar)_0$ is extremely high and it is characterized by multistage "saddle shape" plateaus as well. One possibility is that the excess ^{40}Ar originated from deep layers of the earth and reached the upper crust through outgassing. The distribution of $^{40}Ar/^{36}Ar$ in different tectonic settings was examined in recent studies, and was classified under several types (Kaneoka 1980, 1983; Allègre et al 1983; Ozima and Saito 1983; Sano et al, 1985): MORB type: generally, the $^{40}Ar/^{36}Ar$ value is larger than 10000, which represents the depletion and degassing of the upper mantle; Plume type: the $^{40}Ar/^{36}Ar$ may be less than the atmospheric $^{40}Ar/^{36}Ar$ value or in the neighborhood of 350 (e.g. oceanic island basalt and continental ultramafic rocks), represented the enriched lower mantle(Dalrymple and Moore, 1968). The $^{40}Ar/^{36}Ar$ value of convergent belts is between that of the MORB type and Plume type. Therefore, if only the argon isotope characteristics of the ore-forming elements of the Danzhai gold-mercury deposit are considered, they may probably be interpreted as a consequence of mantle degassing. Some noble gas isotope investigations revealed that some natural gas deposits contain huge quantities of excess argon, and those deposits accordingly may be formed by mantle degassing (e.g. Gold and Soter, 1980; Wakita and Sano, 1983; Wang, 1983; Welhan and Craig, 1979). This kind of natural gas is called non-biogenic natural gas or inorganic natural gas.

There is another possible interpretation of the origin of excess ^{40}Ar, that the formation water or oil brine leached and accumulated the radiogenic ^{40}Ar from potassium-rich strata ($^{40}Ar_K$ originated from ^{40}K decay). The Late Cambrian and Early Ordovician host strata of the Danzhai gold-mercury deposit are dominantly carbonate rocks, but similar deposits are also present in Middle Cambrian (e.g. Wanshan mercury deposit) the Proterozoic Banxi Group, (e.g. Neishan mercury deposit). It is noteworthy that, in the the Lower Cambrian, thick black shale is extensively distributed over the Yangtze craton. The Lower Cambrian black shale is considered to be the oil source strata as well as the ore source for gold and mercury. There are many beds of shale or slate in the Middle Cambrian, Zanian strata and the Proterozoic Banxi Group as discussed in previous chapters. Therefore, the formation water or oil brine may leach radiogenic ^{40}Ar from these potassium-rich strata during its formation and migration, then transported and precipitated it in the mercury, antimony, and gold deposits in the area. This interpretation seems more acceptable and

reasonable than the first one combined with previous geological, fluid inclusion investigations.

§ 6.7. Summary and Discussion

The argon isotope study of the three quartz samples provided some unexpected information. Many investigations demonstrate that argon isotopes in formation water and/or oil brine have their origin in the modern atmosphere (Podosek and Honda, 1980; Mazor and Bosch, 1987). The initial $(^{40}Ar/^{36}Ar)_0$ value in formation water or oilfield brine in some sedimentary basins in the neighborhood of 295.5, the $^{40}Ar/^{36}Ar$ value of modern atmosphere. The geological investigation, fluid inclusion examination and sulfur isotope study show a close relationship to regional petroleum evolution, therefore the initial $(^{40}Ar/^{36}Ar)_0$ values in the samples from the Danzhai gold-mercury deposit should be close to that of a coeval atmosphere. The argon isotope investigation of the three samples, showed excess ^{40}Ar. The initial $(^{40}Ar/^{36}Ar)_0$ ratio for each of the samples or for each crushing step is much higher than the modern atmosphere. The isochron ages for the three quartz samples are 2783 Ma, 3047 Ma and 2250 Ma respectively. Evidently, these are much older than an acceptable mineralization age, and even older than the Cambrian and Ordovician host rocks.

There are two possible interpretations of the abnormal characteristics described above. On one hand, the age spectrum of these samples is similar to that of igneous rocks (e.g. pillow basalt). Its initial $(^{40}Ar/^{36}Ar)_0$ is high and it is characterized by "saddle shapes" spectra as well. The excess ^{40}Ar is probably derived from deeper parts of the earth, for example, the mantle, and reached the upper crust through outgassing. On the other hand, the host strata of the Danzhai gold-mercury deposit belongs to the Cambrian and Ordovician, but similar deposits are also present in older strata such as Middle and Early Cambrian, and even the Proterozoic Sinian and Banxi Group. Clay minerals are enriched in these strata, particularly in the lower Cambrian black shale, which is extensively distributed over the Yangtze craton, and considered a principal oil source strata as well as a source strata for gold and mercury ores in the region. Accordingly, the formation water or oil brine may have leached the radiogenic ^{40}Ar from these K-rich strata, then precipitated it in the Danzhai and

other mercury, antimony, and gold deposits in the area. The latter interpretation seems more acceptable.

Is it possible that a deeply-derived ore-forming fluid ascended in the sedimentary basin and mixed with the formation water or oil brine? No direct answer can be found. The mixing of two distinct fluids is not considered likely as the argon isotopes have no significant change from the second to the last stage of mineralization. If an ore-forming fluid of deep source ascended in the sedimentary basin and mixed with an oil brine, the argon isotopes would vary from stage to stage. The first and second stage of mineralization should be composed of large quantities of excess argon and a high apparent isochron age whereas the last stage or even the second last stage would contain much less excess argon and the apparent age should be close to the mineralization age. This type of variation has not been observed.

^{39}Ar abundance is always low in the three quartz samples, which is to be expected since the host mineral is pure quartz. The only exception is that in the first three steps of crushing in the sample Dz-2, released large quantity of ^{39}Ar relative to others. This may imply that the aqueous fluid inclusions contain higher ^{39}Ar than the liquid methane inclusions, because the solubilities of noble gas in different media, such as formation water, oil, or liquid methane are different.

$^{39}Ar(K)$, $^{38}Ar(Cl)$, $^{37}Ar(Ca)$ show a high degree of positive correlation in the two samples analyzed by crushing, which demonstrates that the argon isotopes come from the fluid inclusions hosted in quartz. The positive correlation between ^{40}Ar and ^{36}Ar may suggest that they have same provenance, and originate from the *in-situ* decay of potassium in the clay minerals or any other K-rich minerals.

CHAPTER VII:

LEAD ISOTOPES

§ 7.1. Introduction

A lead isotope study is a useful adjunct to the examination of the mineralization history of an area (e.g.: Cannon, 1961; Doe and Zartman, 1979, Zartman and Doe, 1981). In most cases, the use of common lead isotopes is more efficient as a geochemical tracer than as a geological dating tool (Slawson, 1983), since distinct patterns of lead isotope abundance are associated with specific geological environments. The isotopic evolution of lead, which results from the radioactive decay of U, Th has effects related to fundamental chemical difference of their source region. The ultimate source of the lead in a deposit can be established by lead isotope studies.

Usually, a lead isotope study in a deposit is based on the isotopic analysis of galena. Unfortunately, no galena is present in the Danzhai gold-mercury deposit (Zhang et al, 1984). The geochemical behavior of lead, mercury and antimony is so different that these elements rarely coexist in a same deposit (Craig et al., 1973). Few examples show galena associated with cinnabar and/or stibnite in a gold-mercury deposit are known. Evidently, an alternative mineral must be found to do lead isotope analysis.

§ 7.2. Sample Selection for Lead Isotope Studies

Sulfide minerals such as stibnite or pyrite may be used as an alternative since no galena samples are available for lead isotope study in the Danzhai gold-mercury deposit. Trace amounts of lead were isolated from stibnite to do lead isotope analysis. This method was first proposed by Ding (1986) for tracing the origin of the Gongguan mercury antimony deposit, Shanxi, Northwest China, and proved to be a practical way to study mercury antimony deposits.

Seven stibnite samples from different ore-bodies in the Danzhai gold-mercury deposit were collected, all of these samples are from the second stage of mineralization, the most important stage for both gold and mercury mineralization. All seven stibnite samples are big prismatic crystals, some of them associated with cinnabar and quartz, some with arsenopyrite and quartz, and the others only associated with quartz as prismatic or acicular crystals.

§ 7.3. Experimental Method

All stibnite samples are carefully selected and hand picking of stibnite is quite easy since stibnite occurs as the big prismatic crystals. The content of lead in stibnite ranges from 0.01 to 0.05%. U, Th contents are low in these stibnite samples, and their contribution to lead can be neglected. The lead was extracted using the technique proposed by Ding (1986).

1. Sample Preparation: The first step is to clean the stibnite by putting samples into a pure alcohol medium and cleaning them ultrasonically, then purging all the surface absorbed matter by washing in pure distilled water. The grain size of these samples ranges from 0.3 to 0.5 mm. Only 200 to 300 mg of sample is required for the analysis.

2. Removal of antimony: Stibnite is a mineral capable of dissolution in HCl. When the temperature is higher than 110 °C, antimony volatilizes as $SbCl_3$ from the solution

while the sulfur also volatilizes as H_2S. If the antimony is precipitated as $SbCl_5$, it will be decomposed as Cl_2 and $SbCl_3$ at 140 °C, but lead will remain in solution.

$$Sb_2S_3 + 6HCl \xrightarrow{150\text{-}200\ ^oC} 3H_2S + 2SbCl_3$$

Samples are placed in a 10 ml tube, with about 3 to 5 ml 12 N analytical pure HCl, heated in an oven at 150 °C, and evaporated. This is repeated three to four times. The trace Pb and other trace elements in the stibnite is extracted while the Sb_2S_3 is eliminated. In the residual solution, the abundance of Tl, Bi are high and are eliminated by HBr. Atomic Absorption spectrum Analysis shows that Sb content is eliminated from 71.7 % in 300 mg stibnite to only 14.1 - 12.3 ppm in the residue as a result of two evaporating runs described above. In the end, 1:100 NH_3 (the extractor of Pb) is added into the beaker containing the residual Pb bearing fraction. Attention is paid to see whether a Pb-bearing precipitate is produced in this step. If so, the precipitate will adsorb Pb and influence the accuracy of the analysis.

3. Diphenyl thiocarbazone and chloroform extraction: In an alkaline medium (pH=7-10), lead ions react with diphenyl thiocarbazone and produce red-colored Pb dithizone $Pb(HD_2)_2$, which can be dissolved in CCl_4. To remove the remaining antimony and sulfide, a 1: 100 NHO_3 solution is used for extracting the Sb and S, in the meantime, adding 25% $(NH_4)_2(OH)Cl$, 50% citric ammonium, 1% potassium cyanide solution. Adjusting the solution to PH = 9-10 by adding ammonia, then extracting the lead by adding diphenyl thiocarbazone, comparing to the standard color solution, to measure the content of extracted Pb. Once again, 1:100 NHO_3 is used to extract the lead in the solution.

4. The Pb abundance in the reagents and the measurement error: the most important reagents in the experiments are HCl, HNO_3, which are superpure reagents, the quantities used in the experiments are small; 12 N HCl < 15 ml, 1:100 HNO3 < 6 ml. Diphenyl thocarbazone and chloroform range from 1 to 2 ml. The water using for making 1: 100 NHO3 is superpure, which is made from ion free water produced from a non-boiling quartz distiller. The exotic Pb taken into the experiment by this reagent is less than 0.1%.

MAT260 Mass spectrometer counter is used for the mass measurement for these samples. The error (σ) $^{206}Pb/^{204}Pb$ = 0.0034 - 0.038; $^{207}Pb/^{204}Pb$ = 0.0034 - 0.062; $^{208}Pb/^{204}Pb$ = 0.0061- 0.067.

§ 7.4. Lead Isotope Composition and Model Age of Ore Lead

All the stibnite samples from different orebodies but from the same mineralization stage in the Danzhai gold-mercury deposit show homogeneous lead isotopic constituents: $^{206}Pb/^{204}Pb$: 18.24 to 18.51; $^{207}Pb/^{204}Pb$: 15.67 to 15.81; $^{208}Pb/^{204}Pb$: 38.32 - 38.55. The analytical result of these samples are given in table 7.1.

As early as 1961, Cannon recognized that lead isotope data can offer three types of major information for ore genesis: (1) the source from which ore metals were derived; (2) the geologic processes that moved them from source to deposition site; and (3) the chronology of the mineralizing event. Research afterward proved that the lead isotope data did provide this information. The ^{206}Pb-^{207}Pb-^{208}Pb trilinear coordinate graph is a useful triangular diagram to distinguish the origin of lead isotope, such as common lead, U-lead, Th-lead and J-lead. The lead isotope data in the Danzhai gold-mercury deposit plots in the common lead sector, that is, in the crescentic area between the two evolution curves in the ^{206}Pb-^{207}Pb-^{208}Pb triangular diagram (Fig. 7.1). This means that the radiogenic lead has a negligible contribution to the trace lead in the stibnite.

Based on Doe and Zartman's(1979) model calculation, μ ranges from 9.05 to 9,47, ω varies from 34.76 to 35.68, and the κ value ($^{232}Th/^{238}U$) is from 3.73 to 3.76. These values also indicate that the lead isotopes belong to common lead (Kanasewich, 1962). This compares with the highly evolved μ value lead in the lead isotope types of most stratabound and stratiform deposits in the P. R. China (Chen, 1981; 1983).

The lead isotope composition in the Danzhai gold-mercury deposit is quite different from that of Mississippi Valley type lead zinc deposits. In this type of deposit, the ore-leads are generally composed by anomalous lead(Fig. 7.1). Lead isotopic analyses for galenas from southeast Missouri, Upper Mississippi Valley and Tri-State area, for

Table 7.1 The lead isotope compositions in the Danzhai gold-mercury deposit

1. Lead isotopes in the Study Area

Sample	Host Min.	$^{206}Pb/^{204}Pb$	$^{207}Pb/^{204}Pb$	$^{208}Pb/^{204}Pb$	Reference
S2-13	stibnite	18.239	15.669	38.322	This Study
S4-02	stibnite	18.468	15.678	38.409	This Study
S5-02	stibnite	18.366	15.695	38.362	This Study
S5-04	stibnite	18.452	15.778	38.527	This Study
S1-10	stibnite	18.209	15.729	38.548	This Study
S1-12	stibnite	18.118	15.686	38.427	This Study
S5-08	stibnite	18.136	15.737	38.377	This Study
Wanshan	galena (5)	18.01	15.52	38.50	1
Cambr. strata	dolomite (3)	18.08	15.52	38.47	1

2. Lead isotopes in typical stratiform deposits hosted in sedimentary rocks

Location	petrography	$^{206}Pb/^{204}Pb$	$^{207}Pb/^{204}Pb$	$^{208}Pb/^{204}Pb$	Reference
Bleiberg, Austria	Triassic (2)	18.41	15.80	38.46	4
	limestones (4)	18.52	15.83	38.87	8
Mibladen, Morocco	Mesozoic	18.34	15.74	38.72	2
	limestone (3)				
Kupferschiefer					
Northern Pennines,	Permian	18.20	15.54	38.15	6
Mansfeld, Germany	rocks (9)	18.17	15.80	38.37	7
Spremberg,	(11)	18.28	15.75	38.50	7
Germany					
Meggen, Germany	Devonian	18.37	15.70	38.60	9
	slates	18.42	15.74	38.62	8
Rammelsberg	Dev. slate(2)	18.15	15.58	38.21	9
Germany					
Cobar, Australia	Silurian rocks	18.21	15.77	39.55	3
CaptainsFlat,	Carbonate (S)	18.18	15.77	38.57	3
Australia					

Bathurst, Canada	metamorphos	18.29	15.78	38.53	3
	ed rocks (O_2)	18.20	15.69	38.24	5
Read Roseberry		18.37	15.75	38.47	3
Austr.					

3. Lead isotopes in Mississippi Valley-type lead zinc deposits

Location	petrography	$^{206}Pb/^{204}Pb$	$^{207}Pb/^{204}Pb$	$^{208}Pb/^{204}Pb$	Reference
	Minimum	19.96	15.65	39.10	10
South Missouri	Maximum	21.46	16.19	41.02	
galena	Average (131)	20.81	15.97	40.08	
	Minimum	21.31	16.00	41.07	3
Tri-State sphalerite	Maximum	22.66	16.28	41.92	
	Average (14)	22.11	16.15	41.46	
Wisconsin-Illinois-	Minimum	20.83	15.96	40.45	11
Iowa sphalerite-	Maximum	24.44	16.33	43.95	
galena	Average (19)	22.54	16.15.	42.31	

References: (1) Hua (1982); (2)Cahen et al. (1958); (3) Ostic et al.(1967); (4) Russell and Farquhar (1960); (5) Doe (1962); (6) Moorbath (1962) (7)Kautsch et al. (1964); (8) Eberhardt et al. (1955); (9) Geiss (1954) (10) Brown (1967); (11) Heyl et al.(1966).

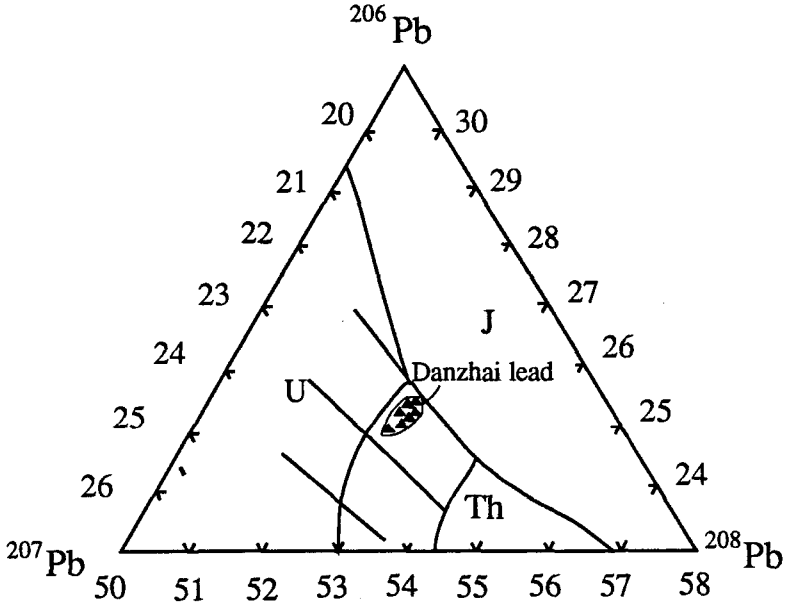

Fig. 7.1 $^{206}Pb - ^{207}Pb - ^{208}Pb$ triangular diagram. The ore leads from stibnite denoted by solid triangles are located in the cresent shaped common lead sector (after Cannon et al. 1961).

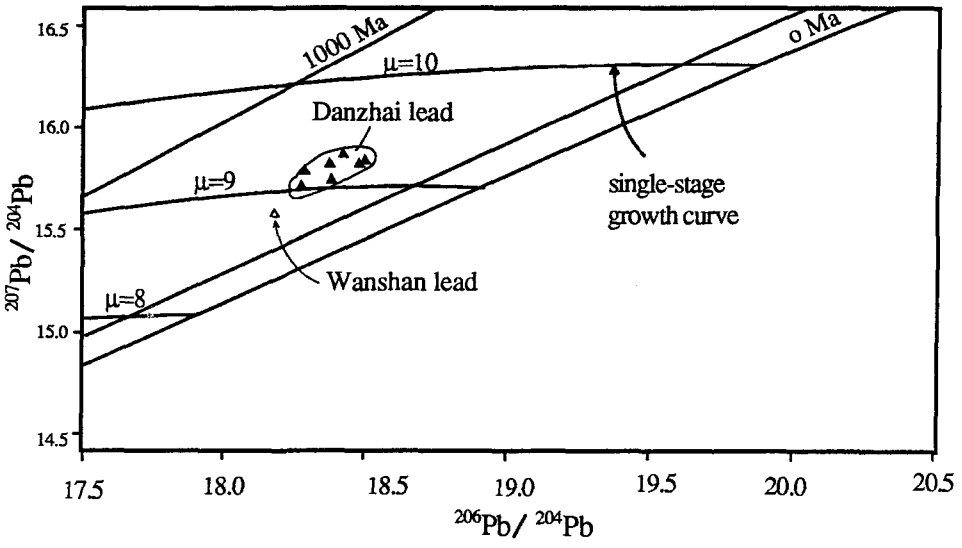

Fig. 7.2 Single stage lead isotope growth curve. The lead isotope data from the Danzhai gold mercury deposit is located near 400 Ma on the model growth curve.

example, indicate that the leads are very radiogenic, all possess values of $^{206}Pb/^{204}Pb$ generally greater than 20.00, $^{207}Pb/^{204}Pb$ usually greater than 15.80, and $^{208}Pb/^{204}Pb$ usually greater than 39.50 (Brown, 1967; Doe and Delevaux, 1972; Crocetti et al., 1988). Geochemically, these data were interpreted as an initial lead homogenized about 1350 Ma and that this lead combined with a variable proportion of an added radiogenic component generated in the period between consolidation of the basement (1350 Ma) and formation of the mineralizing solution (Richards et al. 1971). Geologically, these lead isotope data fit a lateral secretion mechanism for these deposits, perhaps with the source of the lead being the basement rocks(Cannon and Pierce, 1967). Ore genesis in the Danzhai gold-mercury deposit may be distinguished from the Mississippi Valley type lead zinc deposit by the lead isotope data.

Even though the lead isotope value of the Danzhai gold-mercury deposit is quite different from the Mississippi Valley-type lead zinc deposit, they are similar to that of many other sedimentary rock-hosted deposits. For example, the lower part of table 7.1 lists the lead isotope data of some typical stratiform deposits hosted by sedimentary rocks such as stratiform ores in Kupferschiefer Marl-Slate, Germany and Poland, Cobar and Captains Flat, New South Wales, Australia, and Bathurst, New Brunswick, Canada. The lead isotope data in those deposits can be seen to be highly homogeneous and non radiogenic, and have reasonable good agreement with the known age of the wall rocks. One excellent example is the Kupferschiefer Marl-Slate Cu, Au, Pt deposit. Many investigators favor a syngenetic origin for these deposits, but Wedepohl (1964) considered that the syngenetic fluid which deposited the deposits must have been unusually rich in heavy metal contents relative to ocean water. It may be more reasonable and acceptable that the ore-forming fluid in Kupferschiefer Marl-Slate derived from a diagenetic fluid than a syngenetic fluid (Kucha, 1982; Wedepohl et al., 1978).

Detailed studies (e.g. Doe, 1970; Doe and Stacey, 1974) demonstrated that, except in the Mississippi Valley-type lead zinc and fluorite deposits, lead isotope data in many sedimentary rock-hosted stratiform deposits, such as the Kupferschiefer follow the single-stage growth curve, and their model age is identical to their host sedimentary rocks.

The single-stage growth curve is adopted here for the reason mentioned above. The model age from the ore lead is calculated by the method proposed by Doe and Stacey (1974). The parameters used for plotting single-stage growth curves and the isochrons of Fig. 7.2 include the age of the Earth: T=4.57 Ga; primordial lead: $^{206}Pb/^{204}Pb=9.307$, $^{207}Pb/^{204}Pb=10.294$, $^{208}Pb/^{204}Pb=29.497$ (Cumming and Richards, 1975; Köpel and Grünenfelder, 1979); the decay constants: $\lambda(^{238}U)=1.55125\times10^{-10}$/year, $\lambda(^{235}U)=9.8485\times10^{-10}$/year, $\lambda(^{232}Th)=4.9475\times10^{-11}$/year (Jäger, 1979); and the present atomic ratio, $^{238}U/^{235}U=137.88$, $\mu=^{238}U/^{204}Pb$.

Fig. 7.2 shows that the ore lead isotopes fit the single-stage growth curve nicely. The data is located in line in the 400 Ma isochron, as are the leads from the Wanshan mercury deposit. The 400 Ma is the time of the end of Silurian period. Evidently, the model age of ore lead from the Danzhai gold-mercury deposit is a little younger the Cambrian or Ordovician strata. It means that the ore deposit did not form at the same time as the strata and the ore deposits are not syngenetic.

§ 7.5. Origin of the Common Lead Isotope

In the last thirty years lead isotopes have found increasing use in studies of the provenances of ore deposits (e.g. Cannon, 1961, Zartman, 1974, Doe and Zartman, 1979). These applications have generally revealed that if a time interval as geologically short as the Phanerozoic is examined, then distinct patterns of lead isotopic abundances are seen to be associated with specific environments (Doe and Zartman, 1979).

There are several useful and practical ways which have been applied to distinguish the geologic environment of lead isotope (Doe, 1979, Slawson, 1983).

The lead isotope data of the ore is constrained by the origin of $^{238}U/^{204}Pb$ as well as $^{232}Th/^{204}Pb$ (Doe, 1970). Studies indicated that, the μ value of the modern mantle is 6.29, κ of which is 5.91; the μ value of the upper crust is 13.23, , and the κ is 3.43; the μ value of an orogenic zone and/or island arc is 11.32, κ is 3.63 (Zartman, 1981). In the Danzhai gold-mercury deposit, the calculated μ value is in the range of the upper crust, the k value is

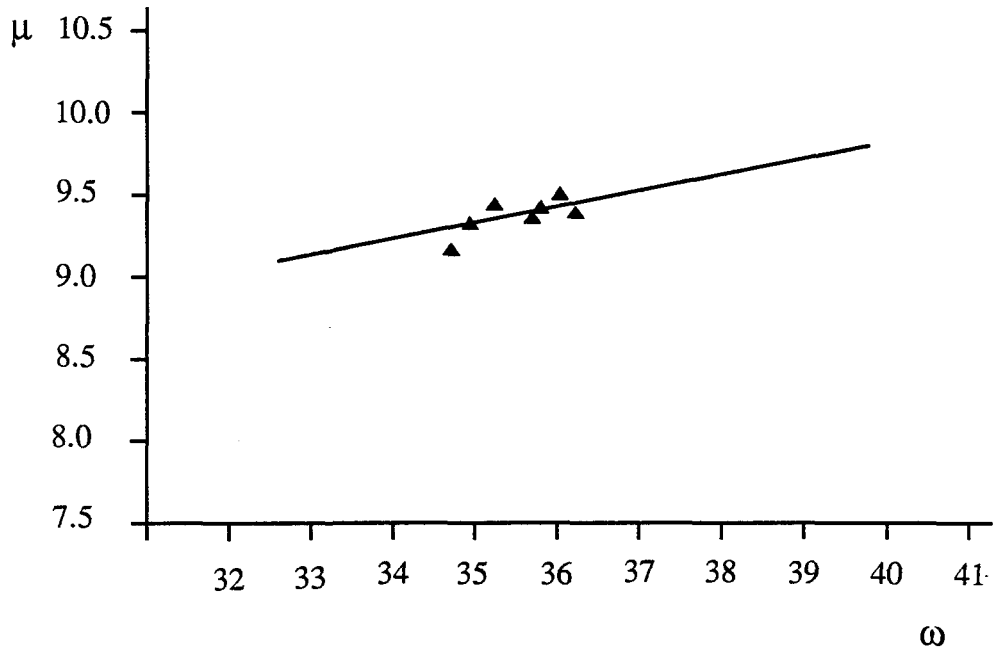

Fig. 7.3 The correlation digram for μ value and ω value of lead provenance based on the calculation of lead isotope of trace lead in stibnite.

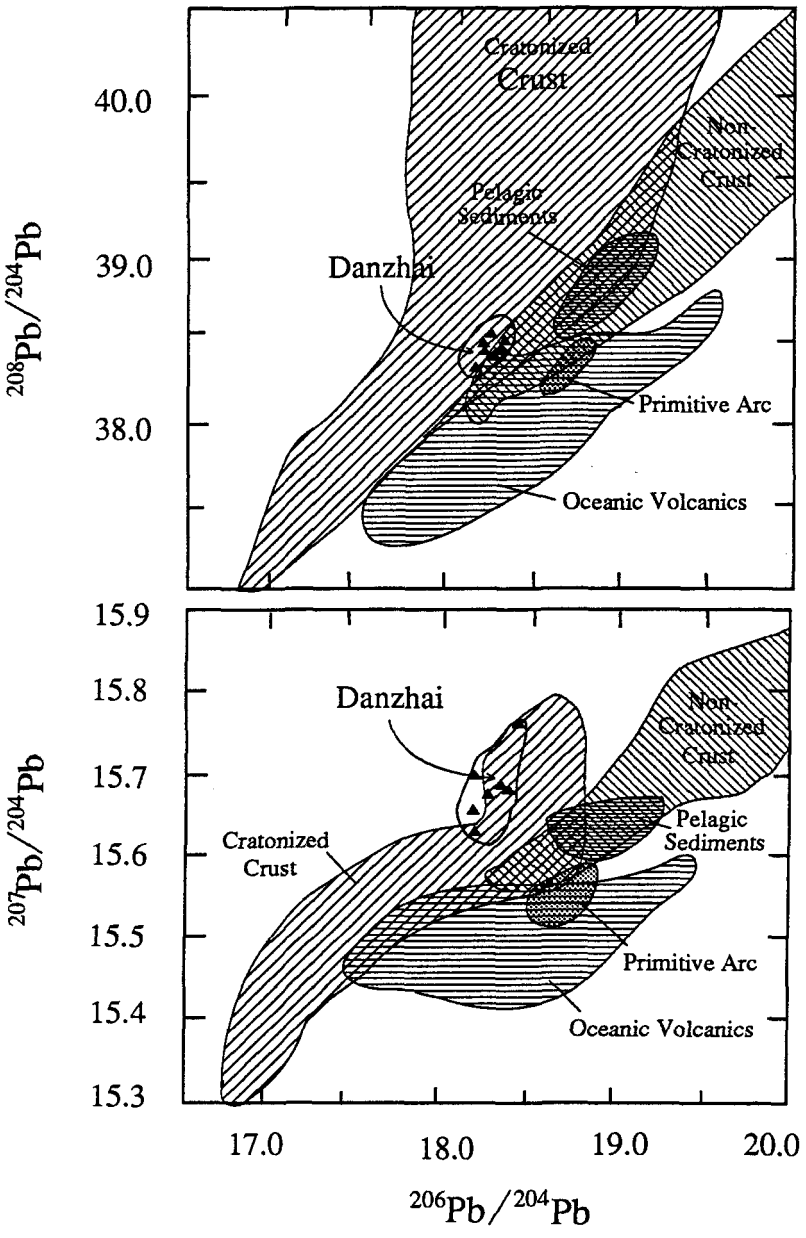

Fig. 7.4 Summary plots for $^{207}Pb/^{204}Pb$ and $^{208}Pb/^{204}Pb$ versus $^{206}Pb/^{204}Pb$ in the crust of the earth. The lead isotope data in the Danzhai gold mercury deposit plots in the sector of cratonized crust.(modified after Doe and Zartman, 1979)

also in the neighborhood of the upper crust. The μ values and ω values of all the samples in the Danzhai gold-mercury deposit and the Wanshan deposit correlate in a line (Fig. 7.3). These correlated μ value and ω values imply they were from the same U, Th, Pb system.

Doe and Zartman (1979) proposed a summary plot for $^{207}Pb/^{204}Pb$ and $^{208}Pb/^{204}Pb$ versus $^{206}Pb/^{204}Pb$ (Fig. 7.4) to present an outline of lead isotope composition for distinct geological environments on the crust of earth, such as oceanic volcanics, primitive arcs, pelagic sediments, non cratonized crust and cratonized crust. The model has been used to distinguish the origin of mineralization(e.g.: Large, 1983; Richards, 1971; Johnson and Richard, 1985). The lead isotopes from the Danzhai gold-mercury deposit, together with some other typical sedimentary rock hosted deposits plot remarkably in the sector of cratonized crust. This is coincident with the geological observation that the Danzhai gold-mercury deposit is located on the Yangtze craton.

On a more detailed scale, lead isotope data from the Danzhai gold-mercury deposit can be compared to sedimentary rock-hosted ore deposits with continental affinities, in which the probability of a close genetic association with igneous activity seems remote. Most of these ore deposits belong to the so-called stratiform and stratabound deposits. These deposits are thought to have formed syngenetically or probably shortly after the surrounding sediments, through action of early diagenesis or postdepositional infiltration. Two distinct groups of lead isotopes are present in these deposits, one group is characterized by common lead and may have model ages in agreement with, or in the neighborhood of, the age of the host rocks, while another group consists of highly radiogenic lead called J-type leads may represent negative or future model ages. The J-lead group is exemplified by the Mississippi Valley-type lead zinc fluorite deposits (Fig. 7.5), which tend to plot below an extension of the orogenic evolution curve in the plot involving thorogenic lead ($^{208}Pb/^{204}Pb$). This phenomenon is interpreted as a characteristic of upper crustal leads in cratonic regions and is believed to be a consequence of enrichment of uranium (relative to thorium) in the upper crust with complementary loss of uranium from the lower crust. Some typical common lead groups in these deposits are listed in table 7.1 such as stratiform ores in Kupferschiefer Marl-Slate, Germany and Scotland, Cobar and Captains Flat, New South Wales, Australia, and Bathurst, New Brunswick, Canada. They are of homogeneous lead isotope composition and have identical model ages with their host

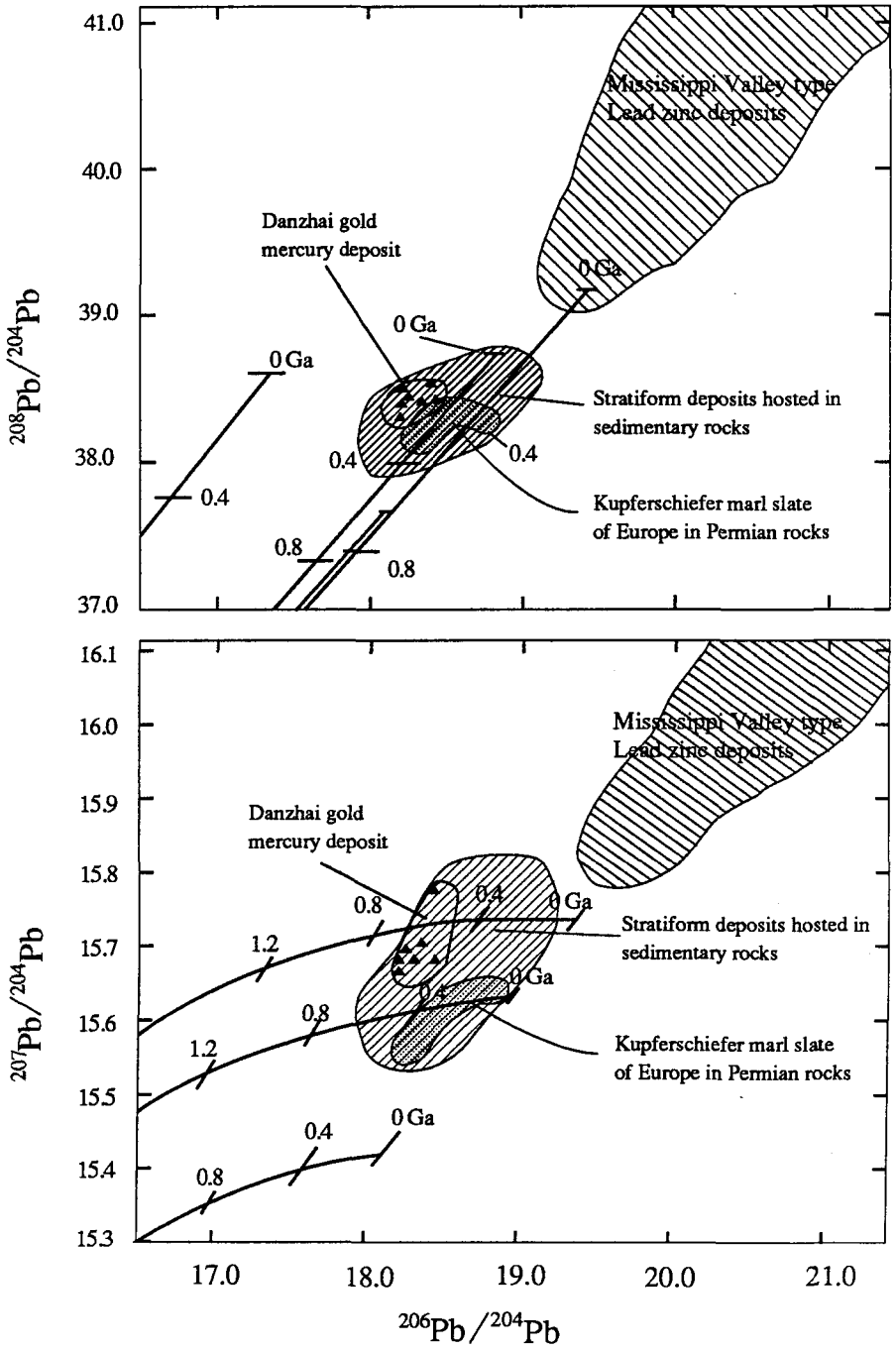

Fig. 7 .5 $^{207}Pb/^{204}Pb$ and $^{208}Pb/^{204}Pb$ versus $^{206}Pb/^{204}Pb$ for mineral deposits hosted in sedimentary rocks without associated igneous activity in a continental environment. The data used in the diagram are given in the table 8.1.

sedimentary rocks. Therefore, they are believed to be either of syngenetic or diagenetic origin. The lead isotopes in the Danzhai gold-mercury deposit are attributed to the common lead group, and are likely of diagenetic origin. Their provenance appears related to Cambrian or Ordovician sedimentary rocks.

The lead isotope investigation in galena samples associated with cinnabar in the Wanshan mercury deposit in the same region (table 7.1) (Hua, 1982) present similar data to the stibnite samples from in the Danzhai gold-mercury deposit, and both lead isotope data from stibnite and from galena are of similar composition to that of dolomite in Cambrian strata (Hua, 1982). Theoretical calculation using lead isotopes from meteorites as primordial ones shows that, the lead isotope composition on earth at 500 Ma is composed of: $^{206}Pb/^{204}Pb$: 18.48; $^{206}Pb/^{204}Pb$: 15.56; $^{206}Pb/^{204}Pb$: 38.05. Lead isotope data from both the Danzhai gold-mercury deposit and the Wanshan mercury deposit are within the range of these calculated values, and they are also coincident with the lead isotope composition of the Cambrian strata. Accordingly, it is acceptable that the ore-lead in the Danzhai gold-mercury deposit is derived from the Cambrian and/or Ordovician strata.

§ 7.6. Summary

Since no galena samples were available for lead isotope investigation in the Danzhai gold-mercury deposit, the trace lead of stibnite is used instead. The trace lead in stibnite was successfully isolated from the major constituents of stibnite such as Sb, S and served for the lead isotope study. The stibnite samples were selected from different ore-bodies, but all from the second mineralization stage, which is the most important stage both for gold and mercury mineralization in the Danzhai gold-mercury deposit.

The lead isotope data indicate that the lead from the Danzhai gold-mercury deposit is common, not radiogenic lead. The lead isotopes of all samples from different orebodies are homogeneous, and have a highly evolved μ value lead, simialr to data from values widely distributed localities in south China. These characteristics are different from the lead isotope of Mississippi Valley-type lead zinc deposits, but they are similar to that of stratiform deposits hosted in sedimentary rocks around the world.

The model age of ore lead is in the neighborhood of 400 Ma, which is the age of the end of Silurian. This is in agreement with other geological facts, because there are many mercury, antimony and gold deposits in that area hosted in Cambrian and Ordovician strata. Lead isotope compositions in the Danzhai gold-mercury deposit are coincident with those of the host Cambrian Ordovician strata, which suggest that the ore-forming elements probably came from the Cambrian and Ordovician strata .

According to the plumbotectonic model of Doe and Zartman (1979) lead isotope data plots on the evolution curve of the upper crust, suggesting that the lead in the deposit is derived from Cambrian or Ordovician sedimentary rocks, and the ore metals such gold and mercury can be considered to be of similar origin.

CHAPTER VIII:

A POSSIBLE GENETIC MODEL FOR THE DANZHAI GOLD AND MERCURY DEPOSIT

§ 8.1. Introduction

A number of models have been proposed for the genesis of Carlin gold deposit in western U.S.A.. For instance, Radtke (1985), Rye et al (1982), Berger and Bagby (1985), Bagby and berger (1991) considered that igneous activity provided heat to convecting meteoric waters, which leached metals from sedimentary rocks and transported them to favorable horizons in the near-surface zone, depositing quartz, pyrite, gold, and associated elements. An integral part of their model was the development of a late-stage, hypogene, acid-leaching phase at higher than ore-stage temperatures due to boiling, which produced much of the oxide ores at Carlin. Cox and Singer (1986) presented a descriptive model for Carlin-type deposits that summarized all of the geological and mineralogical characteristics and grade-tonnage relationships of this deposit, but the model contains no genetic concepts. Rose and Kuehn (1987) tied the formation of Carlin-type deposits to intrusions that de-gas CO_2 and mix it with CO_2 generated from the contact metasomatism of adjacent carbonate rocks. This low-salinity mixed fluid then rises until it encounters and mixes with a lower temperature, low-CO_2 fluid where gold is precipitated. The low-salinity, high-CO_2, and high-H_2S contents would enhance gold transport and inhibit the transport of Ag, Zn, and Pb. Rose and Kuehn(1987) did not consider boiling to be a factor in their genetic model for the Carlin deposit. Bagby and berger (1991) proposed that Carlin-type gold deposit is spatially and temporally related to thermal events associated with relatively reduced, primarily granodioritic magma that may also form tungsten-bearing skarn deposits and/or molybdenum-bearing stockwork deposits. Romberger (1985) believed that the Carlin-type

gold deposit is an epithermal deposit, or a subtype of epithermal deposit, and it is an analogue of present-day hydrothermal systems.

All of these models considered that the Carlin-type gold deposits are an epithermal deposit related to magmatism. As in many other epithermal deposits, particularly present-day epithermal deposit, the following factors are important in the formation of these deposits: (1) heat source from intrusive or eruptive activity is essential for the mineralization; (2) heated ground water participated the mineralization as an ore-forming fluid; (3) subvertical open fractures along which hot solutions rise and precipitate is the key structure in the precipitation of metals; (4) boiling is also an important process in the genesis of the deposits and there is no doubt that this is an effective mechanism for gold deposition. These factors correspond somewhat to the geological characteristics of the Carlin-type gold deposit in western U.S.A., where granodiorite is present within or near these deposits, subvertical fractures control the occurrence of the gold orebodies, but no evidence confirms the boiling process except in the oxidized ores (Radtke, 1980). In the eastern region of Guizhou Province, however, no such magmatism is associated with gold-mercury mineralization, nor with the Carlin-type gold deposits in the southwestern Guizhou Province reported by Cunningham et al.(1988). Therefore, proposed models are obviously not completely adaptable to the genesis of the Danzhai gold-mercury deposit, or other associated mercury, gold, arsenic, antimony and barite mineralization hosted in carbonate in the eastern region of Guizhou Province.

§ 8.2. Formation Water or Oilfield Brine As an Ore-Forming Solutions

A great number of Carlin-type gold deposits and associated mercury, antimony, barite deposits in China are not obviously associated with magmatism. Tu (1983, 1984, 1987, 1988) proposed a genetic model for these stratabound and stratiform mercury, antimony and arsenic deposits hosted in sedimentary rocks, not associated with magmatism or metamorphism, as a process similar to petroleum evolution. The major similarities between the two processes are: (1) oil source strata correspond to the ore source strata; (2) petroleum accumulating strata are equivalent to the precipitating locations of ore-forming fluids; and (3) the structures controlling the mineralization are also similar to that of

petroleum reservoirs. These similarities suggest that mercury, antimony and arsenic mineralization is probably related to petroleum evolution.

Connan (1979) revealed that a genetic relation between oil and ore in some Pb, Zn, Ba deposits. Sverjensky (1984, 1987) proposed that oilfield brines can be an ore-forming solution and can transport base metals such as Pb, Zn, Cu and reduced sulfur to ore formation sites by large-scale migration along aquifers out of sedimentary basins. This hypothesis is supported by the chemical compositions, the pH values, temperature and pressure of present-day heavy metal-bearing oil field brines as well as the petrography of their reservoir rocks. Carter and Cazalet (1984) indicated that hydrocarbon gases in sedimentary rocks can be a pathfinder for mineral exploration.

Hausen and Park (1986) concluded from a study of the Carlin deposit and from comparisons with other deposits that the domed and faulted areas associated with some Carlin-type gold deposits had been petroleum reservoirs, but they believed that the ores at Carlin, Getchell, and Alligator Ridge contain bituminous matter that is mostly petroleum residues emplaced in the host rocks prior to gold mineralization.

Partly because of the absence of magmatism in the eastern region of Guizhou province, and partly because of the intimate spatial and temporal association of the regional gold, mercury, antimony, barite deposits with the former Majiang-Danzhai petroleum reservoir, the Danzhai gold-mercury deposit is considered to be related to petroleum evolution in the region. Prior to illustrating this genetic model, it is necessary to review the general paths of petroleum evolution.

§ 8.3. General Paths of Petroleum Evolution

The processes of generation, development and destruction of petroleum are termed petroleum evolution. A general scheme of the diagenesis of sediments and the evolution of organic matters from deposition to the beginning of metamorphism, is illustrated in Fig. 8.1 by Tissot and Welte (1984) and modified by Barnes et al.(1985) and Bustin (1989). Three important stages of diageneses of sediments are classified as: eogenesis, catagenesis, and

metagenesis, and the associated organic matter evolution is correspondingly divided into: the immature zone, the oil zone, the wet gas zone as well as the dry gas zone.

A variety of organic matter such as dead vegetable or animal matter deposited in a sedimentary basin undergoes the eogenetic stage. Eogenesis covers all low temperature diagenesis of organic matter. Eogenetic reactions are partly biochemical, arising from metabolic processes occurring within organisms, and partly abiotic chemical reactions which incorporate metabolic products released to the sediments. Microorganisms metabolize most of the organic matter to CO_2 and H_2O in oxygenated sediments and to CH_4, CO_2, H_2 and H_2O under anoxic conditions. In the later condition, a natural gas (CH_4) field may be formed in appropriate geological environment. The methane in this stage is called biogenic methane since it is a direct consequence of microorganism metabolism. The remaining organic matter forms humic and fulvic acids. With increasing cross-linkage and loss of functional groups, these acids decrease in solubility and form part of the kerogen fraction. Therefore, in this stage, except for the biogenic methane, oil is not produced, so it is called the immature zone. The boundary between eogenesis and catagenesis is generally considered to be coincident with the boundary between sub-bituminous and high volatile bituminous coals, which corresponds to a vitrinite reflectance of about 0.5%.

The catagenetic stage of diagenesis results from increased temperature and time accompanying burial of the sediments. Kerogen makes up the great bulk of organic matter present at this stage. Kerogen is an irregular geopolymer formed by random chemical recombination of organic compounds released by microbial decomposition of proteins, carbohydrates and lipids.

Based on its bulk H/C and O/C atomic ratios, three types of kerogen have been defined which appear to follow distinct diagenetic pathways. Type I kerogen has high initial H/C and low O/C ratios, and contains many aliphatic chains and few aromatic nuclei. The potential for oil and gas generation of this type of kerogen is the highest. The source material of this type kerogen is mainly algal lipids, or a combination of algal lipids and waxes from higher plants, which have been selectively concentrated by microbial reworking. Type II kerogen has intermediate initial H/C and O/C ratios, and contains more aromatic and naphthenic rings. Both algal and higher plant sources appear to contribute to

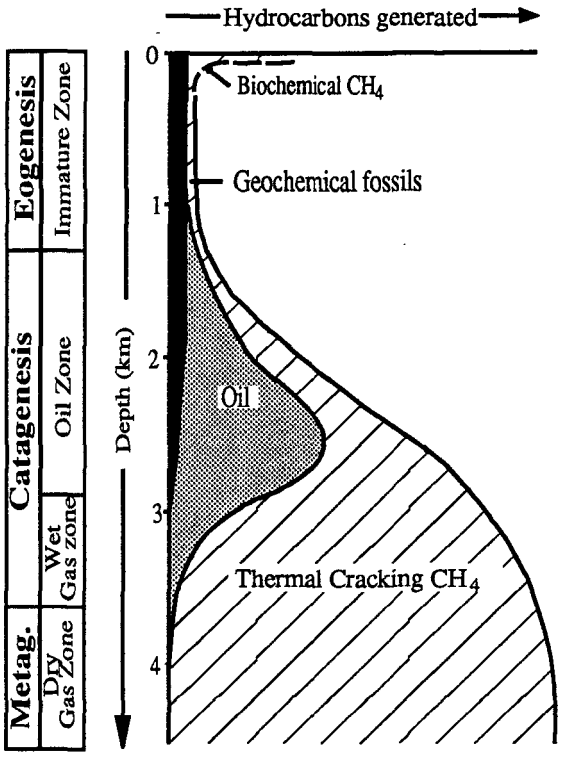

Fig. 8. 1 General scheme of hydrocarbon formation as a function of burial of the source rocks. The evolution of hydrocarbon composition is shown in insets for three structural types. Depths are only indicative and correspond to an average of Mesozoic and Paleozoic source rocks (simplified after Tissot and Welte, 1984).

type II kerogens (liptinite coal macerals). Most type II kerogens are related to marine organic matter deposited in reduced environment, with medium to high sulfur content. The oil and gas potential are lower than that of type I kerogen but still very important. Type III kerogen has a low initial H/C ratio, less than 1, an initial O/C ratio of 0.2 to 0.3, and contains mostly condensed polyaromatics and oxygenated functional groups with minor aliphatic chains. The type III kerogen is derived dominantly from terrestrial plants. Its oil potential is only moderate, although this kerogen may still generate abundant gas at greater depths.

Catagenesis happens at moderate temperatures (50 to 150 °C) and pressures (30 to 150 MPa), corresponding to the zone of oil and wet gas generation. At the end of catagenesis, aliphatic chains are cleaved from kerogens, and the size of aromatic units increases through chemical condensation producing significant ordering. Thermal degradation of kerogen is responsible for the generation of most hydrocarbon and oil is mostly produced in the catagenesis stage. The "oil birth line" denotes the upper limit where oil generation begins and the "oil death line" delimits the end of oil generation thus defining a zone termed as the "oil window". At the "oil birth line", medium to low molecular weight hydrocarbons are produced from kerogens and the vitrinite reflectance is around 0.5% in keeping with the level of catagenesis. On the other hand, the "oil death line" is where kerogen and earlier formed liquid hydrocarbons are transformed through cracking to low molecular weight hydrocarbons with a dominance of methane, commonly described as wet gas. The vitrinite reflectance at this level of diagenesis is around 1.35%. Gas generation from the kerogen can take place all along the "oil window". However, with the increase in the level of catagenesis the cracking increases the proportion of methane. At the level of metagenesis methane is the only component produced through cracking of oil and kerogens and is termed as "dry gas".

Metagenesis is reached only at great depth, however, this last stage of evolution of organic matter begins earlier (vitrinite reflectance approximately 2%) than metamorphism of the mineral phase (vitrinite reflectance of about 4% corresponding to the beginning of the greenschist facies). During this stage, a rearrangement of the aromatic sheets occurs. The stacks of aromatic layers, previously distributed at random in kerogen, now gather to form

larger clusters. At this stage, only dry gas is generated, all oil is thermally degraded to methane.

The geological processes of petroleum evolution are defined as three stages, that is, the formation of petroleum, the migration of petroleum and the accumulation of petroleum. The migration can be defined as primary migration and secondary migration.

With increasing depth, temperature and time of sediments, the kerogen hosted in sediments crack to oil in certain temperature. Meanwhile, compaction in sediments results in an increase in bulk density and loss of porosity. Compaction causing fluid flow through sedimentary rocks was commonly considered as an important factor in petroleum migration. During compaction there is also a marked regular decrease in pore diameters. At greater depths (below 3000 m) in detrital sediments they reach values around 10 to 25 Å, which is in the range of the dimensions of the molecules of certain petroleum constituents.

The most important form of primary migration during the main phases of petroleum formation seems to be a pressure-driven, discrete hydrocarbon phase movement. The generation of low molecular weight hydrocarbons from polymetric kerogen causes combination of the effects of thermal expansion of pore water, rapid burial, and partial transfer of the geostatic stress field from the solid rock matrix to the enclosed pore fluids. In this way pressure centers are created in a source rock that cause a more or less continuous pressure-driven hydrocarbon phase movement. In relatively impermeable source rocks, these pressure centers may even induce microscale rocks fracturing. Pressure build-up, microfracturing, subsequent pressure release, expansion of fluid, and finally transport are a discontinuous process. This process must be repeated many times in source rocks in order to accomplish meaningful petroleum movement. The distances covered by primary migration are commonly in the order of meters or tens of meters.

Secondary migration, the movement of oil and gas through carrier and reservoir rocks, and the subsequent formation of pools is controlled by three parameters. These are the buoyant rise of petroleum in water-saturated porous rocks, capillary pressures that determine multiphase flow, and, as an important modifying influence, hydrodynamic fluid flow. As long as the aqueous pore fluids in the subsurface are stationary, i.e., under hydrostatic conditions, the only driving force for secondary migration is buoyancy. If there

hydrostatic conditions, the only driving force for secondary migration is buoyancy. If there is water flow in the subsurface, i.e., under hydrodynamic conditions, the buoyant rise of petroleum may be modified by this water flow. Capillary pressures in narrow rock pores are the cause for hydrocarbon entrapment. The end of secondary migration, and the final stage in the formation of petroleum pools is the concentration in the highest available part of a trap. The cap-rocks, seal, or barrier that stops moving hydrocarbons by virtue of its general decrease in pore diameters must exert capillary pressures greater than the driving force. Distances covered by secondary migration are in the range of ten to a hundred kilometers, and occasionally even more.

Petroleum is ultimately collected through secondary migration in permeable porous reservoir rocks in the position of a trap. It is characterized by its upward convex shape in combination with porous reservoir rocks with a relatively impermeable sealing cap rock above. Generally one distinguishes between stratigraphic and structural traps. Stratigraphic traps are mainly caused by depositional features, and structural traps by tectonic events. These causes for the formation of a trap may also be combined. Typical examples for stratigraphic traps are barrier sand bars, deltaic distributory channel sandstones and carbonate reefs. Typical examples for structural traps are anticlines, fault traps, and traps associated with salt domes. Petroleum accumulations are found between the surface and depth levels of about 6 to 7 km or deeper. Thus, petroleum must move through pores saturated with water, at fluid pressures ranging between 10^7 pascals and 1.4×10^7 pascals and at temperatures from about 50 °C to about 250 °C.

§ 8.4. Mineralization of the Danzhai Gold-mercury Deposit and Petroleum Evolution in the Eastern Region of Guizhou Province

Even though many geological characteristics are similar between Carlin-type gold deposits in western U.S.A. and the Carlin-type gold deposits in both eastern Guizhou and southwest Guizhou, their tectonic setting and magmatic process are different, that is, Carlin-type gold deposits in western U.S.A. are located in an active continental margin where magmatism is active whereas the Carlin-type gold deposits in southwest of China are situated on the Yangtze craton where magmatism is absent. Therefore, magma as a heat and

metal source of the Carlin-type gold deposits in the eastern and southwest Guizhou is not reasonable. An alternative model should be set up to interpret the geological and geochemical characteristics of these deposits.

The gold, mercury, antimony, arsenic as well as barite mineralization in the eastern region of Guizhou province are associated with Majiang-Danzhai petroleum reservoir. The polymetallic mineralizations and regional petroleum evolution are not only spatially linked, but also temporally related. Detailed fluid inclusion investigation shows that the ore-forming fluid in the different mineralization stages are dominated by hydrocarbons, particularly liquid methane. This relationship may suggest that the regional polymetallic mineralizations are related to regional petroleum evolution. The following discussion is organized accordingly.

§ 8.4.1. The Source Strata for Petroleum and the Source Strata for Ore-Forming Elements

Han et al.(1982) examined the three possible petroleum source strata of the Majiang-Danzhai oil trap, the Lower Cambrian, the Lower Ordovician Honghuaran Formation as well as the Silurian Wengxiang Formation. Calculation shows that the Lower Ordovician can offer 48.49 billion metric tons of crude oil; the Lower Ordovician Honghuaran Formation, 0.22 billion metric tons; and the Silurian Wengxiang Formation, 0.89 billion metric tons. Obviously, the Lower Cambrian is the most important oil source strata since 97.96% of potential crude oil in the Majiang-Danzhai oil reservoir is constrained within it. The lithology in Lower Cambrian is dominated by black shale which was deposited in the reduced marine sedimentary basin. Its thickness can be as great as 1032 meters and the average organic carbon content is 0.70%.

The ore-forming elements in Lower Cambrian black shale over south China was investigated by Fan (1981). She found that gold, arsenic, silver, platinum and palladium were concentrated in the black shale, even some silver-bearing gold grains were discovered. Chen et al. (1986) analyzed seven samples of black shale from the Lower Cambrian to evaluate its possibility as an ore source strata. The results are: gold: 11 ppb to 0.68 ppm; mercury: 3 - 10 ppm; arsenic: 50 - 200 ppm; barium: 100 - 10,000 ppm; silver: 0.1 - 0.5

ppm; organic carbon: 2.9% on average, the highest is 9.12%. All of these values are much higher than the Clarke values of the various metals. Detailed examination showed that mercury, silver, barium, vanadium and chromium tend to enrich in organic carbon-rich black shale while gold and arsenic are concentrated in coarser but organic carbon-poor rocks (e.g.: silty black shale, or argillaceous siltstone). Evidently, the principal ore-forming elements are abundant in the petroleum source strata. It is thus considered that the petroleum source strata of the Majiang-Danzhai oil trap are probably also the ore source strata of the deposits in the Sandou-Danzhai ore belt and other associated mercury, antimony, gold and barite deposits in the eastern region of Guizhou.

§ 8.4.2. Petroleum and Associated Brine as the Ore-Forming Fluid

Shale is commonly a impermeable layer in sedimentary basins, so leaching of metals by ground water may be difficult even though the black shale is metalliferous. How did the Lower Cambrian black shale become the ore source layer of the gold, mercury, arsenic and barite deposits in the eastern region of Guizhou Province?

It is a fact that the metals are extracted with difficulty from black shale by solutions, which happens after consolidation. In the eogenetic stage, however, the metals concentrated in the organic matter-rich argillaceous sediments can be transfered into the hydrocarbon phase of the formation water. These metals can enter the hydrocarbon phase by three possible ways (Ling, 1989): (1) biologic metabolism: some living plants can accumulate metals such as gold from the environment by their metabolism, and the enriched metals will enter into hydrocarbon phase with petroleum evolution of the dead plants; (2) the reaction between organic matters and sediments can take two possible paths, one is that organic matter physico-chemically absorbs the metals in sediments and subsequently enters into hydrocarbon phase of the petroleum evolution while the other is that during the process of formation of hydrocarbons, the hydrocarbons extract the metals from sedimentary rocks; (3) hydrocarbons extract gold from formation water or oilfield brine from different stages of diagenesis.

The first and second methods of metal transfer have been discussed by numerous authors (e.g. Fedoseyeva et al., 1985; Ong and Swanson, 1969; Shacklette et al., 1970).

For example, humic acids and true organic solution can be mineral solvents under supergene conditions (Barker, 1973; Fedoseyeva et al., 1985; Fetzer, 1934, 1946, Moiseev, 1971), these organic acids such as humic acids and amino acids have a capacity to dissolve gold from weathered minerals and transport gold as an ore-forming fluid (Barker, 1978; Benedetti and Boulegue, 1991; Shestopalova and Chernyak, 1975). All these processes correspond to the eogenetic stage of sediments and in the immature zone of petroleum evolution. In the present case the principal concern is the role of oil and associated brine in the extraction and transport of gold, that is to say, the oil and associated brine acting as an ore-forming solution in the catagenetic stage of sediments or in the oil zone of petroleum evolution. Experiments of crude oil and oilfield brine extraction gold was undertaken by Ling (1989). The result shows that the crude oil and oilfield brines have strong capability to extract gold from an experimental gold-bearing solution. The gold extraction rate through oil varies from 21.7% to 96.9%, depending on the type of oil. The heavy oil has high extraction rate while the light oil is the contrary. If the crude oil is rich in heteroatomic compounds such as sulfur, nitrogen as well as oxygen compounds, it tends to have high extracting capability, in the neighborhood of 95%. So the heteroatomic compound may capture the dissolved gold and other metals (Bonati, 1987).

Oilfield brines are considered to be involved in the formation of some important classes of sediment-hosted base metal sulfide ore deposits (Hanor, 1979; Gustafson and Williams, 1981; Sverjensky, 1984, 1987). Fluid inclusion and isotopic data revealed the association of basinal fluids with sediment-hosted ores, particularly, in the Mississippi Valley type lead-zinc-barite-fluorite deposits. By theoretical analysis of water-rock interactions, Sverjensky (1987) indicated that an oilfield brine can also be the ore-forming solution of sediment-hosted Cu-rich deposits. Is it possible that oilfield brines can be an ore-forming fluids for gold and other metallic deposits? Experiments by Ling (1989) also show that the oilfield brines taken from different oilfields in China can extract gold from pure sponge gold. The solubility of gold in the oilfield brines ranges from 0.88 to 1.3 ppm at 70 °C, depending on the compostion of the oilfield brines. It is much higher than that of distilled water, in which the solubility of gold is only 0.003 ppm at 25 °C, but the gold extracting capability of oilfield brine is somewhat lower than that of associated crude oil, so crude oil can extract gold from the oilfield brines.

The intimate association between hydrocarbons and lead, zinc, copper , uranium, mercury, fluorite and barite mineralizations hosted in sedimentary rocks is well documented (e.g.: Saxby, 1976; Parnell, 1988, Dobryanskiy and Gavrish, 1989). In these deposits, many forms of hydrocarbon are found. For example, dispersed bitumen or bitumen veins are associated with mineralizations, bitumens are metaliferous in many occasions (Banikova et al., 1984). Some of them even contain gold (Boyle and Steacy, 1973). Oil inclusions or oil-bearing inclusions are found in sphalerite, fluorite as well as barite (e.g.: Blasch and Coveney, 1988). This close relationship between hydrocarbons and mineralizations does not certainly mean that petroleum is the ore-forming fluid (Parnell, 1988). The role of hydrocarbons might simply be in the deposition of metals and/or sulphides by reduction processes where metal-bearing and hydrocarbon-bearing fluids meet. Alternatively, hydrocarbons may play a role in the transport of metals through the formation of organometallic complexes. In the case of the Danzhai gold-mercury deposit, is it possible for the petroleum to be a gold-mercury ore-forming fluid?

If oil really can be an ore-forming fluid, the investigation of trace elements in petroleum of oilfields around the world is significant (Bnikova et al., 1984; Bergerioux and Zikovsky, 1978; Yen, 1975). What is the abundance of gold in the petroleum of modern oilfield? The analytical results are limited since previously a series of complex processes were needed to analyze gold in oil and bitumen. But recently with the application of Neutron Activation Analysis, gold and many other elements are quite easily examined in the crude oil and bitumen. It is surprising that the gold abundance in crude oil and bitumen may be extremely high, not only much higher than the minimum gold (20 ppb) for an ore-forming solution, but also as high as the oil mineralized by gold, that is, several g/t of gold in crude oil and bitumen. Table 8.1 lists the gold abundance of some samples of crude oil and bitumen for various oilfields over the world. The highest content of gold in oil from Nigeria, is 5.94 ppm, and the highest content of gold in bitumen is from ex-U.S.S.R., 190 ppm. It is therefore believed that gold may be present as gold-bearing organic compounds in oil or bitumen. Therefore, petroleum can probably be a gold ore-forming fluid, extracting gold as well as transporting gold, as does the associated oilfield brine. Actually, as early as in 1931, Freise (1931) indicated that gold can be transported by organic underground solutions.

§ 8.4.3. Constraints on Ore-Forming Fluid From the Fluid Inclusions

The fluid inclusion study revealed that the ore-forming solution in the Danzhai gold-mercury deposit was somewhat similar to, but compositionally different from that of most epithermal deposits. Roedder (1984) summarized the compositions of solutions from which gold precipitated in epithermal systems based on data from fluid inclusions, natural ore, gangue and alteration mineral assemblages. The temperatures of formation for most epithermal deposits were in the 200 to 300 °C range. Many deposits exhibit evidence that the mineralizing solutions boiled at least in some stage of the gold deposition. The solutions had salinities averaging around 3 wt.% NaCl equivalent and rarely exceeded 10 wt.%. Available data suggest sodium chloride is the most abundant dissolved component with smaller amounts of calcium and potassium also present. Carbon dioxide may be present in significant quantities in hydrothermal systems responsible for sedimentary rock-hosted deposits. The fluid inclusion investigation of the Danzhai gold-mercury deposit indicates that: (1) the temperature range is a little lower than that of epithermal deposits, extending from 130 to 210 °C; (2) the salinity is equivalent to that of epithermal deposit, in several percent NaCl eq.; (3) carbon dioxide is unlikely to be present in considerable quantities; (4) liquid methane and many other hydrocarbons such as bitumen, paraffin wax are dominant. Therefore, hydrocarbons occupy an important place in the ore-forming solution.

The burial depth of the Cambrian formations approached 4000 to 6000 meters, the paleotemperature estimated by the geothermal gradient in the eastern region of Guizhou in the Silurian was between 100 to 150 °C (Han et al., 1982). But the bitumen reflectance and fluid inclusions show that the temperature in the mineralization process ranges from 135 to 210 °C. It is obviously higher than the reasonable paleotemperature estimated by the geothermal gradient.

§ 8.4.4. Constraints on Trace Elements

The association of gold with elements such as mercury, arsenic, antimony and barium and the lack of the common base metals such as copper, lead and zinc can both be

Table 8.1 The gold abundance in oil or bitumen in various world oilfields

Location	Type	Gold (ppb)	Reference
Venezuela	crude oil	2.00	1
Venezuela	bitumen	2.00	1
Nigeria	heavy oil	5940.00	2
Nigeria	bitumen	510.00	2
Nigeria	light oil	3800.00	2
Ex. USSR	bitumen	190-370 (ppm)	3
Ex. USSR	bitumen	30-50 (ppm)	3
Ex. USSR	crude oil	70.00	3
Ex. USSR	extracted HC*	1030.00	4
Ex. USSR	extracted HC	420.00	4
Ex. USSR	extracted HC	460.00	4
Shenli, China	crude oil	1690.00	5
Shenli, China	crude oil	2340.00	5
Shenli, China	crude oil	1200.00	5
Shenli, China	crude oil	1890.00	5
Jianghan, China	crude oil	8.00	5
Jianghan, China	crude oil	2.00	5
Miyang, China	crude oil	3.00	5
Keramayi, China	crude oil	6.00	5
Liaohe, China	crude oil	4.00	5
Liaohe, China	crude oil	5.00	5

1. Buenafama and Lubkiwitz (1976); 2. Oluwole, A.F. (1987);
3. Chakhmakhchev, V. A. et al. (1986); 4. Vilenkin, V.A.(1983);
5. Ling Qing (1989); HC*: Hyddrocarbon.

explained by processes taking place at the source. As the oil and associated solutions approach chemical equilibrium with their enclosing rocks, they become more and more reducing, particularly in a petroleum reservoir. As the oil and oilfield brines leach the rocks, the only components that will go into solution are those that are soluble at very low oxygen activities in the presence of sulfur. Such elements are those that are soluble complexes such as gold, mercury, arsenic and antimony. Barium may be included here because it does not form an insoluble sulfide but is insoluble as a sulfate. Thus barium will be mobile in the reducing environment and immobile under oxidizing conditions, as its presence in the oxidized zones as barite indicates. In contrast, those elements which form insoluble sulfides and are soluble as chloride complexes in an oxidizing environment, such as the base metals, will not go into solution in the reduced oilfield fluids. Thus a separation of the gold "group" elements from base metals will occur at the source. Any base metals that are dissolved will become more soluble as the solutions penetrate a more oxidized environment and, therefore, will not be deposited. In contrast, Romberger (1985) has shown that oxidation is a very efficient mechanism for the deposition of gold transported as bisulfide complexes and would apply equally as well to the other metals in solution as sulfide complexes. In addition, the same mechanism would result in the deposition of barite as the activity of sulfate increased during oxidation of sulfide.

§ 8.4.5. Constraints on the Model from the Isotope Study

Previous sulfur isotope investigation (Zhang, 1983; Chen et al., 1986) indicated that sulfur isotopes from cinnabar, stibnite originated from sedimentary rocks. The argon isotope and lead isotope analyses of this study confirm this conclusion.

Argon isotope data show that the excess argon was present in the fluid inclusions of different mineralization stages. This is unexpected because the host sedimentary rocks of the deposit are dominated by carbonates and no potassium-bearing minerals are present in the alteration and mineralization. In this situation, the argon hosted in quartz should be dominated by atmospheric argon, which may modified in certain extent. But considering that both the oil source strata and ore source strata are Lower Cambrian black shale, this enigma can be explained: Shale is a potassium rich sedimentary rock, ^{40}K decays and turns into radiogenic ^{40}Ar. A large quantity of radiogenic ^{40}Ar might be accumulated from the

early Cambrian to Silurian. The oil and associated oilfield brine leached the radiogenic argon from the black shale and other potassium-bearing rocks and transported it to the Majiang - Danzhai petroleum trap, and it was captured as excess argon by quartz in the process of mineralization of the Danzhai gold-mercury deposit.

The lead isotope study shows that the trace lead in stibnite is lead with a highly evolved μ value, which is widely distributed in south China. These characteristics are quite similar to that of stratiform deposits hosted in sedimentary rocks over the world. For example, in Kuperferschiefer in Europe. The lead isotope data plots on the evolution curve of the upper crust according to the plumbotectonic model of Doe and Zartman (1979). Therefore, the origin of the lead isotope in the Danzhai gold-mercury deposit is the Cambrian and/or Ordovician sedimentary rocks.

§ 8.4.6. The Possible Deposition Mechanism of Gold and Mercury

Petroleum and associated oilfield brine are plausible candidates for an ore-forming fluid which can extract and transport gold and other elements, but how were these metals deposited?

The precipitation of gold and other elements may be induced by the variation of temperature, pressure as well as oxygen fugacity. For example, the increase of temperature will accelerate the degradation of the higher hydrocarbons into methane accompanied by the decomposition of gold-bearing sulfur compounds, resulting the precipitation of gold. Regional pressure forces the petroleum and associated brine migration, but a local depression of pressure may bring about the unmixing of liquid methane and brine resulting in the deposition of gold. The oxygen fugacity is always a factor influencing the solubility of metal complexes as well as heteroatomic compounds and gold-bearing sulfur, nitrogen and oxygen compounds are no exception, and may be decomposed to release gold if the oxygen fugacity increased.

Sulfur, nitrogen and oxygen compounds in petroleum have high capability to extract and transport gold (Bonati, 1987, Ling, 1989). Was the petroleum in the Majiang-Danzhai oil trap rich in this kind of heteroatomic compounds as an ore-forming fluid? The abundance

of the heteroatomic molecules in petroleum depends on its precursor, sedimentary environment and maturity. Tissot and Welte (1984) pointed out that most type II kerogens are related to marine organic matter deposited in a reduced environment, with medium to high sulfur content. The Lower Cambrian black shale, deposited in an anoxic reduced marine environment (Fan, 1981), hosts most type II kerogens. The oil cracking from these kerogen is accordingly assumed to be rich in sulfur compounds. In addition, the petroleum derived from carbonate rocks is also generally rich in sulfur compounds and other heteroatomic compounds(Tissot and Welte, 1984). In the eastern region of Guizhou, the Ordovician and Silurian oil source rocks are dominated by carbonates. Therefore, the petroleum in the ancient Majiang-Danzhai oil trap was probably rich in heteroatomic compounds, particularly sulfur compounds. These heteroatomic molecules can capture the dissolved gold and other metals (Ling, 1989; Yen, 1975; Buenafama and Lubkowitz, 1976; Oluwole, 1987). Therefore, the heteroatomic-molecules-rich petroleum in the Majiang-Danzhai oil trap can be the ore-forming fluid of the Danzhai gold-mercury deposit..

In a petroleum reservoir, the temperature increases with increasing depth. As a result, a continuous generation of wet gas parallel to oil generation is produced(Fig. 8.1). Subsequent to oil generation, cracking of oil and kerogen becomes a predominant process due to higher temperature. The reaction of heavy hydrocarbon molecules cracking to methane and other lower molecule hydrocarbons is exothermic, for example, when a mole of CH_4 or CO_2 is formed from heavy molecule, 31, 810 Joule will be released (Shi, 1991). It is known that the high content of heteroatomic compounds in oil tends to accelerate this thermal cracking process (Tissot and Welte, 1984). The heat released from these cracking reactions will increase the temperature in the oil trap. And the higher temperature, in turn, will accelerate the oil cracking to gas. Therefore more and more wet and subsequently dry gas is generated, which results in increasing temperature in the petroleum reservoir.

This mechanism may explain why a temperature as high as 130 to 210 °C was reached.in the Danzhai gold-mercury deposit if magmatism is not responsible. In the Majiang-Danzhai oil trap, the ancient temperature due to geothermal gradient at the depths of 4000 to 6000 meters is only about 100 to 150 °C, which is lower than the temperature (130 to 210 °C) recorded by fluid inclusion and bitumen reflectance. The exothermic reaction of heavy hydrocarbon molecules cracking to methane and other lower molecule hydrocarbons

may explain the difference. In the natural gas stage, the temperature in a petroleum reservoir can be higher than the temperature calculated from its geothermal gradient.

Judging from worldwide oil occurrences, most oil source beds have not been exposed to temperature higher than 100 °C during the time of generation and migration. Light oil and gas, however, are probably generated from source beds at higher temperatures (150 - 180 °C), which in exceptional cases may reach an upper limit of about 250 °C. For example, the highest temperatures recorded in wells drilled for oil and gas are around 270° to 280 °C, observed in two very deep wells (6500 and 7800 m) in South Texas and the Gulf coast (Tissot and Welte, 1984). A fluid inclusion study of the Weiyuan natural gas field in China demonstrated that the homogenization temperatures have two clearly defined ranges. The first ranges from 80-160 °C which corresponds to temperature in the oil window of this petroleum field. The second ranges from 200-240 °C is the temperature coverage of the dry gas stage.

The thermal stability of methane is such that a lower limit - or gas floor - is not determined by high temperatures, but rather by the depletion of hydrogen in the source material. Foreseeable drilling depths, therefore, do not reach the stage where methane becomes thermally unstable. However, methane can be destroyed chemically, for instance by conversion to H_2S in the presence of sulfur or by sulfate:

$$CH_4 + CaSO_4 \text{ ----- } H_2S + CaCO_3 + H_2O + 76.60 \text{ J/mol.}$$

When hydrocarbons are oxidized by sulfate, a significant quantity of heat is released so that the temperature in the oil trap will be increased. What is important is that H_2S is formed and which may react with metals released by cracking of heavy compounds, so the gold and other metals captured by heteroatimic compounds may react with H_2S resulting in gold and mercury mineralization.

The associated oilfield brine can leach and transport gold as well, but how was the dissolved gold precipitated from the brine? Romberger(1985) proposed a possible mechanism. The solubility of gold as a bisulfide complex is shown in Fig. 8.2 for a solution at 250 °C, pH=5, P_{CO_2}=1 atm. It is represented by the heavy line as a function of oxygen activity, increasing to the right. A higher pH will not change the gold solubility significantly

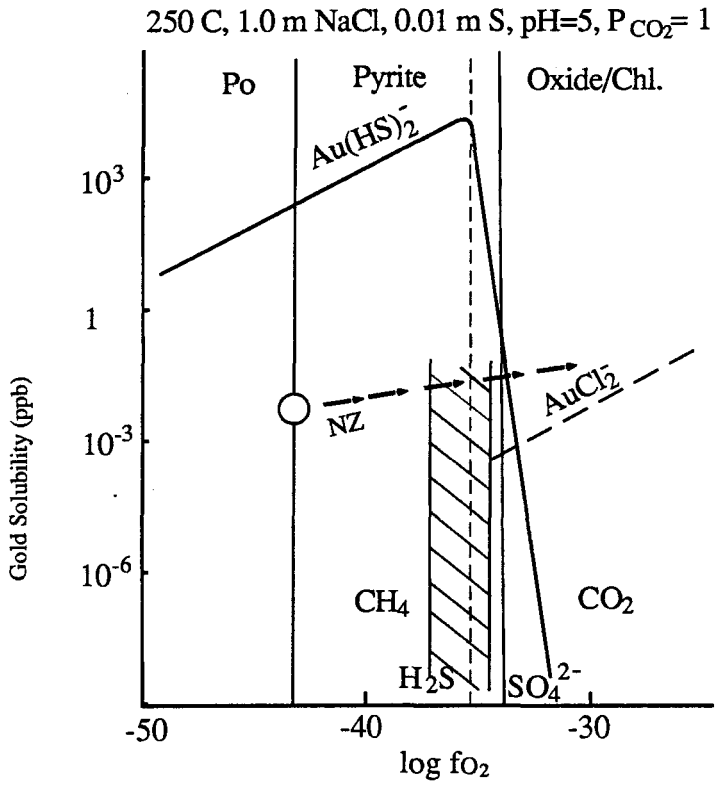

Fig. 8.2 Calculated gold solubility versus oxygen activity at 250 C, pH=5, and CO_2(CH_4) pressure of 1 atm showing the solution path during oxidation of a solution starting with 0.004 ppb Au buffered by the mineral pair pyrite -pyrrhotite (After Romberger, 1984).

if other parameters are are kept constant. The hatched area represents oxidation conditions under which methane, carbon dioxide, reduced sulfide (H_2S) and sulfate predominate. As shown in the diagram, once a solution crosses the light dashed line, that is, from sulfide field to that of sulfate, the solubility of the gold bisulfide complex decreases rapidly. Therefore, gold will be deposited as a result of the oxidation of the gold bisulfide complex. For example, a solution with a gold content of $4X10^{-3}$ ppb indicated by the dashed line with arrows (labelled NZ), starting from a point in equilibrium with the mineral pair pyrrhotite (designated by circle) will be understaturated since it is below the solubility surface of $Au(HS)_2^-$. However, upon oxidation its composition will cross the solubility surface, and gold will precipitate since the solution is oversaturated with the gold bisulfide complex. Note that the solubility of gold as a chloride complex is shown for comparison as a heavy dashed line. Based on the high solubility of gold in bisulfide solution (Seward, 1973) and intimate association between gold and pyrite in most primary ores, Romberger (1985) suggested that most hydrothermal solutions in equilibrium with pyrite never reach saturation with respect to gold and the latter co-precipitates with sulfides. Therefore, gold precipitated from solution either as solid solution in the pyrite or other sulfides (e.g.: arsenopyrite, realgar, orpiment) or as blebs in or coating the grains.

Besides the oxygen activity increasing as indicated by Romberger (1985), the temperature decreasing may be also an important factor for gold precipitation from the hydrothermal ore-forming fluid.

§ 8.4.7. A Possible Alteration Mechanism and the Sites of Gold and Mercury Deposition

Temperature is the primary factor controlling the solubility of silica. The widespread silicification and quartz veins are due primarily to the ore-forming solutions moving down thermal gradients. Silica has a prograde solubility so that cooling is an adequate mechanism for precipitation whereas calcium carbonate exhibits a retrograde solubility. The combination of these two contrasting processes will result in the silicification, that is the replacement of limestone by chalcedony or quartz by a cooling solution saturated with silica. Silica is one of the easiest of the rock-forming components to dissolve in a hydrothermal system, and the deposition of quartz or other forms of silica such as opal or chalcedony is not unusual in

such environments. The brine associated with petroleum in the Majiang-Danzhai oil trap may play the same role as a hydrothermal fluid. It may dissolve the silica from the sedimentary rocks at a higher temperature and precipitate it as silicification or quartz veins in the Danzhai gold-mercury deposit.

Even though the genetic models developed for most epithermal vein-type deposits cannot be completely applied in the Danzhai gold-mercury deposit, the occurrence of gold and mercury orebodies in the deposit are also controlled by subvertical fractures as in most epithermal vein-type deposits. Epithermal vein-type models assume a sub-vertical open fracture system along which hot solutions rise and precipitation occurs as a result of some physico-chemical changes occurring in the system. The result is a mineral deposit with a relatively simple and predictable symmetry and consistent zoning around individual fractures or fracture zones. These models also assume that boiling is an important process in the genesis of the deposits and there is no doubt that this is an effective mechanism for gold deposition (Romberger,1985; Drummond and Ohmoto, 1985). However, evidence for boiling in the sedimentary rock-hosted deposits is sparse (Radtke, 1985). In Danzhai, the regional fault F_1 and associated second order faults played an important role in the mineralization, and all the orebodies are controlled by these faults. As previously discussed in the chapter three, the F_1 fault system was formed during the Caledonian orogeny and reactivated in the Yanshanian orogeny. It is likely that reactivation of the F_1 fault system destroyed the former Majiang-Danzhai petroleum reservoir in Caledonian orogeny, resulted in the temperature and pressure decrease and brought about the depositon of gold, mercury and many other metals from the petroleum reservoir. In this process, unmixing between liquid methane and associated brine likely occurred. However, there is no evidence indicating that these ore-controlling fractures reached the surface since stage by stage investigation of argon isotopes reflect no introduction of atmospheric argon.

§ 8.5. Summary And Discussion

Geological, geochemical and fluid inclusion investigation in the Danzhai gold-mercury deposit demonstrates that gold and mercury mineralizations are related to regional petroleum evolution.

The ore and oil source appears to be the same formation, the Lower Cambrian black shale. Based on the petroleum investigation by Han et al.(1982), the possible oil source strata in eastern region of Guizhou are the Lower Cambrian, the Lower Ordovician Honghuaran formation, as well as the Silurian Wengxiang formation. The Lower Cambrian black shale is the most important oil source strata, and as much as 97.96% of crude oil in the Majiang-Danzhai oil trap might by produced by this black shale. This assumption is also supported by isotope studies, for example, sulfur isotope of cinnabar and stibnite indicate the sulfur was derived from sedimentary rocks. Argon isotopes unexpectedly rich in excess argon, can best be interpreted by the oil and associated solutions as leaching of radiogenic argon from black shale. The study of lead isotopes also shows that the trace lead in stibnite originated from the sedimentary rocks.

Crude oil can extract gold and other metals from sedimentary rocks, which is shown by experiments (Ling,1989). The extraction rate of gold by crude oil varies from 21.7% to 96.9%, depending on the type of oil. The crude oil rich in heteroatomic compounds such as sulfur, nitrogen as well as oxygen compounds has a high extraction capability because the heteroatomic compounds may capture the dissolved gold and other metals. It is important to note that the present-day crude oil in some oilfields contain gold, in abundances up to several ppm. Therefore, the crude oil rich in heteroatomic compounds can be a fifth type of ore-forming fluid (the other four types are defined by Skinner (1979), that is, 1. surface water (including rainwater, lake and river water, seawater and groundwater); 2. connate and deeply penetrating ground water; 3. metamorphic water and 4. magmatic water).

Measurement of reflectance of bitumen indicates that the reflectances are higher than 2%; and fluid inclusion study shows that the ore-forming fluid was dominated by methane

and other highly evolved hydrocarbons. This evidence suggests that the stage of petroleum evolution in the eastern region of Guizhou approached the stage of metagenesis or the dry gas zone. In this stage, the crude oil was thermally cracked to methane and solid pyrobitumen. The gold and other metals were released from heteroatomic molecules. The heteroatomic molecule degradation released sulfur as well, which combines with metals and resulted in mineralization.

The associated oilfield brine can also leach gold and other metals from sedimentary rocks, but its extracting ability is lower than that of crude oil. Besides metals, high temperature oilfield brine has the capability to dissolve the silica from sedimentary rocks. When the temperature is reduced, the silica will replace the limestone or form quartz veins. Metal deposition from oilfield brine may be caused by a temperature decrease, a pressure release, or oxygen fugacity increase. A flow diagram of petroleum evolution and gold-mercury mineralization is shown in Fig. 8.3.

Regional fault F_1 and associated faults played an important role in the gold-mercury mineralization. The F_1 fault system was formed in the Caledonian orogeny and reactivated in the Yanshanian orogeny. It is likely that the F_1 fault system destroyed the former Majiang-Danzhai petroleum reservoir in the Caledonian orogeny, resulting in a temperature and pressure decrease and accordingly deposited gold, mercury and many other metals in the gas field brine. Unmixing between the liquid methane and associated brine likely occurred in this process.

The genetic model differs from other hydrothermal ore deposits, the heat source, actually an external heat source is not considered as an essential component in the mineralization process in the Danzhai gold-mercury deposit and regionally associated mercury, antimony, arsenic, barite deposits.

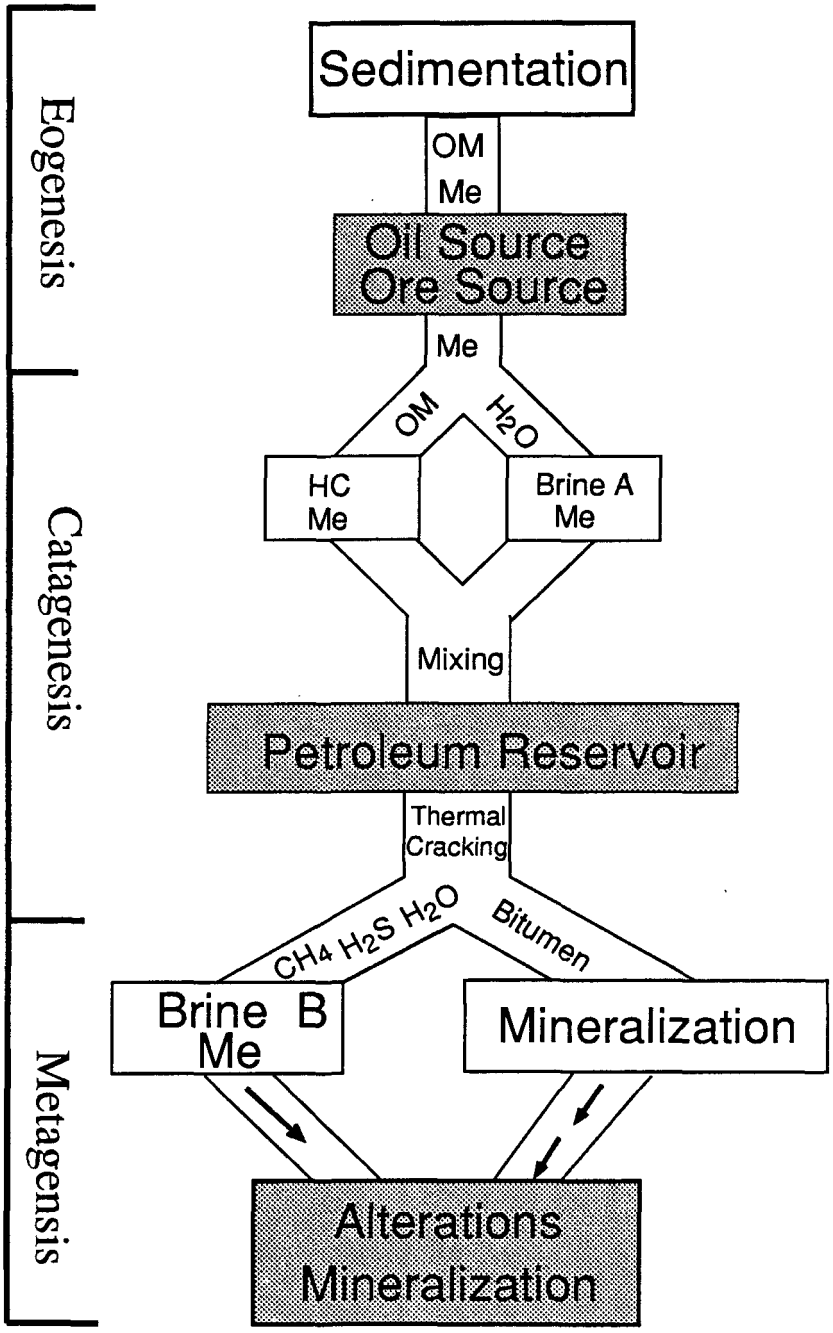

Fig.8.3 Schematic diagram showing petroleum evolution and gold mercury mineralizaitons. OM = Organic Matter; HC = Hydrocarbons; Me = Metals.

CHAPTER IX:

CONCLUSIONS

The principal objective of this thesis is to study the various factors related to the mineralization of the Danzhai gold-mercury deposit, including the host rocks, alteration and gold-mercury mineralization, the relationship between the petroleum evolution and gold-mercury mineralization, the source of the ore-forming fluids and the mechanism of the mineral deposition. The main conclusions are as follows.

1. The host rocks of the Danzhai gold-mercury deposit are Lower Ordovician and Upper Cambrian carbonates with different structures such as brecciated carbonate, banded carbonate, laminated carbonate and thin bedded carbonate.

2. Fault F_1 served as the conduit for the Danzhai gold-mercury mineralization and subsequent faults related to F_1 provided space for mineral precipitation. Most of the gold and mercury orebodies occur in these faults.

3. The peripheral alterations are low temperature assemblages such as silicification and carbonatization, four stages of this alteration and associated vein system are distinguished.

4. The major mineral association are sulfides of arsenic, mercury and antimony such as cinnabar, arsenopyrite, stibnite, pyrite, realgar, orpiment as well as barite. The mineral assemblages related to gold mineralization are: (1) calcite - arsenopyrite- pyrite; (2) chalcedony, quartz - arsenopyrite-pyrite; (3) quartz-realgar-orpiment-quartz,calcite; (4) calcite–stibnite,cinnabar- arsenpyrite, pyrite. The mineral assemblages related to mercury mineralization are: (1) quartz–calcite, dolomite–cinnabar–stibnite; (2) barite-cinnabar-quartz; (3) stibnite–native mercury. Four stages of mineralization and alteration are described.

5. No fine-grained gold or gold minerals have been observed under optical or scanning electron microscope, but chemical analysis show a positive correlation between gold and arsenic indicating that the gold may be mainly associated with arsenic minerals such as arsenopyrite, realgar, orpiment, or arsenian pyrite.

6. The Au/Ag ratios is always greater than 1 in the gold ore but less than 1 in the wall rocks and the mercury ore. Base metals are not concentrated in either ore or wall rocks.

7. Bitumen is distributed pervasively through the Paleozoic sedimentary rocks in the eastern region of Guizhou. Bituminous sandstone occurs in the second member of the Silurain Wengxiang Group ($S_{1\text{-}2}w^2$) as well as the Lower Ordovician Honghuaran Formation(O_{1h}) in the Majiang, Duyun, Danzhai and Kaili areas. All the mercury, antimony, arsenic, gold and barite deposits in the area occur below the ancient interface between petroleum and oilfield brine (-500 M).

8. Bitumen occurs in the host carbonate rocks of the Danzhai gold-mercury deposit in the laminated carbonate and/or banded carbonate and fills stylolites and vugs in the carbonates. Bitumen veins, ranging up to several centimeters thick, occur in the carbonate host rocks. A variety of forms of hydrocarbon are present in the ore and vein system. Dispersed bitumen, which is present in quartz, carbonate and barite veins can be easily distinguished by its color. Patch-like bitumen, veinlet bitumen, as well as stylolite-like bitumen, host sulfide minerals such as arsenopyrite, pyrite and cinnabar. In turn, sulfides such as cinnabar as well as gangue minerals also host bitumen. Reaction zones are not observed around the bitumen grains, which precludes that an earlier formed bitumen reacted with the ore-forming fluid afterwards.

9. Apart from bitumen, another form of solid hydrocarbon, paraffin wax is also found in the Danzhai gold-mercury deposit. It is characterized by a brown to dark brown color, occurs as thin stringers sometimes together with bitumen and sometimes independent. Similar to bitumen, paraffin wax is commonly associated with metal sulfides such as arsenopyrite, pyrite, cinnabar.

10. The reflectance of bitumen from different mineralization stage of the Danzhai gold-mercury deposit is high, and varies from 2 to 3.8%. The temperature calculated from the reflectance ranges from 150 to 210 °C. The bitumen is actually pyrobitumen, of high reflectance, which shows a mosaic texture as well as an anisotropic nature. Fluorescent investigation indicates that bitumen lost its fluorescence, because it is overmature. These characteristics correspond to that of bitumen in the Majiang-Danzhai petroleum reservoir, where petroleum reached the thermal natural gas stage, the last stage of petroleum evolution, when the Danzhai gold-mercury deposit was formed.

11. Hydrocarbons are a significant part of the ore-forming fluid, and the Danzhai gold-mercury mineralization as well as the regional mercury, antimony, arsenic, gold and barite mineralization are derived from the evolution of petroleum and/or the associated oilfield brine of the former Majiang-Danzhai petroleum reservoir.

12. A variety of hydrocarbon inclusions are found in different host minerals and in different mineralization stages, including: (1) liquid methane inclusions; (2) bitumen inclusions; (3) paraffin wax inclusions; (4) heavy oil inclusions, and a combination of all four types.

13. Hydrocarbon fluid inclusions are dominant in minerals from different mineralization stages. The liquid methane inclusions are found in both metal minerals such as cinnabar and realgar and gangue minerals such as quartz, calcite, dolomite and barite. The heavy oil inclusions are abundant in carbonate minerals such as calcite and dolomite. Homogenization temperatures of aqueous fluid inclusions are mainly from 130 to 210 °C, and the salinities of aqueous fluid inclusions range from 5.1-19.3 wt.% NaCl eq.. The temperature range is higher than that of most petroleum fields while the salinity range is lower than that of most petroleum fields, but both temperature and salinity ranges correspond to the temperature and salinity of some natural gas fields.

14. Solid probe mass spectrometry study confirms that the hydrocarbon components, particularly methane, are the most important constituent of the fluid inclusions. The methane in some inclusions is as high as 69.8 mole percent. Some heavy hydrocarbon molecules are also seen in the mass spectra. Unmixing of CH_4-H_2O, or H_2O-CO_2 is the proposed

deposition mechanism for gold and mercury in relevant mineralization stages. Comparison of mass spectrometer spectra of distinct gas phases over total bursts shows a complete separation indicating an unmixing of the CH_4 and H_2O phases in the second mineralization stage. Other spectra however, display an complete separation indicating a marked unmixing of H_2O and CO_2 phases in the third mineralization stage..

15. The argon isotope data of the three samples from the Danzhai gold-mercury deposit show excess ^{40}Ar. The initial $(^{40}Ar/^{36}Ar)_0$ ratio for each of the samples or for each step of crushing is much higher than that of the modern atmosphere. The isochron ages for the three quartz samples are 2783, 3047 and 2250 Ma respectively. The huge quantity of excess argon probably stems from the leaching of radiogenetic ^{40}Ar of the Lower Cambrian black shale. ^{39}Ar is of consistently low abundance in the three quartz samples. The only exception is in the first three crushing steps in the sample Dz-02, which released a high quantity of ^{39}Ar relative to the others. This implies that the aqueous fluid inclusions may contain higher ^{39}Ar than the liquid methane inclusions, because the solubilities of noble gas in different media, such as the formation water, oil, or liquid methane are different.

16. The lead isotopes of trace lead in stibnite from different orebodies are homogeneous, belonging to highly evolved μ value lead. This is quite different from the lead isotope value of Mississippi Valley-type lead zinc deposits, but similar to that of sedimentary rock-hosted stratiform deposits. According to the plumbotectonic model of Doe and Zartman (1979), the lead isotope data plots on the evolution curve of the upper crust. Therefore, the origin of lead isotopes in the Danzhai gold-mercury deposit is from Cambrian or Ordovician sedimentary rocks. The model age of ore lead is in the neighborhood 400 Ma, equivalent to the end of Silurian period.

17. The ore and oil source is the same strata, the Lower Cambrian black shale. The Lower Cambrian black shale is probably also the most important oil source strata since 97.96% of crude oil in the Majiang-Danzhai oil trap might come from this black shale.

18. Crude oil-rich in heteroatomic compounds can be an important type of ore-forming fluid, because the heteroatomic compounds may capture dissolved gold and other metals. It is important to note that the present-day crude oil in some oilfields contain up to

several ppm of gold. The stage of petroleum evolution in the east region of Guizhou approached the metagenesis stage or dry gas zone. In this stage, crude oil was thermally cracked to methane and solid pyrobitumen. The gold and other metals were released from heteroatomic molecules. The heteroatomic molecule degradation released sulfur as well, which combined with metals and induced the mineralization.

19. The associated oilfield brine can also leach gold and other metals from sedimentary rocks, but its extraction ability is lower than that of correspondent crude oil. Besides metals, oilfield brine also has the capability to dissolve silica from sedimentary rocks. When the temperature is reduced, the silica will replace the limestone or precipitate as quartz veins. The metal deposition from oilfield brine may be caused by the temperature decrease, pressure release, or oxygen fugacity increase.

REFERENCES:

Allégre, S.J., Staudacher, D. Sarda P. and Kurz, M., 1983, Constraints on evolution of earth's mantle from rare gas systematics. Nature, 303, 762-766.

Alvarez, A. and Noble D.C., 1988, Sedimentary rock-hosted disseminated precious metal mineralization at Purisima Concepcion, Yauricocha district, Central Peru. Economic Geology, 83, 1368-1378.

Anderson G.M., 1991, Organic maturation and ore precipitation in southeast Missouri. Economic Geology, 86, 909-926.

Anderson G.M. and MacQueen, R.W., 1982, Ore deposit models 6. Misssissippi Valley-type lead-zinc deposits. Geoscience Canada 9, 108-117.

Bagby, W.C. and Berger, B. R., 1991, The geology and origin of Carlin-type gold deposits: in Gold Metallogeny and exploration (Edited by Foster R. P.) Black and son 210-248.

Baker C. and Smith M.P., 1986, Mass spectrometric determination of gases in individual fluid inclusions in natural minerals. Analytical Chemistry, 58, 1330-1333.

Bakken, B. M., and Einaudi, M. T., 1986, Spatial and temporal relations between wall rock alteration and gold mineralization, Main Pot, Carlin gold mine, Nevada, U.S.A. "Gold'86": edited by Macdonald, A. J., Ontario, Konsult International, Inc., 388-403.

Bakken, B.M., Hochella, M.F. Jr., Marshall, A.F.and Turner, A.M. 1989 High resolution microscopy of gold in unoxidized ore from the Carlin mine, Nevada. Economic Geology, 84, 171-179.

Banikova, L.A., Kolesov, G.M., and Barsukov, V.L., 1984, Metals in bituminoids from some hydrothermal deposits. Geochemistry International, 20, 123-131.

Barker, W.E., 1973, The role of humic acids from Tasmanian podzolic soils in mineral degradation and metal mobilization. Geochimica et Cosmochimica Acta, 37, 269-281.

Barker, W.E., 1978, The role of humic acid in the transport of gold. Geochimica et Cosmochimica Acta, 42, 645-649.

Barnes, M.A., Barnes, W.C., and Bustin, R.M., 1985, Diagenesis 8. Chemistry and evolution of organic matter. Geoscience Canada, 11, 103-114.

Barton P.B., 1982, The many roles of organic matter in the genesis of mineral deposits. (abstract) Geological Society American Abstracts with Program, 14, p.140.

Benedetti M. and Boulegue, 1991, Mechanism of gold transfer and deposition in a supergene environment. Geochimica et Cosmochimica Acta, 55, 1539-1548.

Berger, B. R. and Bagby, W.C., 1985, Geologic characteristics of sediment-hosted disseminated precious-metal deposits in the western United States. *In* Geology and Geochemistry of Epithermal systems. eds. Berger B.R. and Bethke P.M. Review in Economic Geology. 2, 169-202.

Berger, G.W. and York, D., 1970, Precision of the $^{40}Ar/^{39}Ar$ dating technique. Earth and Planetary Science Letters. 9, 39-44.

Berger G.W. and York, D., 1981, Geothermometry from $^{40}Ar/^{39}Ar$ dating experiments. Geochimica et Cosmochimica Acta. 45, 795-811.

Bergerioux, C. and Zikovsky, L., 1978, Determination of 18 trace elements in petroleum and its derivatives by nertron activation with a small reactor. Journal. Radioanalytical Chemistry. 46, 277-184.

Bertrand, Ph., Pittion, J-L. and Bernaud, C., 1986, Fluorescence of sedimentary organic matter in relation to its chemical composition. Advanced Organic Geochemistry., Jülich 10, 641-647.

Blasch, S. R., and Coveney, R.M. Jr., 1988, Goethite-bearing brine inclusions, petroleum inclusions, and the geochemical conditions of ore deposition at the Jumbo mine, Kansas: Geochimica et Cosmochimica Acta, 52, 1007-1017.

Bohdan K., 1990, The role of organic matter in the metallogeny of Bohemian Massif. Economic Geology, 85, 1525-1540.

Bonati F., 1987, Gold(1) derivatives of heterocycles. Inorganic Chimica Acta. 1357, 81-85.

Bonham, H.F. Jr., 1988, Bulk mineable gold deposits of the western United States. *In* "The Geology of Gold Deposits: The Perspective in 1988". 193-207.

Bosch A. and Mazor E., 1988, Natural gas association with water and oil as depicted by atmospheric noble gases; case studies from the south eastern Mediterranean Coastal Plain. Earth and Planetary Science Letters 87(3), 338-346.

Boyle, R. W., 1979, The geochemistry of gold and its deposits. Geological Survey Bulletin of Canada. 280, 584p.

Boyle, R.W., 1984, Gold history and genesis of deposits. Van Nostrand Reinhold Company. New York, 676p.

Boyle, R.W. and Steacy, H.R., 1973, An auriferous radioactive hydrocarbon from the Richardson Mine, Eldorado, Ontario Geological Survey of Canada Paper 73-1A, 282-285.

Brown, J.S., 1967, Isotopic zoning of lead and sulfur in southeast Missouri. In: Genesis of stratiform lead-zinc-fluorite deposits (Mississippi Valley type deposits). A symposium, New York, 1966. Economic Geology, Monograph 3, 410-425.

Buenafama, H.D. and Lubkiwitz J.A., 1976, The stability of trace metals suspensions in heavy crudes as determined by neutron activation analysis. Journal radioanalytical Chemistry, 39(1977), 293-300.

Burrus, R.C., 1981, Hycrocarbon fluid inclusions in studies of sedimentary diagenesis. Mineralogy Association, Canada Short Course Handbook 6, 138-156.

Burrus, R.C., Toth D.J. and Goldstein, R.H., 1980, Fluorescence microscopy of hydrocarbon fluid inclusions: Relative timing of hydrocarbon migration events in the Arkoma basin, NW Arkansas (abstract). EOS, Trans. American Geophysical Union, 61, 400.

Bustin, R.M. 1989, Diagenesis of kerogen, In: Hutcheon, I.E. (ed.): Burial diagenesis, Mineralogical Association of Canada, Short Course Handbook 15, 1-38.

Cadogan, P.H., 1977, Palaeoatmospheric argon in Rhymic chert. Nature, 268, 38-41.

Cahen, L., Eberhardt, P., Geiss, J., Houtermans, F.G., Jedwab, J. and Signer, P., 1958, On a correlation between the common lead model model age and the trace-element content of galenas. Geochimica et Cosmochimica Acta. 14, 134-149.

Cannon, Jr., R.S., 1961, The data of lead isotope geology related to problems of ore genesis. Economic Geology, 56, 1-38.

Cannon, R.S. and A.P. Pierce, 1967, Isotopic varieties of lead in stratiform deposits; Genesis of stratiform Lead-Zinc-Barite-Fluorite deposits (Mississippi Valley type deposits) -A symposium, New York, 1966, Economic Geology, Monographs, 3, 427-433.

Carter, J.S. and Cazalet, P.C. D., 1984, Hydrocarbon gases in rocks as pathfindeers for mineral exploration. In: Prospecting in Areas of Glaciated Terrain, 11-14, Glasgow: Institute of Mining and Metallurgy.

Cathelineau, M., Boiron, M.C., Holligeer,P. Marion, P. and Denis M., 1988, Gold in arsenopyrite: crystal chemistry, location and state, physical and chemical conditions of deposition. ed. by Reid R. Keays, W R. H. Ramsay, David I. Groves in "The Geology of Gold Deposits : The Perspective in 1988". 328-341.

Chakhakhchev, A. V., Kurganskaya, E.V. and Punanova, S.A., 1981, Distribution oif trace elements in petroleum fractions. Geochemistry International 18, 177-181.

Chakhakhchev, V.A.Lositskaya, I.F., Dunanova, S.A. and Semenova, R.A., 1985, Trace elements and porphyrins in the geochemical correlation of petroleum and bitumoids. Geochemistry International, 22(9) 1-6.

Chao, E. C. T., Minkin, J. A., Back, J. M., Chen, J. R., Bagby, W. C., Rivers, M.L., Gordon, B. M. and Jones, D. W., 1986, Occurrence of gold in an unoxidized Carlin-type ore sample - a primary synchrotron and micro-optical restudy. Geological Society of America Abstracts with Programs. 18, p. 562.

Chen Haosu, 1981, Lead isotope characteristics and their genetic significane of stratabound and statiform polymetallic deposits in our country. Kexue Tongbao (Science Bulletin), 10, 612-615 (in Chinese).

Chen Haosu, 1983, Lead and sulfur isotope characteristics of stratabound and statiform polymetallic deposits in our country. Kuangchuang Dizhi, 3, 79-85 (in Chinese)..

Chen Qingnian, Jia Rongfen and Liu Dehan, 1986, Some characteristics of organic materials and metals in Danzhai gold-mercury deposit. Annual Report of open organic geochemistry laboratory, Institute of Geochemistry, Academia Sinica. 145-158. (in Chinese).

Colvine, A. C., Andrews, A.J., Cherry, P.M.E., Durocher, M.E., Fyon, A.J., Lavigne, M.J., Macdonald, A.J., Marmont, S., Oulsen, K.H., Springer, J.S. and Troop, D.G., 1984, An integrated model for the origin of Archean lode gold Deposits, Open File Report 5524, Ontario Geological Survey, 98p.

Colvine, A.C., Fyon, J.A., Heather, K.B., Marmont, S., Smith, P.M. and Troop, D.G.,1988, Archean lode gold deposits in Ontario. Ontario Geological Survey Miscellaneous Paper. 139, 136pp.

Connan, J., 1979, Genetic relation between oil and ore in some Pb-Zn-Ba ore deposits. Special Publication of Geological Society South Africa. 5, 263-274.

Cox, D.P. and Singer, D.A., 1986, Mineral deposit models. United States Geological Survey Bulletin, 1693, 379p.

Craig, J. R., Luke, L.L.Y. and William, R.L., 1973, Investigations in the Pb-Sb-S system, Canadian Mineralogist, 12, 199-206.

Craigie, E.R., 1986, Foreword, *In*: Proceedings of Gold '86, An International Symposium on Geology of Gold: Toronto, 1986, *edited* by A.J. Macdonald.

Crocetti, C.A., Holland, H.D., and McKenna, L.W., 1988, Isotopic composition of lead in galenas from the Viburnum Trend, Missouri. Economic Geology, 83, 355-376.

Cumming, G.L., and Richards J.R., 1975, Ore lead isotope ratios in a continuously changing Earth. Earth and Planetary Science Letters, 28, 155-171.

Cunningham, C,G., Ashley, R.P., Chou I-ming, Huang Zushu, Wan ChaoYuan, and Li Wenkang, 1988, Newly discovered sedimentary rock-hosted disseminated gold deposits in People's Republic of China. Economic Geology, 83, 1462-1467.

Curiale, Ja. A., Bloch, S., Rafalska-Bloch, J., and Harrison, W.E.,1983, Petroleum-related origin for uraniferous organic-rich nodules of southwestern Oklahoma. American Association of Petroleum Geologists Bulletin, 67, 588-608.

Dalrymple, G.B. and Moore, J.G., 1968, Argon 40 Excess: submarine pillow basalts from Kilauea volcano, Hawaii. Science, 161, 1132-1135.

Ding Kang, 1986, A Geochemistry study of the Gongguan mercury-antimony deposit. Unpublished M. Sc. thesis, Institute of Geochemistry, Academia Sinica.

Dobryanskiy, L. A. and Gavrish, V.K., 1989, Paragenesis of mercury and hydrocarbons, an important trend in geological studies. Geologicheskiy Zhurnal, no.4, p.3-12 (with English Summary).

Doe, B. R., and Stacey, J. S., 1974, The application of lead isotopes to the problems of ore genesis and ore prospect evolution: a review. Economic Geology, 69, 757-776.

Doe, B.R., 1962, Distribution and composition of sulfide minerals at Balmat. New York, Geological Society of America Bulletin. 73, 833-854.

Doe, B.R., 1970, Lead isotopes. Springer-Verlag 137p.

Doe, B.R. and Delevaux M.H., 1972, Source of lead in southeast Missouri galena ores. Economic Geology, 67, 409-425.

Doe, B.R. and Zartman, R.E., 1979, Plumbotectonics, The Phanerozoic. *In:* Geochemistry of Hydrothermal Ore Deposits. Second Edition. 34-38.

Douglas, A.G., and Mair, B.J., 1965, Sulfur: Role in genesis of petroleum. Science, 147, 499-501.

Drummond, L.J. and Ohmoto, H. 1985, Chemical evolution and mineral deposition in a boiling hydrothermal system. Economic Geology, 80, 126-147.

Eberhardt, P., Geiss, J. and Houtermans, F.G., 1955, Lead and sulfur isotope ratios in galenas. Helvetica Physical Acta. 28, 339-341.

Etminan H. and HOffman C.F., 1989, Biomarkers in fluid inclusions: A new tool for constraining source regimes and its implications for the genesis of Mississippi Valley-type deposits. Geology, 17, 19-22.

Evans, J.G., 1980, Geology of the Rodeo Creek NE and Welches Canyon Gqudrangles, Eureka County, Nevada, United States Geological Survey Bulletin 1473, 81p.

Fan Delian, 1981, Lower Cambrian black sedimentary rock series and stratiform polymetal rich beddings over South China. *In*: Research on Sedimentary Rock, Science Press, 23-45.

Fedoseyeva, V.A., 1985, Interaction of some gold complexes with humic and fulvic acids. Geochemistry International. 23, 106-110.

Fetzer, W.G., 1934, Transportation of gold by organic solutions. Economic Geology, 29, 599-609.

Fetzer, W.G., 1946, Humic acids and true organic acids as solvents of minerals. Economic Geology, 41, 47-56.

Field C.W, 1966, Sulfur isotopic method for discriminating between sulfates of hypogene and supergene origin. Economic Geology, 61, 1428-1435.

Foster, R.P. (ed.), 1984, Proceedings of Gold'82: the Geology, Geochemistry and Genesis of Gold Deposits, Special publication 1, Geological Society of Zimbabwe. Balkena Press.

Foster, R.P. (ed.), 1991, Gold Metallogeny and Exploration. Black and son press.

Freise, F.W., 1931, The transportation of gold by organic underground solutions. Economic Geology, 26, 421-431.

Fu Jiamo, 1988, On several problem of organic geochemistry in stratabound and stratiform deposit. In "Annual Report of Open Laboratory of Organic Geochemistry, Institute of Geochemistry, Academia Sinica". Science Press, 174-184.

Fu Jiamo, 1990, He established golden bridge between petroleum, natural gas evolution and metallic metallogeny. "Exploration, Creation and Advance", Editors: Mineral, Petrology and Geochemistry Society of China and Institute of Geochemistry, Academia Sinica. Chongqin Branch, Chinese Science and Technology Bibliography Press.(in Chinese).

Geiss, J., 1954, Isotope analyses of "common lead", Z. Naturforsch. 9, 218-227.

Giordano, T.H., 1985, A preliminary evaluation of organic ligands and metal-organic complexing in Mississippi Valley type ore solutions. Economic Geology, 80, 96-106.

Gize, A.P. and Barnes, H.L., 1987, The organic geochemistry of two Mississippi Valley-type lead-zinc deposits: Economic Geology, 82, p.457-470.

Gold, T. and Soter, S., 1980, The deep-earth-gas hypothesis. Scientific American, 242, 154-161.

Guha, J. Lu, H.-Z., and Gagnon M., 1990, Gas composition of fluid inclusion using solid probe mass spectrometry and its application to study of mineralizing processes. Geochimica et Cosmochimica Acta, 54, 553-558.

Guha, J. Lu, H.-Z., Dubé B., Robert, F., and Gagnon M., 1991, Fluid characteristics of vein and altered wall rock in Archean mesothermal gold deposits. Economic Geology 86, 667-684.

Guizhou Geologcial Bureau, 1973, Guizhou geological map. *In:* Atlas of geological maps of the People's Republic of China.

Gustafson, L.B. and Williams, N., 1981, Sediment-hosted stratiform deposits of copper, lead and zinc. Enonomic Geology, 75th Anniversary Volume, 139-178.

Han Shiqing, Wang Shoude and Hu Weiyuan, 1982, The discovery of a paleopool in Majiang and its geological significance. Oil & Gas Geology, 3, 316-325. (in Chinese with English Abstract).

Hanor, J.S., 1979, The sedimentary genesis of hydrothermal fluids. In: Barnes, H.L., edited Geochemistry of hydrothermal deposits, New York, 137-172.

Hansley, P.L., and Spirakis C.S., 1992, Organic matter diagenesis as the key to unifying theory for the genesis of tabular Uranium-Vanadium deposits in the Morrison formation, Colorado Plateau. Economic Geology, 87, 352-365.

Harrison T.M. and McDougall I., 1988, Geochronology and Thermochronology by the $^{40}Ar/^{39}Ar$ Method (Oxford Monographs on Geology and Geophysics), Oxford University Press, New York.

Hausen, D. M. and Park, W. C., 1986, Observation on the association of gold mineralization with organic matter in Carlin-type ores: Denver Region Exploration Geologists Society Symposium, Denver, Colorado, April 25-26, 1985, Proceedings 119-136.

Hausen, D.M. and Kerr, P.F., 1968, Fine gold occurrence at Carlin, Nevada. In "Ore Deposits in the United States, 1933-1967" (The Craton-Sales Volume, Ridge, J.D. editor) AIME, New York, 1889, 908-940.

Heizler, M.T. and Harrison, T.M., 1988, Multiple trapped argon isotope components revealed by $^{40}Ar/^{39}Ar$ isochron analysis. Geochimica et Cosmochimica Acta, 52, 1259-1303.

Henry A.L., Anderson G.M. and Héroux Y., 1992, Alteration of organic matter in the Viburnum Trend lead-zinc district of southeastern Missouri. Economic Geology, 87, 288-309.

Heyl, A., M.H. Delevaux, R.E. Zartman, and M.R.Brock, 1966, Isotopic study of galenas from the Upper Mississippi Valley mineral districts. Economic Geology, 61, 933-961.

Hochella, M. F. Jr., Harris, D. W. and Turner A. M., 1986, Scanning Auger microscopy as a high resolution microscope for geologic materials. American Mineralogist, 71, 1247-1257.

Hsü, K.-J., Li J., Chen, H., Wang, Q., Sun, S., and Sengör, A.M.C., 1990, Tectonics of South China: key to understanding the West Pacific . Tectonophysics, 183, 9-39.

Hsü, K.-J.,Sun, S., and Li J., 1987, South China is an orogenic zone not a platform. Chinese Sciences, 10B, 1107-1115. (in Chinese).

Hsü, K.-J.,Sun, S., Li J., Chen, H., Pan H., and Sengör, A.M.C., 1988, Mesozoic overthrust tectonics in South China. Geology, 16, 418-427.

Hsü, K.-J.,Sun, S., Li J., Chen, H., Pan H., and Sengör, A.M.C., 1989, Reply on "Mesozoic overthrust tectonics in South China". Geology, 16, 418-427.

Hua Yongfong, 1982, The genesis and the exploration strategy for mercury deposits in China. Guizhou people's press. 176p.

Jacob, H. 1985, Dispersed solid bitumens as an indicator for migration and maturity in prospecting for oil and gas. Erdol und Kohle -Erdgas-Petrochemie 38(8), 365.

Jacob, H., 1983, Lecture on bitumens at the ICCP meeting, Ovideo (Spain).

Johnsson, A. and Richard D., 1985, Some new lead isotope determinations from the Proterozoic sulfide areas of central Sweden, Mineralium Deposita, 20, 1-7.

Joralemon, P. 1951, The occurrence of gold at the Getchell mine, Nevada. Economic Geology, 46, 267-310.

Kaneoka, I., 1980, Rare gas isotopes and mass fraction and indicator of gas transport into or from a magma. Earth and Planetary Science Letters, 48, 284-292.

Kaneoka, I., 1983, Nobel gas constraints on the layered structure of the mantle. Nature, 302, 698-700.

Kautzsch, E., Birkenfeld, H., Zahn, H., Chang, I., Kaemmel, T. and Kruhme, H., 1964, Lead isotopic abundance of the lead ores of East Germany. Deutsches Akademish Wissenschaft, Chemie, Geologie, Biologie, no.7, 865-876.

Keays R.R. and Skinner, B.J., 1988, Introduction, In: The Geology of Gold Deposits: The Perspective in 1988, edited by R.R. Keays, W.R.H. Ramsay and D.I. Groves, Economic Geology Monograph 6, 1-8.

Kelley S., G. Turner, A.W. Butterfield and T. Shepherd, 1986, The source and significance of argon isotopes in fluid inclusions from areas of mineralization. Earth and Planetary Science Letters, 79, 301-318.

Kelly, W.C. and Nishioka, G.K., 1985, Precambrian oil inclusions in late veins and the role of hydrocarbons in copper mineralization at White Pine, Michigan. Geology, 13, 334-337.

King, L.H., 1963, On the origin of anthraxolite and impsonite: Canada Department of Mines and Technical surveys. Mines Branch, Research Report, R-116, 9p.

Köppel, V. and Grünenfelder, M., 1979, Isotope geochemistry of lead. Lectures in isotope Geology. Edited by: E, Jager and J. C. Hanziker, Springer-Verlag.

Kucha, H., 1982, Platinum-group metals in the Zechstein copper deposits, Poland. Economic Geology, 77, 1578-1591.

Kuehn, C.A. and Bodnar, R.J., 1984, P-T-X characteristics of fluids associated with the Carlin sediment-hosted gold deposit (abstract). Geological Society American Abstract Programs. 16(6), 566.

Kuehn, C.A. and Rose, A.W., 1986, Temporal framework for the evolution of fluids at the Carlin gold mine (Abstracts). Geological Society American Abstract Programs. 16(6), 663.

Kvenvolden, K. A. and Roedder E., 1971, Fluid inclusions in quartz crystals from South-West Africa. Geochimica et Cosmochimica Acta. 35, 1209-1229.

Lamb, J. Cline, J.S. and Wells, D.E., 1992, Preliminary petrographic and fluid inclusion data from the Meikle mine, Carlin Trend, Northern Nevada. in "Fourth Biennial Pan-American Conference on Research on Fluid Inclusions. P.49.

Lanphere, M.A., and Dalrymple, G.B., 1976, Identification of excess $^{40}Ar/^{39}Ar$ age spectrum technique, Earth and Planetary Science Letters, 37, 169-171.

Lanphere, M.A., and Dalrymple, G.B., 1977, Reply to comment by E. Jessberger, Earth and Planetary Science Letters 141-148.

Large, D. and Schaeffer, R., 1983, Lead isotope data from selected galena occurrences in the Noth Eifel and North Saterland, Germany. Mineralium Deposita, 18, 235-245.

Leventhal J.S., Daws, T.A., and Frye, J.S., 1986, Organic geochemical analysis of sedimentary organic matter associated with uranium. Applied Geochemistry, 1, 241-247.

Leventhal J.S., Grauch, R.I., Threkeld, C.N., Lichte, F.E., and Harper, C.T., 1987a, Unusual organic matter associated with uranium from the Claude deposit, Cluff Lake, Canada. Economic Geology, 82, 1169-1176.

Leventhal J.S., Hostra, A.H., Vuletich, A.K. and Mancuso, T.B., 1987b, Sediment-hosted disseminated gold mineralization at Jerritt Canyon, Nevada. III - Role of organic carbon (abstracts) Geological Society of American Abstract Programs, 19, 745.

Leventhal J.S., 1990, Organic matter and thermochemical sulfate reduction in the Viburnum Trend, Southeast Missouri. Economic Geology, 85, 622-632.

Levine, J.R. and Davis, A., 1989, The relationship of coal optical fabrics to Alleghanian tectonic deformation in the central Appalachian fold-and-thrust belt, Pennsylvania: Geophysical Society of America Bulletin, 101, 1333-1347.

Levine, J.R.; Samson, I.M. and Hesse R., 1991, Occurrence of fracture-hosted impsonite and petroleum fluid inclusions, Quebec city region, Canada. American Association of Petroleum Geologists Bulletin. 75, 139-155.

Ling Qing, 1989, The role of organic matter in gold mineralization. Unpublished M. Sc. thesis, Institute of Geochemistry, Academia Sinica.

Macdonald, A. J. (ed.), 1986, Proceedings Volume of Gold'86, An International Symposium on the Geology of Gold: Toronto, 1986, 504p.

Macqueen, R.W. and Powell T.G., 1983, Organic geochemistry of the Pine Point lead-zinc ore field and region, Northwest Territories, Canada. Economic Geology, 78, 1-25.

Marikos M.A, Laudon R. C. and Leventhal J. S., 1986, Solid insoluble bitumen in the Magmont west orebody, southeast Missouri. Economic Geology, 81, 1983-1988

Mazor, E. and Bosch A., 1987, Noble gases in formation fluids from deep sedimentary basins: a review. Applied Geochemistry, 2, 621-627.

McLimans R.K., 1987, The application of fluid inclusions to migration of oil and diagenesis in petroleum reservoirs. Applied Geochemistry, 2, 585-603.

Meunier J.D., P. Landais, and M. Pagel, 1991, Experimental evidence of uraninite formation from diagenesis of uranium-rich organic matter. Geochimica Cosmochimica Acta, 55, 809-818.

Meunier, J.D. Touiller A. Brulhet, J. and Pagel M., 1990, Uranium and organic matter in a paleodeltaic environment: The Coutrs deposit (Gironde, France), Economic Geology, 85, 1541-1556.

Moiseev, A.N., 1971, A non-magmatic source for mercury ore deposits. Economic Geology, 66, 591-601.

Moorbath, S., 1962, Lead isotope abundance studies on mineral occurrences in the British Isles and their geological significance. Philosophical Transactions of Royal Society of London, 254, 295-360.

Moser, M.R., Rankin, A.H. and Milledge, H.J., 1992, Hydrocarbon-bearing fluid inclusions in fluorite associated with thte Windy Knoll bitumen deposit, UK. Geochimica et Cosmochimica Acta, 56, 155-168.

Nagao, K., Takaoka, N., and Matsubyashi, O., 1981, Rare gas isotope compositions in natural gases of Japan. Earth and Planetary Science Letters, 53, 175-188.

Nash, J.T., 1972, Fluid-inclusion studies of some gold deposits in Nevada. United States Geological Survey Professional Paper, 800-c, C15-C19.

No. 4 Geological Team of Guizhou, 1964, Geological report of the Danzhai mercury deposit.(not published).

Noble, D.C. and Vidal, C.E., 1990, Association of silver with mercury, arsenic, antimony, and carbonaceous material at the Huancavelica district, Peru. Economic Geology, 85, 1645-1650.

Oluwole A.F, 1987, Trace elements in Nigerian oil sands and extracted bitumens. Journal of Radioanalytical Nuclear Chemistry, Articles, 110, 275-282.

Ong, H.L., and Swanson, V.E., 1969, Natural organic acids in the transportation, deposition, and concentration of gold. Colorado School Mines Quarterly, 64, no.1, p.395-425.

Ostic, R.G., Russell, R.D. and Stanton, R. L., 1967, Additional measurements of the isotopic composition of lead from stratiform deposits. Canadian Journal of Earth Science, 4, 245-269.

Ozima, M. and Saito, K., 1983, $^{40}Ar/^{39}Ar$ stepwise degassing experiments on some submarine rocks. Earth and Planetary Science Letters, 20, 77-87.

Parnell, J., 1988, Metal enrichments in solid bitumens: A review. Mineralium Deposita. 23, 191-199.

Parnell, J. and Eakin, P., 1987, The replacement of sandstones by uraniferous hydrocarbons: significance for petroleum migration. Mineralogy Magazin. 51, 505-515.

Peabody, C.E. and Einaudi, M.T., 1992, Origin of petroleum and mercury in the Culver-Baer cinnabar deposit, Mayacmas district, Carlifornia. Economic Geology, 87, 1078-1103.

Pering, K.L, 1973, Bitumens associated with lead, zinc and fluorite ore minerals in North Derbyshirte, England. Geochimica cosmochimica Acta, 37, 401-417.

Podosek, F.A., and Honda, M., 1980, Sedimentary noble gases. Geochimica et Cosmochimica Acta, 44, 1875-1884.

Powell, T.G., and Maquen,R.W., 1984, Precipitation of sulfide ores and organic matter: Sulfate reactions at Pine Point, Canadian Journal of Earth Science, 224, 63-66.

Price, L. C., 1979, Aqueous solubility of methane at elevated pressure and temperatures. American Association of Petroleum Geologists, 63, 1527-1533.

Price, L.C., 1978a, Crude oil and natural gas dissolved in deep, hot geothermal waters of petroleum basins - a possible significant new energy source. 3rd Annual Conference of Geothermal-Geopressured Energy, v.1 GI167-249.

Price, L.C., 1978b, New evidence for hot deep origin and migration of petroleum (abs.). American Association of Petroleum Geologists, 62, 556.

Price, L.C., L.M. Wenger, T. Giong and C.W. Blout, 1983, Solubility of crude oil in methane as a function of pressure and temperature in methane. Organic Geochemistry 4, p.201-221.

Qiu Huaning and Dai Tongmo, 1989, $^{40}Ar/^{39}Ar$ Technique for dating the fluid inclusions of quartz from a hydrothermal deposit. Chinese Science Bulletin. 34, No. 22, 1887-1890.

Radtke, A. S., 1985, Geology of the Carlin gold deposit. United States Geological Survey Professional Paper.1267.

Radtke, A.S. and Scheiner, B.J., 1970, Studies of hydrothermal gold deposition (I); Carlin gold deposit, Nevada: the role of carbonaceous materials in gold deposition. Economic Geology, 65, 87-102.

Radtke, A.S., Robert, O.R., and Dickson, F.W., 1980, Geology and stable isotope studies of the Carlin gold deposit, Nevada. Economic Geology, 75, 641-672.

Rama S. N. I., Hart S. R., and Roedder E., 1965, Excess radiogenic argon in fluid inclusions. Journal of Geophysical Research. 70, 509-511

Rankin, A. H., 1990, Fluid inclusions associated with oil and ore in sediments. in "Seventy-five-years of progress in oil field science and technology" (Ala, M., editor, et al) Balkema, Rotterndam, Netherlands. 113-124.

Reymond, C. M. Jr., Leventhal J. S., Glascock M. D. and Hatch J. R., 1987, Origins of metals and organic matter inthe Mecca Quarry shale member and strtigraphhically equivalent beds across theMidwest. Economic Geology, 82, 915-933

Richards, J.R., 1971, Major lead ore bodies --Mantle origin? Economic Geology, 66,425-434.

Robert, P. I. and George, H.B., 1986, Hydrotermal maturation of indigeous organic matter at the Alligator Ridge gold deposit Nevada. Economic Geology, 81, 113-130.

Roedder, E., 1962, Ancient fluids in crystals. Scientific American, 207, 38-47.

Roedder, E., 1967, Environment of deposition of stratiform (Mississippi Valley-type) ore deposits, from studies of fluid inclusions. Economic Geology Monograph 3, 349-362.

Roedder, E., 1979, Fluid inclusion evidence on the environments of sedimentary diagenesis, A review. SEPM Special Publication No. 26, 89-107.

Roedder, E. 1984, Fluid inclusions. Reviews in Mineralogy. 644p.

Romberger, S.B., 1985, Ore Deposits #9. Disseminated Gold Deposits. Geoscience Canada. 13, 23-31.

Rose, A.W. and Kuehn, C.A., 1987, Ore deposition from highly acidic CO2-enriched solutions at the Carlin gold deposit, Eureka County, Nevada (abs.). Geological Society America Abstract Programs. 19(7), 824.

Rudakhov, G.V., 1973, the relationship between incidences of mercury mineralization and the presence of oil and gas. Geologicheskiy Zhurnal, 33, 125-126 (in Russian).

Russel, R.D. and Farquhar, R.M., 1960, Lead isotopes in geology. New York, 243p.

Rye, Robert, O., 1982, A model for the formation of carbonate-hosted disseminated gold deposit based on geologic, fluid inclusion geochemical, and stable -isotope studies of the Carlin and Cotez deposits Nevada, in geologic characteristics of sediment and volcanic - hosted disseminated gold deposits: Search for an occurrence model (Tooker, Edwin W., editor) United States Geological Survey Bulletin. (Washington) 1646, P. 35-42.

Sanada, Y., Furata T., Kimura H. and Honda H., 1973, Formation of anisotropic mesophase from various carbonaceous materials in early stages of carbonization. Fuel, 52, 143-148.

Sano, Y., Urabe, A., Wakita, H., Chiba, H. and Sakai, H., 1985, Chemical and isotopic compositions of gases in geothermal fluid in Iceland. Geochemistry Journal, 19, 135-148.

Saxby, J.D., 1976, The significance of organic matter in ore genesis. in Wolf K.H.editor. Handbook of stratabound and stratiform ore deposite. NewYork, Elsevier, 2, 1111-1338.

Seidemenn, D. E., 1976, An $^{40}Ar/^{39}Ar$ age spectrum for a cordierite-bearing rocks: isolating the effects of excess radiogenic ^{40}Ar. Earth and Planetary Science Letters, 33, 268-272.

Seward, T.M., 1973, Thio complexes of gold and the transport of gold in hydrothermal ore solutions. Geochimica et Cosmochimica Acta, 37, 379-399.

Seward, T. M., 1988, The hydrothermal chemistry of gold and its implications for ore formation: boiling and conductive cooling as examples. edited.by Reid R. Keays, W. R.Ramsay, David I. Groves, in "The Geology of Gold Deposits: The Perspective in 1988". 398-404.

Shacklette, H.T., Lakin, H.W., Hubert, A.E. and Curtin, G.C., 1970, Absorption of gold by plants. United States Geological Survey Bulletin. 1314-B

Shestopalova, L.F. and Chernyak, A.S., 1975, Solubility of gold in amino acids. Zhurnal Prikladoi Khimii. (Leningrad) 48, 718-819 (in Russian).

Shi Jixi, 1991, On the relationship between organic matter and mercury mineralization in eastern Guizhou in special reference to organic inclusions data. Acta Mineralogica Sinica, 11, 341-345. (in Chinese with English Abstract).

Shock, E.L. 1988, Prediction of hydrothermal solubility of hydrocarbons (abst.) Geological Society of America Abstract with Programs. 20 (7) p. A95.

Skinner, B.J., 1979, The many orgins of hydrothermal deposits. In: Geochemistry of hydrothermal ore deposit. Edited by Barnes H.L., A Wiley-Interscience Publication. 798p.

Slawson, W.F., 1983, Isotopic composition of Pb from a paleoland arc: Shasta, Califormia. Canadian Journal of Earth Science, 1521-1527.

Sverjensky, D.A., 1984, Oil field brines as ore-forming solutions. Economic Geology, 79, 23-37.

Sverjensky, D.A., 1987, The role of migrating oil field brines in the formation of sediment-hosted Cu-rich deposits. Economic Geology, 82, 1130-1141.

Tafuri, W.J., 1987, Geology and geochemistry of the Mercur mining district, Tooele County, Utah. Unpublished Ph.D. Dissertation, University of Utah. 180P (referenced by Bagby and Berger, 1991).

Tissot B.P. and Welte D.H., 1984, Petroleum formation and occurrence. Springer-Verlap, 699p.

Tu Guangzhi, 1983, A comparison between petroleum formation and some active elements(Hg, As, Sb) mineralization. Annual Report of the Institute of Geochemistry, Academia Sinica (1982-1983), Guizhou People Press, (in Chinese).

Tu Guangzhi, 1984, Geochemistry of strata-bound deposits in China. Science Press. Volume 1 (in Chinese).

Tu Guangzhi, 1987, Geochemistry of strata-bound deposits in China. Science Press. Volume 2 (in Chinese).

Tu Guangzhi, 1988, Geochemistry of strata-bound deposits in China. Science Press. Volume 3 (in Chinese).

Tu Guangzhi, 1990, The SW Qinling and the SW Guizhou uranium and gold metallogenic belts, and their similarities to the Carlin-type gold deposits in the western states, USA. Uranium Geology, 6, 321-325. (in Chinese with English abstract).

Turner G. and Wang S., 1992, Excess argon, crustal fluids and apparent isochrons from crushing K-feldspar. Earth and Planetary Science Letters. 110, 193-211.

Turner G., 1988, Hydrothermal fluids and argon isotopes in quartz veins and cherts. Geochimica et Cosmochimica Acta, 52, 1443-1448.

Turner G., R., Burgess and M. Bannon, 1990, Volatile-rich mantle fluids inferred from inclusions in diamond and mantle xenoliths. Nature, 344, 653-655.

Varekamp, J. C. and Busack, P. R., 1981, Mercury emissions from Mount St Helens during September. Nature, 239, 55-556.

Vershkovskaya, O.V., Pikovskiy, Yu. I., and Solo'yev, A.A., 1972, Dispersed carbonaceous material in rocks and ores of the Plamennoye antimony-mercury deposit. Dokladi Academii Nauk SSR, Earth Science Section, 205, 220-222.

Vilenkin, V.A. and Fridman, I.D., 1983, Relation of gold and silver to dispersed organic matter of deposits belonging to the gold-sulfide formation. Geokhimiya, 10, 1487-1491 (in Russian).

Wakita, H. and Sano, Y., 1983, $^{3}He/^{4}He$ ratios in CH_4-rich natural gases suggest magmatic origin. Nature, 305, 792-795.

Wang Henian, Chu Tongqing and Chen Laifu, 1991, A hydrocarbon fluid inclusion study of Weiyuan gas field, Sichuan Province. Acta Mineralogica Sinica, 11, 317-324. (in Chinese with English abstract).

Wang Xianbin, 1983, The natural gas from deep in the Earth. Kexue Tongbao (Science Bulletin), 28, 1515-1518.

Wedepohl, K.H., 1964, Investigation of the Kupferschiefer in northwest Germany; a contribution to the explanation of the genesis of bituminous sediments. Geochimica et Cosmochimica Acta, 28, 305-306.

Wedepohl, K.H., Delevaux M.H., and Doe B.R., 1978, The potential source of lead in the Permian Kupoferschiefer bed of Eutope and some selected Paleozoic mineral deposits in the Federal Republic of Germany. Contribution to Mineralogy Petrology 65, 273-281.

Welhan, J.A. and Craig, H., 1979, Methane and hydrogen in East Pacific Rise hydrothermal fluids. Geophysical Research Letters. 6, 829-831.

Wells, J. T. and Mullens, T.E. 1973, Gold-bearing arsenian pyrite determined by microprobe analysis, Cortez and Carlin gold mines, Nevada. Economic Geology, 68, 187-201.

White, D. E., Muffler, L. J. P. and Truesdell, A. H., 1971, Vapor-dominated hydrothermal systems compared with hot-water systems. Economic Geology, 66, 75-97.

Xiong, J., and Coney, P.J., 1985, accredited terranes of China, in Howell, D.G., ed., Tectonostratigraphic terranes of the circum Pacifc: Houston, Texas, council Energy Mineral Resources, Earth Science Series 1, p, 349-361.

Yen, T. F., 1975, The role of trace metals in petroleum, T.F. Yen, Ed., p.167-181, Ann Arbor: Ann Arbor Science.

Zartman, R.E. and Doe, B.R., 1981, Plumbotectonics -the model. Tectonophysics, 75, 135-162.

Zartman, R.E., 1974, Lead isotopic provinces in the Cordilera of the Western United States and their geologic significance. Economic Geology, 69, 792-805.

Zhang Baogui, 1983, Geochemistry of strata-bound Sb, Hg ore deposits. ed. by Tu Guangzhi in "Geochemistry of Strata-bound Ore Deposits in China". Science press. (in Chinese).

Zhang, Z.M., Liu, J.G., and Coleman, R.G., 1984, an outline of the plate tectonics of China: Geological Society America Bulletin, 95, 295-312.

Plate 1

A: Banded carbonate ore in specimen, arsenopyrite concentrated in the carbonate band rather than in the argillaceous band. Arrow shows orientation of thin sections in B and C.

B and C: Banded carbonate ore under the microscope, arsenopyrite significantly concentrated in calcite band, decreases with the increase of argillaceous material (B transmitted light and C reflected light).

D: Arsenopyrite associated with silicification and organic matter. The white part is quartz and arsenopyrite and black part dominated by chalcedony, arsenopyrite and organic matter.

Plate 1

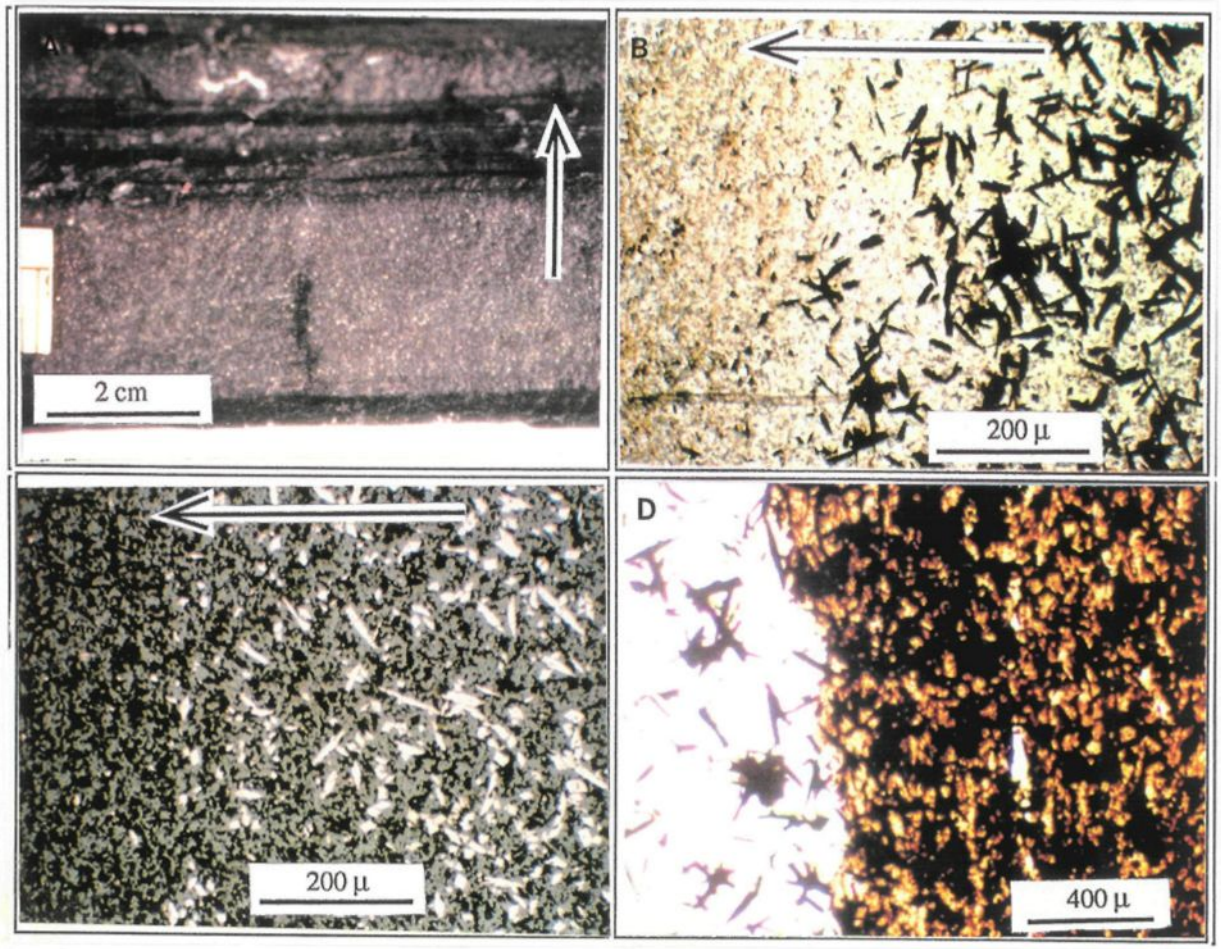

Plate 2

A: Calcite vein rich in cinnabar, arsenopyrite and stibnite. Silicified breccia are distributed in or near carbonate vein and considered to belong to the first stage of gold mineralization (scale is in cm).

B: Silicified limestone rich in hydrocarbon and associated with realgar, orpiment and cinnabar. This sample contains 328.57 ppm gold, the highest in all the samples (scale is in cm).

C: Barite veinlets associated with cinnabar and quartz. The host limestone is slightly silicified or unsilicified (scale is in cm).

D: Calcite vein marbled by black colored hydrocarbon, principally bitumen (scale is in cm).

Plate 2

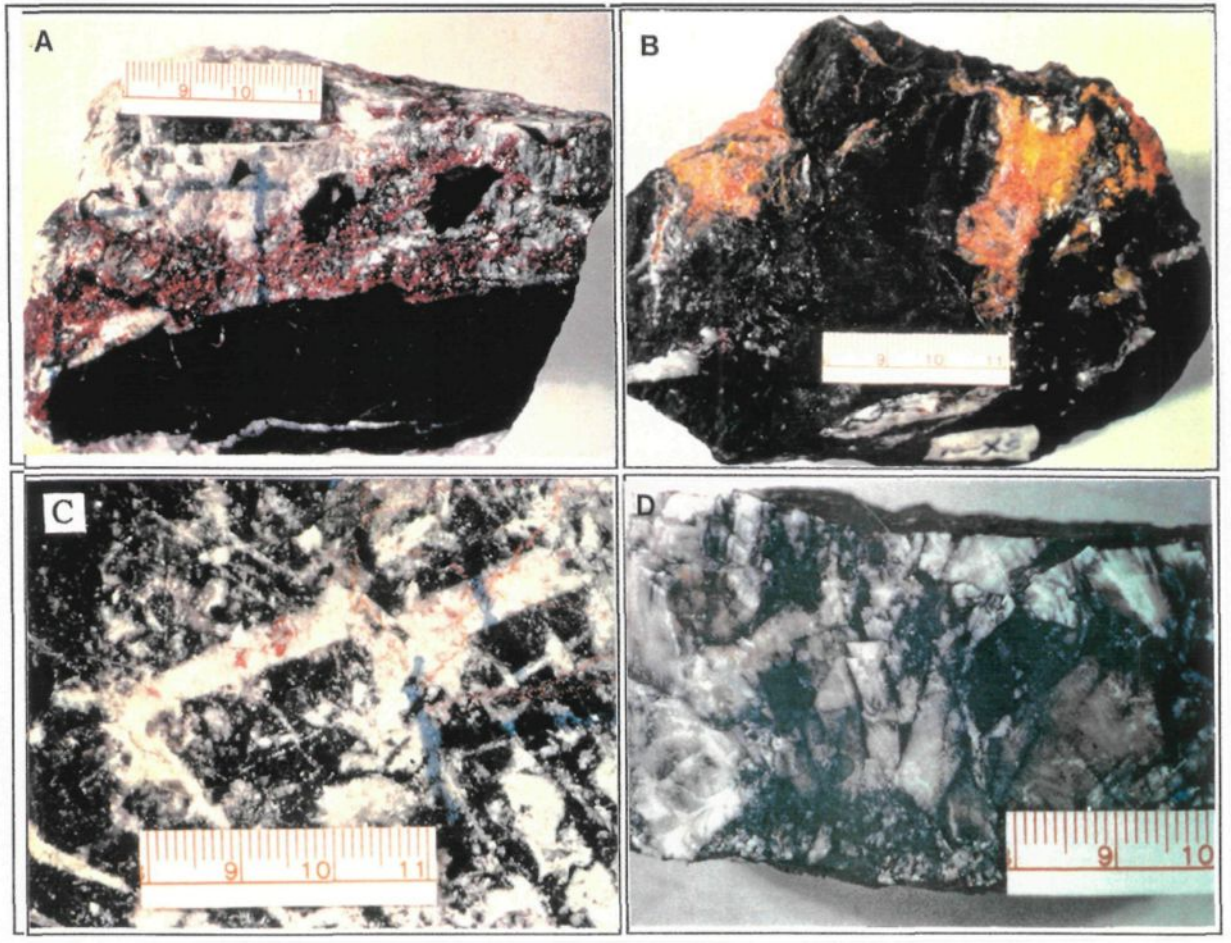

Plate 3

A: Bitumen vein filling fractures along stratification of Cambrian carbonate, the host rock of the Danzhai gold-mercury deposit.

B: Bituminous quartz vein in Cambrian carbonate in the Danzhai area.

C: Arsenopyrite hosted in patch-like bitumen, the host mineral of bitumen is quartz.

D: Arsenopyrite and cinnabar concentrated in hydrocarbon veinlets. The host mineral of these veinlets is calcite but the two crystals in the hydrocarbon veinlet are quartz. The fluid inclusions shown in Plate 9C are hosted in the larger quartz crystal.

E and F: Arsenopyrite and pyrite concentrated in bituminous paraffin wax. The host mineral of the hydrocarbon is quartz. Photo. E was taken under transmitted light while F was taken under reflected light.

Plate 3

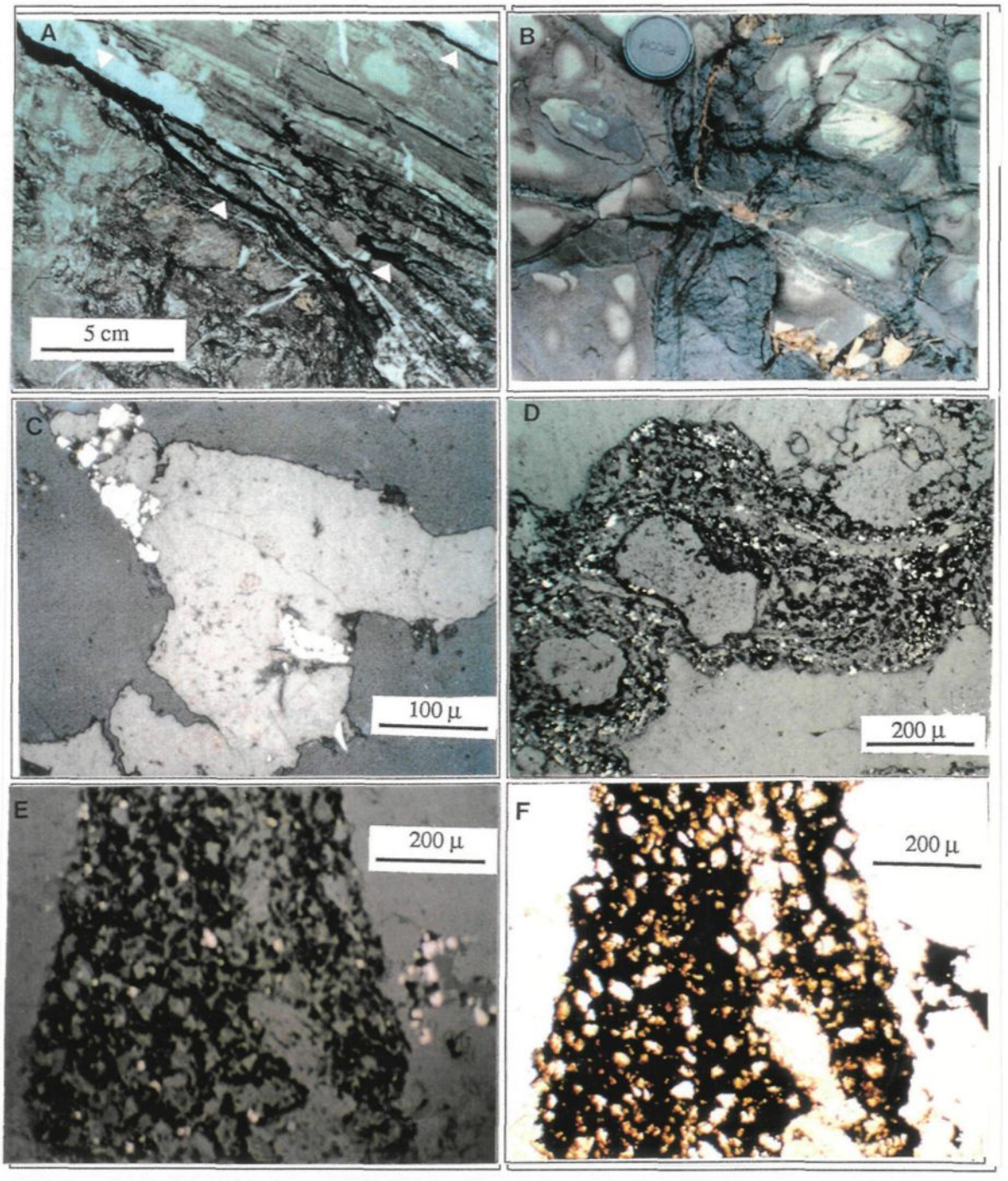

Plate 4

A and B: Arsenopyrite concentrated in stylolitic and patch-like bitumen. The patch-like bitumen is shown in B in higher mangification. The arsenopyrite is only present within hydrocarbon not within quartz.

C: Bitumen grains within quartz and along the border of quartz crystals. These two types of bitumen show no difference in appearance, color and reflectance so they belong to the same generation. The triangular bitumen occurs within the quartz and could be considered as a big solid bitumen inclusion.

D: The fluorescence (?) effect of paraffin wax (red) under 510 nm light wavelength.

Plate 4

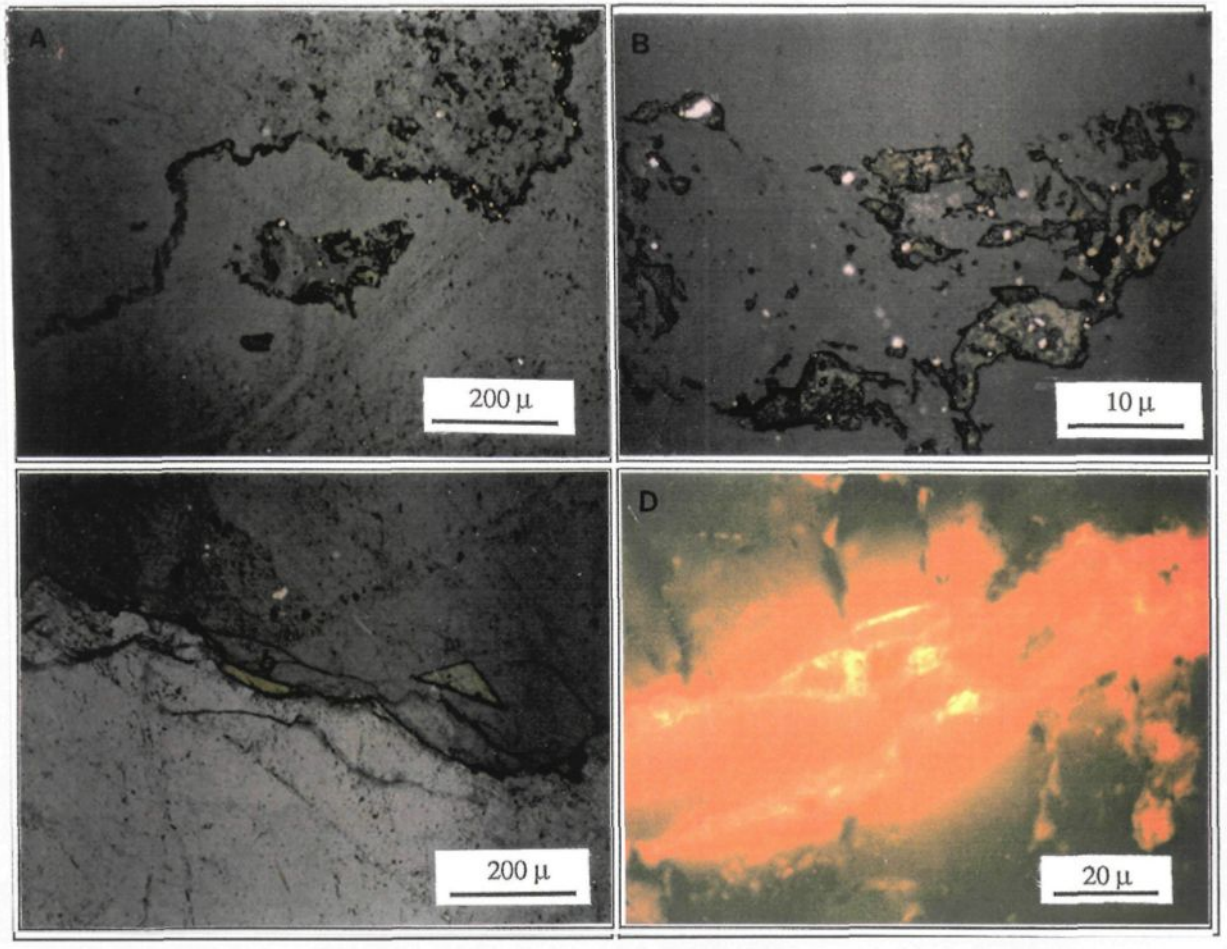

Plate 5

A: Irregular shaped colorless liquid methane inclusions in cinnabar.

B: Inclusion *a* appears to be bitumen inclusion, inclusion *b* is a negative crystal shaped aqueous inclusons

C: Liquid methane inclusions associated with cinnabar crystals, a liquid methane inclusion attached to a cinnabar crystal.

D: Well developed growth zone in a quartz crystal.

Plate 5

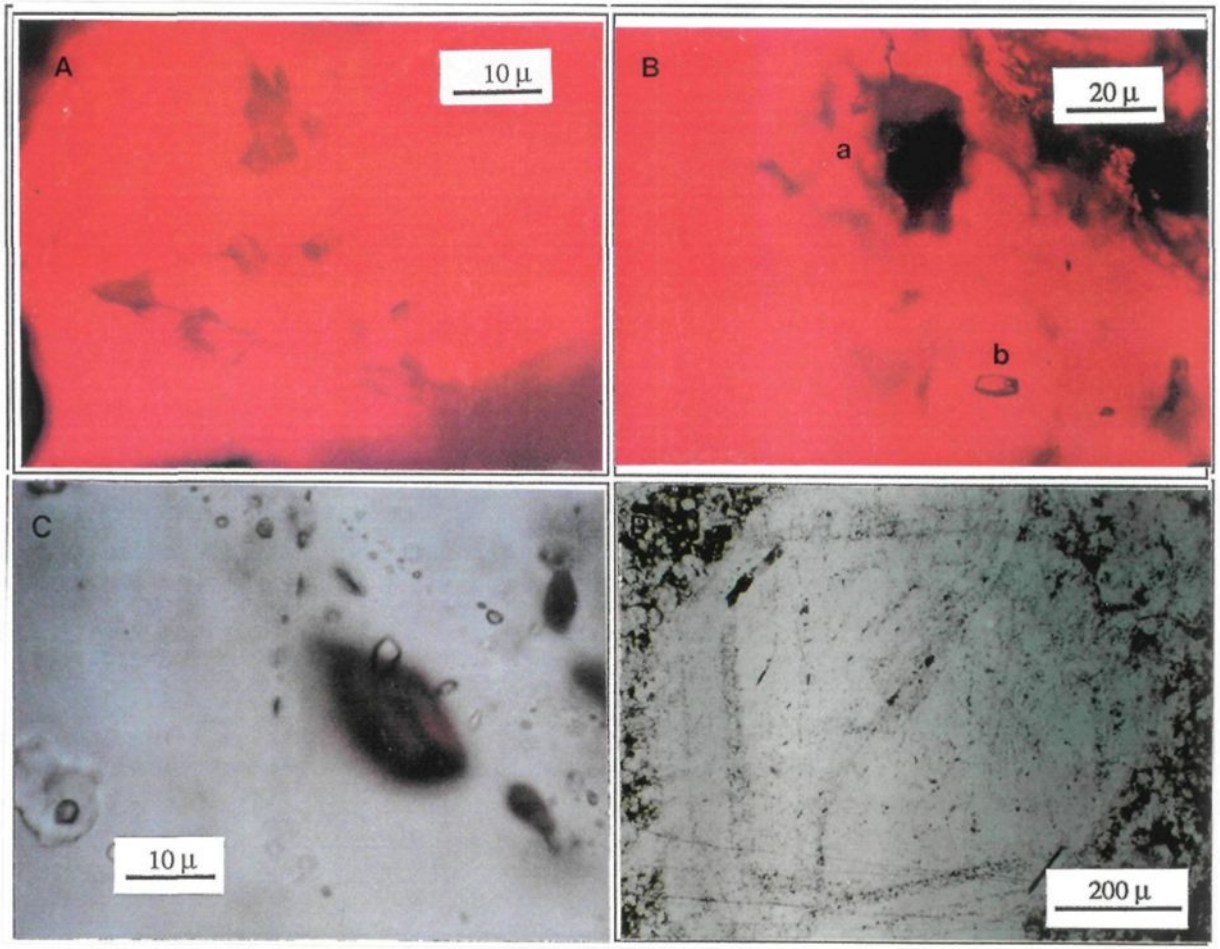

Plate 6

A: The growth zone in Plate 5D is dominated by liquid methane inclusions(e.g.: *a, b*), some bitumen inclusions (e.g.: *c.d*) and other aqueous inclusions(e.g.: *e*).

B: A quartz crystal can clearly be divided into an exterior and interior zone (note the real border of the quartz crystal), the exterior zone is concentrated with densely populated tiny liquid methane and bitumen inclusions so it looks dark, some of the fluid inclusion stretch to the interior zone. The fluid inclusions in the interior zone are pseudosecondary fluid inclusions.

C: One of the fluid inclusions of the belt in B. It consists of liquid methane inclusions, sometimes with aqueous inclusions.

D: Bitumen inclusions in calcite.

Plate 6

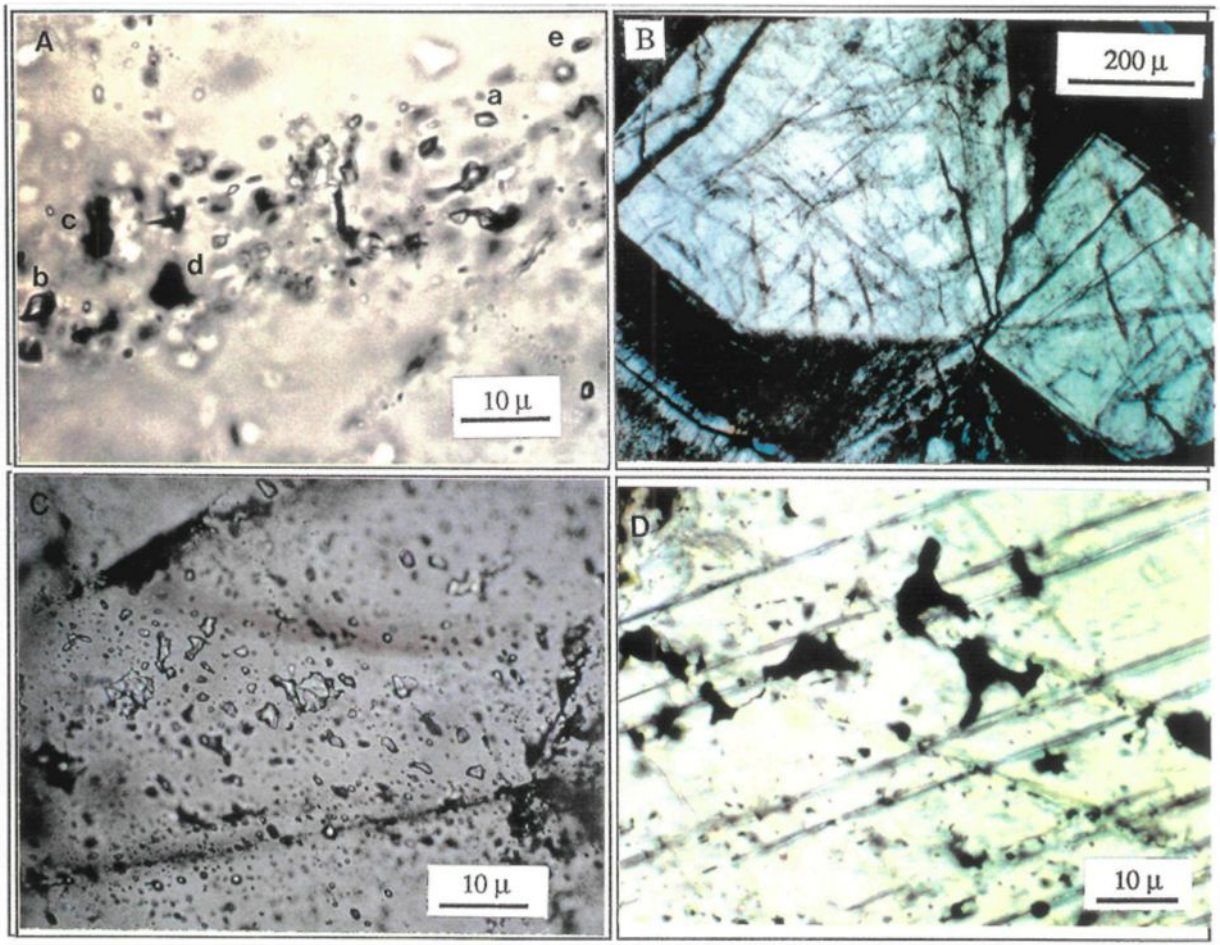

Plate 7

A and B: A group of single solid phase bitumen inclusions in quartz, but one of the biggest inclusions was partly cut in sample preparation and can be seen under reflected light (in B). Reflected light shows that the black fluid inclusions shown in A are solid bitumen.

C: Brown colored, solid bitumen associated with liquid methane in the same inclusion

D: Three solid, translucent with bubbles in a bitumen inclusion, the three white bubbles are composed of paraffin wax.

Plate 7

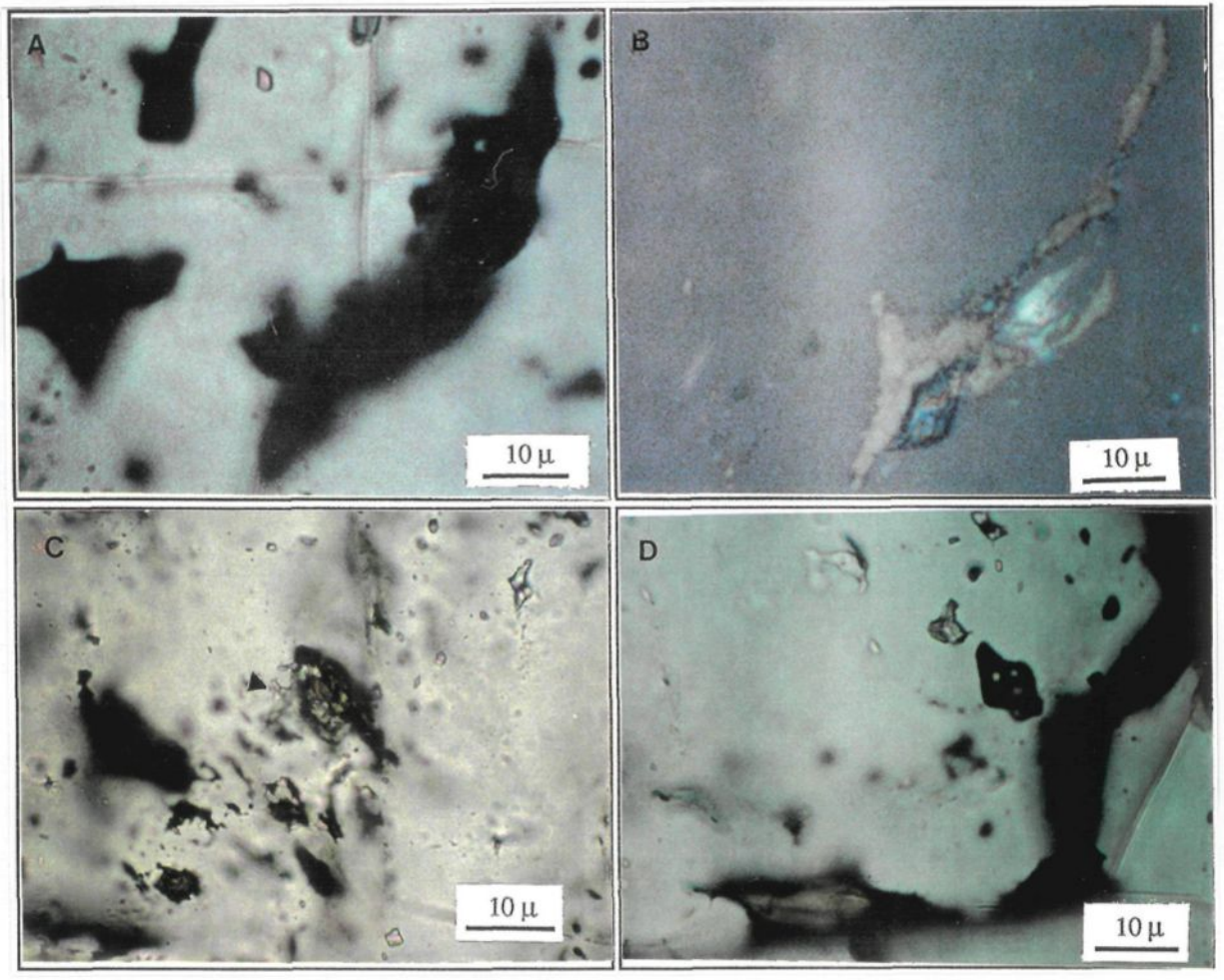

Plate 8

A: Three component bearing hydrocarbon inclusion, including, bitumen (black colored), paraffin wax (white colored, in the upper-right border of the bitumen inclusion) and liquid methane (colorless, separating from bitumen). These two inclusions are actually connected, not separated, but nearly necking down.

B: A small bitumen inclusion and a bitumen-bearing liquid methane inclusion almost necking down.

C: Paraffin wax inclusion hosted in quartz, mixed with some bitumen.

D: Heavy oil droplet inclusions hosted in calcite, in one inclusion (*a*), several viscous, densely-concentrated oil droplets occur together. Adjoining inclusions (*b*, *c*) are probably pure heavy oil inclusions.

Plate 8

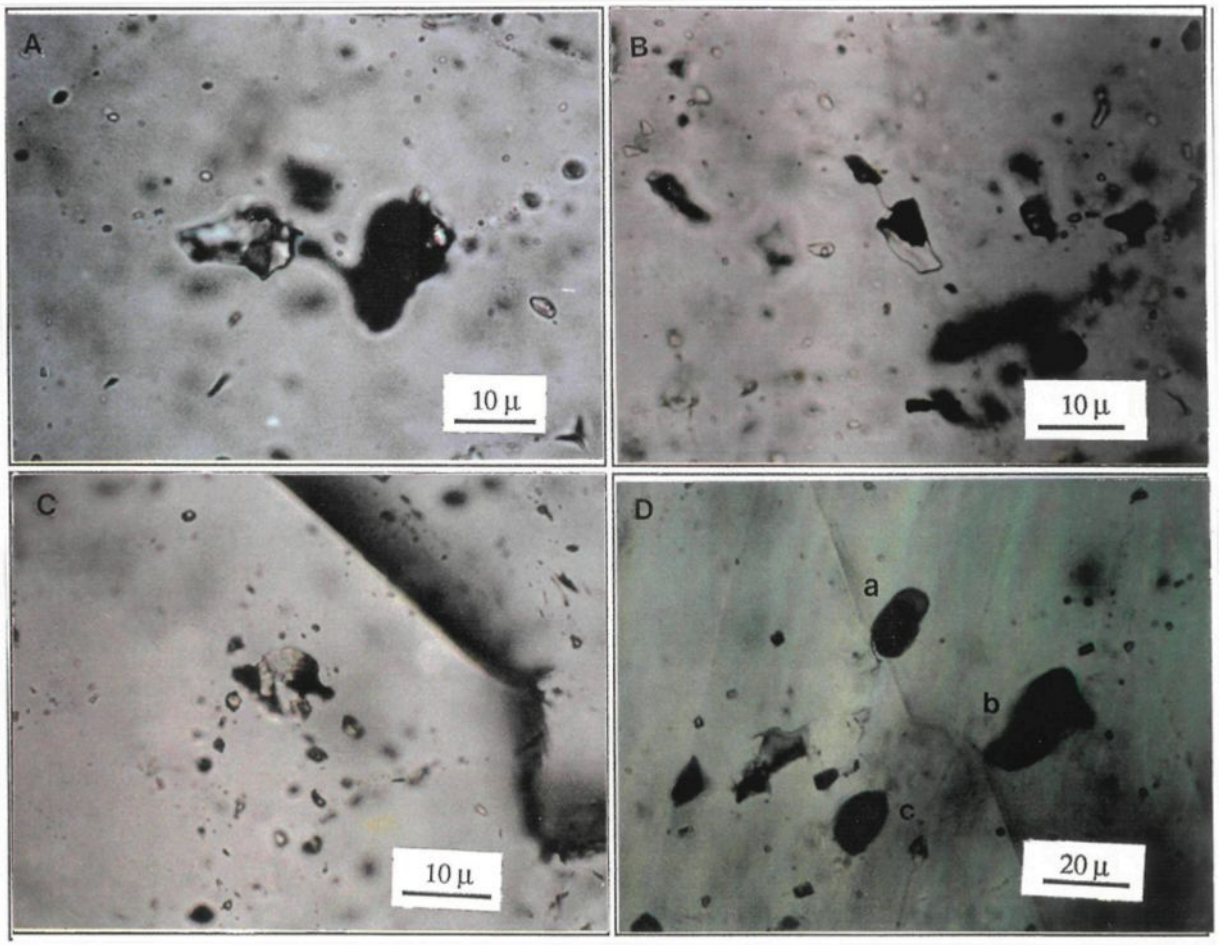

Plate 9

A: Four dark brown droplets occur in an aqueous fluid inclusion, the droplets with dark brown color are probably heavy oil. The fluid inclusion hosted in barite.

B: Two daughter minerals are present in an aqueous fluid inclusion, both of these daughter minerals are columnnar, one with high birefringence and high extinction angle, the other without birefringence and parallel extinction. Black inclusions are bitumen dominated inclusions.

C: A group of fluid inclusions in a quartz crystal (Plate 3D) probably representing the unmixing assemblage of aqueous and hydrocarbon fluid. Bitumen-bearing liquid methane inclusion *a*, aqueous liquid inclusions *b, c, e, f* gas inclusion *d* are present in this unmixing assemblage.

D: Liquid methane inclusion *a* and aqueous inclusion *b* coexist in the same quartz crystal.

Plate 9

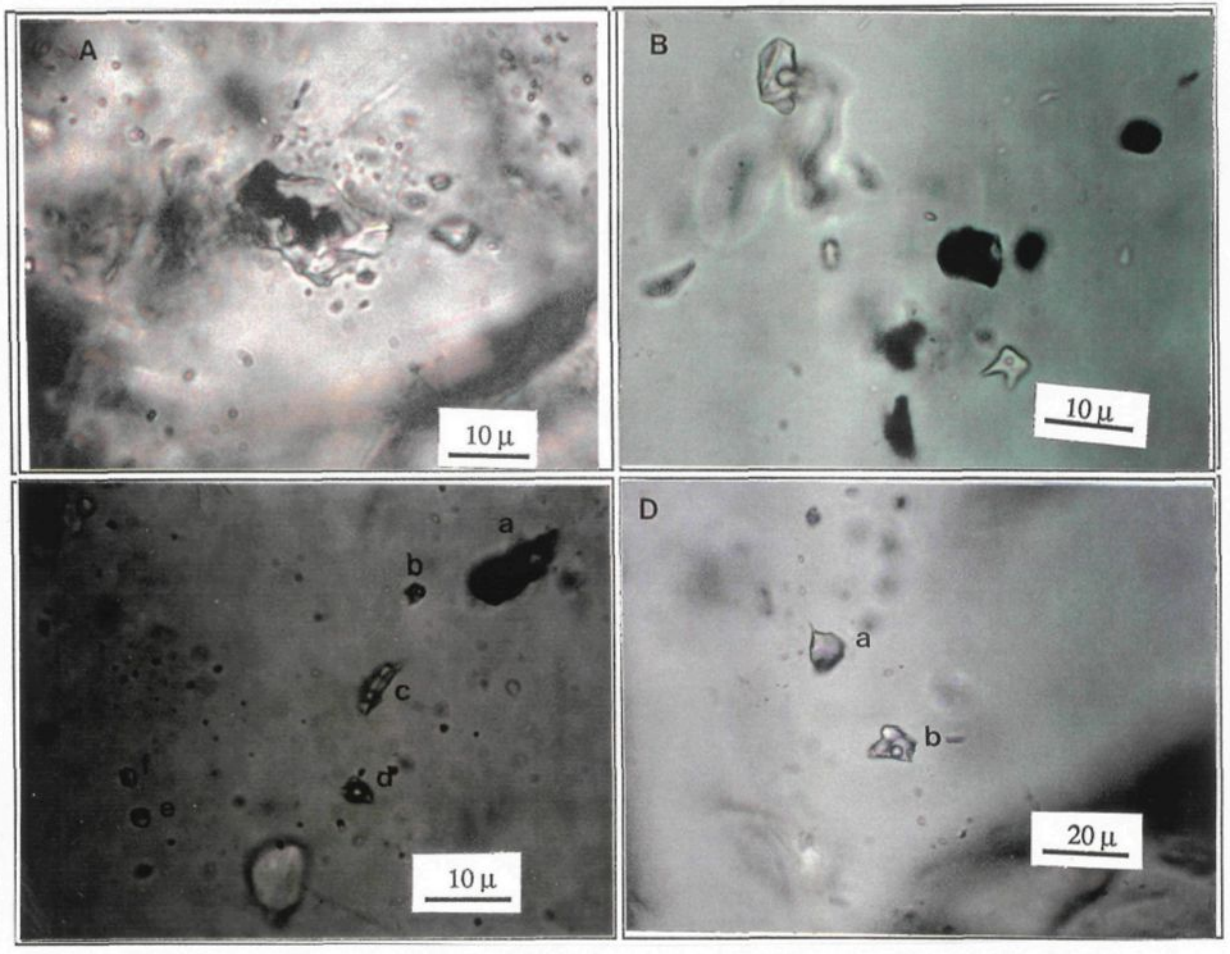

Appendix I

Sample Description

1. Samples from No. 1 orebody

S1-03 Dark gray massive silicified limestone associated with calcite veinlets, with fine-grained disseminated arsenopyrite: first mineralization stage.

S1-06 Black massive argillaceous limestone, rich in organic matter. There is a 3 x 0.3 cm^2 pyrite concret filled in the argillaceous limestone. Calcite veinlets are present in the sample as well.

S1-12 Dark gray massive silicified carbonate. A small quartz vein with aggregated stibnite crosscuts this sample.

S1-15 Fine-grained pyrite disseminated in gray massive argillaceous limestone. Two calcite-pyrite veins cut the massive limestone

S1-22 Banded limestone with low silicification. A sample taken from the argillaceous band demonstrates that arsenopyrite and pyrite are disseminated in the ore: first mineralization stage.

S1-22' The same sample of S1-22, but this part is taken from the carbonate band, in which arsenopyrite and pyrite are highly concentrated. It belongs to first mineralizaiton stage.

S1-26 Dark gray brecciated limestone with strong silicification, rich in bitumen and other forms of organic matter, in which arsenopyrite and/or pyrite are disseminated.

S1-28 Light gray massive limestone associated with calcite veins. Arsenopyrite is

disseminated in bitumens. Silicification is not seen in this sample.

Sx-01 Orpiment and orpiment rich sample with associated cinnabar, quartz and calcite. It is rich in bitumen. It belongs to second mineralization stage. This sample was taken from Level 690.

Sx-02 Orpiment rich sample with associated orpiment, cinnabar. This sample was also taken from Level 690 .

2. Samples from No. 2 orebody

S2-01 Gray thin bedded limestone with low silicification.

S2-02 White quartz vein ranging from 0.3 to 0.8 m thick. It is locally rich in bitumen. Fine-grained pyrite and arsenopyrite are disseminated in the quartz vein. It cuts No. 2 orebody thus it is the last stage of veining.

S2-06 Huge gray calcite vein ranging from 0.5 to 2 m thick. No other minerals is seen except occasionally fine-grained pyrite and arsenopyrite. This vein cuts the whole orebodies thus it belongs to the last stage of vein.

S2-11 Gray banded carbonate, arsenopyrite and pyrite are concentrated in the carbonate band. No silicification is observed.

S2-13 Parallel calcite veins are distributed in this lowly silicified limestone. Arsenopyrite is disseminated in the limestone and stibnite is observed in the calcite vein.

3.Samples from No. 3 orebody

S3-03 Gray brecciated limestone with some calcite veinlets in it. No silicification is observed in this sample.

S3-06 Dark gray silicified thin bedded limestone. Fine-grained arsenopyrite and pyrite are distributed along the bedding. Organic matter such as bitumen is concentrated in this sample.

S3-07 It was taken from a gray calcite vein ranging from 0.3 to 1 m in thickness. No. 3 orebody was cut by this calcite vein, in which no mineralization is observed.

4. Samples from No. 4 orebody

S4-01 Dark gray argillaceous limestone. Aggregated stibnite is distributed in this limestone. A barite vein filled with fine-grained cinnabar, but no silicification is observed in this sample.

S4-01' Dark gray argillaceous silicified limestone is rich in organic matter. Barite veins are seen and silicification is observed with differing intensity. It belongs to the third mineralization stage.

S4-02 Dark gray argillaceous limestone, rich in bitumen. Aggregated stibnite is distributed in this limestone, but no silicification is observed.

S4-03 Fine-grained arsenopyrite is disseminated in this gray argillaceous limestone, stibnite is seen locally.

S4-05 Light gray argillaceous limestone with barite and calcite veins. Locally aggregated stibnite is present .

S4-07 Dark gray argillaceous limestone, with disseminated arsenopyrite and pyrite. Silicification is not observed in this sample.

S4-13 Gray banded limestone, with fine-grained arsenopyrite and pyrite concentrated in a carbonate band. No silicification is observed in this sample.

5. Samples from No. 5 orebody

S5-01 Silicified limestone breccia trapped in huge calcite vein. Cinnabar crystals are distributed around the silicified limestone breccia.

S5-02 Sample taken from principal No. 5 orebody. Calcite and quartz vein ranging from 2 to 5 m thick are associated with cinnabar and stibnite. It belongs to the second mineralization stage, an important stage for both gold and mercury mineralization.

S5-03 Find-grained cinnabar and stibnite are disseminated in this huge calcite-quartz vein up to 4 m thick.

S5-04 Brecciated limestone taken from the wall of the huge calcite-quartz-cinnabar-stibnite vein. The brecciated limestone is silicified with varing intensity. Fine grained arsenopyrite and pyrite are observed in the sample.

S5-04' Sample taken from the principal No. 5 orebody, calcite and quartz vein ranging several meters is associated with stibnite: second mineralization stage.

S5-06 Silicified limestone breccia in calcite-cinnabar-stibnite vein, which ranges from 1 to 2 meters: second mineralization stage.

S14-01 Sample taken from strongly silicified brecciated limestone, rich in pyrite, arsenopyrite and bitumen: first mineralization stage.

S14-12 Sample taken from strongly silicified limestone, rich in pyrite, arsenopyrite and bitumen.

6. Samples from wall rocks

W-01 Brecciated carbonate from Yangjiawan formation, upper Cambrian. No alteration or mineralization is observed.

W-02 Unmineralized thin bedded limestone from Sandou formation, upper Cambrian.

W-03 Dark gray banded micrite limestone Goutang formation, lower Ordovician. No mineralization is seen.